Additives for the reduction of NOx emissions in large scale solid fuel combustion

Richard Ian Birley

Submitted in accordance with the requirements for the degree of Doctor of Philosophy as part of the Integrated PhD with MSc in Bioenergy

30 June 2020

University of Leeds
Centre for Doctoral Training Centre in Bioenergy,
School of Chemical and Process Engineering.

Declaration of Authorship

The candidate confirms that the work submitted is his/her/their own, except where work which has formed part of jointly authored publications has been included. The contribution of the candidate and the other authors to this work has been explicitly indicated below. The candidate confirms that appropriate credit has been given within the thesis where reference has been made to the work of others.

Work within Chapters 6, 7 and 10 are from the paper:

Birley, R., Jones, JM, Darvell, LI, Williams, A, Waldron DJ, Levendis YA, Rokni, E, Panahi, A. 2018. Fuel flexible power stations: Utilisation of ash co-products as additives for NOx emissions control. Fuel. 251, p8.

Acknowledgements

Throughout this work there has been many influences (possibly too many to mention in one page) and driving forces that have helped me to achieve the goal of completing the research and this tome. At the forefront has to be my ever-patient supervisors, Prof. JM Jones, Prof. A Williams, Dr. LI Darvell, who have graciously steered me through the minefield of academia. Research funding from EPSRC (EP/L014912/1) and BF2RA (Grant 23); P Sage and Dr. J Ashman have been essential in achieving a successful conclusion. An external consultant Dr. D Waldron has been of great influence and a font of modelling knowledge. All of the academic staff at the University of Leeds, who have been invaluable.

From a non-academic perspective, there have been many people who have been influential, in particular all of the 2015 CDT in Bioenergy cohort. Some individual names from the university that have been prominent in maintaining a level of sanity for a variety of reasons, Daisy Thomas, Nicola Wood and Ghinwa Yaghy.

Finally, I would like to extend a high level of thanks to all of the staff at the Library, who have kept me in constant supply of coffee and conversation, without which completion may have been on rocky ground.

Abstract

Oxides of nitrogen (NO_X) are gases that can cause harm to flora, fauna and human health. NO_X emissions can result in acid rain, act as a nucleus to form particulate matter (PM) and have been known to cause respiratory disorders in humans. Recent regulations to curtail the emissions of NO_X (and other emissions) have been implemented globally. The current legislation, the Industrial Emissions Directive (IED) has set ever more stringent limits for NO_X from existing power stations across the European Union (EU). To meet these targets, power stations operating with pulverised fuels will be required to use multiple reduction technologies.

This research is focussed on using by-products of biomass combustion, pulverised fly ash (PFA) and furnace bottom ash (FBA) in co-combustion with coal to reduce NO_X in fuel flexible power stations. The increase in K, Ca, Na and Mg in the fuel blends may provide catalysts to promote a reduction mechanism for NO_X to diatomic nitrogen during combustion. Three bituminous coals, representative of those used for power production were selected for co-combustion with the two ash additives. To compliment the research, a low reactivity coal was also examined under the same conditions. A high reactivity biomass was also examined using coal PFA as an additive, with relatively high Fe. The experimental work investigated the nitrogen partitioning and carbon conversion of the fuel blends through a variety of conditions; Low heating rate (LHR) and high heating rate (HHR) analysis was carried out. The range of experimental work revealed, through the addition of the FBA and PFA to all of the coals, volatile nitrogen was increased and char nitrogen reduced. Carbon conversion was also increased across all of the coals. The addition of the coal PFA to the biomass also realised the same trends in volatile nitrogen and carbon conversion. These are favourable conditions in a large-scale furnace fitted with Low-NO_X technology.

A slice model was used to represent of a well stirred pulverised fuel furnace. By dividing the furnace into several 3-dimentional slices the model can calculate the overall performance of a furnace. The slice model can be used for the prediction of NO_X emissions from a furnace based on the fuel properties, and furnace operating conditions. When the adapted model was applied to the bituminous coals with and without the additives, accuracies within 10% of experimental work were achieved.

The use of PFA and FBA may present a cost-effective NO_X reduction technique when combined with other low NO_X technologies in fuel flexible power stations.

Contents

List of Figures

List of Tables

Nomenclature

ϕ	Work function
ϕ	Equivalence ratio
µm	Micro-meters
AGRI	Agricultural residue
$A\ s^{-1}$	Pre exponential factor
A/F	Air fuel ratio
Al_2O_3	Aluminium oxide
A_N	Pre exponential factor for nitrogen
ar	As received
ASTM	American Standards, Tests and Measurements
BAT	Best Available Technology Reference Document
B-BOT	2, 5-Bis (5-tert-butyl-benzozazol-2-yl) thiophene
BS	British Standards
BT	Burnout temperature
CaCl	Calcium chloride
CaO	Calcium oxide
CAS	UK Clean Air Strategy
CBK	Carbon burnout kinetics
CCS	Carbon capture and storage
CH_4	Methane
CHNO	Carbon, hydrogen, nitrogen, oxygen
CHNS	Carbon, hydrogen, nitrogen, sulphur
CO	Carbon monoxide
CO_2	Carbon dioxide
Coal PFA	Coal pulverised fly ash
CPD	Chemical percolation and devolatilisation
daf	Dry ash free
db	Dry basis
dc	Diameter of carbon core
Defra	Department for Environment, Food and Rural Affairs
$DeNO_X$	NO_X removal systems
Dm/dt	First derivative mass/time
dmmf	Dry mineral matter free
dp	Diameter of particle µm
DTF	Drop tube furnace
e	Exponential
Ea	Activation energy kJ/mol
Eb	Photoelectron energy eV
ED	End of devolatilisation
EEA	European Economic Area
Ek	Photoelectron kinetic energy
EPA	Environmental Protection Agency
ESP	Electrostatic precipitation
EU	European Union
eV	Electron volts

FBA	Furnace bottom ash (white wood)
Fe_2O_3	Iron oxide III
FGD	Flue gas desulphurisation
FG-DVC	Functional Group Devolatilisation Vaporising and Cross-linking
FGR	Flue gas recirculation
Fo	Oxygen correction
FOP	Furnace outlet plane
Fp	Pressure correction
FR	Fuel ratio
Ft	Temperature correction
GC	Gas chromatography
GHG	Greenhouse gases
GWP_{100}	Global warming potential (100 years)
HCl	Hydrogen chloride
HCN	Hydrogen cyanide
HHR	High heating rate
HTVY	High temperature volatile yield
hv	X-ray photon energy
I	Intensity of light
Ic	Ion chromatography
IEA	International Energy Agency
IED	Industrial Emissions Directive
I_o	Intensity of light in sample chamber
k	Rate constant
K	Temperature in Kelvin
K	Potassium
K_2O	Potassium oxide
kc	Composite pre exponential rate constant char
KCl	Potassium chloride
Kg	Kilogram
Kt	Kiloton
kW_{th}	Kilo-watt thermal
kδ	Composite pre exponential rate constant side chains
LCPD	Large Combustion Plant Directive
LHR	Low heating rate
LOI	Loss on ignition
M	Inert molecule
m/z	Mass spectra
m_{add}	Mass added
Mg	Magnesium
mg Nm^{-3}	Milligrams per normalised cubic meter
MJ	Mega joules
mL	Milli-litre
Mn_3O_4	Manganese tetroxide
MS	Mass spectroscopy
MW	Mega Watts
MW_{th}	MW thermal
N_2	Molecular nitrogen

N_2O	Nitrous oxide
N-4	Quaternary nitrogen group
N-5	Pyrrolic nitrogen group
N-6	Pyridinic nitrogen group
Na	Sodium
Na_2O	Sodium oxide
NECD	National Emissions Ceiling Directive
NH_3	Ammonia
NHO_2	Nitrous acid
NHO_3	Nitric acid
NNH	Nitrogen, Nitrogen and hydrogen
NO	Nitric Oxide
-NO	Nitroxo groups
NO_2	Nitrogen dioxide
NO_X	Oxides of nitrogen (NO and NO_2)
N-Q	Quaternary nitrogen group
NSCEP	National Service Centre for Environmental Publications
O_3	Ozone
OC	Onset of combustion
OD	Onset of devolatilisation
OFA	Overfire area
P	Height between fuel/air injectors
P_2O_5	Phosphorus pentoxide
PAC	Particulate activated carbon
PACT	Pilot-scale Advanced CO_2 Capture Technology
PAH	Poly aromatic hydrocarbons
PCC	Pulverised coal combustion
PFA	Pulverised fly ash (white wood)
PFC	Pulverised fuel combustion
PID	Proportional integrated derivative
PM	Particulate matter
ppmv	Parts per million by volume
PT	Peak temperature
R	Reactant/reactions
Ri	Intrinsic reactivity kJ/mol
rpm	Revolutions per minute
SCR	Selective catalytic reduction
SE	Secondary electron
SEM	Scanning electron microscope
SiO_2	Silicon dioxide (Silica)
SNCR	Selective non-catalytic reduction
SO_2	Sulphur dioxide
SO_3	Sulphur trioxide
St	Stoichiometry
STA	Simultaneous thermal analysis
TGA	Thermogravimetric analyser
TiO_2	Titanium dioxide
Tp	Temperature of particle

TWh	Terawatt hours
UHC	Unburnt hydrocarbons
UK	United Kingdom
US	United States of America
UV	Ultraviolet
v	Velocity m s^{-1}
V_2O_5	Vanadium pentoxide
VOC	Volatile organic compounds
Vol	Volatile
WHO	World Health Organisation
WOU	Western Oregon University
wt	Weight kg
WW	White wood
w/w	Weight per weight
XPS	X-ray photoelectron spectroscopy
ϐ	Labile bridge
δ	Thickness of porous ash film μm
λ	Excess air
Ψ	Fraction of carbon converted to CO_2

Chapter 1 Thesis overview

1.1 Introduction

The research is focussed on the emissions of NO_X from large scale combustion, in particular from power production. Emissions of NO_X from power stations have a variety of control technologies deployed to reduce the emissions to the atmosphere. Advancements in regulations are reducing emissions further, creating difficulties for the current technologies to comply with the future emissions targets. Coal, as a primary fuel for combustion to produce electrical power is being reduced in the UK and across the EU, however the new emission targets are to come into effect from 2020, with power stations to be compliant by 2021. Some coal fired power stations are being converted to biomass fuels, as such there is an increase in the ashes from solid biomass combustion in fuel flexible furnaces. The ashes from biomass combustion tends to be relatively high in alkali and alkaline earth metal compounds. The research is focussed on utilising the ash from biomass as an additive to change the nitrogen partitioning of coal during combustion. The interaction of the reactive compounds in the ash additives can act as catalysts, providing reactive sites for the conversion of fuel nitrogen during pyrolysis.

1.2 Experimental

Initial investigations focussed on analysis of four reference coals and the ash additives. This included proximate and elemental analysis, together with some low heating rate analysis (10°C min^{-1}) at temperatures of 1000°C to find evidence of any catalysis and to obtain the apparent first order rate parameters for pyrolysis of the coals with and without ash additives. This was then extended to high heating rate studies (10^4-10^5 K s^{-1}) and at 1100°C utilising two different drop tube furnaces (DTF). DTF1 at the University of Leeds (UK) was used under devolatilisation conditions for the creation of chars for comparative analysis. DTF2 at Northeastern University, Boston (USA), was

used under un-staged combustion conditions for emissions during devolatilisation and char combustion. A smaller parallel study examined whether coal ash could act to influence N-partitioning during biomass combustion.

Further analysis was carried out using scanning electron microscopy (SEM) to ascertain the physical morphology of the coals and coal chars with ash additives. X-ray photoelectron spectroscopy (XPS) was carried out to determine the nitrogen functional groups within the coals and coals with additives.

1.3 Modelling

The final stage of the research is focussed on modelling. An established model that utilises Chemical Percolation and Devolatilisation (CPD), was applied in a DTF model to compare the measured and predicted nitrogen partitioning from a DTF. This model was calibrated for the presence of additives based on experimental DTF results-this provided a more flexible model for subsequent modelling of a coal furnace. A second model carbon burnout kinetics (CBK) is applied to calculate carbon conversion from a fuel during devolatilisation and char carbon conversion. Using these models and details appertaining to a specific furnace, a large-scale furnace slice model was adapted to predict the emissions from a large-scale furnace for a given fuel/additive combination. The model can be used to predict the NO_X emissions from a furnace.

1.4 Aim of the research

The aim of the research is to investigate the impact of biomass ash on NO_X emissions during coal combustion in large scale power production, with a particular focus on the N-partitioning during the devolatilisation stage. Biomass ashes tend to have high levels of reactive components, (alkali and alkaline earth metals) which may act as catalysts to change the nitrogen partitioning during combustion of coal.

1.5 Objectives

1. To understand the impact of the emissions directives set for current and future emissions control. In specific the directives that are applicable to the power generation industry. This will include all large-scale furnaces above 50MW_{th}. Of particular importance, for this research are the implications for NO_X production and emissions.
2. Establish the current knowledge about nitrogen emissions and evolution from coal and biomass.
3. To perform laboratory based experiments that closely replicate industrial scale furnaces and the emissions from coal combustion. This will take the form of tests at high heating rate and high temperatures of 1100°C and performing devolatilisation and combustion experiments.
4. To carryout analysis of a range of fuels relevant to power stations, consisting of 3 bituminous coals (Shotton, UK, La Loma, Columbia and Galatia, USA) and a low reactive coal Ffos-y-fran, UK. The analysis of 2 white wood (WW) ashes, a pulverised fly ash (PFA) and a furnace bottom ash (FBA) (both from the same source).
5. Determine the nitrogen partitioning and carbon conversion from the fuels, and any changes observed when the fuels are combined with the additives.
6. Examine the kinetics for devolatilisation of the fuels and the fuels with the additives.
7. Establish a working model for the nitrogen emissions from an industrial furnace and the nitrogen partitioning data from devolatilisation in a drop tube furnace.
8. Carry out comparative work on a high reactivity fuel, olive cake, with a coals PFA additive. All work in objectives 5-8 to be carried out on the olive cake and olive cake with coal PFA.

1.6 Tasks to achieve the objectives

Task 1

To review the historical emissions directives within the EU and UK, and the wider political arena.

Establish the future emissions regulations that act as a driver for industry to reduce the emissions from the exhaust stack.

Critically review NO_X control strategies available to meet emissions directives.

Task 2

A review of historical and current literature related to nitrogen evolution from solid fuels.

A review of current literature on nitrogen emissions and devolatilisation and the potential effects of additives on the release of NO_X in the atmosphere.

Task 3

Through the use of laboratory equipment, experimental work simulating combustion and reactions within a furnace, will be used to show the devolatilisation and combustion characteristics of a range of fuels will be established. The experimentation will include: combustion, devolatilisation, nitrogen partitioning analysis and emissions analysis.

Task 4

Coals have been selected that are representative of those used in large scale furnaces. The white wood ash additives selected are from a fuel flexible furnace. The ashes may have alternate uses as building aggregate or as potential concrete additives.

They will be analysed using a range of experimental apparatus including ISO Standard Testing Methods, thermal gravimetrical analysers, drop tube furnaces, mass spectroscopy, x-ray photoelectron spectroscopy, flash elemental analysers.

Task 5

Using data from CHNS elemental analysers from the fuels and the fuels with additives, and an ash tracer method to calculate the partitioning of nitrogen released during devolatilisation and retention in the char. Carbon conversion can be calculated through the same methodology.

Task 6

Through the use of thermogravimetric analysis and assuming apparent first order global kinetics, together with the Arrhenius equation, the kinetic parameters of the fuels and fuels with additives can be calculated.

Task 7

Using a previously established model, refining CPD and CBK 8 in the presence of additives, and combining this with data from experimental work and from the kinetic evaluation, a working model can be built to predict the emissions from the fuels and any changes brought about by using the additives with the fuels. The furnace model (without additive) will be calibrated against power station data.

1.7 Thesis outline

Chapter 1 lays down an overview of the research carried out, including the main aim and the objectives of the work. Finally within this chapter is a breakdown of the thesis by chapter.

Chapter 2 introduces some background information explaining why coal is an important fuel source. It then discusses atmospheric pollution and presents information on anthropogenic emissions into the atmosphere. The emissions from the power sector are discussed, with an introduction to oxides of nitrogen and the environmental impact they have. There is an introduction to alternate sources of energy for power production, i.e. renewable energy alternatives to coal. Due to the anthropogenic emissions, there

have been a series of regulations implemented to restrict emissions, in particular to emissions from large scale furnaces. There is an insight into the future of coal globally and within Europe. Finally there is an introduction into NO_X reduction strategies adopted in large scale furnaces.

Chapter 3 investigates the origins of coal and reviews some of the physiological and chemical properties. A more in-depth analysis of the nitrogen content of coal is explored, with an introduction to the nitrogen containing functional groups there within. The formation of NO_X from coal combustion is reviewed, exploring the main routes of formation, Fuel-NO_X, Thermal-NO_X and Prompt-NO_X, with an introduction to short lived intermediary species N_2O and NNH. Photochemical smog is explored, and the processes involved in its formation from NO_X emissions. An exploration into the industrial technologies deployed to reduce the emissions of NO_X from large scale furnaces is presented.

Chapter 4 explains the experimental procedures and processes employed for the analysis of the fuels and the emissions characteristics from the coals and the additives.

Chapter 5 presents and discusses the results from the fuel analysis. The fuel analysis includes the proximate and elemental analysis of the fuels and the additives. Particle size distribution is data is presented and is used later in Chapter 8, modelling. SEM microscopy of the coals and additives are presented here. Further analysis examined the functional groups present in the coals with and without additives by XPS.

Chapter 6 is the presentation of the data from devolatilisation. Devolatilisation and pyrolysis was carried out with low heating rates (LHR) analysis and high heating rate (HHR) techniques. LHR analysis consisted of TGA at heating rates of 10°C/min, to examine the reactivity and kinetics of the coals with and without additives. The HHR analysis was carried out in two drop tube furnaces (DTF): University of Leeds, UK (DTF1) and Northeastern University, Boston, US (DTF2). Chars were produced in DTF1 for the coals with and without additives, for further nitrogen partitioning and char

analysis, including carbon burnout and HHR total volatile yield. Comparative analysis for nitrogen partitioning was carried out using a low nitrogen elemental analyser. Data from this chapter explains the changes in nitrogen emissions from the coals as a result of catalysis from the additives.

Chapter 7 explores the interaction between the coals and the additives during combustion. DTF2 was used for emissions analysis during pyrolysis, char combustion and coal combustion, all analysis was for the coals with and without additives. Emissions analysis consisted of CO_2, CO, NO and NO_2, total NO_X and SO_2. The output data was used to convert to industrial emissions values. Using both image analysis from scanning electron microscope (SEM) and XPS. The SEM is use to explore the effects of devolatilisation on the coal particles with and without additives. This technique was used to investigate the morphology changes of the particles. XPS was used to interpret the changes in nitrogen functional groups within the fuels and the changes to the functional groups as a result of the devolatilisation of the coals when blended with the additives.

Chapter 8. In this chapter, the data from Chapters 5, 6 and 7 is used as input information for modelling. The modelling is divided into three model outputs: a DTF model, a carbon burnout and kinetics model (CBK 8) and a furnace model. The DTF model was used to predict the nitrogen partitioning during devolatilisation within a DTF. The CBK 8 model was used to predict the amount of carbon conversion that takes place within a DTF for both coal burnout and char carbon burnout. The CPD model is refined for the presence of additives and this enables predictions from the furnace model of NO_X reduction due to the presence of additives.

Chapter 9 investigates the data from the experimental work using a biomass, olive cake, and coal PFA as an additive. This was a feasibility study to compare the potential NO_X reduction capabilities of blending coal PFA with biomass. The chapter draws

together information in previous chapters (6 and 7) and introduces some supplementary information to consolidate understanding.

Chapter 10. The final chapter explores the results and summarises the data and draws conclusions. The conclusions are reviewed in a discussion, drawing on information from literature reviews and comparative data.

2.1 Introduction

The first industrial revolution started in Britain in the late 1700's, and quickly spread to Europe and the US through the 1800-1900's. The industrial revolution facilitated the conversion of small-scale cottage industries into large scale production. The advent of the steam engine by Thomas Newcomen in 1712, saw the use of coal on an industrial scale to produce steam. The steam engine was improved by James Watt in the 1770's. The Watt steam engine went on to be used in industry, coal mines, ships and locomotives. Using coke as a fuel instead of charcoal, Abraham Darby designed a more efficient and cheaper method of cast iron production in the late 1700's (Tylecote, R. F.,1992, Rolt and Allen, 1997). In 1878, Lord Armstrong used water from a lake to power a small-scale hydroelectric power station in Cragside, England. (Pevsner, N., Richmond, I., 2002). By 1882, Thomas Edison project, organised by Edward Johnson saw the World's first public coal fired power station built in London. The second industrial revolution (1870-1914), saw the increase in use of fossil fuels for powering industry, transport and increasingly the spread of electricity use in industry and for domestic use (Landes, D.S., 1969). During these periods, the pursuit of technological advancement took precedence, with little knowledge or concern for environmental issues.

2.2.1 Atmospheric pollution

In the atmosphere there are several sources of pollution. Some pollution sources derive from natural processes, including volcanoes, physical and chemical erosion, soil erosion, microbial action, natural fires and lightning. These processes can lead to natural levels of potentially harmful compounds, i.e. SO_2, CO, CO_2, NO_X (NO and NO_2) N_2O O_3 NH_3, volatile organic compounds (VOC) and particulate matter (PM).

Some of these compounds produce secondary pollution products. One example of this is ozone (O_3), which is a major contributor to photochemical smog, particularly around large urban areas. CO_2, N_2O, O_3 and CH_4 are known powerful greenhouse gases (GHG). SO_2, CO, CO_2 and NO_X can form acid compounds and fall as dry acid particles or as acid rain. Normal rainfall has a pH of 5.2-5.6 due to dissolved CO_2. Additional acid gases, particularly NO_X and SO_X result in rain with lower pH, 4.3, which can devastate trees and other plant life, and can result in acidification in water bodies,

2.2.2 Anthropogenic pollutions

Anthropogenic processes can produce large quantities of emissions and can increase the natural levels of harmful compounds to untenable levels. Industrial processes such as combustion plants, fuels and fuel processing, agriculture, mining, transport and product manufacture can be significant contributors to elevated levels of SO_2, CO, CO_2, CH_4, NO_X, N_2O, O_3, NH_3 and PM. As with natural processes, see section 2.2.1, CO_2, N_2O, CH_4, and O_3, are powerful GHG and can be major contributors to man-made global warming. Because of its long atmospheric lifetime (~121 years), N_2O on the Global Warming Potential (GWP_{100}), is approximately 298 times more powerful than CO_2 as a GHG. (Myhre, 2013)

Secondary pollution effects can also be found in anthropogenic emissions. SO_2, NO_2, CO and CO_2 from man-made processes can form acid rain, see Section 3.5.2. Anthropogenic induced acid rain can be more strongly acidic, with values as low as pH 4.3. Acid rain can cause severe damage to flora and fauna. Figure 2.1 is a forest in Czechoslovakian Republic that has been damaged by acid rain.

Figure 2.1 Effects of acid rain on forestry in Jizera Mountains, Czech Republic (Lovecz, 2006)

2.2.3.1 NO_X emissions

Whilst GHG emissions and climate change are the highest priority for emissions control, the emissions of NO_X, are of significant importance and as such, also subject to stringent regulations, see Section 2.6. From 1990-2016, NO_X emissions in the EU fell by more than 50%, from 18.1 to 7.6 million tonnes (Eurostat, 2018), see Section 2.8. There are natural sources of NO_X, atmospheric and biogenic. Atmospheric sources are derived from lightning, where the increased levels of heat ionise the N_2 and O_2 in the air to form NO, see Section 2.2.1. Biogenic source predominantly comes from plants, where they fix nitrogen from the soil and emit oxides of nitrogen. Soil based nitrogen compounds are readily converted to N_2O. (Skiba, 2006). The two largest sources of anthropogenic NO_X in Europe are from vehicle exhausts and from combustion power production with distribution, at 50% and 25% respectively. Figure 2.2 shows the NO_X emissions from source in the EU. The fitting of catalytic converters to road vehicles has been the main reduction strategy for the reduction of NO_X from vehicle exhausts. Within the power industry, NO_X reductions have been realised through the implementation of Low-NO_X burners, other firing strategies and flue gases abatement technologies (SCR/SNCR). The conversion of some facilities from solid

fuels to gas has also yielded reductions in NO_X emissions from power production. (Eurostat, 2018).

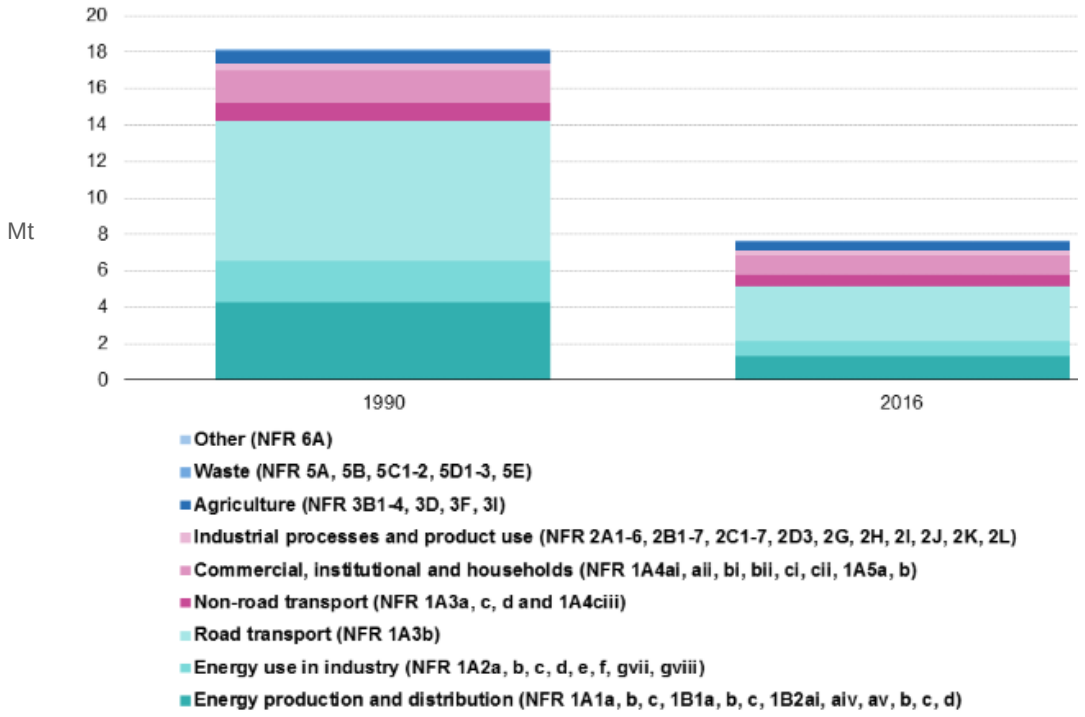

Figure 2.2 NO_X emissions by source sector across the EU-28 from 1990 to 2016 (Eurostat, 2018)

2.2.3.2 What's wrong with NO_X emissions/Global /EU emissions?

NO_X is the combination of two oxides of nitrogen NO and NO_2. NO_X can be harmful to fauna and flora in gas form and to human health in gaseous form. NO_2 at levels of 40 µg m^{-3} annual mean and a 1 hour maximum exposure limit of 200 µg m^{-3}, have been recommended by the World Health Organisation (WHO) (WHO, 2006). The exposure limits are expressed in the form of NO_2. NO does not have specified limits as it tends to oxidise in the atmosphere to NO_2 within minutes of emission from source (WHO, 2006). NO_X emissions can also result in secondary pollution effects. NO and NO_2 can act as a nucleus for the formation of aerosols, i.e. particulate matter (PM), $PM_{2.5}$ and PM_{10}, which are harmful to human and animal health. NO_X and $PM_{2.5}$ are known to cause disorders in the lungs. NO, is a known source of tropospheric ozone (O_3), when it reacts with O_2 in the atmosphere in the presence of sunlight. Whilst ozone in the

stratosphere helps to protect life from harmful UV radiation, in the troposphere it is harmful to life. O_3 is poisonous as a gas and can be a precursor for the formation of photochemical smog, see Section 3.5.1, NO_X gases can also contribute to nitrogen enrichment in water, through nitrate deposition and result in eutrophication. It is estimated that between 12-44% of water nitrification comes from atmospheric nitrogen (NSCEP, 1997). Eutrophication of the water course can lead to increases in algae blooms. Increased algae blooms can seriously diminish the oxygen content in the water leading to the death of other plants and animals. The increase in decomposing matter creates a hypoxic water layer near the bottom of the water column, making the region uninhabitable.

2.3 Power production

Across the globe electrical power production reached approximately 26 700 TWh in 2018, (IEA, 2019). The main producers of electrical power are predominantly the countries with larger populations. Developed countries tend to have higher levels of electrical power production per capita. China and the US are the largest producer of electricity, accounting for nearly 70% of Global electricity produced (Enerdata, 2019).

Coal still has the major share in power production accounting for approximately 26% of global power production (power production includes all primary energy demands, including industrial processes and domestic heating, etc). Within the electrical power generation, coal still accounts for 38% globally (IEA, 2019). Despite showing a reduction in the global share from 41% down to 38% from 2017-2018. Coal power production still accounted for 26% of the increases in electrical power production in 2018. The main area for the increase was in countries such as China, India, Pakistan and Indonesia (IEA, 2019). These increases in Asia far outweighed the reductions in Europe, the US and Japan.

2.4 Alternate energy sources to coal

In Europe, the use of coal for electrical power generation has started to decrease, and has dropped to 669 TWh in 2017, Figure 2.3, whilst renewables have seen an increase up to 679TWh. Biomass for electricity production has increased its share in the EU reaching 196 TWh, (Sandbag, 2018) Figure 2.4.

Hard coal has seen its share of electricity generation drop to 357 TWh, whilst lignite has maintained its levels at 312 TWh (Sandbag, 2018). Whilst EU countries are running their hard coal fired power plants down, lignite plants in Poland, Germany, Greece and the Czech Republic are maintaining their reliance on lignite, as illustrated in Figures 2.3 and Figure 2.4.

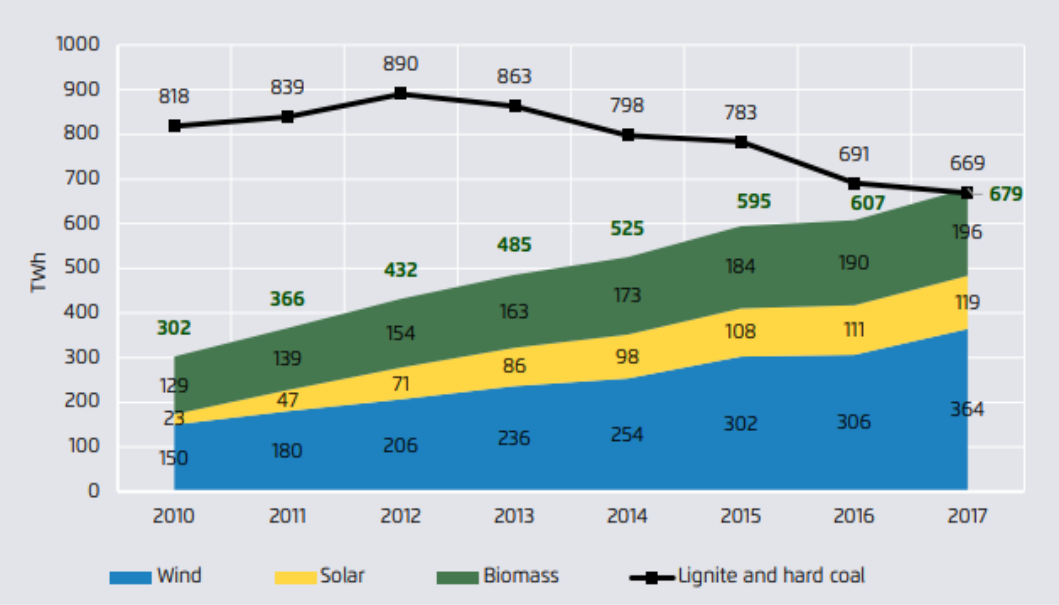

Figure 2.3 Comparison of fuel sources in the EU. (Sandbag, 2018)

There is continued emergence of alternate and renewable primary power sources for the production of energy. Several sources have developed, including solar, wind, nuclear, tidal and the use of biomass in converted coal combustion plants. The increased use of biomass in converted coal fired power plants has led to the development of fuel flexible power stations. Figure 2.3 shows that while the increase is still slow, the alternate sources of electricity and heat generation are starting to grow.

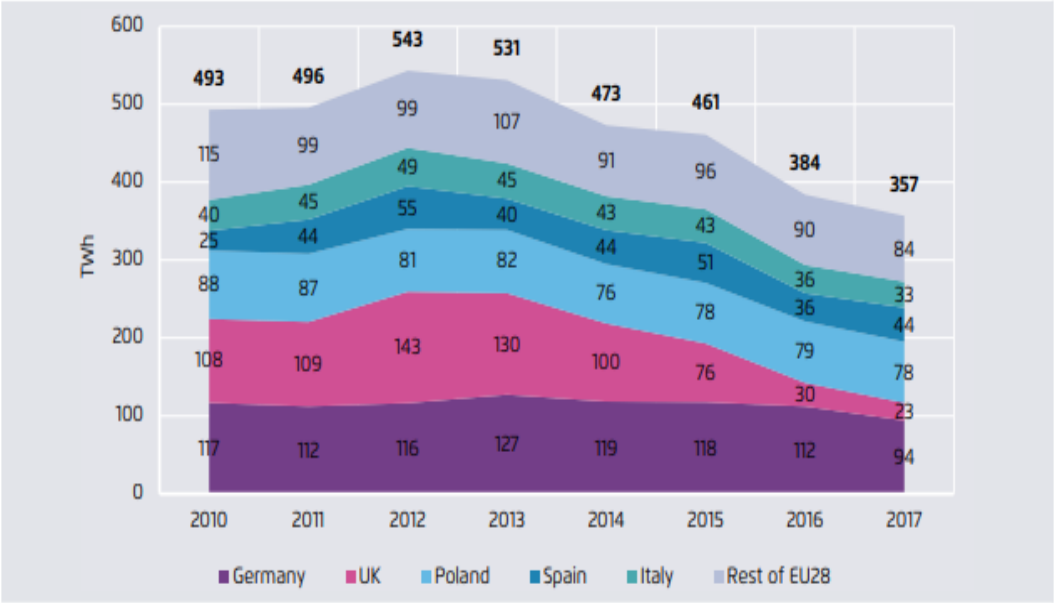

Figure 2.4 The gradual decline of hard coal for power production in the EU (Sandbag, 2018)

When grown sustainably, the use of biomass in combustion power plants can have a large carbon reduction effect on GHG emissions (Sami et al., 2000). The emissions of other gases, SO_2 and NO_X however are more dependent on the type of biomass, the growing environment and control technologies. Some biomass types are higher in fuel nitrogen, and so can be higher emitters of NO_X than coal during combustion, see Section 3.4.2.

2.5 Emissions from combustion plants

Large scale combustion plants are considered to be high pollution areas. Combustion plants are generally designed to run on specific fuel sources, i.e. oil, gas, biomass and coal. From coal combustion gaseous emissions of concern, include CO, CO_2, SO_X and NO_X. In large and uncontrolled quantities these can be harmful to human, fauna and flora. In response to regulations, Section 2.6, there are many control measures that are employed within coal fired power plants. Of particular interest are the measures incorporated to control NO_X, Figure 2.5, shows an overview of emissions from combustion and the control measures.

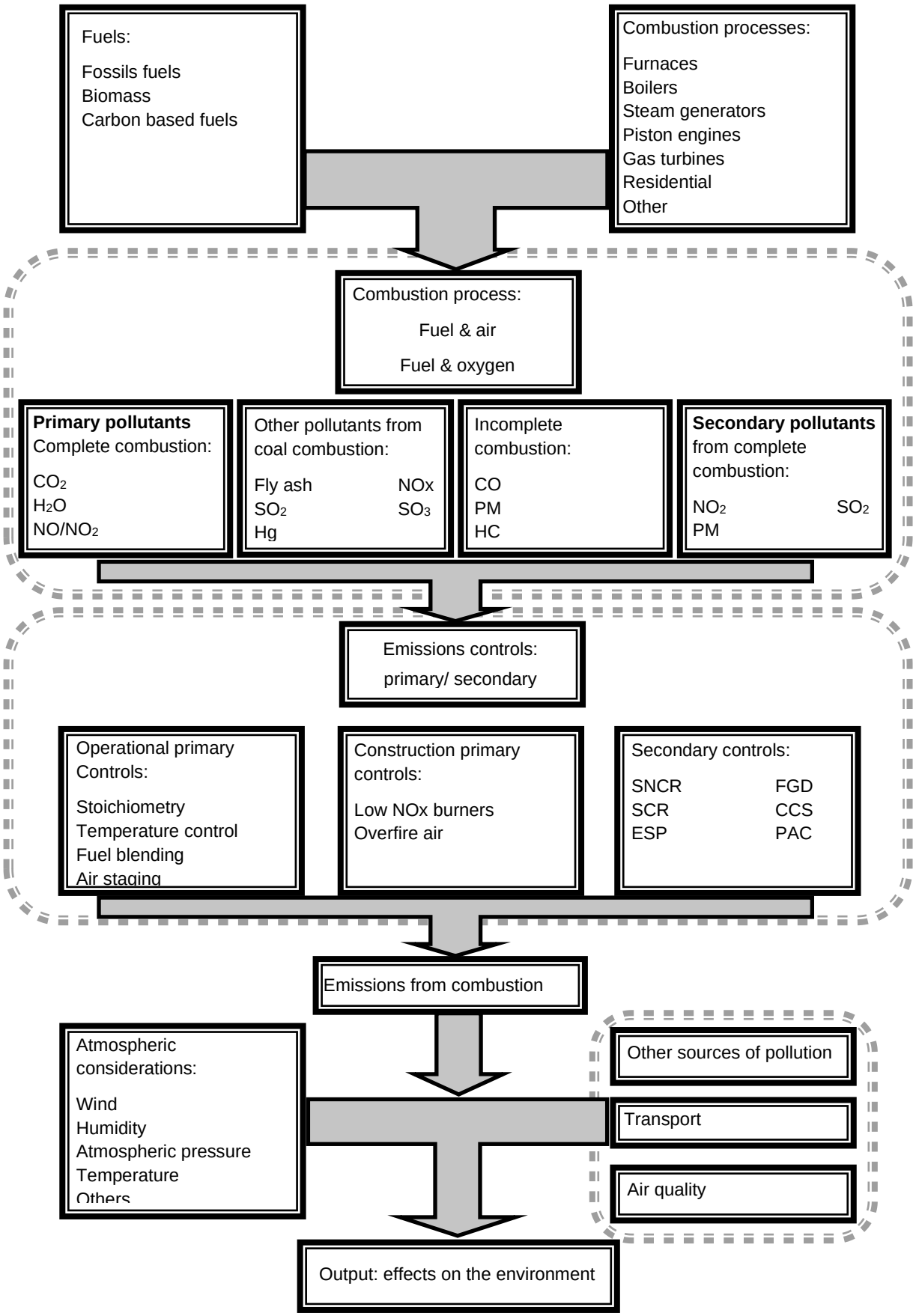

Figure 2.5 Emissions from combustion processes, adapted from (Popescu, 2010)

There are a range of technical solutions utilised, within the power production industry to combat the emissions of NO_X, see Section 2.8. Figure 2.5 shows an overview of the combustion processes that can lead to certain types of emissions from anthropogenic activity. This figure only covers some of the larger production emissions of concern, and does not include items such as VOC, polycyclic aromatic hydrocarbons (PAH), furans or dioxins.

Figure 2.5 only show the pollutants from direct emissions, these do not take into account the secondary pollutants. The secondary pollutants include O_3, particulate matter PM_{10} and $PM_{2.5}$ and photochemical smog. The secondary pollutants can form as a by-product of the direct emissions after leaving the stack. Emissions controls are covered in more detail in Section 2.8 and in Section 3.6.

2.6 UK and European regulations

The Clean Air Act was originally established in 1956, in response to the levels of smoke and smog in larger cities in the UK. The aim of the act was to decrease the quantities of dark smoke from industrial chimneys. Over the following years, the Clean Air Act has been improved up to the amendment in 1993 and culminating in the Clean Air Bill 2017-19.

In May 2018, Department for Environment, Food & Rural Affairs (Defra) launched the UK Clean Air Strategy (CAS). The CAS was established to set out strategies to combat the emissions of a range of air pollutants, $PM_{2.5}$, NH_3, NO_X, SO_2 and O_3.

Across the EU, there have been more directives implemented.

- National Emissions Ceiling Directive (2016/2284/EU) (NECD). The NECD came into effect in December 2016. The 2016 update superseded previous versions and sets targets for future emissions with respect to emissions levels in 2005 as a baseline. The NO_X emissions has been set from 2020 to be 59% (711kt) of

the 2005 figures, and from 2030, 41% (494kt) of 2005 values. (EU, 2016; EEA, 2010)

- Large Construction Plant Directive (LCPD, 2001/80/EC). With ever more stringent regulations on the permissible levels of emissions from power production, improved technologies were needed to reduce the emissions to comply with the LCPD regulations. The LCPD set standards across the European Union, limiting flue gas emissions from combustion plants with a thermal capacity of 50 MW_{th} or greater. It was principally aimed at fossil fuel combustion plants, i.e. power stations, steel works, petroleum works and refineries. The directive aimed to curb the emissions of nitrogen oxides, oxides of sulphur and dust (EU, 2001).

- Industrial Emissions Directive (2010/75/EU) (IED). The LCPD has subsequently been superseded by the IED at the start of 2016. This has set NO_X limits of as low as 200 mg/Nm^3 for power plants >300 MW_{th} from 2020. Under the IED, a new set of targets are to be implemented of 150 mg/Nm^3 for NO_X, using the Best Available Technology Reference Document for Large Combustion Plants (BAT). The cost of implementation of the BAT for emissions reduction has been instrumental in some power station operators electing to cease operations.(EU, 2010) (EU, 2017).

NO_X emission across the UK have shown significant reductions from 1970 through to 2017. Figure 2.6 shows how the NO_X emissions have reduced in the attempt to comply with NECD targets. The NECD and Gothenburg targets for 2020 and onwards are yet to be realised.

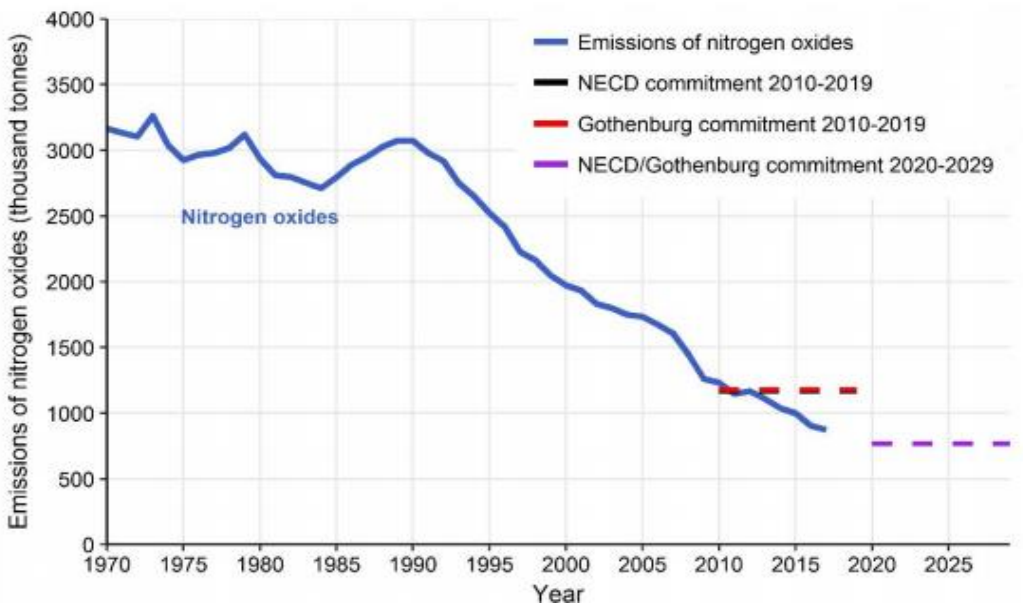

Figure 2.6 Annual NO_X emissions for the UK from 1970-2017, and the targets to be achieved set by the NECD. (Defra, 2019)

Figure 2.7 shows the national NO_X emissions from the major contributors from 1990-2017. Road transport is the largest contributor, with the energy industries as the second largest NO_X emissions. These figures can be compared to the EU figures shown in Figure 2.2, Section 2.2.3.1. The UK figures, as percentage of the total NO_X emissions by sector shows the same trend as the EU figures with road transport being the greatest contributor, followed by the energy industries.

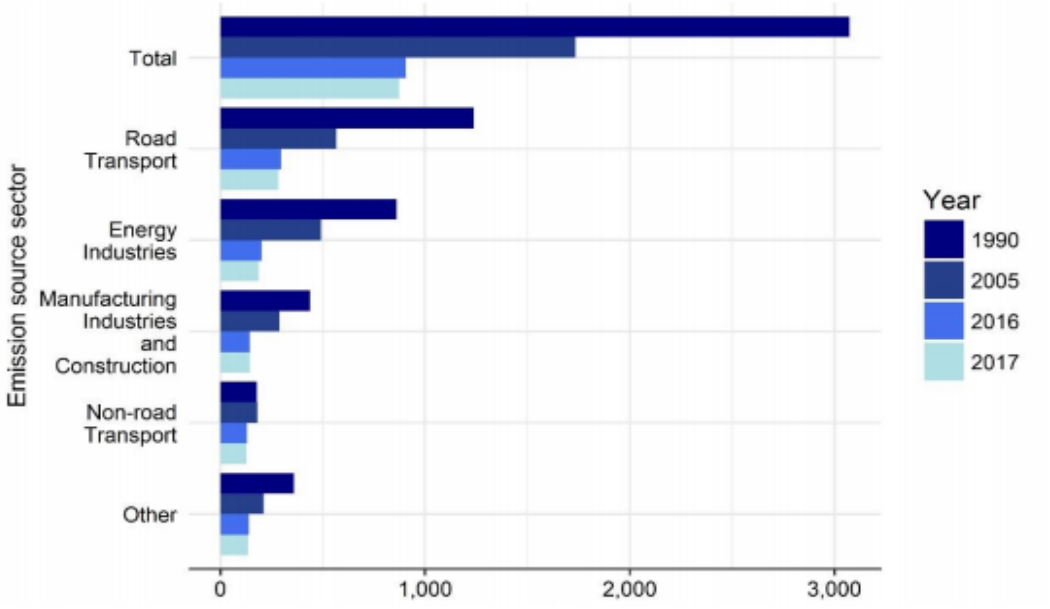

Figure 2.7 Emissions of NO_X by contributors in the UK from 1990 through to 2017 (thousand tonnes) (Defra, 2019)

Table 2.1 shows a comparison between the EU, the United States and China for NO_X emissions standards. The standards shown for the US and China are already in place.

Table 2.1 Emissions standards for power plants operating at > 300 MW_{th} (Wynn, 2017)

		Emissions standards mg Nm^{-3}		
		Europe (BAT)	United States	China
NO_X	New plant	85	117	100
	Existing plant	150-175	117-160	100-200

Note: to achieve the emissions targets set, the use of post combustion technologies will be essential for new and existing power stations.

2.7.1 Future of coal (Globally)

Across the globe there is a range of coals used for power production, including lignite, bituminous, sub-bituminous and anthracites. The choice of coals used for power production is primarily a commercial decision and dependent on the fuels available either locally or cost effectively.

China has coal fired power production of approximately 965 GW, with power stations currently under construction providing 128 GW, and future plans to build a further 70 GW's. (Evans, 2019) With the expansion of the Chinese power plant building, there are proposals to build over 200 coal fired power plants in countries ranging from Egypt to Indonesia (Evans, 2019).

Within the EU, electricity is produced from the combustion of hard coals (bituminous, sub-bituminous and steam coals) and from lignite.

Within the US there have been reductions in the use of coal for power production, with some US states declaring they are to go coal free. (eia, 2019) Oregon has voted to stop producing electrical power from coal by 2035. California was only operating one coal fired power station as of 2017, and it only provides 0.2% of the energy demands of

the state. New Mexico, the US state most dependant on coal for power production has declared it intends to be carbon free by 2045 (Irwin, 2016; eia, 2018).

2.7.2 Future of coal in the EU/UK

Across the EU, there is a trend to remove coal fired power stations in several countries, including the UK. Many of these closures are necessary to bring electricity production into compliance with the LCPD and IED. Figure 2.8 shows the countries that are scheduled to phase out coal, those under deliberation and the countries with no plans to phase out coal, as of June 2020. Whilst the power plants operating on hard coals are systematically being closed, many of the lignite coal fired plants are not scheduled for closure (Sandbag, 2018).

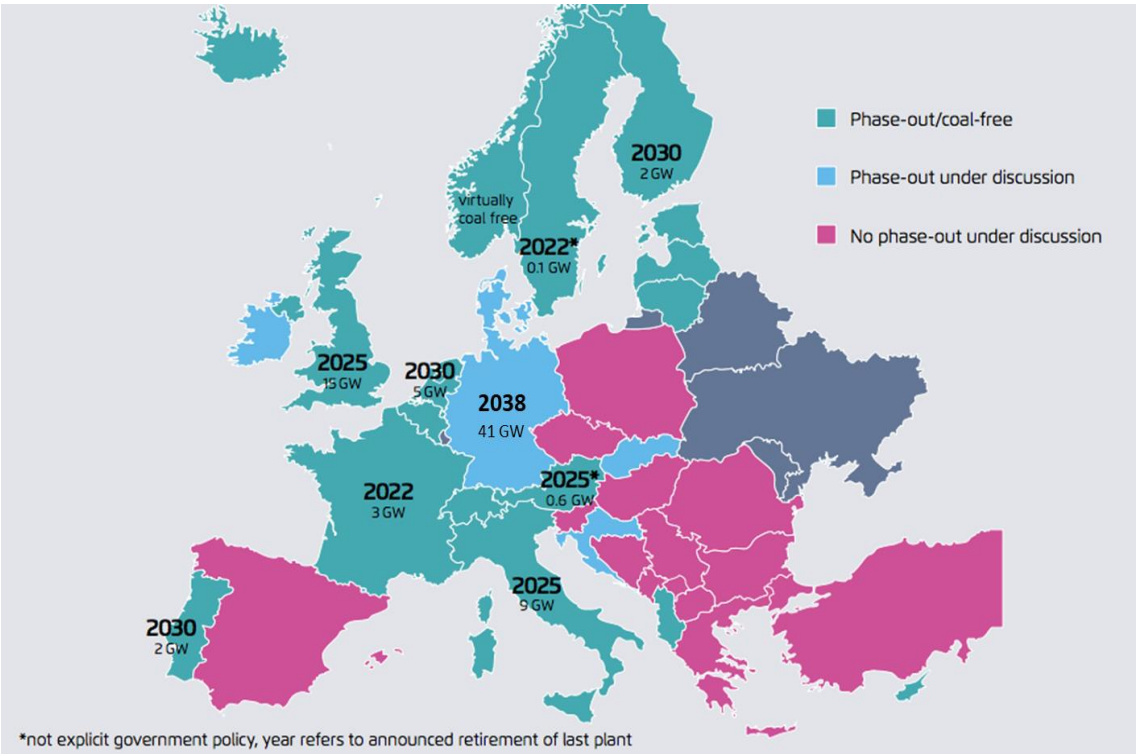

Figure 2.8 Proposed cessation of coal fired power stations across the EU. Adapted from (Sandbag, 2018)
Note: The closures stated are not governmental proposals but declarations of retirements of the last coal plant operation date.

Across the UK, eight legacy coal fired power station have elected to close in response to the emissions targets set under the IED, as the cost of implementation of control

technologies would not be financially viable. Table 2.2 shows the coal fired power plants currently in operation and their future with respect to the future emissions directives (PowerstationsUK, 2019).

Table 2.2 Coal power stations currently in operation or under conversion to biomass in the UK, adapted from (PowerstationsUK, 2019)

NAME	LOCATION	STATUS	CAPACITY	AGE
Aberthaw B	Vale of Glamorgan	Running reduced hours to comply with emissions limits.	1,586 MW	48 Years
Found to be emitting illegal levels of air pollution in September 2016 and has been running reduced hours in order to comply with emissions limits.				
Cottam	Nottinghamshire	Decommissioned September 2019.	2,008 MW	50 Years
Drax (Units 5-6)	North Yorkshire	Plans to convert further units to gas.	1,290 MW (coal) (3,885 MW total)	33 Years
Drax has been working on their move away from coal for some time now. 4 of the 6 units have been converted to fire Biomass, the first in 2013 and the most recent in 2018. Plans are in the pipeline to convert the remaining two units to gas as part of a larger expansion project.				
Fiddlers Ferry	Cheshire	Closed 31 March 2020.	1,961 MW	48 Years
One unit closed on March 2019, leaving a total capacity of 1,510 MW. In March 2020 SSE announced the power station has closed.				
Lynemouth	Northumberland	Converted to biomass	420MW	47 Years
Kilroot	County Antrim	May 2018. Contract extended by 12 months.	520 MW	38 Years
Kilroot and the nearby oil-fired Ballylumford power stations were sold to the Czech firm EPH in April 2019. They have both faced closure over the last few years.				
Ratcliffe	Nottinghamshire	No plans to close.	2,000 MW	51 Years
Ratcliffe is fully compliant with current emissions regulations.				
West Burton	Nottinghamshire	No plans to close.	2,012 MW	51 Years
Uskmouth	Gwent	Conversion to Biomass and waste ongoing	220MW	60 Years

2.8 Strategies for NO_X reduction

To comply with past and future NO_X emissions regulations limits, operators of combustion plants need to deploy emissions control technologies. Within a combustion chamber, there are four principle methods where NO_X is produced.

- Prompt NO_X
- Thermal NO_X
- N_2O mechanism
- Fuel NO_X

Prompt NO_X is the result of molecular nitrogen from the air being reduced by fuel radicals to N and NH radicals and HCN in a fuel rich environment and then subsequently oxidised to NO.

Thermal NO_X is produced at temperatures in excess of 1373 K and is the result of molar nitrogen and oxygen in the air reacting at higher temperatures.

The N_2O mechanism is an intermediary process, originally proposed by Malte, (Malte and Pratt, 1975) that tend to dominate at lower combustion temperature of ≤1800K. It is an accepted process mechanism for the formation of NO_X during combustion. Later works have suggested a temperature range of 300-1900 K (Klippenstein et al., 2011).

Fuel NO_X can account for in excess of 75% of all NO_X produced during combustion. (Mitchell, 1998). It is the result of oxidisation of the fuel nitrogen, released initially as mainly HCN, ammonia or tar-N, see Section 3.4.2. There is a further method of NO_X formation, the NNH mechanism. The NNH mechanism has an intermediary function so is not a principle target for NO_X production. See section 3.4.3. To combat the NO_X emissions from combustion power plants, a range of technologies have been deployed. These can be separated into primary reduction and secondary reduction technologies.

Primary reduction technologies include:

- Low NO_X/ultra-low NO_X burners

- Fuel staging
- Air staging

These technologies are designed to target some of the design characteristics shown in Table 2.3.

Table 2.3 shows the primary reduction processes and technologies incorporated within pulverised coal furnaces. The primary technologies are designed to focus on the fuel characteristics, the combustion processes and the designs of combustion chambers to reduce emissions.

Table 2.3 Primary reduction processes used in industry to control the emissions from pulverised coal combustion, in particular NO_x. (Van der Kooj, 1997)

Design characteristics within a pulverised coal combustion furnace to control NO_x	
Boiler Design	Boiler Type- i.e. wall fired, tangential Capacity Burner type, low NO or conventional Number and type of burners Residence time Burning zones Advanced overfire ports Flue/Exhaust Gas Recirculation
Operation	Burner operation-swirl, air ratio (primary to secondary) Air levels (stoichiometry) Burner angles Milling operations Load
Coal Properties	Chemical Breakdown- C:H and O:H ratios, N content, ash content Calorific value (CV) Volatility Volatile release Moisture

Secondary technologies include selective catalytic reduction (SCR) and selective non-catalytic reduction (SNCR) and flue gas recirculation (FGR). Secondary NO_X reduction technologies focus on the effluent gases after they have left the furnace, see Section 3.6.8.

2.9 Chapter summary

NO_X within the atmosphere is harmful to fauna and flora. NO_X has been linked to lung disorders and can lead to acid rain and eutrophication of waterways. NO_X can form through natural processes such as ionization of the air during lighting and thunderstorms. Anthropogenic sources, such as furnaces and transport contribute more significantly to atmospheric NO_X than natural processes (Eurostat, 2018; Schumann, 2007). Large scale power plants are a major source of a range of emissions, including NO_X. Through combustion, NO_X has three main formation routes, prompt and thermal NO_X, which both form from the nitrogen and oxygen in the air, and fuel NO_X, where the nitrogen comes from the fuel. To reduce the emissions of NO_X (and other pollutants), regulations have been implemented to curtail their release into the atmosphere. The most recent regulations in the EU has resulted in the IED, with the intent of large-scale combustion reducing the NO_X emissions to ≥ 150 mg Nm^{-3} by 2021.

In response to ever more stringent regulations, several types of technology have been developed to control NO_X emissions, including Low NO_X burners, furnace operating conditions and secondary control measures such as SCR and SNCR.

Page intentionally blank

Chapter 3-Literature review

3.1 Coal formation

Coal is a metamorphosed sedimentary rock found around the globe. Figure 3.1 shows the distribution of known coal fields around the planet. The oldest economically extractable coals are no more than ~330M years old, and as such formed during the carboniferous era, Figure 3.2.

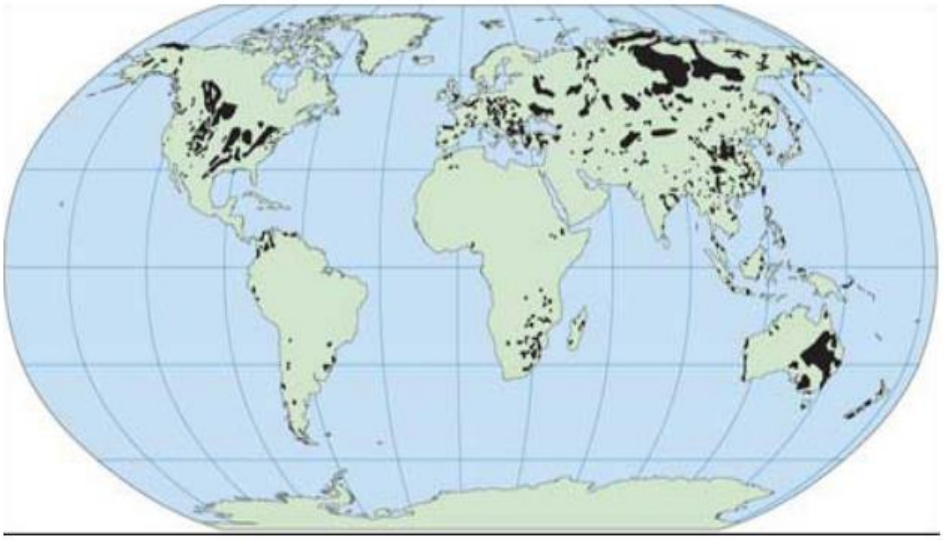

Figure 3.1 Known coal distribution around the globe. (Thomas, 2002)

Prior to this time, there was insufficient carbonaceous plant matter to form substantial coal beds. As plant material dies, it falls the ground. If this is in an anoxic environment, i.e. a swamp, peat bogs or in brackish waters at coastal lagoons, then the material is unlikely to go through decomposition. As further biogenic material is layered on top, the lower levels of material is preserved. If there is no erosion of the laid down biogenic material, it is likely to become buried by sediment. As the layer of plant material becomes buried deeper it is subject to compression and heat. Within this environment, the original plant material compresses by about 90% (Veriskovsky, 1956; Thomas, 2002). As coal is formed from biogenic and mineral matter, it is heterogeneous in nature. Coal is the product of compression, heat and time, therefore there are no coals

younger than 2-3M years old. Carbonaceous sedimentation that fall within 2-3M years old are more likely of peat class than a low-grade coal, see section 3.2.

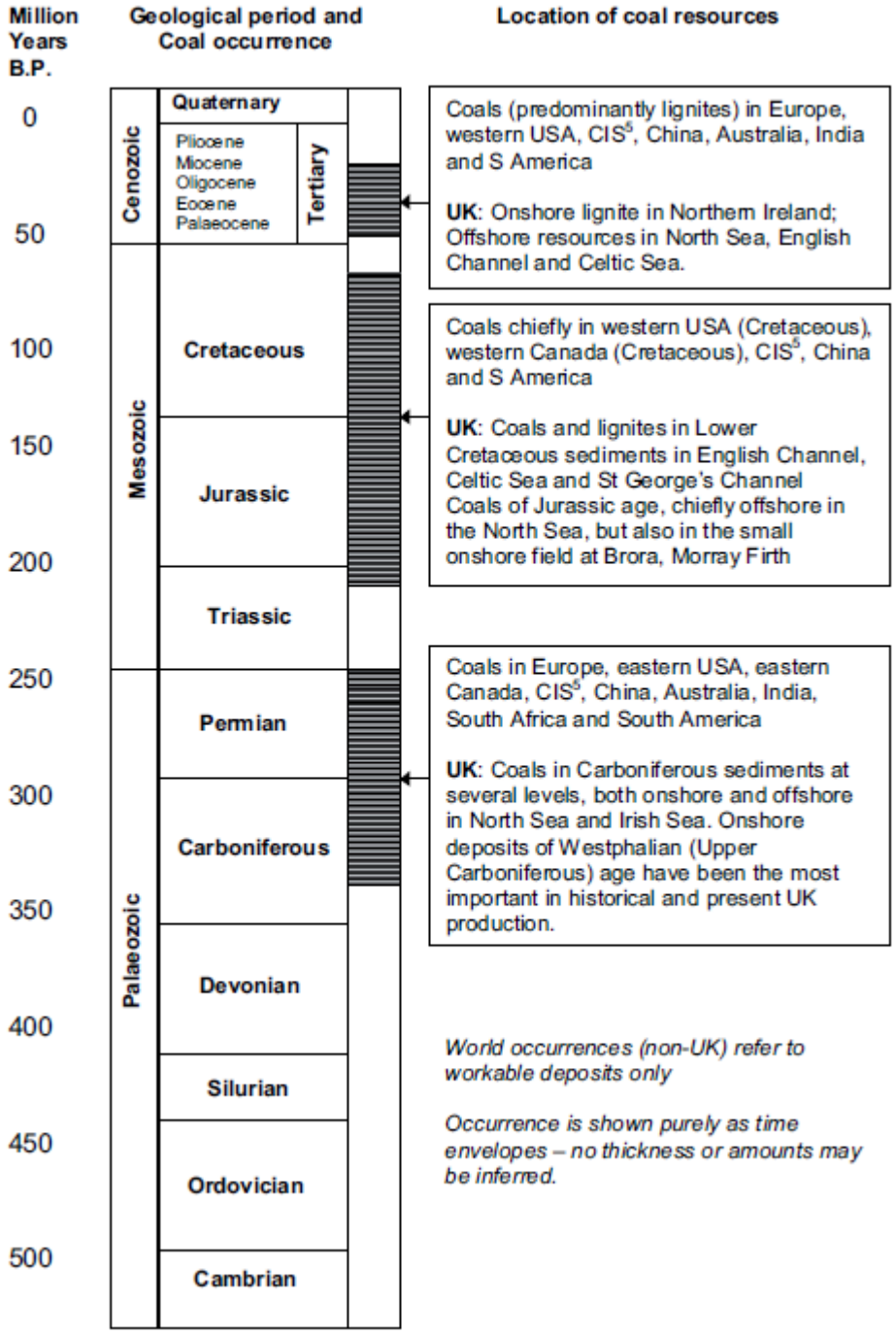

Figure 3.2 Profile of coal formations with respect to geological eras from the perspective of UK coals. (Kendall, 2010)

Coals seams can be as thin as a few millimetres up to 30m in thickness. As coal forms from biogenic material, generally in rain forests and swamps, there can be an in-wash

of biogenic material and mineral matter from other sources. The mixing of plant materials and sediments can lead to wide variations in the elemental composition of the sedimentation. In turn this variation will lead to compositional variations not only in a coal fields, but also from one coal seam to another.

There is a large area of coal bearing rocks under the Amazon basin. The coal bearing reserves are deeply buried beneath younger sedimentary rocks. The size of the reserve is not clearly known, however due to the complex geological nature of the environment, it is unlikely to be commercially exploited.

3.2 Coal rank and grade

As coal forms under differing conditions and different environments, there are several ranks and grade of coals. Whilst there are several systems for classifying coals, there is a consensus that they start from the lowest grade of lignite through to anthracite. Peat is the lowest grade having the lowest percentage value of carbon, but many of the classifications do not consider peat as a coal. Graphite has the highest carbon content, but is also not given a coal classification. Table 3.1 shows an adaptation of the ASTM 388-12 classification.

Table 3.1 Classification of coals based on the ASTM 388-12 ranking (ASTM; ASTM, 2012)

Coal classification by rank based on ASTM 0388-12				
Coal Rank		Volatile content % dmmf	Fixed carbon % dmmf	Gross calorific value MJ/kg
Anthracite	Meta-anthracite	<2	≥99	
	Anthracite	2 to 9	92 to 99	
	Semi-anthracite	9 to14	86 to 92	
Bituminous	Low Volatile	14 to 22	79 to 86	
	Medium volatile	22 to 31	69 to 79	
	High volatile A	>31	<69	>32.54
	High volatile B	>31	<69	30.23 to 32.54
	High volatile C	>31	<69	26.74 to 30.23
Sub-bituminous	A			24.42 to 26.74
	B			22.09 to 24.42
	C			19.30 to 22.09
Lignite	A			14.65 to 19.30
	B			<14.65

Note: dmmf = dry mineral matter free

Hilts Law is considered the fundamental rule of coal formation, whereby the grade of coals is consistent with the time/compaction of the original plant material (Skinner, 1976). The longer the time and greater the compaction, the higher the grade of coal is likely to be produced. With increased depth temperature rises, with temperatures rising 30°C per km of depth (Francis, 1954). The rise in temperature can be significantly increased in areas of igneous activity. Increases in pressure (at depth) may have a detrimental effect on coalification, if it restricts the escape of methane and other volatile materials (Skinner, 1976). There is still a dependency on the original plant material and the initial environment for the accumulation and sedimentation. Figure 3.3 shows that as there is greater compression, so the oxygen content (% wt) decreases as the carbon content increases.

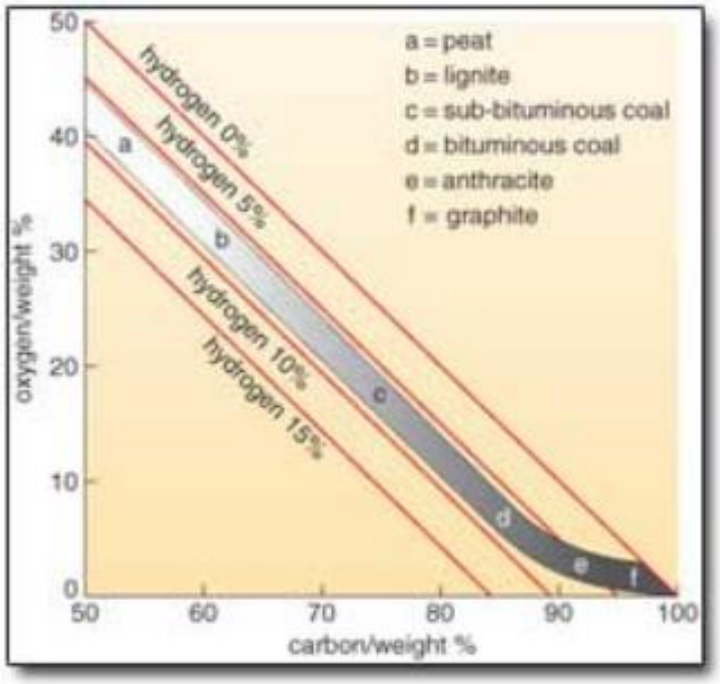

Figure 3.3 Relationship between coal rank/ grade, with comparison of carbon to oxygen content (Skinner, 1976)

From Figures 3.2 and 3.3 an assumption can be drawn that the coals from the Tertiary era will be of lower grade than those from the carboniferous geological period. As coal goes through greater time, compression and metamorphosis, anthracite is likely to form, especially under geological plate boundary conditions, where high pressure and

temperatures are achieved. Coals from the Tertiary era have had insufficient time to form high grade coals (Skinner, 1976; Thomas, 2002).

3.3.1 Nitrogen in coal

The nitrogen content within coals can show great variation not only from coal type, but also within a mine area. The nitrogen within the fuels can also take different chemical forms, pyrrole, pyridine, pyridinic and quaternary. The nitrogen in coal generally forms hexycyclic bonds in the aromatic matrix and heteroaromatic compounds.

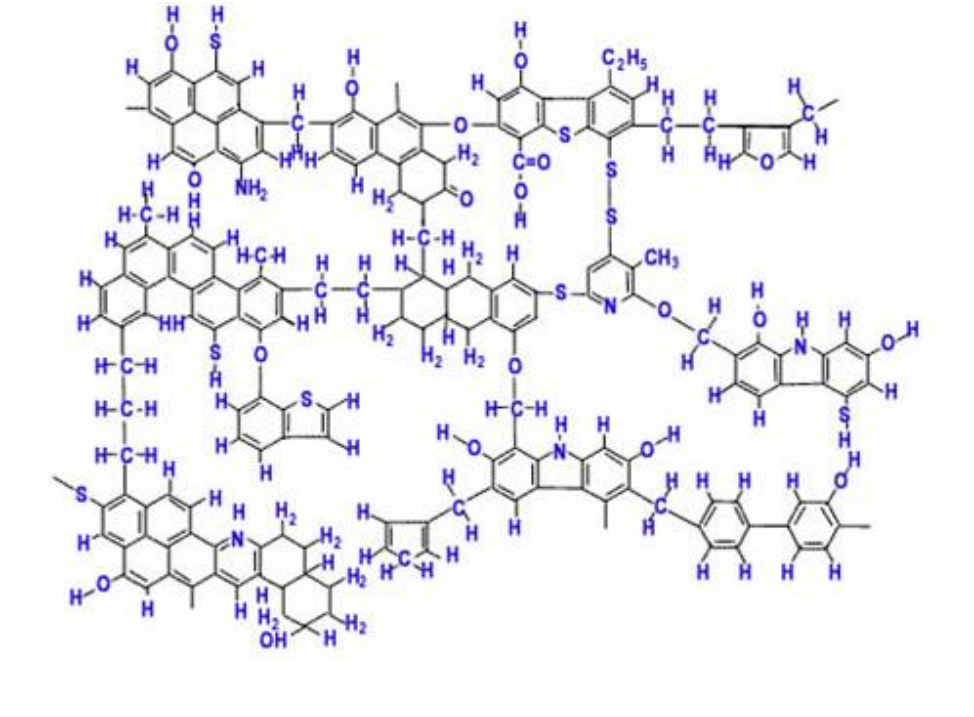

Figure 3.4 Representation of the 2-D structure of bituminous coal, based on the Wiser model (Wiser, 1975; WOU, 2006)

As the rank of a coal increases, so the structure changes and the carbon content increases. With the increase in carbon content, the nitrogen locked into the coal lattice tends to show a relative decrease.(Nelson, 1992b; Nelson et al., 1990). Figure 3.4 shows a 2-D representation of the structure of a bituminous coal. Within the lattice of the coal, the elemental structure of the CHNO is shown, it does not include other

elements, but can be useful tools for predicting how the chemical structures breakdown under heating conditions.

3.3.2 Pyrrolic Pyridine/ Pyridinic/ Quaternary nitrogen

Coal is a complex heterogeneous structure; the carbon content tends to form aromatic and heteroaromatic compounds. The nitrogen content forms some distinct functional chemical groups with the carbon complexes; pyrrolic, pyridinic and quaternary groups. Figure 3.4 shows the nitrogen in hexicyclic and 5-membered heterocyclic formations with the carbon atoms. These groups can be divided into the following: pyridine group has N-6 formations, the pyrrole group has an N-5 formation and quaternary is constructed of N-4 formations. The fourth bond in the quaternary structure is often associated with a hydroxyl or oxygen in an intra or intermolecular formation (Nelson, 1992a; Davidson, 1994). Figure 3.5 shows the structures of the functional groups and their electron volts (eV) binding energies. The binding energies are used in X-ray photoelectron spectroscopy (XPS) analysis, see section 4.11. Although there are other nitro-complex functional groups, pyridine, pyrrole and quaternary are the main sources of nitrogen in coal, with pyrrole containing between 50-80% of the nitrogen content across all coal ranks (Deng, 2008; Gong, 1999; Kambara et al., 1994; Liu, 2001; Woitowicz et al., 1995)

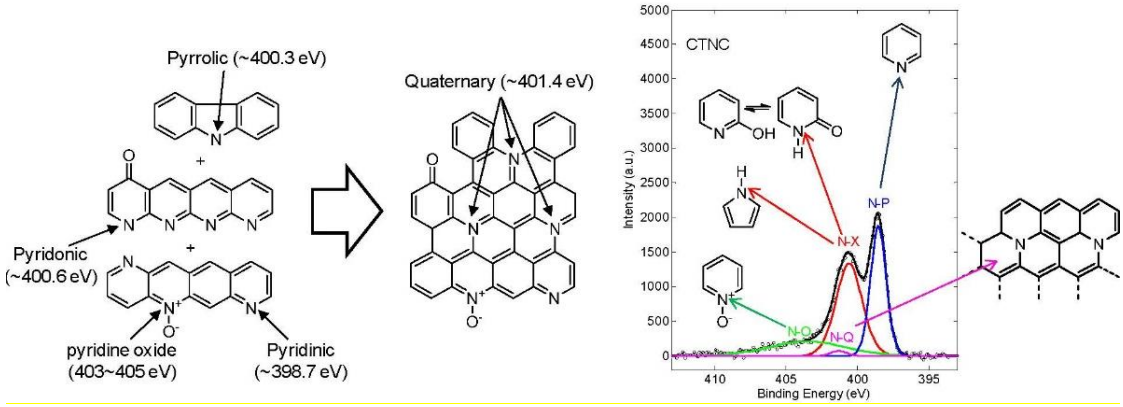

Figure 3.5 The degradation of pyrrolic and pyridine nitrogen to form quaternary nitrogen compounds. (Pels, 1995b)

When the coal is subjected to thermal degradation, initially the aromatic clusters separate and the aliphatic groups are liberated, but the fuel nitrogen (Fuel-N) are retained in their functional groups. As the temperature increases, the functional groups begin to degrade. The nitrogen contained in the functional groups becomes the principle source of fuel NO_X as the coal is subject to thermal degradation. Different coals contain different percentages of the nitrogen functional groups, as such, the fuel NO_X released under the same combustion conditions will differ dependant on the functional groups. (Ji, 2009; Johnsson, 1994; Liu, 2001; Taniguchi, 2010; Watanabe, 2011; Zhao, 2004), The NO_X emissions are not solely limited by the percentage of the functional groups. Whilst the functional groups are linked to the carbon content of the coal, the functional groups will be different in different ranks of coals. There is a relationship between the emissions levels and the functional groups. Therefore, the formation of fuel NO is dependent on; coal grade and functional groups. (Kambara et al., 1994). As coal rank increases, so the carbon content increases. With the increase in carbon, the nitrogen percentage content has a tendency to decrease. The decrease is mainly felt in the pyridine and quaternary functional groups and less so in pyrrole. There has been conflicting work with respect to the functional groups nitrogen content when compared to carbon content of coal. Kambara showed with increases in carbon content, pyridinic and quaternary nitrogen contents decreased, while the proportional nitrogen content of pyrrole increased (Kambara et al., 1994). Keleman, Woltowics and Nelson (in separate works) showed that as the carbon content increased, the quaternary nitrogen decreased across all three results. The pyridinic nitrogen increased across all three sets of results, however while Keleman indicated a slight increase in pyrrolic nitrogen Nelson and Wojtowics indicated modest reductions in pyrrolic nitrogen (Nelson, 1992b; Kelemen S. R., 1994). All four sets of data showed that the main nitrogen bearing functional group for all of the coals was pyrrolic (Davidson, 1994), "*More pyrrole than pyridine in coal lead to high yields of fuel-NO_x"* (Zhang et al., 2015).

3.4.1 NO_X formation

Despite many studies into NO_X formation through combustion, the complete mechanism of fuel-N evolution to NO_X is still not fully understood, (Glarborg, 2003; Klippenstein et al., 2011; Niksa, 1996a; Liu, 2019; Glarborg et al., 2018). There are three principle routes to the formation of NO_X during the combustion of coal: fuel-NO_X, prompt-NO_X and thermal NO_X. Fuel NO_X is responsible for between 75-95% of all NO produced during the combustion of coal (Mitchell, 1998). From approximately 1200°C, thermal NO_X starts to become prevalent (Mitchell, 1998). NO_2 only account for approximately 5% of the fuel NO_X, dependent of the fuel type. (Matsuda, 1994; Sarofim, 1995). A fourth intermediary process is also considered, a free radical compound NNH. The NNH process was proposed by Miller et al (Miller and Bowman, 1989) and experimental work by Selgran indicated a life span of approximately 0.5 µs (Selgren, 1989). Further theoretical work by Bozkaya suggested life spans of 10^{-8}-10^{-10} s, and Klippenstein used lifetimes of 10^{-9} s for NNH in a furnace (Bozkaya, 2010; Klippenstein et al., 2011).

Until approximately 2000, industrial combustion furnaces used for power production were held at 1200-1500°C (Bilbao, 1995; Lanigan, 1994; MacPhail, 1997). More recent operating temperatures of a PCC using bituminous coal operate between 1500-1700°C.(IEA, 2018). This maintains a balance between fuel-NO_X and thermal-NO_X. Figure 3.6 shows the relationship for the three main routes of NO production. Thermal NO starts to become prevalent at 1100°C, showing an exponential increase from 1200°C onwards. Fuel NO stabilises at around 1800°C. Prompt NO shows a slight increase at 1800°C. This combination of factors shows why controlling the temperature in a furnace is imperative to controlling NO_X emissions, see Section 3.6.

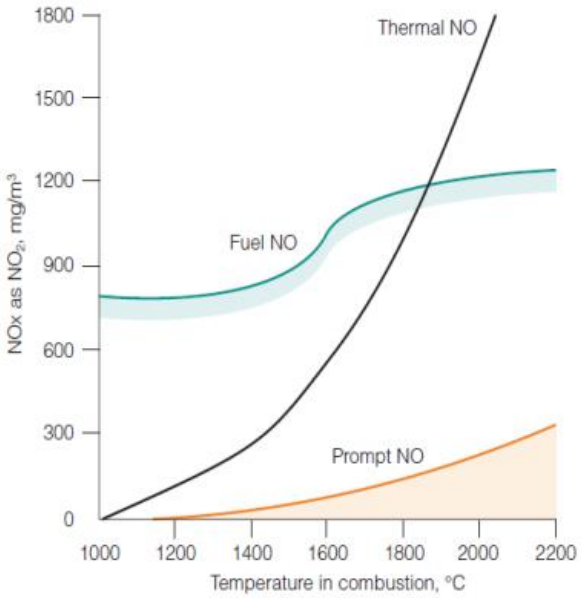

Figure 3.6 Relationship between nitrogen oxides formations and temperature. (BHEL, 2016)

The nitrogen content of most coals is between 0.5-2% by mass (Turns, 2012), although dependent of the geology and petrology there may be higher percentage values. The nitrogen content within a fuel, and the functional groups in which it is entrained are critical factors to the amount of fuel NO_X emissions, Section 3.3.2.

3.4.2 Fuel NO

During combustion of coal, there are three main stages: drying, devolatilisation and char combustion. For the formation of NO_X, devolatilisation and char combustion are intrinsic. During devolatilisation, nitrogen is released from the functional groups. As the nitrogen is released it can form nitrogen containing radicals, molecular nitrogen, ammonia (NH_3) and hydrogen cyanide (HCN). NH_3 and HCN are known to be intermediary species for the formation of fuel NO. Not all of the Fuel-N is released during devolatilisation, some is retained in the char and heavier volatiles as tars. The partitioning of the Fuel-N is critical; to the control of NO_X emissions from a furnace, see Section 3.6

The hydrogen cyanide released during pyrolysis can react with free oxygen radicals to form NO, at equivalence ratios of 1.2 or less (Glarborg et al., 2018), Equation 3.1-3.4.

$$HCN + O \leftrightarrow NCO + H \quad \text{Eq 3.1}$$

$$NCO + H \leftrightarrow NH + CO \quad \text{Eq 3.2}$$

$$NH + H \leftrightarrow N + H_2 \quad \text{Eq 3.3}$$

$$N + OH \leftrightarrow NO + H \quad \text{Eq 3.4}$$

As the equivalence ratios increases above 1.2 the HCN can be returned back into N_2. Therefore if the equivalence ratio can be controlled, then this can be an important process in controlling the final formation of NO_X, in particular prompt NO_X. (Miller and Bowman, 1989).

The hydroxyl groups can form further reactions with hydrogen radicals. Figure 3.7 highlights some of the key reactions and mechanisms that take place for the conversion of Fuel-N to molecular nitrogen during the devolatilisation and subsequently char combustion. (Fenimore, 1970). During devolatilisation and into combustion, an intermediary product from Fuel-N to fuel NO can readily develop. During the tar phase, heavier volatiles can be released. In a fuel rich environment, the volatiles can be oxidised through pyrolysis in hot gases. During pyrolysis, nitrogen is released from the tars and form intermediary species of NH_3, but predominantly HCN (Glarborg, 2003).

When the fuel is combusted under fuel lean conditions, even under moderate flame conditions, the Fuel-N can readily react with the free oxygen radicals to form NO. The complete range of reaction pathways are not known or completely understood, the abstraction of hydrogen forms a reaction with the hydrogen cyanide via oxy-cyanosis of HNCO and NCO to form ammonia species NH_i, (where i=1, 2 or 3).

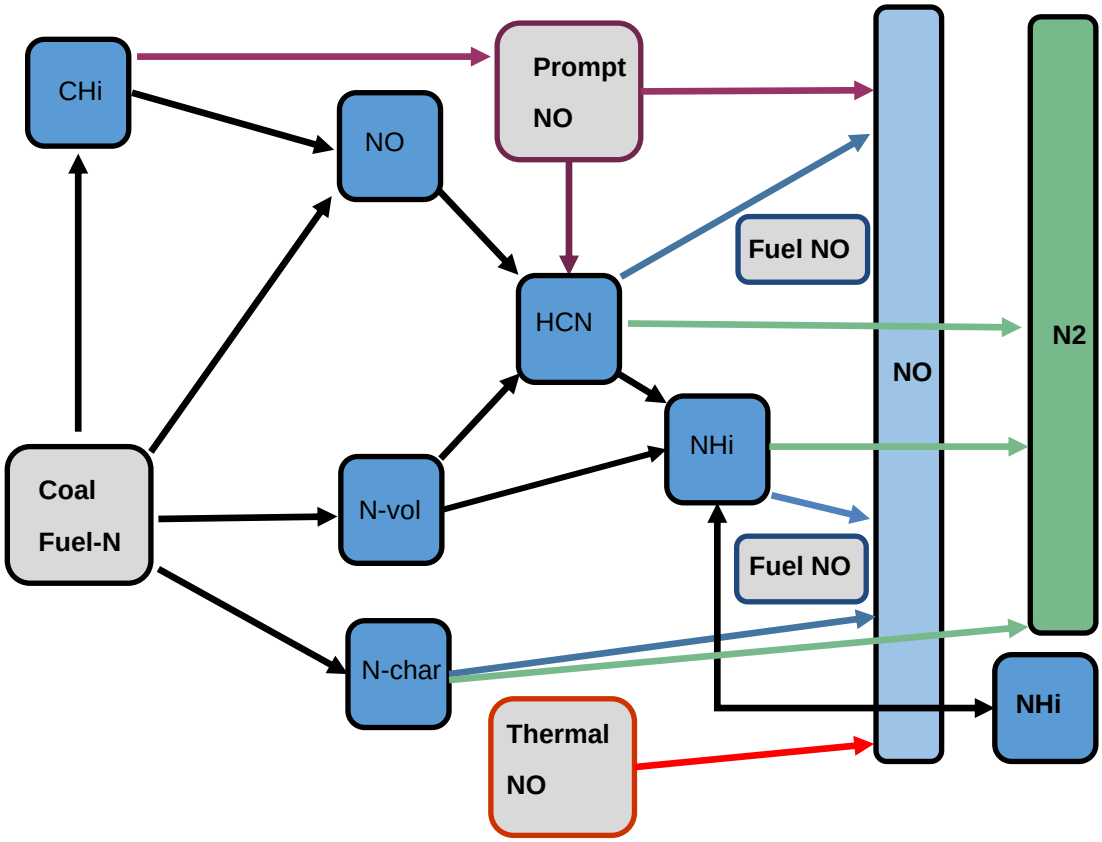

Figure 3.7 Simplified production of NO from combustion of hydrocarbons containing N within the fuel matrix. (Adams, 2017; Fenimore, 1970)

In a fuel rich environment amines are released during pyrolysis and can react with the NO. Through this process, Fuel-NO can be reduced back to molecular nitrogen. NO can also readily react with C_xH_y species, thus complicating the NO reduction. The main product of this interaction and reactions is HCN. Under fuel rich conditions however, HCN can be reduced to N_2, see Section 3.6.2.

After the devolatilisation stage, char combustion takes place. Fuel-N retained in the char is then released. The char combustion stage is the last to happen and generally lasts longer than both the devolatilisation and the tar pyrolysis phases. Occasionally Fuel-N is retained in the ashes after combustion is complete, however during complete combustion of coal, all of the nitrogen will be released. Whilst the process is not fully understood, or all of the chemical reactions known, the char-N is predominantly released as HCN, with lesser quantities of NH_3. As char combustion takes place in the presence of O_2, the remaining Fuel-N may convert directly to NO. The formation of

HCN from the char and ash, through thermal dissociation, is highly exothermic, which will tend to release any remaining fuel bound nitrogen. (Niksa, 1996a) Fuel-N converted to NO can be reduced to molecular nitrogen via the solid-gas reaction, Equation 3.5:

$$2C + 2NO \rightarrow 2CO + N_2. \qquad \text{Eq 3.5}$$

The reduction of NO to N_2, can occur on the surface of the char, (Jones J.M, 2004; Molina et al., 2009). There is a correlation between carbon burnout and NO_X and carbon burnout in coal boilers and furnaces.

Fuel-N converted to NO can have a broad range of between 15-40%, dependent on the operational conditions within a furnace, including stoichiometry, flame temperature, furnace temperature, air and fuel staging. Fuel properties are also instrumental in how much NO is produced, i.e. nitrogen content, nitrogen functional groups and volatile matter, see Section 3.6 (Baxter et al., 1996; Pels, 1995b). The primary product of char nitrogen combustion is NO. The reaction rates of char combustion is much slower than volatile and tar combustion. NO accounts for approximately 25% of the char-N. (Cahill, 1991).

The following reactions are the likely pathways for Fuel-N under fuel rich conditions (Mitchell, 1998):

$$HCN + OH \rightarrow NH_2 + CO \qquad \text{Eq 3.6}$$

$$NH_2 + RH \rightarrow NH_3 + R \qquad \text{Eq 3.7}$$

$$H_2 + NO \rightarrow N_2H + OH \rightarrow N_2 + H_2O \qquad \text{Eq 3.8}$$

NO can be depleted via the following mechanism:

$$CH + NO \rightarrow HCN + O \qquad \text{Eq 3.9}$$

$$C + NO \rightarrow 0.5N_2 + CO \qquad \text{Eq 3.10}$$

Under fuel lean conditions, with stoichiometry, $\lambda \geq 1$, the following reactions can be assumed: (GRI2, 1996).

$$HCN + O \leftrightarrow NCO + H \quad \text{Eq 3.11}$$

$$HCN + O \leftrightarrow NH + CO \quad \text{Eq 3.12}$$

$$HCN + O \leftrightarrow CN + OH \quad \text{Eq 3.13}$$

These reactions are followed by:

$$NCO + O \leftrightarrow NO + CO \quad \text{Eq 3.14}$$

$$NH + OH \leftrightarrow NO + H_2O \quad \text{Eq 3.15}$$

$$CN + O \leftrightarrow N + CO \quad \text{Eq 3.16}$$

Under fuel rich conditions, the reaction pathways in Equations 3.11 to 3.16 will be different.

3.4.3 NNH mechanism

The NNH mechanism is a short lived intermediary reaction pathway for NO production *of* 10^{-8}-10^{-10} s, whilst Selgram indicated durations in the region of 5 μs. (Bozkaya, 2010; Selgren, 1989). The NNH mechanism was originally suggested by Miller and Bowman and again later by Bozzelli and Dean through the rich fuel environment represented in Equations 3.17-3.19. (Miller and Bowman, 1989; Bozzelli and Dean, 1995). Although the pathway is only an intermediate step, it may be intrinsic to the formation of NO during combustion.

A comparative route for the formation of NO occurs in a fuel rich environment:

$$N + OH \leftrightarrow NO + H \quad \text{Eq 3.17}$$

In fuel rich conditions a further reaction mechanism can take place (Bozzelli and Dean, 1995):

$$H + NN = NNH \quad \text{Eq 3.18}$$

$$NNH + O = NO + NH \quad \text{Eq 3.19}$$

Within a turbulent flame, the O radicals can be intrinsic to the formation of NO, (Bilger, 1975) where fuel nitrogen can form compounds with the highly reactive O radicals.

The fuel-N will be liberated under high energy conditions i.e. when heat is applied, and in an environment where oxygen is present, the Fuel-N is likely to form NO. In the post flame environment, where heat is greater than in the flame region in a combustion chamber, char-N will readily form NO. (Mitchell, 1998). Within the post flame environment, therefore, the temperature needs to be controlled to reduce NO_X formation, see Section 3.4.5.

3.4.4 Fenimore (Prompt) NO_x

Prompt NO_X is the formation of NO from the interactions of atmospheric nitrogen, oxygen radicals and hydrocarbons. Originally proposed by Fenimore, (Fenimore, 1970). The NO formation happened in the early stages of combustion of a fuel and occurs at the flame front. The reactions are short timescales; however hundreds of reactions take place over this time frame. Prompt NO_X forms differently than fuel NO_X as this is the result of atmospheric nitrogen, however it does follow some of the same reaction pathways. As the formation occurs early on in the combustion process, the process is different than thermal NO_X, which often takes place in the hotter part of the furnace, above the flame zone. Radicals are produced, and react with the atmospheric nitrogen, and small quantities released from the fuel. Equations 3.20-3.25 shows that cyano compounds are produced which can develop into amines with the nitrogen. Further dissociation takes place resulting in NO and hydrogen radicals.

Whilst hundreds of reactions take place, the principle reactions are shown in Equations 3.20-3.21.

$$CH + N_2 \leftrightarrow HCN + N \qquad \text{Eq 3.20}$$

$$C + N_2 \leftrightarrow CN + N \qquad \text{Eq 3.21}$$

After this process the hydrogen cyanide can react with free oxygen radicals to form NO, at equivalence ratios of 1.2 or less. The second Equations 3.22-3.25 are the same as those shown in Fuel NO_X formations.

$$HCN + O \leftrightarrow NCO + H \quad \text{Eq 3.22}$$

$$NCO + H \leftrightarrow NH + CO \quad \text{Eq 3.23}$$

$$NH + H \leftrightarrow N + H_2 \quad \text{Eq 3.24}$$

$$N + OH \leftrightarrow NO + H \quad \text{Eq 3.25}$$

As with fuel NO_X, these reactions are reversible, if the equivalence ratio is greater than 1.2. This can be instrumental in inhibiting the formation of NO_X, and the potential to reverse NO_X into molecular nitrogen (Miller and Bowman, 1989).

The contribution of prompt NO_X to the overall NO_X formation within a PCC is not completely known, especially as some of the reactions are shared with fuel NO_X, but it is small, <5%. The amount of prompt NO_X formed during combustion has been established to be proportional to the concentrations of carbon atoms. The carbon atom formation however is independent of the hydrocarbon species (Hayhurst and Vince, 1980; Tomeczek and Gradon, 1997). As conditions within the combustion chamber takes place, so the formation of prompt NO_X changes. Prompt NO_X will always form in the combustion zone as long as there are hydrocarbons present where nitrogen from the air can be oxidised.

3.4.5 Zeldovich (Thermal) NO_x

Thermal NO_X is a reaction pathway for atmospheric nitrogen that occurs at higher temperatures generally starting around 1100°C (1370K) (Zeldovich, 1946). After this temperature there is an exponential increase, see Figure 3.6, Section 3.4.1. Temperatures higher than this do not readily form in the flame zone. Therefore most thermal NO_X forms above the flame zone within the overfire air region (OFA), see

Figure 3.10, Section 3.6.6. Whilst the oxygen is primarily dissociated from the air, it can be derived from H and O radicals from the coal, which readily form NO with the nitrogen which can also come from the fuel (Bozzuto, 1992; Mitchell, 1998). The principle reactions are shown in Equations 3.26-3.29:

$$N_2 + O_2 \rightarrow 2NO \qquad \text{Eq 3.26}$$

The extended Zeldovich equations can then be applied and the reversible equations are formed:

$$N_2 + O \leftrightarrow NO + N \qquad \text{Eq 3.27}$$

$$N + O_2 \leftrightarrow NO + O \qquad \text{Eq 3.28}$$

$$N + OH \leftrightarrow NO + H \qquad \text{Eq 3.29}$$

Whilst these reactions are heat dependent, they form more readily in a fuel lean environment, stoichiometry <1. The higher temperatures dependencies for the formation of thermal NO_X, as the nitrogen triple bond of N_2 is strong and so requires high levels of energy. If the oxygen and nitrogen are in a steady state, the Zeldovich mechanism can be best described as a shuttle reaction. Hydroxyl and hydrogen species are intrinsic in the oxidation of nitrogen for NO formation. The mechanism is responsive to temperature, stoichiometry and residence time. Thermal NO_X can occur in fuel rich conditions; however, the reactions pathways are different. Increased reactions are required to compensate for the elevated concentrations of hydrogen radicals and hydroxyl radicals. Under fuel rich conditions, extra heat energy may be required to help break the O_2 and N_2 bonds (Mitchell, 1998).

3.4.6 N_2O mechanism

The N_2O mechanism is a low temperature intermediary process in the formation of NO_X. The initial reaction to form N_2O from diatomic nitrogen from the air and oxygen is shown in Equation 3.30. The reaction pathways for N_2 and O is not well researched or

understood. The reverse reaction of disassociation of N_2O has been experimentally studied over a range of conditions (Glarborg et al., 2018) The original proposal for the mechanism was from Malte (Malte and Pratt, 1975). Experimental work using CH_4 and air during combustion revealed the potential reactions shown in Equations 3.30-3.34:

$$N_2 + O + M \leftrightarrow N_2O + M \quad \text{Eq 3.30}$$

$$N_2O + O \leftrightarrow 2NO \quad \text{Eq 3.31}$$

$$N_2O + O \leftrightarrow N_2 + O_2 \quad \text{Eq 3.32}$$

$$N_2O + H \leftrightarrow N_2 + OH \quad \text{Eq 3.33}$$

$$N2O + H \leftrightarrow NO + NH \quad \text{Eq 3.34}$$

An alternate pathway for the atmospheric nitrogen is shown in Equation 3.35 (Bozzelli and Dean, 1995).

$$H + N2 + M \rightarrow NNH + M \quad \text{Eq 3.35}$$

The route shown in Equation 3.35 starts the formation of NNH mechanism as shown in Section 3.4.3.

The NH may go on to further reactions with OH or O_2 to form NO, or react with NO to form N_2O or N_2 (Glarborg et al., 2018).

The N_2O mechanism is a low temperature process Malte suggested ≤1800K (Malte and Pratt, 1975). Later work by Klippenstein et al (Klippenstein et al., 2011), bracketed the reactions to a temperature range of 300-2200 K for the N_2O + H reactions in Eq 3.33. Experimentally, Yokoyama (Yokoyama et al., 1991) showed the N_2O + H reaction accounts for 70-90% of the total reaction rates, with N_2 + OH accounting for 10-30%. This was later confirmed theoretically by Klippenstein (Klippenstein et al., 2011). At this range, there would be some overlap into thermal NO_X, which starts at ~1370K, and becomes predominant at ~1800 K (Zeldovich, 1946). Above 2200 K, only two studies have been carried out in shock tubes for the NH + NO mechanism, 2200-3500 K by Mertens et al (Mertens et al., 1991), and at 3500 K by Yokayama (Yokoyama et al.,

1991). The rate constants for $k_{(NH+NO)}$ reported by Yokayama were between and one and three orders lower than those reported by Mertens.

3.5.1 Photochemical Smog

Photochemical smog forms from hydrocarbons and oxides of nitrogen in the troposphere, through the dissociation of NO_2 with light from the electromagnetic spectrum from visible light to ultraviolet. Equations 3.36 and 3.37 show the mechanism involved on the formation of ground level O_3 at wavelengths of <430 nm. The NO_2 dissociates to form NO and a free oxygen radical. The second stage involves a stable secondary molecule which interacts to form a stable transition for molecular oxygen and free radical to form ozone. (Finlayson-Pitts, 2015) The stable molecule acts as a catalyst for the reaction.

$$NO_2 + hv\ (X< 430nm) \rightarrow NO + O \qquad \text{Eq 3.36}$$

$$M + O + O_2 \rightarrow O_3 + M \qquad \text{Eq 3.37}$$

The same process can occur with NO, where the NO is dissociated to form nitrogen and oxygen free radicals. The reactions in Equation 3.36 are then followed for the formation of O_3. The nitrogen radical will readily form a new molecule with other nitrogen radical to form stable molecule nitrogen. (Turns, 2012) This process can also occur naturally, where lightning can act to dissociate the N_2 and O_2 to produce the free radicals N and O.

3.5.2 Acid rain

A further problem associated with NO_X is the secondary pollutant acid rain. Sections 2.2.1 and 2.2.2, highlights some of the issues associated with acid rain. Acid rain from NO_X can take the form of two different compounds HNO_3, nitric acid and HNO_2, nitrous

acid. The NO_2 molecules in the atmosphere are subject to hydrolysis, the acid compounds formation are shown in Equation 3.38.

$$2\ NO_2/N_2O_4 + H_2O \rightarrow HNO_2 + HNO_3 \qquad \text{Eq 3.38}$$

The reaction can be reversed, where the nitric acid is converted back to NO_2, H_2O and O_2 Equation 3.39.

$$4HNO_3 \rightarrow 4NO_2 + 2H_2O + O_2 \qquad \text{Eq 3.39}$$

Whilst the principle concerns are from acid rain, as shown in Figure 2.2, if the NO_2 particles do not go through hydrolysis, they may fall to the ground as a dry solid acid, which is also harmful to flora and fauna.

A further problem can be the formation of PM, where the NO_X particles can act as a nucleus for the formation of fine particulate matter, both $PM_{2.5}$ and PM_{10}.

3.6 Industrial NO_X reduction techniques

The BAT in Section 2.6, showed the emissions standards to be met by 2021 in the EU. Table 3.2 shows the primary and secondary reduction technologies incorporated within pulverised coal furnaces.

Table 3.2 Primary and secondary NO_X reduction technologies used in industry to control the emissions from pulverised coal combustion. (Van der Kooj, 1997)

Primary and secondary technologies for the control NO_x		
Technology	Reduction %	Application or restrictions
Low NO_X burners	30-55	Stoichiometry is used as a control measure. Flame length is important for maintaining efficient combustion. Not suitable for cyclone furnaces.
Low NO_X burners with air staging	35-70	Injection location and height of the overfire air ports is essential. Not suitable for cyclone furnaces.
Gas re-burn	60	Retrofit injectors required which require large amounts of space. Can have an impact on boiler heat distribution
Low-NO_X burner with gas re-burn	60-70	As with Low NO_X burners and gas re-burn
SNCR	30-50	Temperature is critical to avoid ammonia slip and the production of N_2O.
SNCR with natural gas re-burn	90	As above. Reburn stoichiometry of 1 is required.
SCR	90	Costly refurbishment. Operating temperatures restricted 300-360°C. Catalyst poisoning from alkali and alkaline metals allowing ammonia slip

3.6.1 Primary Reduction

The primary technologies are designed to focus on the fuel characteristics, the combustion processes and the designs of combustion chambers to reduce emissions.

3.6.2 Low NO_x burners

NO_X reductions of 30-55% can be achieved through the deployment of a Low NO_X burners in a PC furnace (Sen, 2010). Low NO_X burners inject fuel and air at different stoichiometric levels between the primary, secondary and tertiary inlets. Figure 3.8 shows a Low NO_X burner outlet from a small PC combustion chamber (250KW_{th}). Whilst the burner is from a small-scale pilot test facility, it shows the main characteristics of a large-scale furnace burner design.

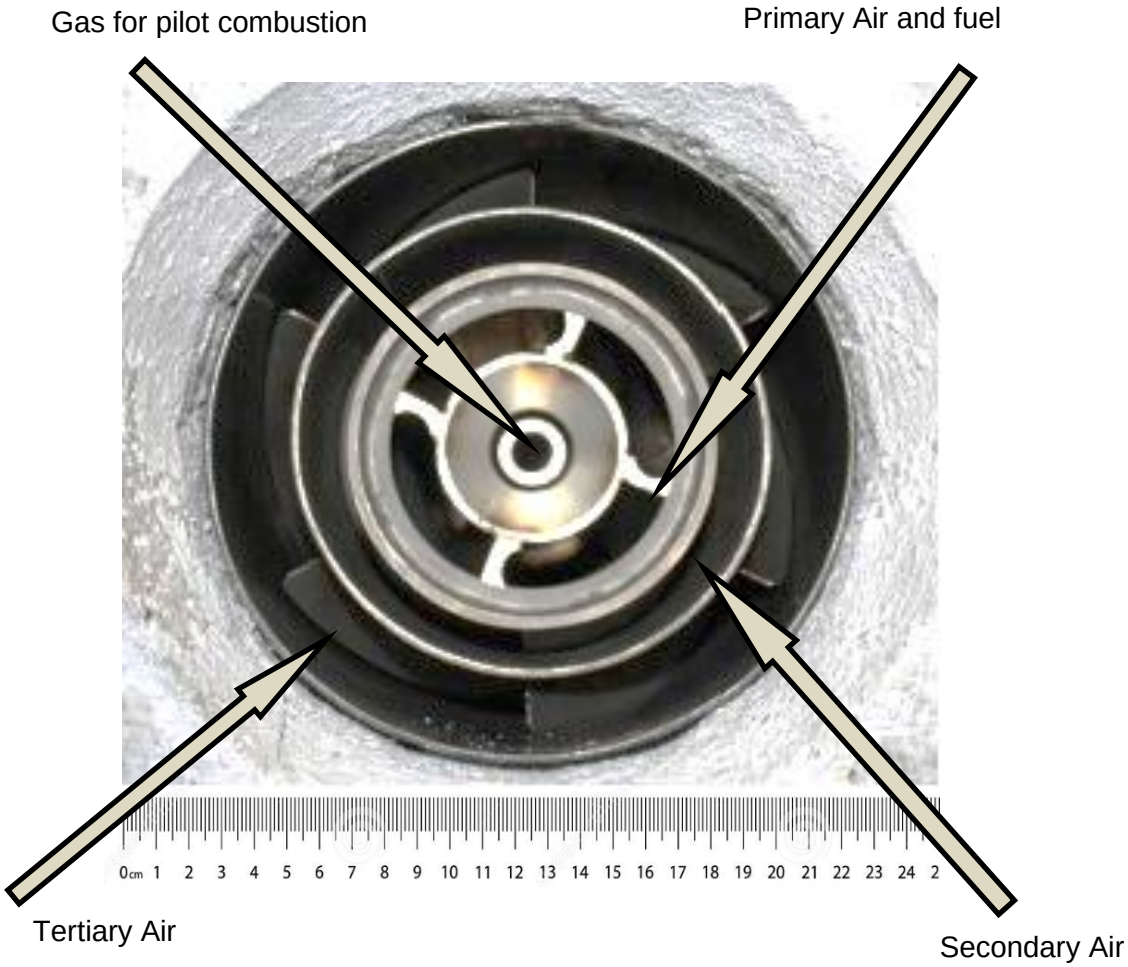

Figure 3.8 Outlet into the combustion chamber of a low NO_x burner from a 250kW_{th} PC combustion chamber at the PACT facility Sheffield**.** Adapted from (Nimmo, 2016)

For coal to achieve continuous combustion, the operating temperature of the furnace needs to achieve 750-800°C for incipient combustion. To achieve these temperatures, natural gas is introduced through the pilot port. Within large scale furnaces, gas or industrial oil may be used to initiate start up in a furnace. From a cold start, a large-scale furnace (>500MW), can take up to 10 hrs to achieve operational temperature. The reaching of operational temperature does not include production of steam for electrical power production. When operating temperature is reached, the natural gas supply can be turned off, and the furnace will be self-sustaining on pulverised coal under the correct stoichiometric conditions.

The primary, secondary and tertiary zones within the Low NO_X burner, contain angular vanes designed to create vortices of air. The vanes provide a swirl motion to the fuel

and air in the combustion chamber. The fuel is injected with the primary air and is picked up in the vortices and mixed with the air. Maintaining the fuel and air mixture within the heat cycle for the correct length of time ensures a more efficient combustion cycle. A more efficient combustion cycle ensures less carbon is left in the ash. Through this action, greater efficiency can be achieved in the furnace and the mass of solid waste product is reduced.

The stoichiometric levels are maintained as a fuel rich combustion environment. As the air levels are comparatively low, this leads to lower NO levels by reducing the amount of reactive oxygen present. The reduced O_2 reacts more readily with the carbon in preference to the volatile nitrogen. The nitrogen releases as volatile fuel-N forms triple bonds with other available nitrogen species in the absence of readily available oxygen, to form N_2, Equations 3.5 and 3.10. A second stage of combustion is at a stoichiometric value of ~1. The nitrogen now in N_2 form would require higher energy levels to break the strong triple bond, and so is less likely to become reactive with the oxygen in the air. The controlled stoichiometry achieves lower temperatures leading to lower values of thermal NO_X. The operating conditions of a Low NO_X burners are a compromise between NO reduction, emission of other gases (CO and CO_2) unburnt hydrocarbons (UHC) and flame stability.

Figure 3.9 shows the stoichiometric conditions within a furnace and the effects this can have on the emissions characteristics of CO_2, CO, HC, NO and particulate matter. Through small changes in the stoichiometric values, significant changes in the emissions can be realised. It can be seen that changing the ratio λ from 1.01 to 1.04 can achieve large reductions in CO, UHC and particulate matter. Over this range there are only slight increases for the CO_2 and NO. To achieve reductions of CO_2, however, ultimately stoichiometry in excess of 1.03 is required. Increasing stoichiometry over 1.01 starts to see a rise in NO values. The tuning of a combustion chamber into combustion zones with different characteristics is essential, in an attempt to achieve emissions values inside regulation standards see Section 2.6.

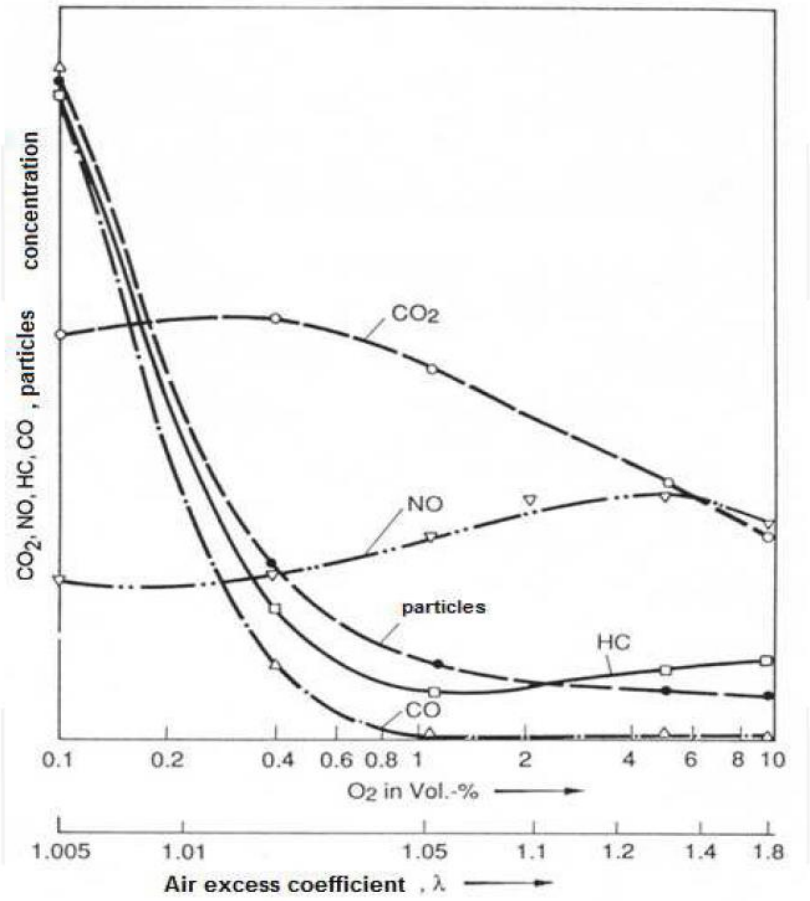

Figure 3.9 Emissions concentrations as a function of air in excess of λ, air fuel ratio above stoichiometry (Popescu, 2010)

3.6.3 Furnace conditions and design

The burner geometric design can have significant effects on the combustion process, and a specific fuel type may require different design characteristics. The geometric design will not be discussed further, however the operational conditions within the furnace appertaining to NO_X reduction follow.

3.6.4 Stoichiometry

Stoichiometry is the control of the air/fuel (A/F) ratio. The ratio is critical in controlling the temperature, emissions of gases, particulate and unburnt hydrocarbons. Figure 3.9 shows how changing the value can change the proportions of these. The stoichiometric values that a furnace operates on is dependent on many aspects; geometry of the

furnace, type of furnace (tangential or side wall fired), number and type of burners, fuel type and load. Furnaces will normally be run with a stoichiometry (λ) of less than 1, i.e fuel rich conditions. Most PCC furnaces operate at between 0.7 – 0.85. The air fed into the combustion chamber is divided between the primary combustion zones and the overfire air Figure 3.10. If the A/F ratio exceeds these figures, then the oxygen in the air, not required for combustion, will readily form NO with the Fuel-N. If excess O_2 levels are maintained at approximately 5%, then NO emissions can be kept to a minimum and controlled using stoichiometric values. These observations were noted by Chen and Gathitu (2011), when using lignite and bituminous coals in a down fired furnace, with a residence time of 1 s for the fuel. (Chen and Gathitu, 2011). Much research has been carried out exploring the potential to optimise stoichiometry in an attempt to control NO_X. Hesselmann et al, carried out experiments in a combustion chamber using a single Low-N burner (160kW_{th}) using a Polish bitumen coal. Within the primary combustion zone they operated stoichiometry of 0.9, in an excess O_2 value of 3%, in the primary combustion zone. With these values set, they found that NO_X emissions were dependent on the distances between the primary combustion port and the overfire air. As the distances between the primary combustion zone and the overfire air increased, so NO_X reductions were observed (Hesselmann, 1997; Mitchell, 1998).

Rozendaal Van Vliet experimented with stoichiometry values between 0.75-0.95 in an electrically heated furnace, using a high volatile bituminous coal. When operated at 0.95 in the primary flame zone, reductions in NO_X from 700 ppmv to 400 ppmv were observed. These figures were reduced further to 350 ppmv when the combustion was complimented with burnout air. Reduction of the stoichiometry down to 0.75 shown significant reductions of NO_X down to 100 ppmv. The final burnout of the char led to an increase in the NO_X emissions back to 170 ppmv. (Greul, 1996; Rosendaal, 1996).

At stoichiometry values of 0.8 and using a blended coal of bituminous and brown coals, Bose et al, found that NO was the principle nitrogen compound formed. When

operating stoichiometry of 0.6, more HCN and NH_3 were formed. Smart and Webber (1998) found the same results, when operating with residence time. Longer residence times lead to lower NO emissions, when using a premixed burner and blended bituminous with brown coals. (Bose, 1988; Smart, 1989).

3.6.5 Temperature

As shown in Thermal NO_X (Section 3.4.5) temperature can have a significant effect on the amount of NO_X produced during combustion. Temperature in the primary combustion zone is dependent on the fuel type, and stoichiometry. Temperature can also be controlled via residence time. Complete combustion is more likely to take place if the residence time is increased. Complete combustion and thus complete carbon burnout can lead to higher temperatures if stoichiometric conditions are maintained. Higher grade coals tend to have higher carbon contents. Whilst higher carbon content can lead to higher temperatures in a furnace, they also require higher temperatures to start and maintain combustion, due to lower volatile contents. Nitrogen content tends to be lower in high carbon coals, see Section 3.3.1. If the volatile content is reduced then the amount of volatile nitrogen may well be reduced, leading to a relative increase in char-N (Courtemanche and Levendis, 1998). Volatile-N, when released from fuel in a Low-N burner, see section 3.6.2, can be controlled and reduced back to molecular nitrogen. In a Low-N burner, char-N can account for as much as 60% of the NO_X produced, therefore, whilst the percentage of nitrogen content may be lower in a high carbon fuel, the relative amount of NO_X produced may be increased (Mitchell, 1998).

3.6.6 Overfire (Air Staging)

Overfire air, or air staging is a process of partitioning out primary air, which is fed in with the fuel, and a parcel of air which is used in the overfire air, see Figure 3.10. The

overfire ports are situated above the main combustion zone, and approximately 20% of the total air is fed into these ports.

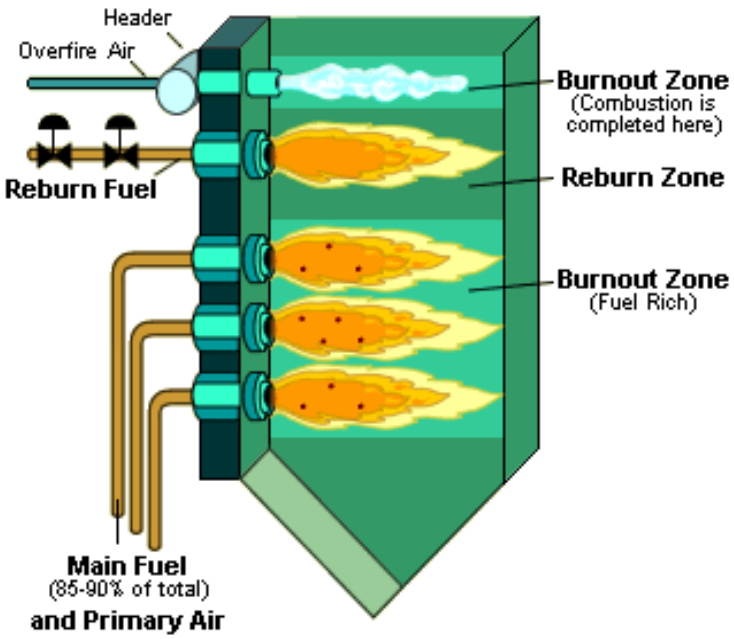

Figure 3.10 Basic design of a furnace with overfire ports. (EPA, 2018)

The net result of partitioning off the air to overfire, is a fuel rich environment in the main combustion zone, see Section 3.6.4. The creation of the fuel rich zones leads to an NO reducing environment. Further reductions are felt through the control of the temperature in the main flame zone. Above the main flame zone is the overfire air. The temperatures are higher in this region. The overfire air is fed in which reduces the temperature. The reduction in temperature due to the overfire air helps to reduce thermal NO_X and creates an environment for complete combustion. The location and height above the main combustion zone is critical to achieving a reducing environment. The combination of Low-NO_X burners and overfire air can achieve NO reductions of as much as 70%.

3.6.7 Fuel Staging

Fuel staging utilises a secondary fuel to supplement the primary fuel in the combustion chamber to create different combustion zones. The secondary fuel can be of the same

fuel type as the primary or an alternate fuel, in the case of coal the secondary could be oil or gas. The secondary fuel can be fed in via the overfire system and can be used to create a fuel lean environment.

Primary fuel is supplied to the main combustion zone with an excess of air. Within the primary combustion zone high levels of NO are initially produced. When the secondary fuel is injected, there is no extra air provided. The excess air/O_2 from the primary combustion is used with the secondary fuel. The secondary fuel can also be combined with overfire air. Under these conditions the excess air can be used to reduce the excess CO produced in primary combustion. The combustion of the excess O_2 with the secondary fuel restricts the oxygen available to form NO_X. The NO is converted to molecular nitrogen in the reducing atmosphere in the absence of hydrocarbon radicals. Excess hydrocarbons are consumed in the overfire region.

Stoichiometry is an essential part of the process to control and restrict the amount of available air and O_2 in the primary and secondary combustion zones. Stoichiometry of 0.9-0.95 is applied in the re-burn zone to control temperatures between 1300-1800 °C. This control measure offers the optimum performance for NO_X reduction for bituminous coals, yielding residence times of 2-5 s in the combustion chamber (Garner, 1997). Re-burning can offer NO_X reductions of 70%, when operating with natural gas as a secondary fuel to coal. When coal is used as a secondary fuel over the primary fuel of coal, reductions of 50-60% can be achieved (Doig, 1997; Bell and Buckingham).

3.6.8 Secondary control measures

Secondary control measures involve NO_X and emissions control measures after combustion. The control systems are in the effluent exhaust systems and consist of mechanisms designed reduce the NO_X emissions before emission from the exhaust stack. Whilst the secondary NO_X control measures provide necessary control technology, they have no direct impact on this research. Their inclusion is for reference

and for the potential effects this body of research could have on the performance of an SCR incorporated in a PCC furnace.

3.6.8.1 Exhaust Gas Recirculation (flue gas recirculation)

Exhaust gas recirculation extracts a volume of gas from the effluent gases and feeds this back into the furnace. The exhaust gases tend to be low in oxygen, and comparatively high in CO_2. When fed back into the furnace, the CO_2 from the exhaust gases replaces some of the oxygen in the air supplied (on a relative basis). The reduced O_2, results in a fuel rich environment, with reduced oxygen for the nitrogen to form NO_X.

3.6.8.2 Selective non-catalytic converters (SNCR)

SNCR's are used to reduce NO_X via the injection of reactant, aqueous ammonia or urea direct into the exhaust stream of a PCC furnace. The operating temperature of a SNCR is normally in the range of 870-1150°C. The ammonia is vaporised at these temperatures and acts as a reactant to form diatomic nitrogen from the NO_X, water and CO_2. SNCR's can give conversion rates of 30-70%.

The reaction pathways for the interaction between NO and ammonia are shown in Equations 3.40 and NO and urea in Equation 3.41.

$$4\ NO + 4\ NH_3 + O_2 \rightarrow 4\ N_2 + 6\ H_2O \qquad \text{Eq 3.40}$$

$$4\ NO + 2\ NH_2CONH_2 + O_2 \rightarrow 4\ N_2 + 4\ H_2O + 2\ CO_2 \qquad \text{Eq 3.41}$$

3.6.8.3 Selective catalytic converters (SCR)

SCR's are deployed within the exhaust gas system of a PCC to control NO_X emissions and can yield reductions of 80-90%. The effluent gases pass over a catalyst, often manufactured from oxides of base metals, i.e. titanium or vanadium pentoxide. The catalysts are often honeycombed in design, which provide large surface areas for

reactions to take place. Reactants ammonia or urea are combined with the catalyst, using the same pathways as shown in Equations 2.34 and 2.35. The operating temperatures of a SCR are much lower than for SNCR, and normally in the range of 300-400 °C. If operating temperatures exceed 400 °C, rapid degradation of the catalyst will ensue. Due to this limited operating temperature, an SCR is positioned further down the exhaust system compared to a SNCR.

SCR's are subject to degradation and poisoning, which can dramatically affect the performance. Ultrafine particles and nanoparticles can become embedded on the surface of the catalysts, reducing the effectiveness. Chemical attack and poisoning can occur from alkali metals (sodium and potassium). Alkali metals are generally higher in biomass than in coals, see Section 3.7. As this research is focussed on utilising biomass ashes as a method of NO_X reduction, there may be further implications for SCR systems installed if the alkali metals were to reach the SCR high concentrations. (Dai et al., 2008)

3.6.8.4 Ammonia slip

Both SNCR and SCR can be subject to ammonia slip. Ammonia slip is caused when some of the ammonia from the system is not completely used and passes through to the exhaust stack. HN_3 is a powerful GHG and a pollutant, therefore the release of NH_3 into the atmosphere is undesirable.

Ammonia slip can occur if the operating temperatures are too low for complete reaction in an SNCR or SCR. Within a SCR if the catalyst has become less reactive over time or has a reduced performance through poisoning, then ammonia slip may also occur.

3.7 Ash products from combustion

During combustion of solid fuels, there is the effluent gases as emissions, but also a solid waste product in the form of ash is produced. The ashes are primarily the non-

combustible inorganic minerals of, silicon, iron, potassium, calcium, magnesium, aluminium and sodium. Other minor or trace elements may also be present in the ashes. During the high energy environment of combustion, the minerals are released from the fuel matrix often as ions. The mineral ions readily form bonds with available oxygen or other ions. The ash can take 2 main forms: furnace bottom ash and fly ash. The furnace bottom ash tends to form larger particles which drops to the bottom of the furnace. The furnace bottom ash can be directly removed from the furnace as solids. Dependant on the furnace type, these may be quenched in water for rapid cooling. The fly ash takes the form of finer or less dense particles, which are carried on the thermal currents of the effluent gases. Due to the finer nature of fly ash, specialised collection systems are required, consisting of electrostatic precipitators and filter bags.

3.7.1 Coal Ash

Coal forms from plant material in swamps, mires and coastal lagoons, see section 3.1. The plant material gets laid down in strata, which is permeated with eroded rocks, minerals and soils. The combination of the permeated mineral matter, and the minerals taken up by the plants during growth can form the base of the ash materials during combustion. Through the coalification process, heat and compression, mineral matter in coals can become concentrated on a percentage basis. Ash is formed from the inorganic mineral matter either forming part of or within the coal matrix. Coal ashes can be dominated by aluminosilicates from rock minerals and iron oxides and sulphates from pyrite.

Table 3.3 shows breakdown of a selection of coals from the Phyllis 2 data base. Ash analysis is often taken on an oxides basis only (although other compounds may be present in lower concentrations), therefore only the oxide of the major element analysis is shown in Table 3.3.

Table 3.3 Major elemental ash analysis from Phyllis 2, for a selection of 9 bituminous and sub-bituminous coals from around the globe (www.ecn.nl/phyllis2, 2016)

Ash composition		Minimum	Maximum	Mean	Std dev	No of Samples
SO_3	wt% (ash)	3.60	9.99	6.75	2.99	4
Cl	wt% (ash)	0.01	0.01	0.01	0.00	1
P_2O_5	wt% (ash)	0.60	1.90	1.23	0.65	3
SiO_2	wt% (ash)	13.70	59.90	39.44	13.01	9
Fe_2O_3	wt% (ash)	4.80	21.50	12.39	6.19	9
Al_2O_3	wt% (ash)	5.20	31.10	18.72	9.26	9
CaO	wt% (ash)	1.80	44.80	13.19	13.77	9
MgO	wt% (ash)	0.70	13.30	4.23	4.02	9
Na_2O	wt% (ash)	0.40	7.30	1.83	2.12	9
K_2O	wt% (ash)	0.40	2.80	1.29	0.73	9
TiO_2	wt% (ash)	0.30	1.50	0.82	0.42	9

3.7.2 Biomass Ash

In its initial formation whilst growing, ashes from white woods may be considered similar to coal, as coal forms from woody materials, Sections 3.1, 3.2 and 3.7.1. Wood biomass will take up some elements from the environment in which they grow, however, these are then not concentrated through the coalification process. Elemental uptake in woody biomass can be from the soil, local geology or the atmosphere in which they grow. (Darvell LI, 2010; Gudka, 2015). As noted in Section 3.1 and 3.2, coals are millions of year's old, woody biomass may be at most only a few hundred years old, and generally much younger. The uptake of minerals and elements (other than those needed for growth) may be affected by anthropogenic emissions. Therefore, if grown in areas of higher pollution the biomass may take this into the plant structure. (Bogush et al., 2018; Gudka, 2015; Lanzerstorfer, 2015) Biomass naturally tends to be high in alkali and alkaline earth metals potassium, calcium, magnesium and sodium. Plant material may also contain elevated levels of chlorine. During combustion the alkali/alkaline elements are released and can be highly corrosive in a furnace. These elements may also form salts KCl and NaCl, which may be highly corrosive to the furnace and the steam systems within. (Tillman et al., 2010).

Table 3.4 shows the major elements present in pelleted white wood biomass ashes Elemental chlorine is not shown in the biomass ashes, and only a trace amount in the coal.

Table 3.4 Major elemental oxides in the ashes from a selection of white wood pellets (www.ecn.nl/phyllis2, 2016)

Ash composition		Minimum	Maximum	Mean	Std dev	No of Samples
SO_3	wt% (ash)	1.62	1.62	1.62	0.00	1
P_2O_5	wt% (ash)	0.10	5.27	3.39	2.86	3
SiO_2	wt% (ash)	23.53	46.06	36.20	11.52	3
Fe_2O_3	wt% (ash)	2.00	4.48	2.74	1.05	5
Al_2O_3	wt% (ash)	1.76	14.00	6.86	5.37	5
CaO	wt% (ash)	12.30	33.58	27.56	8.05	6
MgO	wt% (ash)	0.60	6.50	3.26	2.50	6
Na_2O	wt% (ash)	0.19	1.30	0.67	0.43	6
K_2O	wt% (ash)	1.00	13.06	7.57	4.42	6
TiO_2	wt% (ash)	0.06	0.17	0.12	0.08	2

When the oxides of potassium and calcium are reviewed, the biomass has significantly higher percentages of these in the ash compared to the coal. In the case of CaO, the values is twice as large, whilst for the K_2O, the value is nearly four times greater. The higher values of these oxides may be important catalytic pathways for the reduction of NO to molecular nitrogen during combustion.

When biomass is subjected to thermal degradation in a furnace, the chemical composition of the created oxides and particulate matter are shown in Figure 3.11. A variety of size fractions are achieved, ranging from 0.01 µm up to 50 µm. Agglomeration, condensation and coalescence may cause larger particle to form. Incomplete combustion may also result in larger particle size being found (Kleinhans, 2018).

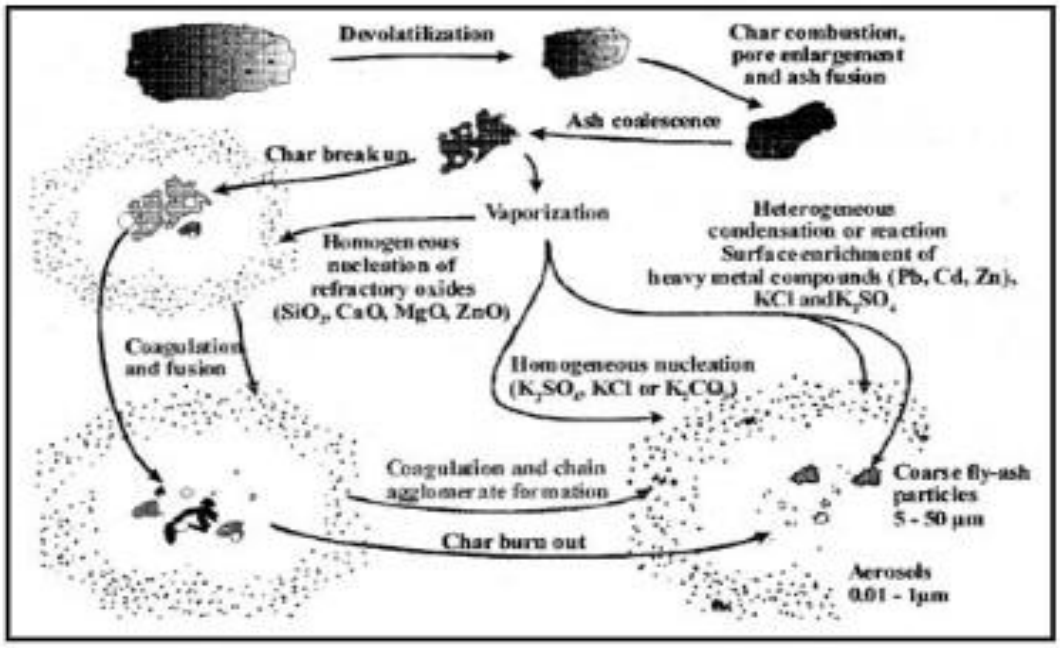

Figure 3.11, The formation of elemental ashes through combustion of biomass (Van Loo, 2008)

3.7.3 Utilisation of ash

When comparing coal to biomass, coals tend to have higher percentage values of ash. When referring to Phyllis 2, for the fuels selected the coals shows ashes of 0.4% to 40.30%, whilst the white wood pellets are 0.07% to 6.4%. In a review of ash from biomass and from co-combustion of biomass and coal, James, suggested there may be an increase in the amount of ash produced during co-combustion of certain fuel types. When combined with agricultural biomass, values of 5-10% ash were noted, whilst coals in co-combustion with rice husks increases to 30-40% (James et al., 2012). Much of this increase in ash may have resulted from incomplete combustion leading to higher values of carbon in the ash (James et al., 2012; Duan, 2012; Gomez-Barea, 2009). The energy density of biomass also tends to be lower than that of coal, therefore more fuel is required for the same heating value. The variation in biomass ashes is highly dependent on parent biomass source. For white wood pellets, the parent biomass may be virgin white wood, with low ash content, off-cut branches or the

inclusion of bark will significantly increase the ash contents (Vassilev et al., 2013; James et al., 2012; Olanders and Steenari, 1995).

The known elemental composition of the ash is essential for future potential use of the ash. Fly ash has potential secondary uses in the following areas: fertiliser, construction industry and cement additives. The use of fly ash as an additive for lightweight blocks, as a cement additive or for concrete emulsifier has been reviewed. Woody biomass fly ash has some limitations as a cement enhancer, above 20%, it can weaken the structural integrity (Berra et al., 2015; Rajamma et al., 2009; Gomez-Barea, 2009). Furnace bottom ash can also be used as an aggregate and as a concrete additive (Beltrán et al., 2014). The use of coal fly ash as a fertiliser or soil improver has been reviewed by Silva. It was noted whilst there is some uses in amelioration of the soils and macro-nutrient enhancement, correct certification of the ash is essential to denote ash to waste and reusable ash (Silva, 2019). Maschio noted bottom ash could be used as a cement and concrete additives when applied in *"equivalent mass of 5, 10, 20 and 30 wt. %*", fly ash to bottom ash. (Maschio S., 2011).

The carbon content of an ash can be intrinsic to any future usage. Biomass ash carbon content with respect to biomass boiler and furnace efficiencies has been reported (Duan, 2012; Gomez-Barea, 2009). Carbon content figures between 10-60% have been recorded by Gomez-Barea. More modest percentage values of 10-30% were reported by Duan et al. The higher carbon content figures are found in the furnace bottom ash rather than the fly ash (Duan, 2012; Gomez-Barea, 2009). Boiler design, stoichiometry and combustion process can have a significant effect on the efficiency of combustion and thus the amount of carbon retained in the ash, see Sections 3.6.3-3.6.5. Complete combustion of biomass can also be affected by the type and density of the biomass. Lower density biomass fuels can be affected by the turbulent flow in the furnace. Lighter or less dense particles can be forced to the side of the furnace in turbulent flow, away from the main flame zone. Particles removed from the main flame zone are unlikely to go through complete combustion, resulting in carbon left in the ash.

Ashes with higher carbon content could be potential secondary fuels. The ashes would be low in volatiles, and the carbon content may be in char form, therefore higher flame initiation temperatures would be required for combustion to take place. The increased alkali/alkaline metals would need to be considered if used as a fuel, as these can have implications for ash slagging and fouling, (James et al., 2012) see Section 3.7.5, Chapter 8 and 10. When biomass has gone through partial combustion, resulting in high carbon content, the carbon will have high relative surface areas. The increased surface areas would provide reaction sites for the potential reduction of NO to N_2 and O_2.(Illan-Gomez et al., 1995a; Illan-Gomez et al., 1995b; Illan-Gomez et al., 1993). The increased reaction sites on the carbon may be instrumental for the current research if a high carbon content is present in the ash.

3.7.4 Reactivity of Ash

The main compounds in coal and biomass ashes have been shown in Sections 3.7.1 and 3.7.2. The oxides were summarised in Tables 3.3 and 3.4, where biomass ashes showed higher levels of alkali and alkaline metals compared to the coals (Tumuluru, 2011). The total reactivity ratio of ashes can be calculated using Equation 3.42.

$$R_{b/a} = \frac{(Fe_2O_3+CaO+MgO+Na_2O+K_2O)\%}{(SiO_2+Al_2O_3+TiO_2)\%} \qquad \text{Eq 3.42}$$

Equation 3.42 uses the known alkaline and acid oxide products in the ash as percentages. This calculation can be used to assist in predicting the potential slagging and fouling potential of a fuel from the ash analysis. When co-combustion of coal and biomass is used, this can also act as an indicator of reactivity, since the basic components, especially alkali metal oxides, can be important catalysts for different reactions increase in reactive alkaline of the biomass. The alkali metal oxides can be important for reactions during combustion.

During combustion, the reactive elements are released during devolatilisation, including hydrogen, potassium, sulphur and chloride. The chloride can combine to form highly corrosive compounds KCl and HCl. When the fuel contains moisture, potassium hydroxide and hydrochloric acid can develop. In the presence of vapour, all of the reactive compounds in equation 3.42 can form alkaline and acids compounds, respectively. (Dayton, 1996; Garba, 2012).

Sections 3.7.1 and 3.7.2 show biomass to have higher percentage weights of alkaline, K, Mg, Na and Ca (Nunes et al., 2016) in the ash. The alkali and alkaline metals may be important in the partitioning of nitrogen during combustion. If the partitioning of nitrogen can be controlled, and released more readily during devolatilisation, then using reactive ashes may be a method of controlling NO_X emissions (Hernandez, 2005; Illan-Gomez et al., 1993). The higher levels of K and Ca are the main focus of investigation in this research, however other reactive compounds and elements may also be significant in the reduction of NO to N_2.

During combustion, secondary reaction pathways are present. The secondary reactions may also continue after combustion has finished. Table 3.5 shows some of the major secondary reactions (Boström, 2012).

Table 3.5 Primary and secondary reaction pathways during and post combustion of biomass ashes (Boström, 2012)

Ash Forming Reactions	
Primary	Secondary
K_2O	$P_2O_5 + 2KOH \leftrightarrow 2KPO_3 + H_2O$
KOH	$SO_3 + 2HOH \leftrightarrow K_2SO_4 + H_2O$
NaOH	$HCl + KOH \leftrightarrow KCl + H_2O$
Na_2O	$SiO_2 + 2KOH \leftrightarrow K_2SiO_3 + H_2O$
CaO	$CO_2 + 2KOH \leftrightarrow K_2CO_3 + H_2O$
MgO	$P_2O_5 + 3CaO \leftrightarrow Ca_3P_2O_8$
P_2O_5	$SO_3 + CaO \leftrightarrow CaSO_4$
SO_2	$2HCl + CaO \leftrightarrow CaCl_2 + H_2O$
SiO_2	$SiO_2 + CaO \leftrightarrow CaSiO_3$
HCl	$CO_2 + CaO \leftrightarrow CaCO_3$
Cl_2	$K_2SiO_3 + CaO \leftrightarrow$ K-Ca-silicates
CO_2	$KCl + SiO_2 + Al_2O_3 \leftrightarrow$ K-Al-silicates + HCl

3.7.5 Co-combustion

Within modern power station, fuel flexible furnaces are being used for the combustion of fossil fuels and biomass. The co-combustion of coal and biomass can be used as a CO_2 reduction mechanism (Priyanto et al., 2016). Biomass has a lower calorific value, so during co-combustion can be used as a mechanism to control temperature within the furnace, however the increased volatile content of biomass, compared to coal can lead to higher temperatures if flame stability is not controlled (Sahu et al., 2014; Gil et al., 2010). Reduced temperatures can be used to reduce NO_X, See section 3.4.5. (Wang, 2009; Sahu et al., 2014; Gil et al., 2010). Coal and biomass also have different combustion characteristics. Bituminous coal has two overlapping combustion phases at 315-615°C. Biomass tends to have two distinct phases; devolatilisation and volatile combustion between 200-360 °C, whilst char combustion occurs between 360-490 °C (Gil et al., 2010). Despite the potential increases in alkaline metals, which may increase slagging and fouling, Section 3.7.4, the reduced heat in the furnace can be used as a method of reducing slagging in a furnace (Arvelakis and Frandsen, 2010). Slagging and fouling issues enhanced by increasing potassium levels in the fuel may be mitigated against by the use of coal ashes, where potassium can be absorbed onto the coal ash surfaces (Liu et al., 2017).

Testing of fuel characteristics during combustion in a large-scale furnace, however is impractical through cost and operational considerations. Even in a pilot scale furnace the cost implications can be prohibitive. (Gil et al., 2010).

Laboratory scale equipment can be used to simulate the conditions found within large scale furnaces. Thermogravimetric analysers (TGA) are used for fuel characterisation and for calculating the kinetic reactivity, see Section 4.8. The TGA provides useful rapid screening to compare combustion characteristics of different fuels. TGA can be used to differentiate between volatile combustion and char combustion phases. The data from the TGA can be used for fundamental analysis between samples under test. (Arenillas, 2004; Rubiera, 2002). A drop tube furnace (DTF) can be used for simulating

the devolatilisation and combustion processes in a furnace. The DTF can be used to create chars for devolatilisation analysis, or for combustion and emissions analysis see Sections 4.4.1 and 4.4.3. The DTF can be used to closely simulate the conditions in a large scale pulverised fuel furnace (PF). (Munir, 2009).

3.8 Chapter summary

Coal forms over millions of years from the degradations and coalification of plant materials, under anoxic conditions. There are a range of coals ranging from high rank anthracite through to lignite. A further grade, peat can be included, however this is not a coal classification. Coal is made of a range of elements, of importance for the formation of NO_X are carbon, hydrogen, oxygen, sulphur and nitrogen. The nitrogen is bound into the coal in heterocyclic formations. There are several functional groups of nitrogen in coal, including, pyrrole, pyridinic and quaternary nitrogen. As the rank of coal increases, so the carbon content increases. An increase in carbon often leads to a reducing of fuel nitrogen.

During combustion there are a range of products including: CO_2, CO, SO_X, NO_X and ash. Within a furnace, the nitrogen is released as part of the combustion process and can form many species of nitrogen compounds, including NH_3 and HCN. Ammonia and hydrogen cyanide are intermediary species for the formation of NO_X. Whilst the formation of NO_X is highly complex, involving thousands of intermediary reaction pathways, there are three principal methods of NO_X formation from combustion: prompt, thermal and fuel NO_X. Prompt and thermal NO_X, are products of nitrogen in the air, supplied for combustion. An important process for NO_X production is the N_2O mechanism, a low temperature (300-2200 K) process of producing NO from atmospheric nitrogen and oxygen. Fuel N accounts for as much as 95% of the NO_X produced during combustion.

To control NO_X emissions, a range of technologies have been employed, including Low NO_X burners to control the stoichiometric ratios in the furnace, fuel and air staging to control the temperature and secondary measures such as SCR and SNCR to reduce the emissions at the exhaust stack.

With the advent of fuel flexible furnaces, co-combustion of coal with biomass has been employed as a method of emissions control for a range of gases. Including NO_X. The combustion of biomass has resulted in ashes that are relatively high in reactive elements, K, Ca, Na and Mg. Within this work there is an exploration of co-combustion of coal with biomass ash. The reactive elements within the biomass ash may present an opportunity to act as a catalyst during co-combustion to reduce NO_X to diatomic nitrogen.

Page intentionally blank

Chapter 4 Experimental Methodology

4.1 Introduction

This chapter explains the equipment, instrumentation, processes and procedures followed in the subsequent experimental chapters. The chapter is broken into the following main sections: overview of the materials under analysis, equipment used for fuel analysis and the procedures followed.

4.2 Materials

Three types of reference coals were selected, Galatia from the US, La Loma from Columbia and Shotton, UK. A further low reactivity coal Ffos-y-fran from the UK was selected for a comparative analysis. Two additives were selected for use with the coals, white wood pulverised fly ash (PFA) and white wood furnace bottom ash (FBA). Both of the ash additives were from the same fuel source, i.e. white wood pellets with ~5 wt. % w/w of wheat, oat and Miscanthus added pre combustion. See Figure 4.1. The additives were from the same combustion cycle within a furnace.

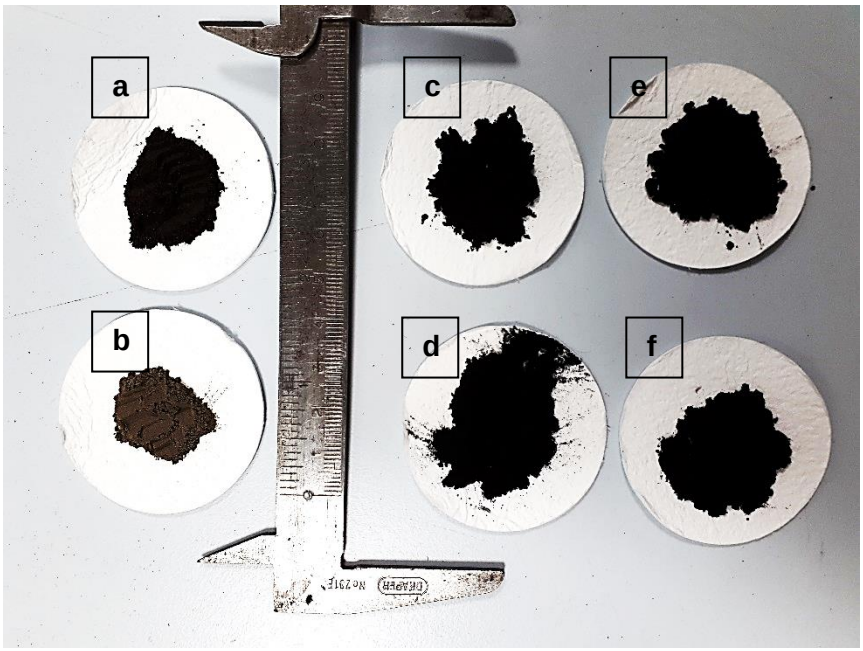

Figure 4.1 Coals and ash additives dried and milled: a. FBA, b. PFA, c. Galatia, d. Shotton, e. Ffos-y-fran, f. La Loma.

A biomass, olive cake from Spain was used to ascertain if the same type of reactions could take place within a high reactivity fuel. A third additive was selected for combining with the olive cake, a coal pulverised fly ash (coal PFA). Figure 4.2.

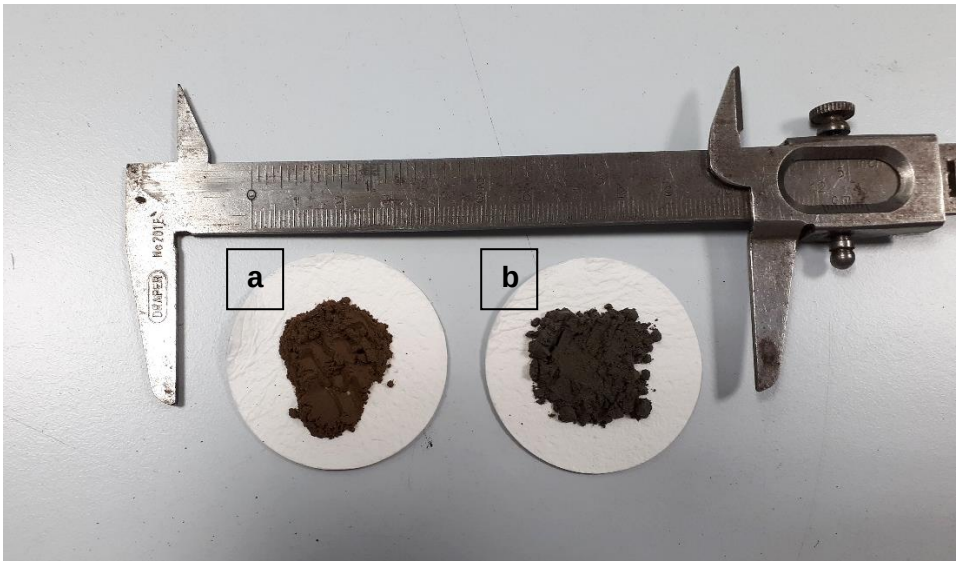

Figure 4.2 Olive cake and additive dried a. Olive cake, b. coal PFA

4.3 Sample preparation

All of the samples were dried, milled and processed for each experimental stage as per the procedures listed in this chapter.

4.3.1 Ball mill

All samples were milled using a Retsch PM 100 ball mill, Figure 4.3. The samples were then separated into size fractions using a Retsch PM 300 sieve shaker. Size fractions taken were 152-212 µm for initial proximate analysis, 75-152 µm for elemental analysis and <75 µm for thermogravimetric analysis (TGA) and drop tube furnace char manufacture.

The La Loma and Shotton were milled as received. Galatia had retained a significant amount of surface moisture, and thus required drying before milling could be carried out. The drying stage was conducted at 80°C for 24 hours prior to milling. The weight of

the sample was taken before and after drying to ascertain the moisture loss. The weight loss of moisture was carried forward for further calculations and included in the proximate analysis, Section 4.5. The FBA also required oven drying before milling due to the amount of moisture retention. The mass loss from drying was again calculated for subsequent proximate calculations, Section 4.5. The PFA and coal PFA were milled as received.

The olive cake required further milling to achieve size fractions of <75 µm, see Section 4.3.3. A Retsch cryo-mill was used to produce the smaller size fractions from the milled samples from the Retsch PM 300 planetary ball mill.

Figure 4.3 Retsch PM 100 ball mill

The ball mill consists of an electronic program controller, a rotating sample crucible with stainless steel balls for mechanical breaking of samples. The crucible is made of stainless steel and has a capacity of 250 mL. There are 15 × 20 mm stainless steel balls within the crucible. The crucible is locked into place mechanically and an electronic safety switch ensures the mill cannot operate if the safety catch is not engaged. The crucible rotates on the sun wheel opposite to the counterbalance weight. The combination of mechanical action and friction breaks the samples into finer particles. A sample was placed in the crucible with the 15 steel balls. The crucible, balls and sample were weighed, and a counterbalance weight was set to hold the equipment stable. Settings of 300 rpm for 2 minute cycles was selected for grinding the samples.

Short time cycles were selected to prevent any build-up of heat. Heat at this stage may cause some devolatilisation.

4.3.2 Retsch AS 200 sieve shaker

The sieve shaker is a vibrating plate on which different mesh size pans were placed, Figure 4.4. A base pan with no mesh was placed on the base with subsequent increasing mesh sizes of 75 µm, 152 µm and 212 µm. A lid was placed on the top to prevent any losses. The pans were clamped into place at the top. The sieve shaker was then programmed to run at a cycle of 80 rpm for 3 minutes residence time to produce homogenous samples at each mesh size.

Figure 4.4 Sieve shaker AS200

4.3.3 Retsch cryo-mill

Due to the less brittle nature of olive cake, compared to coal, finer grade samples were not possible from the ball mill. For the production of finer samples, a Retsch cryo-mill was used, where liquid nitrogen was used to cool the chambers, Figure 4.5. Liquid nitrogen freezes the sample making it more brittle and so easier to break mechanically. The chambers were made of stainless steel and the balls also of stainless-steel

construction. The chambers were filled to two thirds with sample, and stainless-steel balls were added to mechanically break the sample into finer particles.

The mill was pre-programmed to run through a cooling cycle, followed by a milling cycle. After the cycle finished, the chamber was removed and allowed to return to ambient temperature. The sample was placed in a 75 µm sieve, and gently moved around with a brush and passed through the sieve to ensure a homogenous sample of < 75 µm was produced.

Figure 4.5 Retsch Cryo-mill

4.3.4 Sample drying

All four coals, ashes and olive cake were pre-dried to remove surface and residual moisture for use in Section 4.4, char production. Sample particle sizes were <75 µm and 75-152 µm. The samples were weighed and spread evenly across the surface of a plastic tray. The samples were heated in a drying oven for a minimum of 12 hours. The sample containers were heated in the oven over the same period to ensure no moisture was present in the sample tubes.

After drying, the samples were weighed again, and the mass loss recorded for future proximate calculations, Section 4.5. The dried samples were placed in the heated sample containers and stored in a desiccator for future use. See Chapter 5.

4.3.5 Blended samples

To produce the blended samples for each phase of experimental work, individual blended samples were made. The mass of additive to be added was calculated as per Equation 4.1:

$$m_{add} = \frac{m}{(1-\frac{x}{100})} - m \qquad \text{Eq 4.1}$$

Where:

m_{add}=mass of additive to be added (g)

m=mass of coal or olive cake (g)

x=percentage of additive required

4.3.6 Malvern Mastersizer Hydro 2000E

The Mastersizer 2000E was used for measuring the abundance of the relative surface areas of the particles under analysis, Figure 4.6. In practice, a measurement of a few milligrams of sample can be used to make an approximation of the particle size distribution of many tonnes of material, provided the sample preparation is homogeneous and representative of the bulk sample.

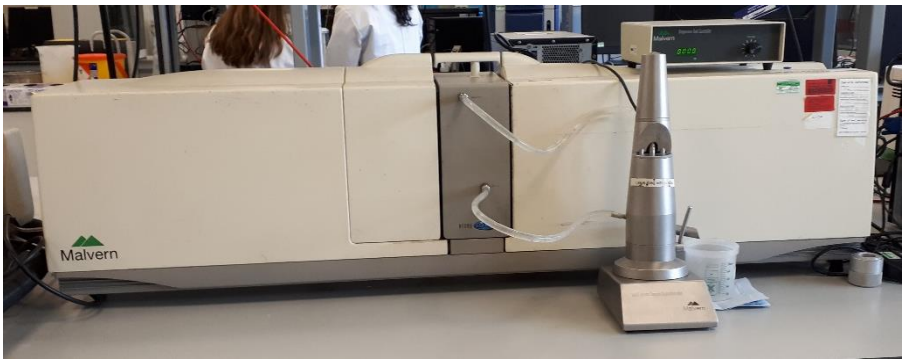

Figure 4.6 Malvern Mastersizer 2000E

The main process utilises Beers Law, Equation 4.2, to calculate the concentration of the particles that are in suspension in a dispersant.

$$\frac{I}{I_0} = e^{-\propto b} \qquad \text{Eq 4.2}$$

I=Intensity of light at distance b in the particle field of absorbance $\propto$.

I_0= Intensity of light beam entering the sampling chamber.

$\frac{I}{I_0}$= Relative transmission T of the beam.

This equation can be rearranged to calculate the absorbance $\propto$, Eq 4.3a:

$$\propto = \frac{-1}{b} Ln\langle T \rangle \qquad \text{Eq 4.3a}$$

The term α incorporates information about the attenuation (scattering and absorption) of the particles under test. The attenuation can be expressed as Equation 4.3b:

$$a = Q\pi r^2 n \qquad \text{Eq 4.3b}$$

Q=Efficiency of light extinction (scattering and absorption)

r =particle radius

n =number of particles

The Mastersizer 2000E operates on a red-light source:

Red Light: Class 111a HeNe gas laser

Maximum output power: 4mW

Beam diameter: 0.63 mm ($1/e^2$)

Beam divergence: 1.5 mrad

Wavelength: 633 nm

The red-light source has a relatively long wavelength, therefore smaller particles may be passed by the waveform with no disturbance. If no disturbance is felt on the

waveform, it will be read as no particle present. To compensate for particles that may be small enough to be missed in the waveform, over 2000 snap shots are taken for each measurement, with an average snapshot taken every 1 ms.

There are a range of detectors in the optical bench, each detector collects scattered light from a narrow range of angles. As a single detector only gives one reading from a narrow angle, all of the detectors take a snapshot and these are added together to create an average measurement. Ten consecutive readings were taken using the above method, and an average summation result was taken across the averaged ten measurements.

The equipment uses Mie theory for calculating the particle sizes (Malvern, 2010). Mie theory allows for particle sizing of 0.1-1000 µm, using the red-light sources in the Malvern 2000E. Mie theory utilises an assumption the particles are spherical, and the reflectance and absorption are known for the particles.

The Mie method is more accurate than the Fraunhofer theory for a greater range of particle sizes dependant on the light source, however is limited for particles that are not spherical (Malvern, 2010). The Fraunhofer theory can be more adaptable for a range of different shaped particles, however it can lead to large errors when the refractive index of the suspension medium and the particles are similar. Mie theory is used to predict the way light is scattered, absorbed or passes through the particles. The reflectance of the material under test is required to gain an accurate measurement from the Mastersizer. Figure 4.7 shows a representation of incident light approaching a particle and some possible routes the light can take.

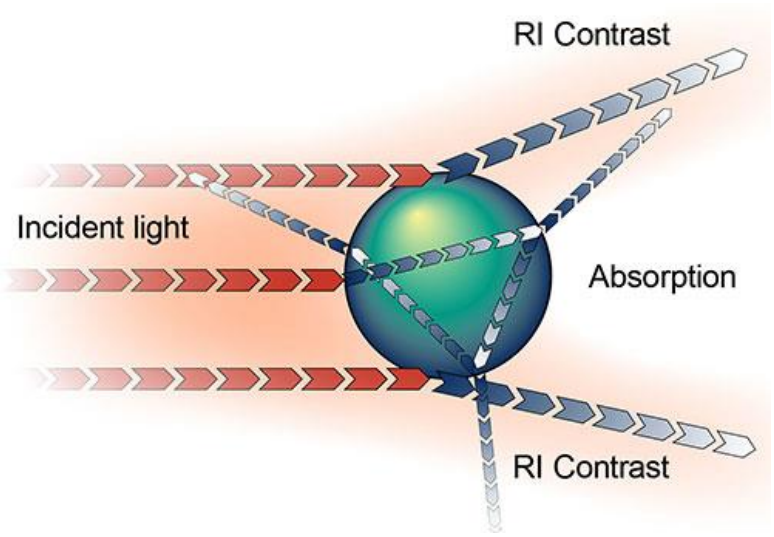

Figure 4.7 Mie theory used for particle size and distribution in the Mastersizer 2000E. (Malvern, 2010) RI= Reflective index contrast, i.e the difference between absorption and scattering.

4.3.7 Mastersizer operation

The auto-sampler and system were initially flushed through with de-ionised water. The water flow was checked to ensure no air bubbles were present. The auto sampler impeller was set to 960 rpm to ensure continuous sample flow past the optical sensor without destruction of the sample.

The dry samples was suspended in de-ionised water (from the same source as used to fill the auto-sampler) and placed in an ultrasonic bath to maintain particle suspension. The software was set to measure the light scattering disturbance of the de-ionised water medium.

Once the disturbance of the de-ionised water was complete, the sample solution was added to the medium slowly. When the obscuration reached between 10-20%, the concentration of sample to medium was in the optimum conditions for analysis. Analysis of each sample was carried out within this obscuration level.

Once the analysis was complete, the data was extracted from the bespoke Mastersizer software as data tables and images of graphs. The data from the Mastersizer is presented in Chapter 5.

4.4 Char preparation

Chars were prepared for analysis using 2 different drop tube furnaces (DTF); University of Leeds, UK (DTF1), Northeastern University, Boston US (DTF2). The chars produced in the DTF's were under high heating rate (HHR) chars, with heating rates of 10^4-10^5 K/s. The chars were used for analysis to determine the effects of different heating regime on the coals with and without both additives (FBA and PFA) and the olive cake and the olive cake with the coal PFA. Proximate and elemental analysis was carried out on the chars with data used for nitrogen partitioning calculations, see Section 4.5, Section 4.6 and Chapter 6.

4.4.1 Drop tube furnace (DTF1), University of Leeds, UK

The DTF1 at the University of Leeds was manufactured by Elite Thermal Systems from a design commissioned by Dr Leilani Darvell. Figure 4.8.

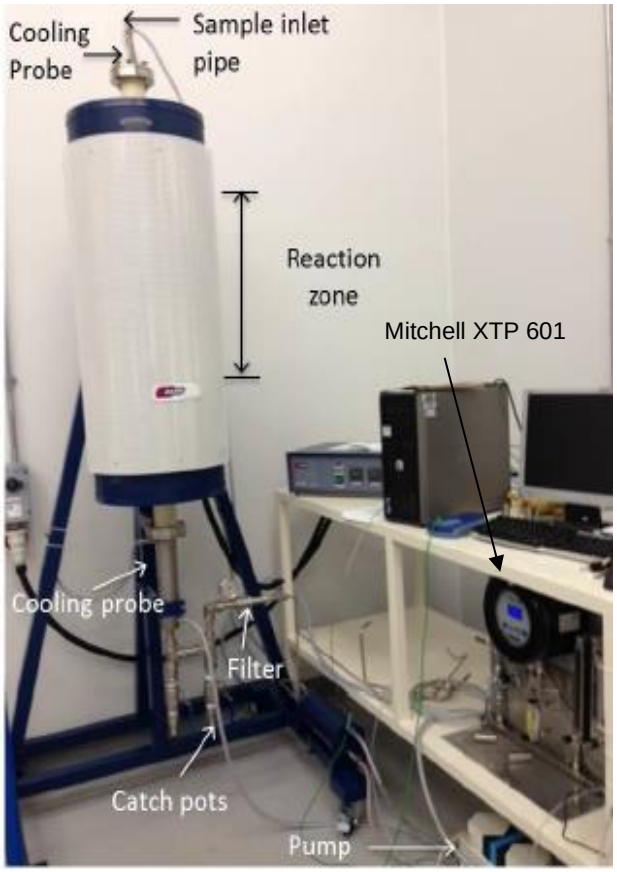

Figure 4.8 DTF1, Elite thermal

DTF1 consists of a manually fed fuel system into a cylindrical combustion zone. The combustion tube is an electrically heated alumina tube 1400 mm long, and 65 mm id. The furnace zone is 1165 mm long, with a reaction zone of 610 mm, with three independent heaters regulated by PID controllers. Contained in the heated reaction zone is a 455 mm isothermal zone, Figure 4.9.

At the top of the furnace is a fuel inlet pipe which directly feeds into the furnace reactor tube. Particles of fuel are fed in through the inlet pipe. Ambient air is drawn in through the fuel inlet pipe. Pure N_2 is fed into the reactor chamber via a manifold, whereby the flow is controlled by a flow meter with a needle valve. The combination of gases are pulled through the reactor tube by a pump at the bottom of the DTF.

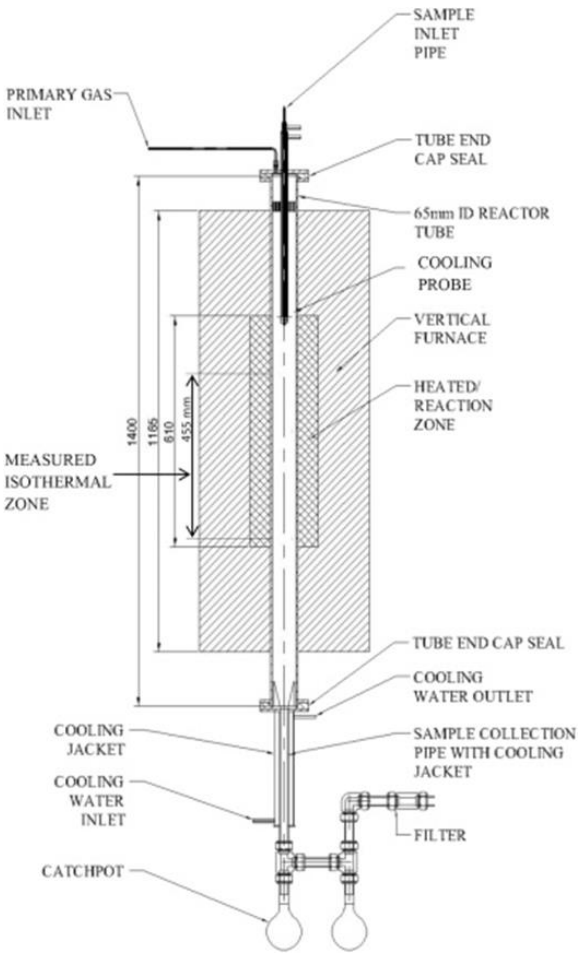

Figure 4.9 Schematic diagram of DTF 1

The nitrogen oxygen ratio and percentages are controlled by controlling the amount of entrained air with a needle valve and monitored with a Mitchell Instruments XTP 601 paramagnetic oxygen analyser, Figure 4.10. A minimum of 300 ml of gas flow is required through the analyser to maintain accurate control of the O_2 flow. The gas flow through the analyser is controlled via a manifold and flow meter. The oxygen content was set between 1-2% ± 0.1 to ensure all tars were converted to gas phase, whilst still retaining the chars of the fuel. The gas analyser was pre-calibrated using laboratory cylinder gas of 5/95% oxygen/nitrogen.

Figure 4.10 Mitchell Instruments XTP 601 paramagnetic oxygen analyser

The inlet and outlet of DTF1 are water cooled. At the outlet are two catchpots, the cooled chars collect in the catchpots. There is a sintered filter in the extraction pipe after the second catch-pot to prevent losses of the chars through the extraction of effluent gases. DTF1 was used for the production of chars from the coals, coals with ash additives, the olive cake with and without coal PFA. The DTF was heated to 1100°C at a heating rate of 10°C/min. Once at 1100°C, the fuels were entered manually at the inlet pipe. Through the reaction zone, the fuels were subject to heating

rates of 10^4-10^5 K/s. The tars and gases were not collected from the DTF. The data from the chars produced from DTF1 is presented in Chapter 6 and Chapter 7.

4.4.2 Calibration and temperature profiles of DTF1

To ascertain the temperature profile of the DTF, a type k thermocouple was inserted in through the inlet pipe. The gas mixture was maintained as a nitrogen atmosphere with 1% ± 0.1 oxygen. Temperature profiles measurements were taken at 15 cm intervals down the reaction tube. Temperatures were measured via a Picolog every second over a one-minute time frame. Average values over the minute were reported and captured in Figure 4.11. The temperature was raised to the operating temperature of 1100°C at a rate of 10°C/min. 1100°C was used for calibration as this is the operating temperature for char creation. The thermocouple measured an average of 1062°C ± 33°C.

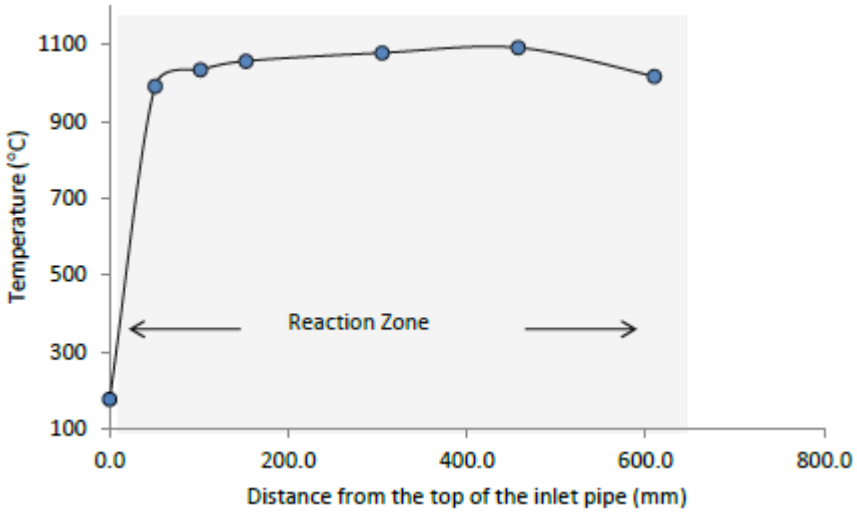

Figure 4.11 Temperature profile for DTF 1 at 1100°C

4.4.3 DTF 2, Northeastern University, USA

The DTF at Northeastern University was used for char production, devolatilisation and combustion analysis. DTF2 was connected to gas analysers for the analysis of the effluent gases during devolatilisation and combustion, see Section 4.4.4.

The DTF used for the pyrolysis and combustion of the fuels and blends (and re-firing of the chars obtained from the pyrolysis experiments) consisted of an electrically heated alumina drop tube manufactured by ATS, Figure 4.12.

Figure 4.12 -DTF 2 with Harvard Apparatus constant speed syringe injection and vibration for fluidisation of the fuel. B-Metered gas supply adjustable for air, N_2, CO_2 or O_2. C-bank of gas analysers CO, CO_2, O_2, NO_x and SO_2.

The reaction area within the DTF has dimensions of 250 mm long and 35 mm id. A test tube with sample was fitted to a Harvard Apparatus constant speed syringe pump. A 1.8 mm id capillary tube was connected to the inlet of the DTF, at the top, and connected to the sample test tube with an airtight bung. When in operation, the sample tube and capillary tube were vibrated to ensure fluidisation and continuous delivery of the sample to the reactor tube. The vibration of the sample and capillary tube is provided by 2 variable 12v, 2000 rpm, 0.5A DC mini vibration motors, Figure 4.13 (Ren et al., 2017).

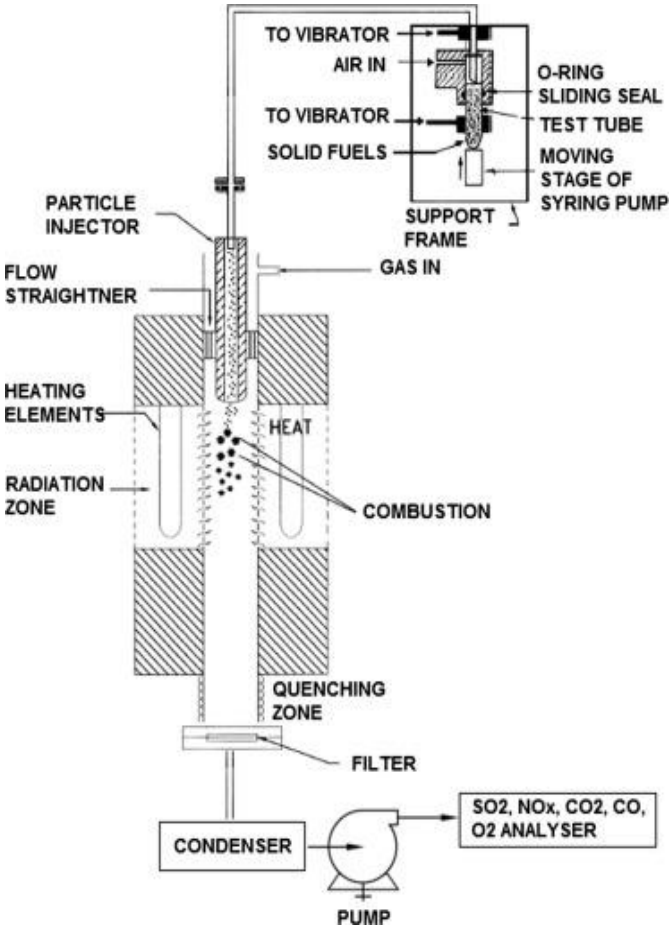

Figure 4.13 Schematic of DTF 2

All samples used in DTF 2 were of size 75-152 µm and dried using the method in Section 4.3.4. Approximately 1.5-2 g of sample was weighed out for each devolatilisation or combustion run in DTF 2. For the blended fuels (coals with FBA or PFA), the coals were pre-weighed at 1.5-2 g, 15% w/w of additive was then added, the blended samples were then mixed until an even colour to the eye was achieved. Each sample, either with or without additives was then transferred to a pre-weighed test tube. The weight of the test tube was taken with the contents to confirm the mass of sample. The samples were delivered into the radiation (reaction) zone in the furnace via the capillary tube. The furnace was set at 1100°C. Through the reaction zone, the fuels were subject to heating rates of 10^4-10^5 K/s. The weight of the test tube was again taken after the fuels were fed through the DTF. The difference between the tube with

fuel and tube after the procedure, was the mass of sample through the reactor tube in the DTF.

Gas was delivered to the top of the furnace at a rate of 4 L/min. The gas was divided before the DTF, 2.5 L/min was fed through the fluidised fuel to entrain it into the DTF via the capillary tube with the sample. The remaining 1.5 L/min, was delivered direct into the DTF via a flow straightener into a concentric area. The DTF was water cooled at the top (fuel and gas input) and at the quenching zone housing the ash or char collection filter as the base of the DTF. The collection filter was a WV 417 paper filter. The effluent gases passed through the collection filter and enter into a condenser. The condenser was immersed in an ice bath. Within the condenser was glass fibre wool. Any residual moisture and tar from the DTF were collected at this point to prevent them being taken into the gas analysis equipment. The effluent gases were also cooled at this stage. The temperature within the DTF was held at 1100°C and monitored by two type-S thermocouples. The centre line temperature is estimated to be 50°C below the temperatures read at the thermocouples. Figure 4.14, shows a calibration curve from work carried out by (Kazanc et al., 2011).

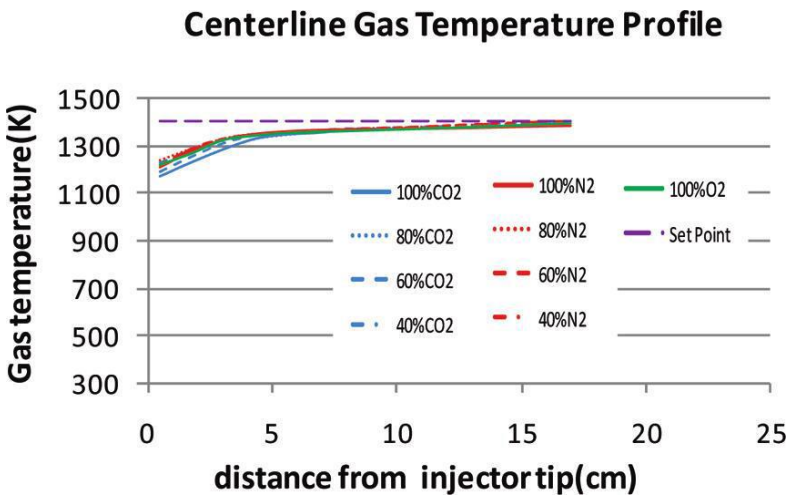

Figure 4.14 Calibration and thermal profile for DTF 2

4.4.4 Effluent gas analysis DTF2

Effluent gases from combustion and pyrolysis was captured and recorded using a range of analysers, Figure 4.12c and Table 4.1:

Table 4.1 Equipment used for effluent gas analysis from DTF2

Gas measured	Model	Equipment
CO_2 and CO	Model 200	California Analytical Instruments
NO_x	Model TH200H	chemiluminescence analyser, Teledyn
SO_2	Model TH100H	UV analyser, Teledyn
O_2	MPA510	Horiba
CO_2	VIA510	Horiba
CO	VIA510	Horiba

To ensure consistency of analysis and consistency in readings, CO and CO_2 were analysed with the California Analytical Instrument and the two separate Horiba instruments. Data was recorded using the above instruments and fed to a PC via a PCI 6221 data card. Data was extracted from Labview and is presented in Chapter 6.

4.4.5 Particle residence time within DTF1 and DTF2

The residence time for a particle within the DTF was calculated using fluid flow through a straight pipe, as the furnace reaction zone is a cylindrical alumina tube. An assumption was made, that the size of the particles were such that they maintain the same velocity as the gas travelling through the tube.

The velocity of flow through the DTF was calculated using Equations 4.4 to 4.8.

$$v = \frac{Q_a}{60\pi(\frac{d}{2})^2} \qquad \text{Eq 4.4}$$

Equation 4.5 was used to calculate the gas flow rate through the pipe at ambient temperature. This is to be converted to the furnace temperature to allow for heating of the gases and samples

$$v_{(T°C)} = v_{(amb)} \times (\frac{T_{sample(K)}}{T_{amb}(K)}) \qquad \text{Eq 4.5}$$

The gas residence time in the furnace can now be calculated using the length of the furnace tube.

$$t = \frac{l}{v_{gas}} \qquad \text{Eq 4.6}$$

The gas residence time needs to be calculated at the centre line velocity. The centre line velocity is twice the mean velocity, due to sheer stresses of the gas on the tube walls (Reynolds, 1901).

$$v_{(cl)} = \frac{l}{(v_{gas} \times 2)} \qquad \text{Eq 4.7}$$

The fuel flow rates through the DTF can be calculated by using the mean gas velocity, delivery time and mass of fuel.

$$flow\ rate = \frac{m(fuel)}{time(\min)} \qquad \text{Eq 4.8}$$

This was used to indicate the fluidisation of the fuel and the amount of time the fuel took to pass through the combustion zone in the DTF. The mean gas velocity was used as the velocity of fuel flow through the combustion zone; therefore the assumption was made that all fuel transited through the combustion zone at the average centre line velocity.

The same calculation process was applied to both DTF1 and DTF2. Data on residence time and flow rates is utilised in Chapters 6 and 7.

4.5 Proximate analysis

Proximate analysis was carried out to establish the moisture, volatile, fixed carbon and ash contents of the fuels and additives. All samples were carried out in duplicate and in accordance with the following standards for the coals: moisture, ISO 11722 BS 1016-104.1:1999; volatiles, ISO 562 BS 1016-104.3:1998; ash, ISO 1171:1997 BS 1016-104.4:1998.

The ash additives were analysed using the above standards. Loss on ignition (LOI) analysis was also carried out on the ash samples using D7348-08.

The proximate analysis for the olive cake was carried out in accordance with. BS EN 14774-3:2009 for the moisture, BS EN 14775:2009 for ash and BS EN 15148:2009 for the volatiles. Average values are reported with associated estimated errors. All of the proximate data, moisture, volatile, fixed carbon ash and loss on ignition is presented in Chapter 5.

4.5.1 Moisture content of coals and additives

Size fractions as stated in Section 4.3, were used for moisture analysis for all of the samples. A number of glass crucibles and lids were pre-dried in an oven at 105°C until a constant weight was achieved. The crucibles were then removed from the oven, allowed to cool to room temperature, in a desiccator until ready to use. Once the crucibles and lids were cool, approximately 1 g of each of the coals and each of the additives was weighed and placed in individual crucibles. This procedure was carried out in duplicate. The samples were dried for 60 minutes in an N_2 atmosphere in a Carbolite MFS oven, Figure 4.15.

Figure 4.15 Carbolite MFS oven

The samples were then removed and the lid replaced on the crucibles and allowed to cool to 30 °C above ambient. The crucibles complete with lid and sample were then placed in a desiccator. Once at room temperature the crucibles were weighed. The

samples were put back in the oven for a further 30 minutes to ensure no change in weight was observed.

$$\omega_M = \frac{m_2 - m_3}{m_2 - m_1} \times 100 \qquad \text{Eq 4.9}$$

Where:

m_1 = the mass of empty dish and cover

m_2 = the mass of dish plus lid and the coal before drying

m_3 = the mass of dish plus lid and the coal after drying

All of the masses are in grams.

The olive cake moisture content was carried out using the same procedure.

4.5.2 Volatile content of the coals and additives

The samples were milled to the size fractions as at Section 4.3, sample preparation. A Carbolite VMF (+PID/CHIM) furnace was heated to 900°C (±5), Figure 4.16.

Figure 4.16 Carbolite VMF 11.18 Furnace Oven

Silica crucibles with lids fitted were placed in the oven for 7 minutes. These were then removed and allowed to return to ambient temperature. The crucibles and lids were then weighed. Approximately 1 gram of sample was placed in each crucible and the lid put back on. The crucibles were put into the furnace at 900°C (±5) for 7 minutes (±5 s). It was established that the temperature returned to a stable 900°C after the cold samples were introduced into the oven. If this was not achieved the samples was to be rejected.

After devolatilisation, the samples were removed from the furnace and allowed to cool to room temperature, and then weighed. The mean of duplicates was recorded. The volatile content was calculated using Equation 4.10.

$$V = \frac{100(m_2 - m_3)}{m_2 - m_1} - M \qquad \text{Eq 4.10}$$

Where:

m_1 = the mass of empty crucible and lid

m_2 = the mass of crucible plus lid and the sample before heating

m_3 = the mass of crucible plus lid and the sample after heating

M = the moisture content as a percentage of mass see section (moisture content)

All masses are in grams.

The volatile content for the Olive cake was carried out using the same procedure.

4.5.3 Ash content of the coals and additives

Samples were prepared as shown in Section 4.3. The porcelain dishes and lids were dried in a preheated Carbolite AAF (+PID/CHIM), Figure 4.17, furnace to 815°C (±10).

The dishes were allowed to cool to room temperature in a desiccator, then weighed. Approximately 1 g of sample was weighed and added to each dish. The dishes with

samples were placed in the oven at room temperature. The furnace was then raised at 10°C/minute up to 500°C and held at this temperature for 30 minutes. A further heating cycle at 10 °C/min up to 815°C was set. The samples were held at to 815°C for 60 minutes. The samples were removed from the furnace and allowed to cool for 10 minutes, then transferred to a desiccator to return to room temperature. When at room temperature, the crucibles complete with samples were weighed. If any signs of carbon was observed, the samples was placed back in the furnace for a further 15 minutes. If any doubt that complete combustion had taken place the samples were reintroduced into the oven for a further 15 minutes, until a change in weight of no more than 1 mg was observed. All samples were carried out in duplicate and a mean value recorded.

$$A = \frac{m_3 - m_1}{m_2 - m_1} \times 100 \qquad \text{Eq 4.11}$$

Where:

m_1 = mass of empty crucible and lid

m_2 = mass of crucible plus lid and the sample before heating

m_3 = mass of crucible plus lid and the sample after heating

All masses are in grams

Figure 4.17 Carbolite AAF 11.18 Furnace Oven

4.5.4 Ash content of the olive cake

The sample size was prepared as shown in Section 4.3, sample preparation. Ash content was carried out in a Carbolite VMF (+PID/CHIM) furnace at 550°C (±10), Figure 4.17. Porcelain dishes were pre-dried in an oven at 105°C until a constant mass was achieved. These were then stored in a desiccator until required. Approximately 1 g of samples was added to each porcelain dish. The dishes with sample were then placed in an oven at room temperature and heated to 250°C at a rate of 7°C/min. The oven was then held at 250°C for 1 hour to ensure the volatile content was expelled from the samples. The oven was then raised to 550°C at a heating rate of 10°C/min. The oven was maintained at 550°C for a further 2 hours. Once completed the dishes with samples were removed and allowed to return to room temperature in a desiccator. Once at room temperature the samples were weighed. If any carbon was suspected the dishes and samples were returned to the oven for a further 15 minutes. All sample analyses were carried out in duplicate and the mean recorded.

$$A = \left(\frac{m_3 - m_2}{m_2 - m_1}\right) \times 100 \times \left(\frac{100}{100 - M}\right) \quad \text{Eq 4.12}$$

Where,

$m1$ = mass of the empty dish (g)

$m2$ = mass of the dish and test portion (g)

$m3$ = mass of the dish and ash (g)

M= moisture content, as a percentage of mass, in the sample being analysed

4.5.5 Loss on ignition

LOI was carried out on samples prepared as in Section 4.3. The oven used for LOI was the same as described in Sections 4.5.3. Duplicate samples were weighed to 1 g. Moisture analysis was carried out on the samples, see section 4.5.1. The samples were loaded into ceramic crucibles. A two-step method was used for the analysis in

accordance with ASTM D7348-08. Where the samples were heated from ambient temperature up to 500°C at a heating rate of 7.5°C/min. The furnace was held at 500°C for 1 hour. The furnace was heated for the second step up to 750°C at a heating rate of 5°C/min. The temperature was held isothermally for 2 hours. The samples were removed from the furnace and allowed to cool to ambient temperature in a desiccator. The samples in their crucibles were weighed. The samples were then returned to the oven for a further hour at 750°C. The weighing process was repeated. If a loss in weight was recorded, the process of a further hour of heating at 950°C was repeated until no further loss of weight was recorded.

$$\mathrm{M} = \left[\left(\frac{\mathrm{W}-\mathrm{C}}{W}\right)\right] \times 100 \qquad \text{Eq 4.13}$$

$$\mathrm{A} = \left(\frac{\mathrm{D}}{W}\right) \times 100 \qquad \text{Eq 4.14}$$

To calculate the LOI:

$$LOI = \left(\frac{W-C-D}{W}\right) \times 100 \qquad \text{Eq 4.15}$$

Where:

A= percentage of ash

C= mass of sample after drying for moisture

D= mass of ash after heating for LOI

LOI= percentage mass lost through test

M= percentage of moisture

W= Mass of test sample

All masses are in grams

4.6 Elemental analysis for the coals and ash additives

Elemental analysis was carried out to calculate the carbon, hydrogen, nitrogen, sulphur and oxygen content of the fuels, ash additives and chars. The CHNS analyses of the coals, ashes and coal chars were conducted using an EA1112 Flash Analyser, Figure 4.18 and in accordance with BS ISO 29541:2010. The furnace tube was cleaned, a clean wad of quartz wool was inserted in the bottom of the reactor tube and the flash analyser was gas leak tested in accordance with standard operating procedures. The furnace was then heated to 900°C. Calibration standards were prepared in tin capsules. The tin capsules were pre-weighed, then approximately 2.5 mg of each standard was prepared from the following: 2, 5-Bis (5-tert-butyl-benzozazol-2-yl) thiophene (B-BOT), atropine, methionine, cysteine and sulphanilamide. An empty tin capsule was also prepared. Between 2.5-3 mg of sample was prepared for each sample and placed in pre-weighed tin capsules. Vanadium pentoxide (V_2O_5) was added to all of the fuels under test and to the B-BOT. As these fuels contain relatively high levels of carbon, the V_2O_5 provided extra oxygen to ensure complete carbon conversion to CO_2. Once the samples were prepared, the capsules were folded closed to remove the air and prevent loss of sample. The data from the elemental analysis is presented in Chapter 5.

Figure 4.18 EA 1112 Elemental analyser

When each sequence of samples was prepared, the standards and sample information was entered into the software. The standards and samples were loaded into the auto-sampler. The blank capsule was loaded first, then the standards, followed by the samples. After each ten samples, a calibration standard was prepared and inserted in the sequence. At the end of the sequence a calibration standard was included.

Sequentially the standards and samples were fed into the reactor tube. Combustion took place in an excess of O_2, with CO_2 and CO produced from the fuel carbon, H_2O from the hydrogen, N_2 and NO_X from the fuel nitrogen and SO_2 and SO_3 from the sulphur. The products of the combustion process were removed from the reactor with a helium carrier. The evolved gases were fed across copper in a reduction tube, which removes any excess oxygen by converting the copper to copper oxide. During the reduction phase (at 650°C), any NO_X was reduced to N_2 and the SO_3 is converted to SO_2. The gases were then passed over copper oxide, where the CO was converted to CO_2. The mixed gases were then analysed in a gas chromatographer (GC) and separated out at different rates for each gas type. Upon leaving the GC, the gases passed over a thermal conductivity detector, where they were detected in the order of N_2, CO_2, H_2O and SO_2. The output from the elemental analyser are presented as a percentage and on an as received bases. The oxygen can be calculated by difference.

4.6.1 Elemental analysis of the olive cake

For the ultimate analysis of the olive cake, BS EN 15104:2011 was followed. The preparation of the samples and standards was the same as for the coals and additives.

4.6.2 Prediction of high heating value (HHV)

The HHV of the individual samples was calculated from the composition of each fuel based on its elemental and proximate analysis. For coal, Equation 4.16 (ASTM, 2012) and for biomass Equation 4.17 (Friedl et al., 2005), the HHV can be calculated on an

as received (ar), dry basis (db) or dry ash free (daf). The DuLong method is calculated from a db only (Eq 4.18) (Nizhou, 2014). With all methods, ar, db, daf can be calculated through extrapolation.

The HHV(ar) for coal can be calculated in MJ's using a formula from Milne et al:

$$\mathrm{HHV\ (MJ)} = 0.341\mathrm{C} + 1.322\mathrm{H} - 0.12 \times \mathrm{O} - 0.12\mathrm{N} + 0.06865S - 0.0153\mathrm{Ash} \quad \text{Eq 4.16}$$

Biomass HHV (ar) can be calculated in kJ's using an equation from Friedl et al:

$$HHV(kJ) = 3.55C^2 - 232C - 2230H + 51.2C \times H + 131N + 20600 \quad \text{Eq 4.17}$$

The ash additives FBA, PFA and coal PFA, HHV (db) can be calculated in kJ's using an equation from DuLong:

$$HHV\ kJ(db) = 333xC(db) + 1442(H(db) - O(db)\ /\ 8) + 93xS(db) \quad \text{Eq 4.18}$$

All of the calculations of HHV are presented in Chapter 5 and utilised in Chapters 6 and 7.

4.7 EA 5000 Low N analyser

To carry out analysis of the nitrogen content of the fuels an alternate method of testing was trialled. The data from this analysis was used to compare against the nitrogen partitioning method, Chapter 6.

An Analytika Jena EA 5000 Elemental Analyser (Low N) was used for nitrogen content analysis, Figure 4.19. The Low N analyser carried out complete combustion of a fuel to analyse the nitrogen content. The process was carried out over two separate stages: devolatilisation and combustion.

Figure 4.19 Analytika Jena EA 5000 elemental analyser

As the data was produced over devolatilisation and combustion, the N split between volatile-N and char-N can be determined. During devolatilisation and combustion, the nitrogen (and other gases) were given off from the samples. The gases were passed through a dryer to remove any moisture. The gases were then passed through each gas type analyser. For this work, only the chemiluminescent NO_X (nitrogen analysis) was used. All effluent gases were then removed through an extraction system.

All samples used in the Low N were of <75 µm. Sample masses of between 2-3 mg was weighed for each coal, coals with ash additives, chars and chars with additives. The samples were weighed on Metzler Toledo scales XPR with accuracy of 0.001 mg. All of the samples were of high carbon content; therefore a test standard was required to confirm correct operation of the analyser. Olive stone was selected as the standard due to the high carbon content. The olive stone standard was analysed first, to ensure there was no drift in the nitrogen analyser. Each sample was loaded into a clean silica boat and sequentially loaded into the solids auto-sampler. The data for all of the samples was entered into the bespoke software. The Low N was set to the operating temperature of 1050°C. The gases selected for devolatilisation and then combustion were argon and oxygen respectively. Argon was selected as it is an inert gas for devolatilisation. The oxygen was used to ensure complete combustion at 1050°C. The temperature was maintained at 1050°C throughout the analysis. A sample was loaded into an external sealed chamber. The combustion chamber was purged with argon gas,

and the sample then loaded into the combustion chamber. The sample was heated in argon to carry out complete pyrolysis. After the flame sensors detect no more NO_X given off from the sample, the gas selection in the sample chamber was changed to oxygen. Once oxygen was selected, complete combustion took place of the remaining char. The analysis process was repeated for the gases given off. When no more combustion product gases were detected, the sample has completed combustion, the silica boat containing the residue ash was removed from the furnace.

Data is taken from the software in the form of a pdf printout and an excel spreadsheet, see Figure 4.20.

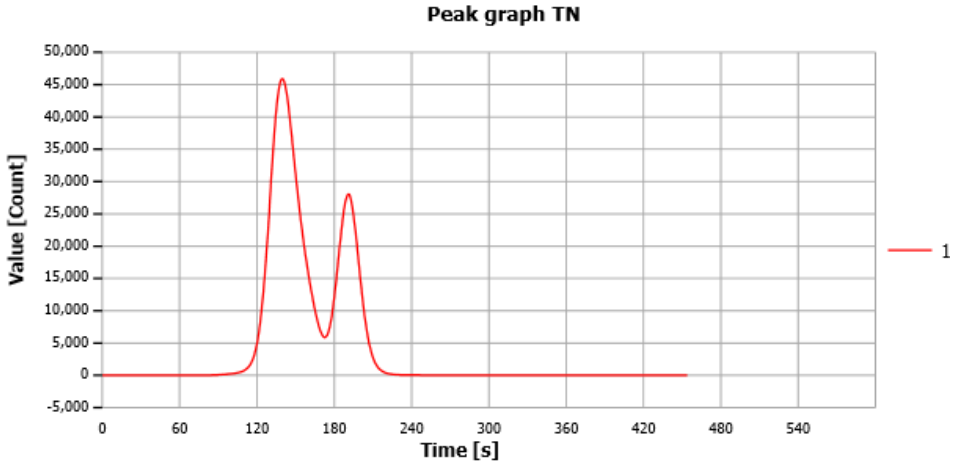

Figure 4.20 Example of a pdf printout from the software for the Low N analyser

4.8 Thermogravimetric analyser (TGA)

A TA Q5000 IR was used for TGA analysis, see Figure 4.21. The TGA was used for two main areas of analysis, isothermal oxidation kinetics and ballistic heating analysis. The TGA could also be used for producing small amounts of char for comparative analysis against other chars produced from alternate methods, see Sections 4.4, DTF1 and DTF2. The TGA was programmed to operate from two gas sources, nitrogen and air, and was programmed via the TA Instruments software for a variety of heating regimes. Four IR halogen lamps were used to facilitate precise controlled heating. Data

analysis was taken from the software and converted into a text document and an excel format.

To carry out any analysis the following processes are extant: the high temperature platinum pans are cleaned with a brush to remove any residual from previous work, the pans are further cleaned in a Bunsen burner to ensure all residue is removed, the pans are tarred on the equipment. Nitrogen is used for devolatilisation and air for combustion. All samples were oven dried as per Section 4.3.4 before analysis.

Figure 4.21 Thermogravimetric Analyser TA Q5000 (IR)

4.8.1 Kinetic evaluation

For kinetic evaluation, the TGA was programmed for the same devolatilisation run for all fuels and fuel with additive blends. A sample was selected from the auto-sampler. Gas 1 (N_2) was selected with a flow rate of 100 mL/min, which was used as an atmosphere within the furnace to prevent contamination of the balance. This flow rate was held isothermally at 50°C for 5 min. The balance flow rate was reduced to 20 mL min^{-1} and held isothermally for a further 5 min. The temperature was then raised at a rate of 10°C/min up to 105°C. The temperature was held at 105°C for 20 minutes to

remove any latent moisture left in the fuel. The temperature was then raised to 1000°C with a heating rate of 10°C/min. The temperature was held isothermally for 30 min, then returned to ambient temperature. The calculation for kinetic evaluation assumes first order kinetics was carried out using Equation 4.19-Equation 4.21.

$$k = \frac{-1}{W_t} \times \frac{dW}{dt} \quad \text{Eq 4.19}$$

Where:

k= Reactivity at time t

W_t= Weight of combustible material at time t (% wt g)

$\frac{dW}{dt}$= slope of the tangent of the curve at time t (5 wt g/s)

$$k = Ae^{-\frac{E_a}{RT}} \quad \text{Eq 4.20}$$

$$lnk = lnA - \frac{E_a}{RT} \quad \text{Eq 4.21}$$

Where:

k = reaction rate constant (cm^3/mol/s)

e = exponential function

A = pre-exponential factor (cm^3/s)

Ea = activation energy (kJ/mol)

R = Universal Gas constant (J/mol K)

T = temperature (Kelvin)

ln = natural logarithm

Using the assumption that the reactivity is 1st order, an Arrhenius plot can be constructed, from the data as the weight loss can be taken from multiple points on the weight loss time curve to calculate the kinetics. Data for the kinetic analysis is

presented in Chapter 5. Figure 4.22 shows a mass loss curve for a coal under low heating rate conditions.

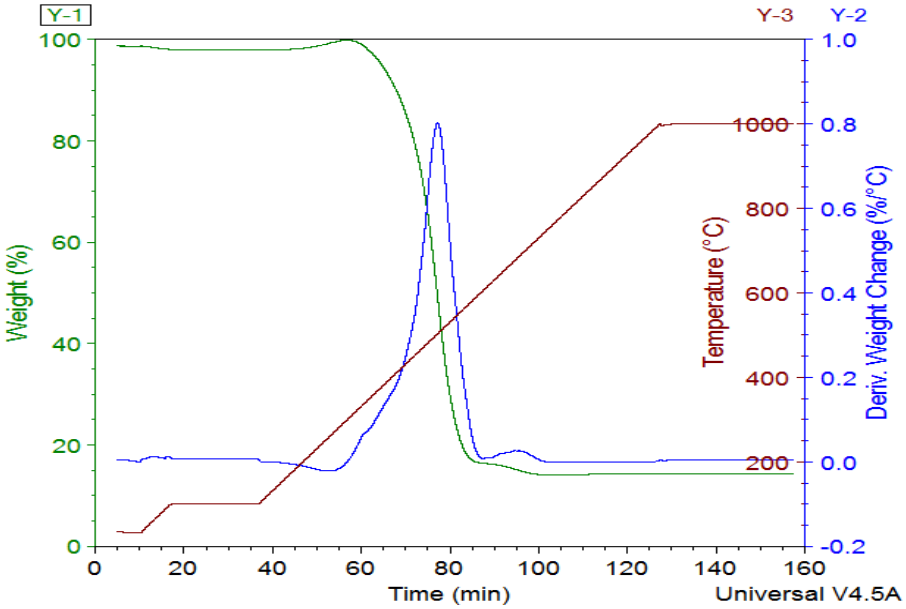

Figure 4.22 TGA mass loss profile for a coal.

4.8.2 Ballistic heating

Ballistic heating can be used as a comparative method for high heating rate volatile yield and high heating rate char production. Samples were loaded from the auto-sampler into the furnace. Gas 1 (N_2) was selected with a flow rate of 100 mL/min, which was used to prevent contamination of the balance. This flow rate was held isothermally at 50°C for 5 min. The balance flow rate was reduced to 50 mL/min and held isothermally for a further 5 min. Temperature was increased to 1000°C, using step function. The step function allowed the furnace to heat up to 1000°C taking ~30 s producing a heating rate of 33°C/sec. Figure 4.23 shows an output from ballistic heating. The data from the ballistic heating is presented in Chapter 6.

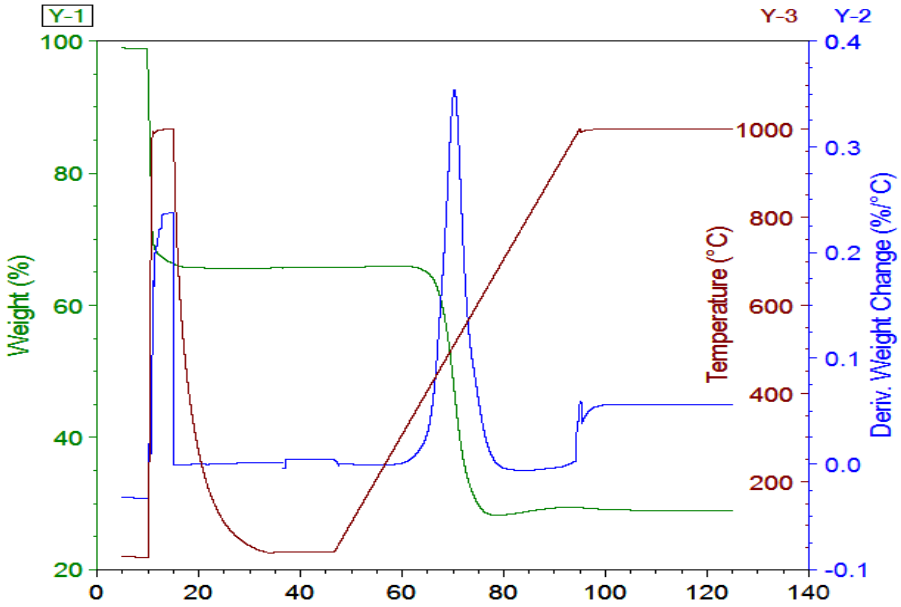

Figure 4.23 TGA plot showing ballistic heating of a sample in the TA Q5000 IR.

4.9 Scanning electron microscope (SEM)

Prior to SEM imaging, a small amount of the fuels and chars (~2mg) were each coated on an adhesive sticker on an aluminium stub. The samples were then spluttered with a gold coating to create a conductive layer across the sample to prevent charging during analysis. A non-conductive surface can build up a static negative charge which interferes during imaging. A Carl Zeiss EVO MA15 SEM was used for the analysis, Figure 4.24. Images of varying magnification were then acquired with an incident electron beam of 20 kV across different segments of the stubs using either secondary electrons or backscattered electrons (described below) to acquire images. During SEM analysis, a beam of electrons was focussed on to the sample within the chamber induced from an electron gun (cathode). The electrons were finely focussed on to the sample using an anode and series of electromagnetic condenser lenses. The electrons then scanned the sample (left to right and up and down) depending on the degree of magnification selected i.e. greater magnification = smaller scanning area. There were two modes of obtaining an image; secondary electrons (SE) or back-scattered electrons (BSE) were released. In the case of the former, when the electron beam hit the sample, the sample absorbed the electrons and gave off its own electrons. The

emitted electrons were attracted to a positively charged faraday cage and then sensed at the detector. The detector then used the information from these electrons to create an image of the sample on a computer monitor. In the case of back-scattered electron imaging, the electrons from the beam hit the sample and were reflected back out of the sample on to a detector attached to the pole piece (above the sample). Back scattered electrons penetrate deeper than secondary electrons. Images from the SEM is presented in Chapters 5 and 7.

Figure 4.24 Carl Zeiss EVO MA15 SEM

4.10 Ion mobility

Ion mobility was carried out to ascertain if the alkali and alkaline earth metals in the additives are able to become mobile in solution. If mobile in solution, then this could be representative of the mobility during devolatilisation and combustion. The ash additives, 5 g of each of FBA, PFA and coal PFA were individually placed in separate conical flasks in 200 ml de-ionised water. A magnetic stirrer was introduced into the solution. The conical flask was placed on a heated magnetic hotplate. The hotplate was set to maintain 100°C with a stir rate of 300 rpm. This was maintained for 1 hr. After the hour, the solution was left to cool and then decanted into a further conical flask through a filter paper to capture the ash solids. This filtered solution was made back up to 200 ml using de-ionised water from the same source. The solids were returned to the first conical flask and 200 ml of de-ionised water was again added, and the cycle repeated.

This process was repeated to gain four consecutive solution samples for each ash type.

The solution samples were analysed via ion chromatography (IC) in a Metrohm 850 Professional IC with an 858 sample processor. The IC column used was a Metrosep C4-100/4.0, with a sample loop of 10 µL. The eluent used was 1.7 mmol HNO_3 and 0.117 g/L of 2, 6-pyridinedicarboxylic acid. Analysis was extracted using MagIC net 3.1 software. Data from ion mobility is presented in Chapter 5.

4.11 X-ray photoelectron spectroscopy (XPS)

XPS is a method of carrying out an analysis of a sample to ascertain the functional groups of elements contained within. The system operates on the photoelectric field effect. The core electrons of an atom have a specific binding energy. When a beam of photons are fired at an atom, and a photon strikes an electrons, the electron is energised and reaches an excited energy state. If it escapes the atom, it is referred to as the photoelectron. The photoelectron will have a specific amount of kinetic energy dependent on the element, see Figure 4.25. Equations 4.22 and 4.23 show the energy calculations for the XPS photoelectron emission.

$$h\nu = Eb + Ek + \phi \qquad \text{Eq 4.22}$$

$$Eb = h\nu - Ek - \phi \qquad \text{Eq 4.23}$$

Where:

$h\nu$ =X-ray photon energy = Kα

Eb=photoelectron energy

Ek =kinetic energy of photoelectron, measured by the energy analyser

ϕ =work function induced by the analyser, about 4~5 eV.

All energy units in this calculation are eV.

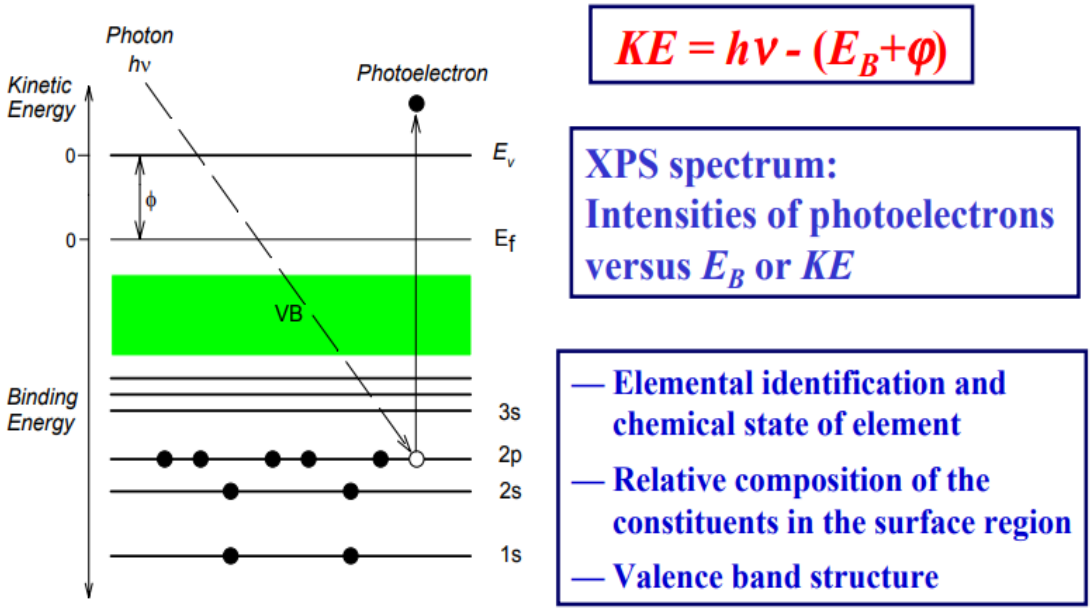

Figure 4.25. Representation of a photon stricking an electron in the 2p shell of an atom, and the photoelectron released as kinetic energy (Smart, 2016)

XPS is a surface scan technique of ~10 nm thickness, therefore there is an assumption made that the surface is representative of the whole sample.

All of the samples for analysis were pre-dried, see Section 4.3.4 sample dying. The samples were mounted onto carbon tape, and then mounted onto metal plates into the Thermo Escalab 250 XPS. The XPS is fitted with a mono-chromated aluminium K-alpha X-ray source, which emits photon energy of hν =1486.6eV. The XPS analysis operates within a vacuum, the chamber was purged for 2 hours to ensure any surface and atmospheric moisture was removed from the chamber.

Analysis was conducted for a variety of elements; however the focus was on the functional groups of nitrogen N 1s (electron configuration) with binding energies between 398-405 eV, see Table 4.2. Figure 4.26 shows the configuration of quaternary nitrogen and refers to Table 4.2.

Table 4.2 Binding energies of nitrogen species. (Wang et al 2012)

Binding energy eV	Nitrogen Species	Reference
398 ±0.3	Pyridinic	N-6
400.2±0.3	Pyrrolic or pyridine and nitroso complex[a]	N-5
403.1± 0.3	Pyridinic N-Oxides	N-X
399.2, 401.4±0.3	Quaternary[b]	N-Q
>405	Nitro type complexes	$-NO_x$

a. Pyridine and nitroso complexes when combined equal the same energy values as Pyrrolic nitrogen
b. Binding energies for quaternary nitrogen A=399.2 eV, B and C=401.4±0.3eV, Figure 4.26.

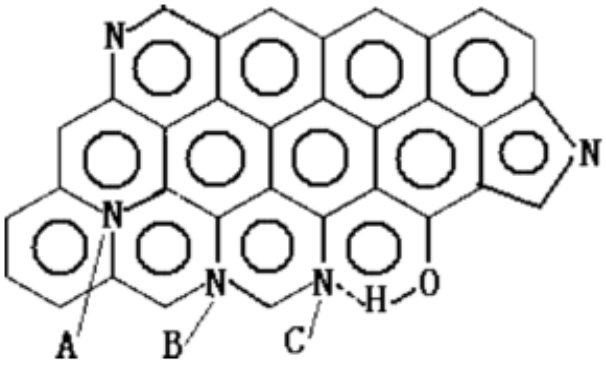

Figure 4.26 The structure or quaternary nitrogen found in coals and their respective chars (Garcia, 1995)

The spot size for the x-ray beam was 500 μm with a power of 150 W. Using 20 eV with step intervals of 0.1 eV, a detailed spectra of each individual peak was taken. To compensate for drift in the spectra, the carbon 1s peak was set to 285eV, see Figure 4.27. Carbon was used for drift correction as it is the most abundant element in the samples. Using CASAXPS software and a de-convoluted Gaussian-Lorentzian fit, the detailed spectra was plotted against a Shirley or linear background. Details of the XPS analysis is shown in Chapters 5 and 7.

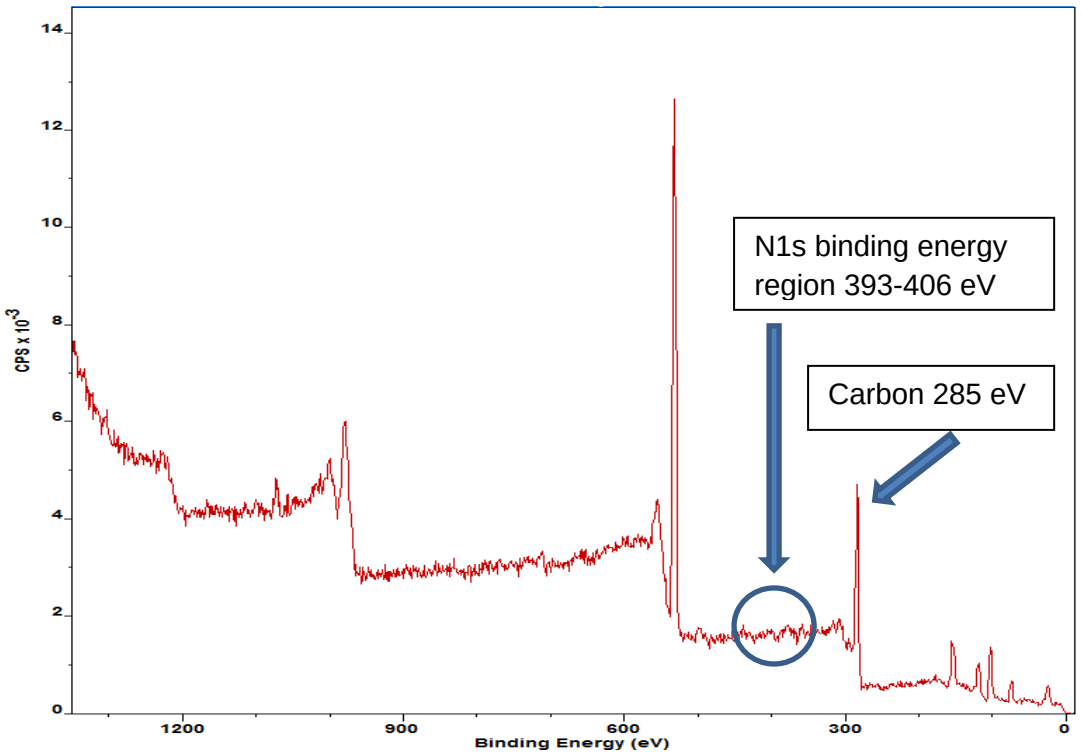

Figure 4.27 Binding energy analysis from an ESCALAB XPS with the N1s region highlighted and the carbon at 285 eV utilised to compensate for time drift.

4.12 Simultaneous thermal analysis-mass spectroscopy (STA-MS)

The STA-MS was used for measuring the reactivity of the chars for the coals and olive cake, with and without additives. The nitrogen species evolution from the char was also measured from the MS.

4.12.1 STA

A Netsch STA 499/QMS403, Figure 4.28, was used to measure char reactivity for the four coal chars with and without additives. The process for calculating the reactivity kinetics was the same as shown in Section 4.8.1, however the measurements were carried out in He and O_2, Section 4.12.3.

Figure 4.28 Netsch STA 499/QMS403

4.12.2 Quadupole MS

The MS element is used to find the mass percentage of a range of emissions given off from the chars during combustion. The emissions that can be calculated from the MS are CO, CO_2, NO, HCN and C_2N. An Aeolos Quadupole is used for the MS data gathering of the gas analysis. Through the use of variable DC and AC voltages through the quadupole, the transition of ions on a mass basis can be controlled for collection at the detector. The gases analysed have different masses, "*m/z 14 (N_2^2+ and CO_2+), m/z 27 (HCN+tail end of m/z 28 signal), m/z 28 (predominantly $^{12}C^{16}O$), m/z 30 (NO +$^{12}C^{18}O$), m/z 43 (HCNO+ tail end of m/z 44 signal), m/z 44 (predominantly $^{12}C^{16}O_2$), m/z 46 (NO_2+$^{12}C^{16}O^{18}O$), and m/z 52 (C_2N_2)*" (Jones et al., 2012). Pure graphite was initially tested as a known standard. From the data collected from the pure graphite analysis, corrections were made to allow for the contributions of C^{12} and O^{18} and corrections to the tail of m/z44, from $^{12}C^{16}O^{18}O$.

4.12.3 Procedure for STA-MS

Duplicate samples of ~5 mg of pure graphite was initially loaded into a crucible for analysis. The product of pure graphite is CO and CO_2, which were used for correction

factors and reference (Darvell LI, 2010; Jones J.M., 1995). The chamber was purged with He gas. Gas levels of 50% He and 30% O_2 was then selected. The input gases realised a 12.5% O_2 value in the combustion chamber. A heating rate of 10 K/min up to 1200°C (1473 K) and held isothermally. The process was repeated for the coal chars with and without ash additives to ascertain the nitrogen evolution from the chars. The results are presented in Chapter 6.

4.13 Chapter summary

To establish the effects of blending biomass ash with coal on the NO_X emissions during combustion, a range of low heating rate and high heating rate techniques were employed.

Low heating rate analysis included: elemental and proximate analysis was carried out on the coals, biomass ashes, olive cake and coal ash. A range of physical characteristics were employed to establish morphology changes to the coal during analysis. Particle size distribution was established for all of the fuels and ashes and SEM microscopy was used to find any physical changes to the coal during pyrolysis, the use of TGA was employed to give small scale representation of a furnace under controlled conditions. From the TGA, mass loss profiles and apparent first order DTG analysis for reaction rates was carried out. Nitrogen functional groups of the coals and chars with and without additives were established using XPS analysis. An analyses of the ashes was carried out to establish the mobility of the cations, K, Na, Ca and Mg.

High heating rate analysis: The TGA was used for ballistic heating of the samples to evaluate any changes to the characteristics under high heating rate conditions. A drop tube furnaces were utilised for the production of chars for further analysis and differential calculations and a second drop tube was used to establish gas emissions from the coal with and without additives. The chars were further analysed using elemental analysis and the use of STA-MS to find the nitrogen species evolution. A

comparative method of nitrogen release from the fuels was carried out using a nitrogen elemental analyser (Low N).

Page intentionally blank

Chapter 5 Fuel characterisation

5.1 Introduction

Through this chapter, the analysis of the coals with and without additives is presented. This will encompass the data from the fuels analyses, including proximate and elemental analyses, reaction kinetics, particle size distribution, XPS nitrogen functional group analysis and SEM images. To understand the potential effects of the two biomass ash additives on the thermal behaviour of the coals, the chemical and physical structures are required for the coals and for the ash additives. The elemental composition of the coals and the ashes is important to understanding: the devolatilisation and char formation during devolatilisation and combustion and the potential reaction pathways for fuel nitrogen evolution.

5.2 Fuel properties

Analysis of the coals and additives was carried out using the methods in Chapter 4.5. The results of the elemental and proximate analysis of the fuels is presented in Table 5.1.

Table 5.1 Elemental and proximate analysis of the fuel and additives

	Ffos-y-fran	Shotton	La Loma	Galatia	FBA	PFA
C[a]	81.9±2.2	86.5±3.7	73.2±2.7	77.3±1.4	93.9±0.23	36.5±0.2
H[a]	3.2±0.2	4.5±0.1	5.3±0.3	5.0±0.06	4.7±0.06	0.6±0.15
N[a]	1.0±0.02	1.9±0.1	1.5±0.04	1.9±0.02	0.3±0.01	0.2±0.01
S[a]	0.8±0.2	1.1±0.01	0.6±0.1	1.2±0.17	0.0±0	0.8±0.04
O[ad]	13.1±2.2	6.0±1.2	19.4±2.3	14.6±1.4	1.0±0.3	61.9±0.14
Vol[b]	8.1±0.14	32.3±0.4	38.8±0.1	40.0±0.12	25.7±1.0	2.9±0.5
FC[a]	87.6±0.77	57.9±0.6	49.1±0.3	49.7±1.6	16.3±1.4	9.4±2.0
Ash[b]	4.3±0.36	9.8±0.1	12.1±0.1	10.3±0.5	58.0±	87.7±1.18
LOI	-	-	-	-	41.4±2.6	12.3±1.2
M[c]	3.9±0.27	7.4±0.2	5.4±0.3	12.4±0.9	2.4±1.2	0.4±0.3
FR	10.8	1.8	1.3	1.2	0.6	3.3
HHV[be]	28.04	31.08	25.79	27.72	15.14	-

a=daf, b=db, c=as received, d=by difference, e=coal HHV-Milne, ash HHV-DuLong. HHV shown as MJ/kg db

The carbon, nitrogen and volatile contents are of particular importance. The carbon content of the ash additives is of interest, as carbon compounds that has been through combustion can have large surface areas. Larger surface areas can act as a reactive substrate for other reactions such as the reduction of NO and NO_2 to N_2. (Illan-Gomez et al., 1995a; Illan-Gomez et al., 1995b; Illan-Gomez et al., 1993). NO and NO_2 can form from the nitrogen and oxygen from either the fuel or from combustion air, Chapter 3.4.1 to 3.4.5. The volatile content can be used as a metric for the partitioning of nitrogen between devolatilisation and retention in char, as nitrogen devolatilisation tends to follow mass volatile release.

5.3 Ash analysis

The ashes of the three bituminous coals and the two ash additives were analysed for their oxide contents. The results of the analysis are shown in Table 5.2. The coal ash analysis shows high proportions of SiO_2, Al_2O_3 and Fe_2O_3, as expected for coal samples.

Table 5.2 Ash analysis of coal and additives

Wt % db	Shotton	La Loma	Galatia	FBA	PFA
SiO_2	46.7	57.3	51.0	52.8	47.4
Al_2O_3	28.0	22.3	19.2	17.4	18.1
TiO_2	1.0	1.1	1.0	0.7	0.8
Fe_2O_3	13.4	7.9	16.6	8.2	5.8
CaO	6.5	3.1	3.9	9.8	11.7
MgO	2.0	1.9	0.9	2.8	3.3
Na_2O	0.4	3.4	0.9	1.2	1.3
K_2O	1.9	1.8	2.4	3.5	5.9
Mn_3O_4	0.0	0.0	0.0	0.4	0.5
P_2O_5	0.0	0.3	0.1	0.9	1.2
SO_3	0.0	2.6	3.8	0.3	0.7

The biomass ashes also exhibit high levels of the oxides of Si, Al and Fe. This was not anticipated for wood biomass ashes. The biomass may have been grown on brown field sites, leading to uptake of heavier elements or the biomass ash was exposed to coal ashes. (Gudka, 2015; Bogush et al., 2018) The second option was the most viable

for these samples. Despite the potential contamination with coal ash, the two biomass ashes still present relatively high levels of the reactive compounds expected, i.e CaO, K_2O, MgO and Na_2O.

The elemental abundance of the four Group 1 and 2 elements and the Fe are shown in Table 5.3. The three bituminous coals show a small mass of each of these elements. The two ashes have relatively high proportions compared to the coals. Of particular importance is the Ca and the K, which in homogenous vapour form have been shown to have potential catalytic effects on the reduction of NO to N_2. (Hernandez, 2005). Zhong et al, has suggested that during heterogeneous reactions in bituminous coals, CaO, CaS and calcined limestone may act as catalysts for the reduction on NO to N_2. (Zhong et al., 2001). Coals impregnated with potassium have also been shown to be promising in SCR systems for NO reduction. (Chen and Gathitu, 2011; Illan-Gomez et al., 1995b; Illán-Gómez et al., 1998). However, K_2O has been shown to act as a poison for SCR, whereby particles of K_2O, which are <5µm can become ingrained on the surface of the catalyst and reduce the effectiveness of the reaction zones (Baxter, 2005; Benson et al., 2005; Larsson et al., 2006). Coal chars impregnated with KOH have also shown a reducing effect on NO emissions, potentially through the reduction of activation energy affecting the NO reaction on the surface of the chars. (Zhong et al., 2001) Recent research of co-firing coals with biomass has indicated a reduction in NO_X may be due to elevated levels of alkali and alkaline earth metals. (Rokni et al., 2018) The Fe_2O_3 has been shown to be a potential catalyst for affecting the formation and reduction of NO to N_2 during heterogeneous combustion when combined with an SCR system. (Daood et al., 2017). Steer et al, has suggested that particle size of the fuels alone is not the only characteristic that affects burnout. Chemical composition and mineral deposition on the surface of ground particles may also be instrumental in the burnout rates of coal. (Steer, 2015).

Table 5.3 Elemental analysis of the coals and ashes (%)

	Shotton	La Loma	Galatia	FBA	PFA
Ca	0.45	0.27	0.29	4.06	7.33
Mg	0.12	0.14	0.06	0.97	1.74
K	0.15	0.18	0.21	1.68	4.29
Na	0.03	0.31	0.07	0.52	0.85
Fe	0.92	0.67	1.20	3.33	3.56

5.4 Ash additive ion mobility

The mobility of the cations is instrumental to the effectiveness of them acting as catalysts for the conversion of NO to elemental nitrogen during coal combustion. To ascertain their mobility, the ashes were dispersed in de-ionised water as described in Chapter 4.10. Table 5.4 and 5.5 show the results of successive washes of the ashes.

The mobility in water is an indication of the potential mobility during the heating process (Shannon and Fine, 1974). The ash additives have been through a combustion process in a large-scale furnace. Oxides are the expected products from the mineral matter when the combustion takes place in air, however other compounds and salts may be present in the ash e.g. $CaCl_2$, KCl, which are soluble in water.

Table 5.4 WW PFA ion mobility as a % of ions in ash

	Wash 1	Wash 2	Wash 3	Wash 4	Total %
Sodium	14.60	9.79	5.60	5.61	35.60
Calcium	10.15	10.64	10.12	8.96	39.87
Potassium	15.25	2.59	1.31	1.46	20.61
Magnesium	1.80	1.69	0.56	1.01	5.06

Table 5.5 WW FBA ion mobility as a % of ions in ash

	Wash 1	Wash 2	Wash 3	Wash 4	Total %
Sodium	7.19	6.13	5.35	4.71	23.37
Calcium	13.40	14.79	10.93	10.82	49.94
Potassium	3.17	2.87	1.97	1.85	9.87
Magnesium	4.12	2.71	2.90	2.11	11.84

From Table 5.4 for the PFA, it can be seen all four of the elements of interest are mobile in the successive washes. The calcium and potassium ions are of particular

interest. The potassium becomes highly mobile during the first wash of the sample. Successive washes show a significant reduction. The calcium shows high levels of mobility across all four of the washes for both PFA and FBA. Calcium in its oxide and chloride state are soluble in water, which is shown across the repeated washes of the samples. The magnesium shows some mobility in the water, but to a lesser extent than the sodium, calcium or potassium in the PFA.

The ion mobility from the FBA in Table 5.5 shows the calcium is again highly mobile across all four of the washes. The potassium ions also show mobility across the four washes, though to a lesser extent than the calcium and sodium. The Mg shows similar trends as the potassium mobility, with proportionally similar amounts of these ions liberated in solution.

The high mobility of the alkali and alkaline elements from both ashes is a good indication the alkali and alkaline earth metals may become readily available to act as catalysts for homogenous reactions during combustion. Since the K and Ca contents in PFA are much higher than in FBA (See Table 5.2), it is expected that there will be a higher availability of catalytic species when using PFA compared to FBA additives.

5.5.1 Coal particle size distribution

All of the samples of coal were processed as shown in Chapter 4.3. The particle size distribution is shown in Figure 5.1. The particle size distribution could be an indication of the applicability of the coal within an industrial furnace mill. If all of the particles are smaller, there is a possibility of greater carbon burnout over a shorter time frame. For the coals that produce a larger range of particle size for the same milling time, then an inconsistent burnout may result in the furnace.

The range of particles for each coal type showed different characteristics. La Loma showing the narrowest particle distribution for sizes ranging from 1-100 µm. La Loma shows a peak between 50-60 µm and no particles below ~2.5 µm. Shotton shows a

wider distribution, with some fines shown as small as 0.25 µm. The peak area for Shotton is centred around 40-50 µm. Galatia shows a similar distribution to Shotton with smaller particles at 0.3 µm and a peak distribution centred at 40-50 µm. A larger fraction of smaller particle sizes may be indicative of potential reactivity through greater surface areas. Ffos-y-fran has a peak distribution of 100 µm. There are no particles shown below 1 µm in Ffos-y-fran.

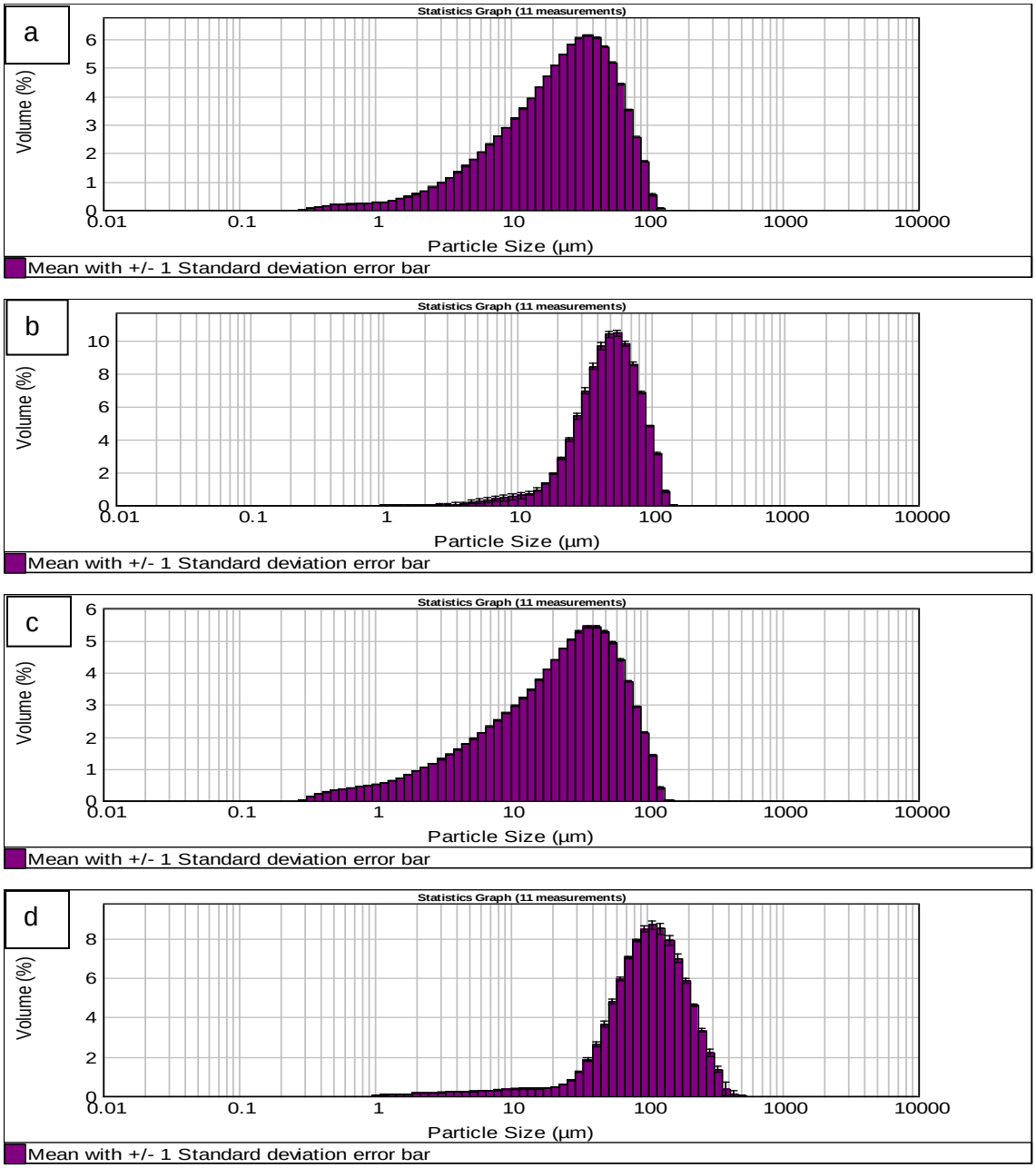

Figure 5.1 Particle size distribution of the four coals. a=Shotton, b=La Loma, c=Galatia, d=Ffos-y-fran

Table 5.6 shows the comparative distribution of particle sizes by percentage value. The values were separated into size groups for use in the slice model, shown in Chapter 8. The particle distribution was separated into size ranges of 0-50 µm, 50-100 µm, 100-150 µm and >150 µm. The data was broken into 4 categories for ease of use in the model, and to reduce computational time. From Table 5.6, the two biomass ashes and the bituminous coals, all show the greatest percentage of particles are <50 µm, with 50-100 µm the second largest group. For the Ffos-y-fran, the distribution is more even, with the 50-100 µm being the largest particle size group.

Table 5.6 Mean particle size distribution for the four coals and two biomass additives

Particle size	0-50µm	50-100 µm	100-150 µm	>150 µm
Ffos-y-fran	16.2	34.06	25.02	24.72
Shotton	71.65	17.18	10.57	0.6
Galatia	55.58	40.41	1.81	2.20
La Loma	81.97	14.06	3.97	0
FBA	68.29	21.58	6.35	3.78
PFA	95.72	4.19	0.09	0

5.5.2 Biomass ashes particle size distribution

The two biomass ashes particle size distribution are shown in Figure 5.2. The FBA has a distribution spread from 0.3 µm up to 800 µm, with a broad peak centred at 40 µm. Conversely, the PFA exhibits two peaks, one in the lower range of 0.7 µm and a second larger % peak at ~15 µm. The greater range, and the larger abundance of smaller particles in the PFA would indicate the potential to act as a catalyst with higher surface areas per mass. From Figures 5.2a and b it can be seen the greatest proportion of particles are in the 0-50 µm range for both of the additives.

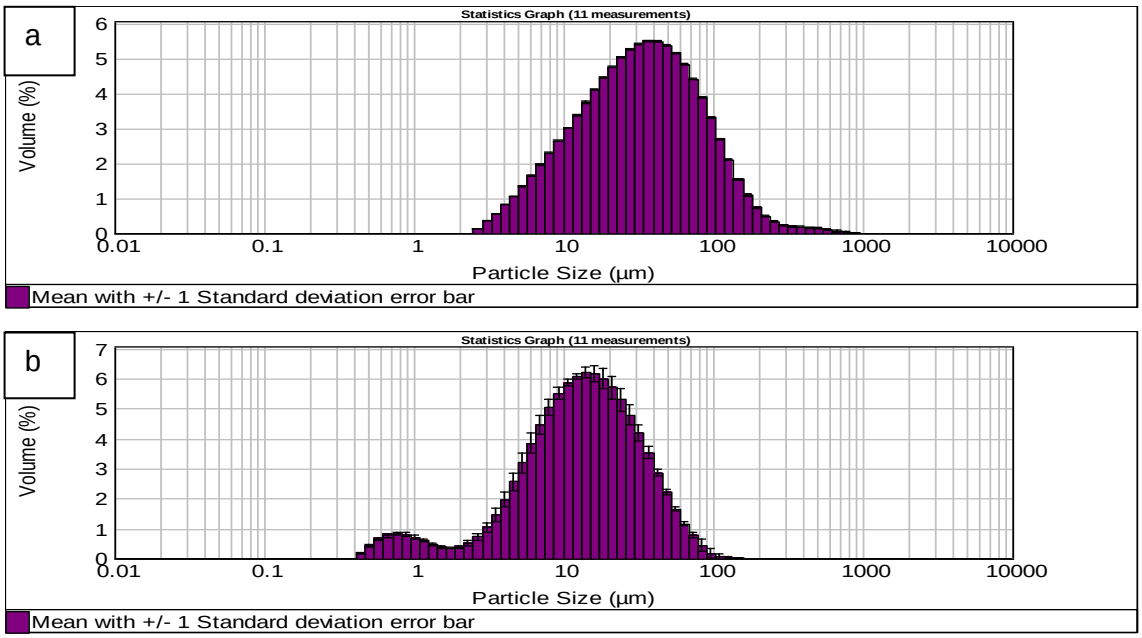

Figure 5.2 Particle size distribution for biomass ashes. a=FBA, b=PFA.

5.5.3 SEM coal images

From the SEM images of the bituminous coals in Figures 5.3, different physical characteristics are shown after grinding despite all coals being processed using the same procedure in Chapter 4.3.

Both La Loma and Galatia show strong cleavage lines, forming distinct clean lines of breakage with few small fines. Shotton has the same larger cleaved particles, however there are also large quantities of fines, shown in Figure 5.3a. The quantities of fines would indicate the coal is more susceptible to fragmentation. Shotton is a blended coal, which may lead to the finer grinding of some of the coal types in the blend. With the larger quantity of fines, the Shotton may be expected to produce larger burnout figures than the other bituminous coals. Steer (Steer, 2015) suggested that different grinding regimes can lead to different burnout characteristics. In this work, the same milling regime was used for all of the coals, therefore burnout is likely to be linked to coal type and particle size rather than the milling process.

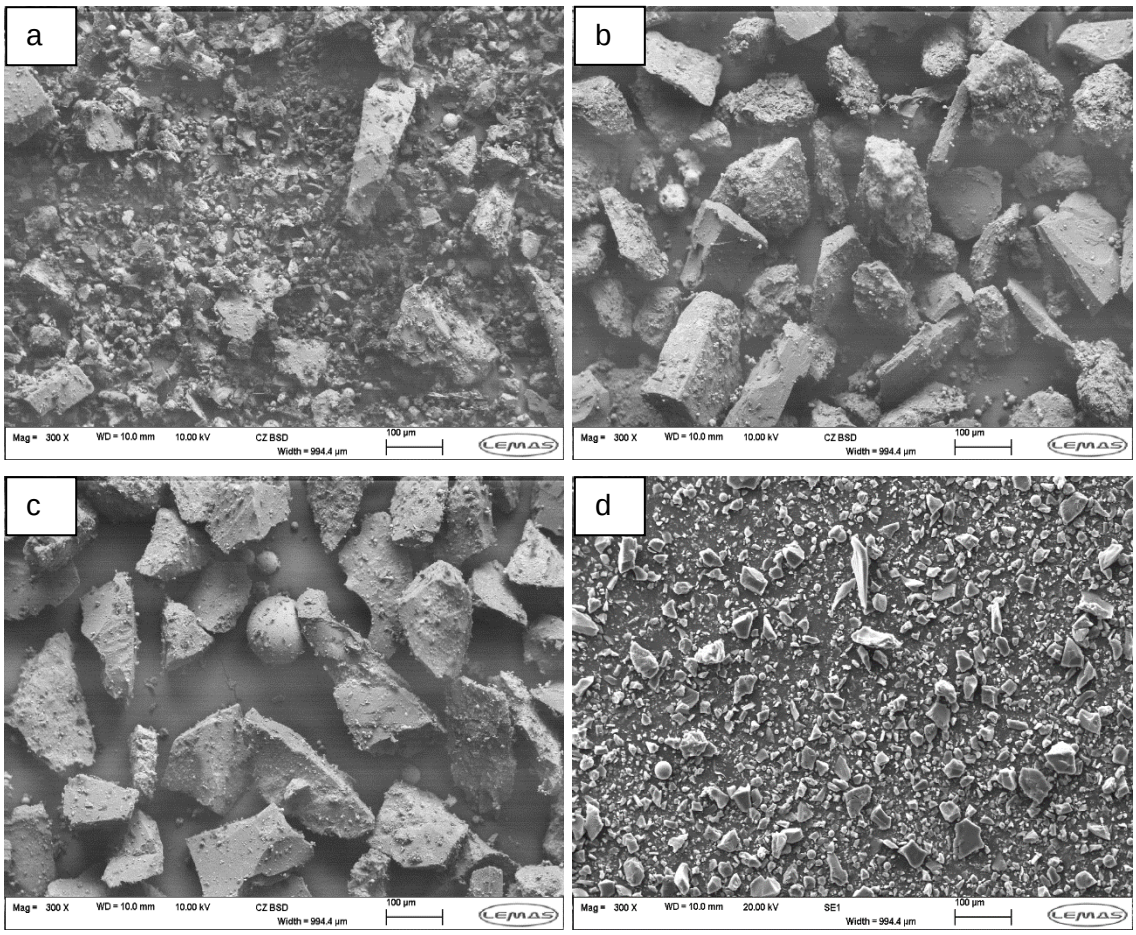

Figure 5.3 SEM images of the four coals at 300x magnification scale bar=100µm, image width=994.4µm. a=Shotton, b=La Loma, c=Galatia, d=Ffos-y-fran

When the particle size distribution graphs are compared against the SEM images, it can be seen that Shotton does have a large array of particle sizes ranging from 2.5 µm through to over 100 µm. The greatest proportion of these are below 30 µm. The Galatia particle size graph shows a similar trend; however, the same distribution is not seen in the SEM images. There are smaller particle sizes present, however not in the same proportions as Shotton. During combustion and devolatilisation, the physical structure of the coals are expected to change. (Cai, 1996; Lester, 1995) SEM images in Chapter 7 is used to show any morphology changes from Figure 5.3. The effects of the catalysts on the devolatilisation of the fuels may become apparent in the coal morphology.

5.5.4 SEM FBA and PFA images

Figure 5.4 a and b show the differences in the morphology of the FBA and PFA respectively. The FBA shows some larger particles which appear to consist of carbonaceous biomass materials. Figure 5.4a shows some material which appears to be lignocellulose. The carbon content in the FBA, Table 5.1, is indicative this is unburnt carbon. There are also spherical mineral ash particles. The PFA shows higher levels of mineral ash particles and more consistent range of particle sizes. These images are consistent with proximate and elemental analysis where the FBA has higher levels of carbon and less ash minerals.

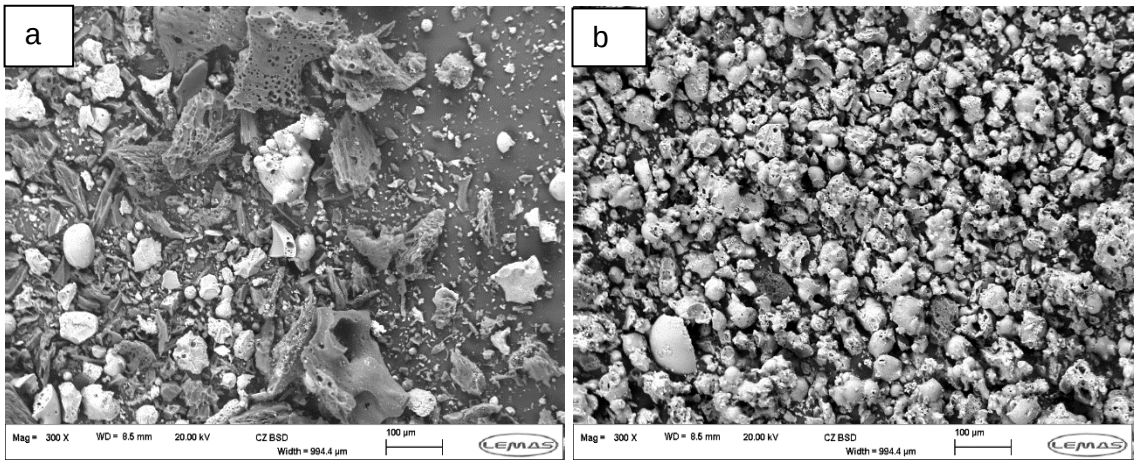

Figure 5.4 SEM images of the biomass additives, 300x magnification scale bar=100µm, image width=994.4µm. a=FBA, b=PFA

5.6 Nitrogen functional groups (XPS)

The nitrogen within the coals form into distinct functional groups: pyridine, pyridinic, pyrrolic and quaternary, see Chapter 3.3.2. The coals were prepared as shown in Chapter 4.3 for the XPS and carried out in accordance with Chapter 4.11. Figure 5.5 shows the four coals and the functional groups contained.

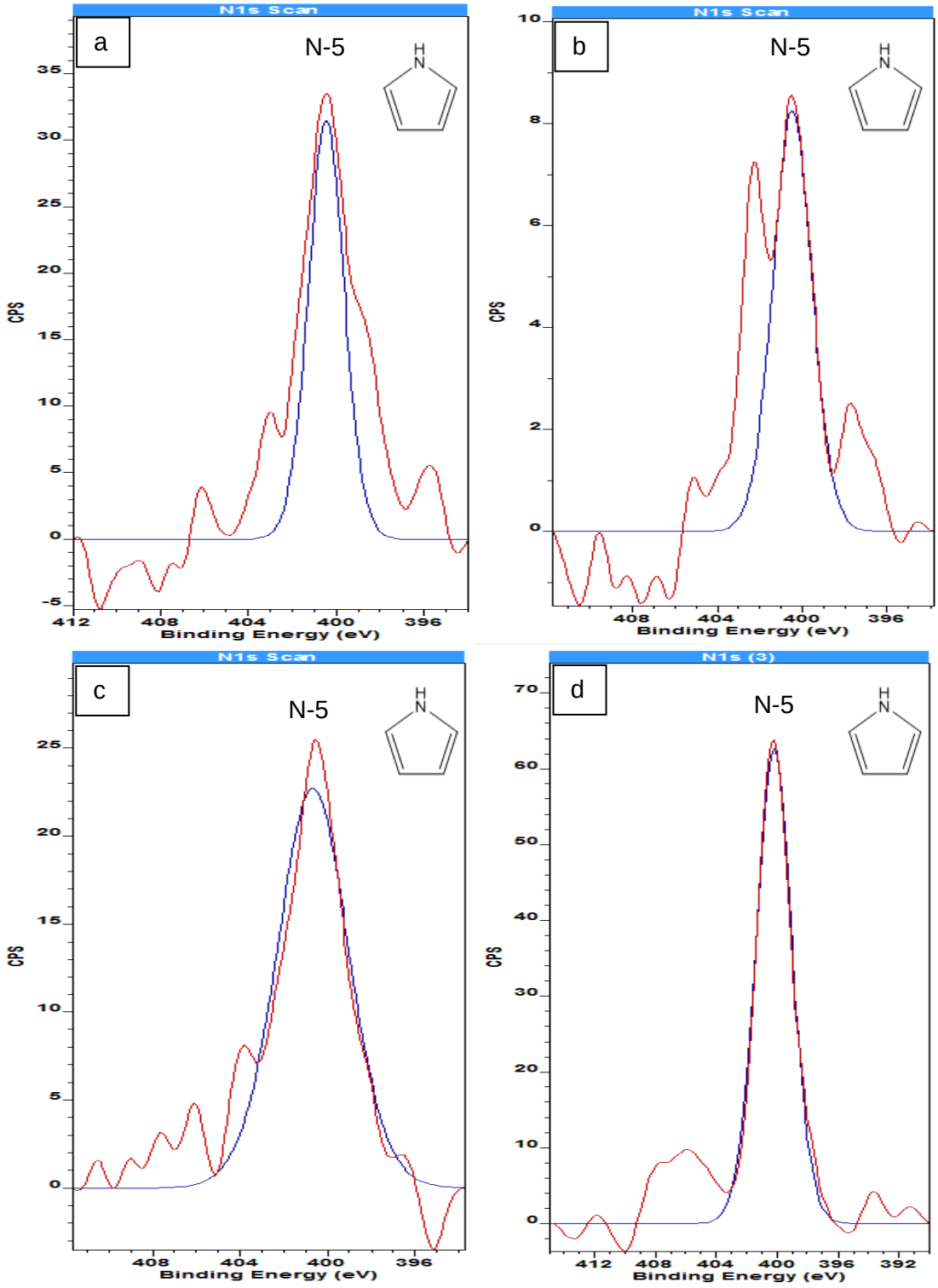

Figure 5.5 N functional groups in the four coals. a=Shotton, b=La Loma, c=Galatia, d=Ffos-y-fran. ——— Functional group, ——— raw data

All four of the coals show a distinct peak for pyrrole, which is consistent with previous findings for coal where 50-80% is pyrrolic (N-5). (Deng, 2008; Gong, 1999; Kambara et al., 1994; Liu, 2001; Woitowicz et al., 1995). Peaks at <403 eV are shown for the Shotton and La Loma, however these peaks do not conform with the correct eV for any

of the N-functional groups, Table 4.2 and Figure 4.25. Table 5.7 and Figure 5.5 show the distribution of functional groups and the percentage value of each functional group. No other nitrogen functional groups were present for the four coals. The lack of other nitrogen functional groups detected, may be a result of the noise present in the raw data signal.

Table 5.7 % functional groups within the coals

Coal	Functional group	% in group
Shotton	Pyrrole	100
La Loma	Pyrrole	100
Galatia	Pyrrole	100
Ffos-y-fran	Pyrrole	100

5.7 FBA and PFA functional groups

The additives FBA and PFA have shown no detected nitrogen functional groups within the XPS profiles, therefore no data is presented.

5.8 Chapter Summary

Throughout this chapter the chemical and physical characteristics of the four coals and the two ash additives have been examined. The proximate and elemental analysis has shown the coals have a range of nitrogen contents ranging from 1-1.9% db; HHV from 25.79-28.04 MJ/kg db; fuel ratios of 1.2-10.8 and volatile contents 8.1-40% db.

The chemical composition of the coal ashes show high levels of SiO_2, Al_2O_3 and Fe_2O_3, with smaller percentages of other oxides, including the alkali and alkaline earth metals. The two ash additives have relatively high levels of K, Ca, Na and Mg, which may act as catalysts for the reduction of NO to N_2, especially since water-washing experiments show that a high fraction of these are expected to be mobile during combustion

The physical characteristics of the coals may be indicators of their behaviour during devolatilisation and combustion. A greater range of smaller particles will potentially yield higher burnout rates. Surface chemistry and mineral composition and deposition on the surface of the coals may also influence burnout.

For the ash additives, the FBA showed particles sizes ranging from 2.5 µm up to 800 µm, although at the larger size they are non-spherical as they have been passed through 75 µm sieves. The structure and composition of the FBA is quite varied with high levels of unburnt carbon and ash particles.

The PFA shows a more consistent range of particles, however there are larger quantities of smaller particles. Fuels or additives with smaller particles tend to be better catalysts due to containing a higher surface area to mass ratio. The composition of the PFA, with higher surface areas and higher percentage masses of alkali and alkaline earth metals would indicate this is a viable catalyst for blending with the coals to illicit changes to the nitrogen partitioning from the coals.

The four coals all show a consistent pattern for the functional groups, with all of the coals under investigation have pyrrole nitrogen as the functional group at 400.3 eV binding energy.

Page intentionally blank

Chapter 6 Devolatilisation

6.1 Introduction

During combustion there are three distinct phases: drying, devolatilisation and char combustion. A fourth phase, gas combustion also happens simultaneously with devolatilisation and before char combustion. All samples under analysis were pre-dried. This chapter focusses on the devolatilisation of the coals and coals blended with ashes. The chapter is divided into two different types of analysis: low heating rate and high heating rate devolatilization/pyrolysis. Changes to the heating rates can yield changes in the results, in particular to the reaction kinetics and volatile yields, therefore all heating rates were maintained. Each of the two heating rates were the same for both types of analysis.

Low heating rate analysis was carried out in the TGA, using a heating rate of 10°C/min. Low heating rate (LHR) data can be used to calculate the reaction kinetics, onset of devolatilization (OD), peak reactivity temperature (PT) and maximum rate of devolatilization (ED). The reaction kinetics were used within the model shown in Chapter 8.

High heating rate (HHR) analysis can be used to simulate the thermal gradients that occur in a furnace. By using high heating rates, the devolatilisation and nitrogen partitioning can be calculated for the coals and coals with additives. The high heating rate analysis was further segregated into TGA, DTF and a comparative analysis using the Low N analysers.

The HHR used in ballistic heating in the TGA were carried out for studying the N-partitioning and to measure high temperature volatile yields (HTVY) for comparison against proximate analysis and against measurements in the DTF.

The DTF analysis was used for the studying of volatile and char yields and for N-partitioning analysis. The char data is presented in Chapter 7.

The Low N analyser was used for assessing of the N partitioning. This method is an alternative evaluation method for attempting to confirm the N partitioning.

6.2 Low heating rates (LHR)

The LHR analysis was carried out in the TGA. The samples were prepared and processed as shown in Chapter 4. LHR analysis was used to find the reaction kinetics, mass loss and dm/dt analysis and proximate analysis.

6.2.1 Evaluation of devolatilisation profiles

The onset of devolatilisation for the four coals shows a trend as the grade of coal increases, so the OD value increases, with La Loma having the lowest value at 554 K, and Ffos-y-fran at 754 K, Table 6.1. The OD can be linked to volatile content and devolatilisation rates, as in the early stages of combustion devolatilisation can occur. The coals with higher volatile content tend to devolatilise more readily. The size of the particles can have an effect on both the devolatilisation and burnout of a coal in a 1 MW furnace. Lower grade coals tend to have a higher burnout, and thus less carbon in the ash than higher grade coals for coals milled to the same size proportions (Barranco et al., 2006). Steer has suggested that dependent on the grinding regime, larger particle sizes can also lead to improved combustion burnout. (Steer, 2015) The grinding regime can change the physical behaviour, devolatilisation and combustion characteristics of the coal particles, leading to the formation of cenospheres, network chars and the swelling properties of the coals. (Steer, 2015). Using blended coals in a TGA/DTG, Su et al (Su et al., 2001) has shown that higher volatile coals tend to have better OD characteristics, whilst higher heating values can produce greater flame stability. Fuel ratio can be used as a guide to carbon burnout for coal blends. (Su et al., 2001).

The inclusion of higher ash and moisture content coals can affect both OD and flame stability through heat diffusion. It has been proposed by Zou, that CaO_2 may act as a catalyst for improved efficiency of coal combustion by lowering the temperature for OD and PT, (Zou, 2016). In this work, the same effect was not observed across all of the coals, however in this work the CaO_2 was not isolated out as a single reactant or catalyst. The combination of potential catalytic alkali and alkaline elements may therefore have conflicting effects on the OD, PT and ED. However, the catalytic species may have an influence under combustion conditions, or under HHR conditions and this is discussed in Chapter 7 and Section 6.3.1 respectively.

Table 6.1 OD, PT and ED for the coals with and without additives (K)

Coal and additives	OD	PT	ED	LHR Vol % (db)
Ffos-y-fran	754	804	878	8.09
Ffos-y-fran plus FBA	702	808	876	10.36
Ffos-y-fran plus PFA	756	806	876	7.06
Shotton	662	739	837	32.31
Shotton plus FBA	641	785	857	31.32
Shotton plus PFA	663	790	867	27.90
La Loma	554	700	814	38.78
La Loma plus FBA	584	736	848	36.82
La Loma plus PFA	579	743	855	33.40
Galatia	643	776	845	40.00
Galatia plus FBA	605	765	857	37.86
Galatia plus PFA	662	826	941	34.43
FBA	545	712	802	25.74
PFA	626	730	901	2.88

Note: LHR vol % (db) is the contribution to the measured volatile yield from the coals alone

The coals when blended with the FBA, show a reduction in OD for all of the coals except La Loma, where an increase is observed. The lowering of the OD for the coals may be due to the higher volatile content of the FBA, which leads to the FBA showing an OD of 545 K. La Loma had the highest volatile content of the coals, therefore the effects of the volatile content of the FBA showed an increase in OD. The PFA has an OD of 626 K. Increases in OD were observed across all of the coals blended with PFA. The peak mass loss temperatures show a similar trend across all of the coals with and

without additives, with La Loma having the lowest peak temperature (PT), and Ffos-y-fran the highest, with Galatia and Shotton being comparable.

The ED temperature has been assigned to the point where mass loss is equivalent to 1%/min (~0.1 %/K) and decreasing. (Cumming, 1982; Unsworth, 1991). Complete devolatilisation is achieved at 800-878 K across all of the coals with and without additives. The exception is Galatia blended with PFA, where an increase to the ED is recorded (941 K), Table 6.1.

6.2.2 Pyrolysis behaviour of coals with and without additives

The coals and coals blended with additives were prepared as per Chapter 4.8.1 for analysis with the TGA. The displayed results for the blends were normalised to allow for the mass of the additives compared to the coals without additives. Percentage mass loss profiles were taken for all of the coals and coal and additive blends. Figures 6.1 show the derivative mass loss/temperature (dm/dt) curves for each coal compared to the coals with additives.

Data for the OD, PT and ED are presented in Table 6.1 The pyrolysis information can provide information on the effects of the ashes in the coals in an LHR environment. From all four coal dm/dt curves, both additives have reduced the peak mass loss for all of the coals. The PFA showed the greatest change of the two additives across all of the four coals.

All four of the coals show the same characteristics of small amounts of moisture loss, chemisorption and devolatilisation. Figure 6.1 show dm/dt curves for the four coals. From the dm/dt curves it can be seen the higher carbon content fuels tend towards higher peak temperatures PT and ED. The lower volatile content of the low reactivity coal is also represented by the higher OD temperature.

When the coals were blended with the additives, a distinct change in the dm/dt curves can be seen. When the FBA is blended with the coals, a distinct bump is observed at

~630 K. The FBA has retained ~25.7% (daf) volatiles. The volatiles from the FBA is released at this point, which helps to accelerate the onset of devolatilisation for the coals.

The PFA has a much lower value of volatiles ~3% (daf). The coals when blended with the PFA do not show the same onset of devolatilisation but dm/dt curves tends to follow those of the coals without additives mass loss curves across all of the four coals.

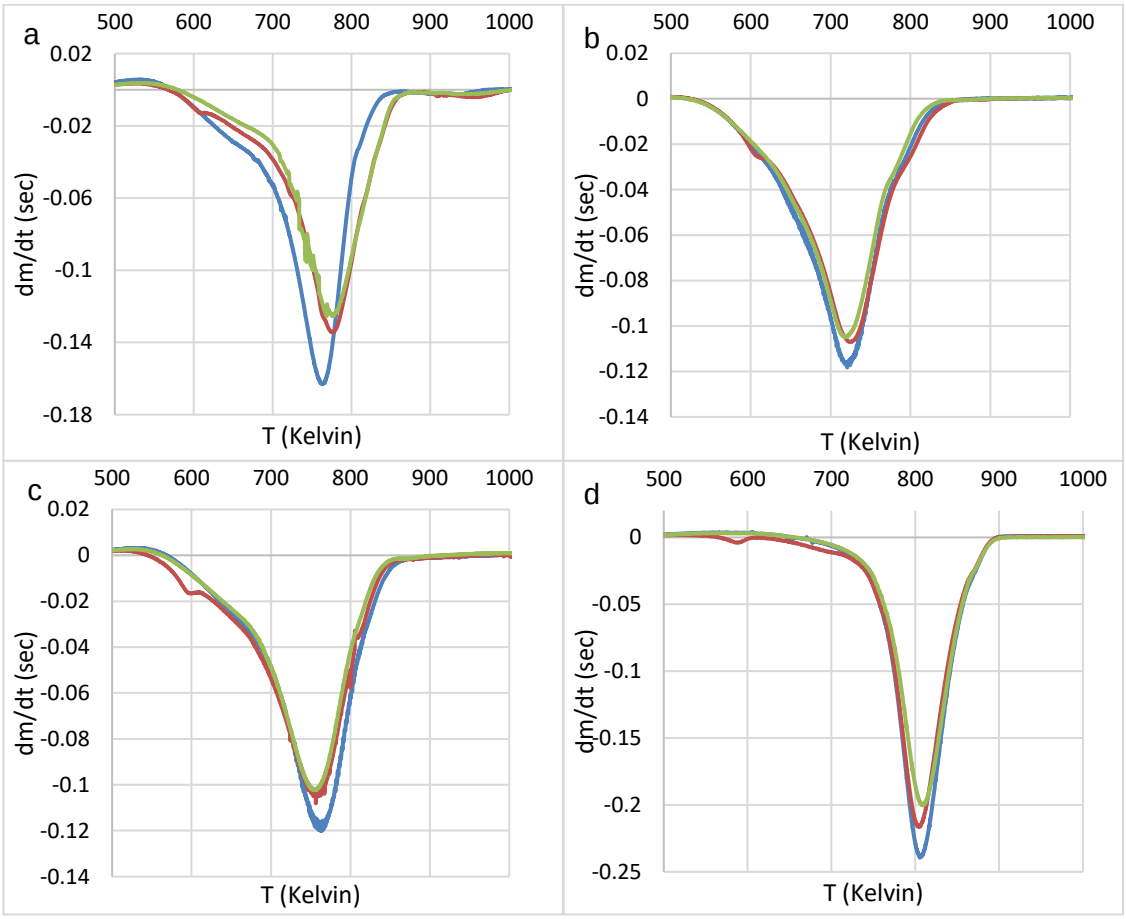

Figure 6.1 dm/dt for the four coals with and without additives a. Shotton, b. La Loma, c. Galatia, d. ffos-y-fran. — coal, — coal plus FBA, — coal plus PFA

6.2.3 Coal reactivity

When the reactivity of the coals and coals blended with additives are compared, there is a marked change in the reactivity. Figure 6.2 shows the data for Ln k and 1000/T, using Equations 4.19-4.21.

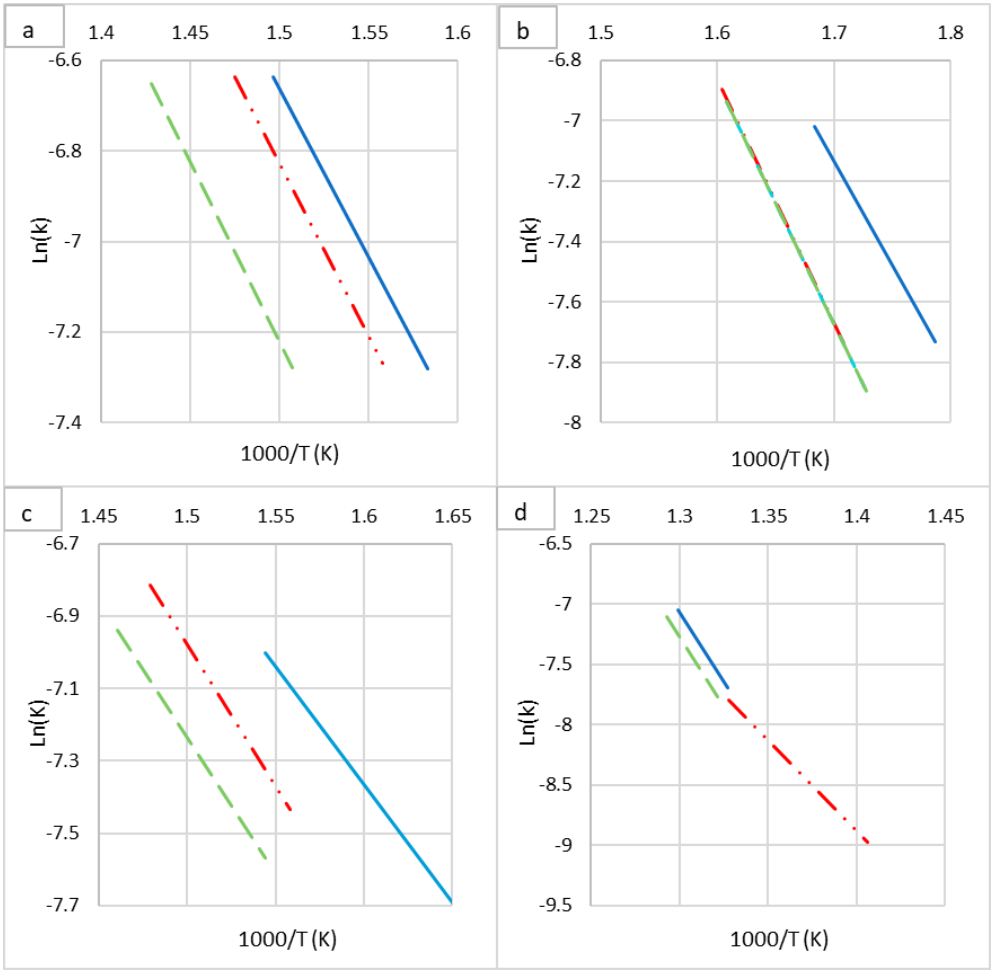

Figure 6.2 Kinetic parameter for the four coals with and without additives a. Shotton, b. La Loma, c. Galatia, d. ffos-y-fran.—— coal, —— coal plus FBA, —— coal plus PFA When blended with the FBA, all of the coals show a change in the reactivity values.

In general, the reaction rate constants (calculated for the start of devolatilisation) of La

Loma samples were faster than those of Galatia and Shotton, see Table 6.2.

Table 6.2 Kinetic parameters of coal and coal/ash blends

Sample	E_a (kJ/mol)	A (cm^3/s)	k_{630K}/s
Ffos-y-fran	194.755	1.55E+10	1.03E-06
Ffos-y-fran plus FBA	107.88	99599.01	1.35E-05
Ffos-y-fran plus PFA	182.81	6.34E+10	1.36E-06
Shotton	61.85	90.55	6.68E-04
Shotton plus FBA	68.6	181.1	3.90E-04
Shotton plus PFA	61.7	61.25	4.19E-04
La Loma	58.95	144.3	1.74E-03
La Loma plus FBA	47.1	13.65	1.30E-03
La Loma plus PFA	58.65	138.3	1.57E-03
Galatia	65.35	112.4	4.38E-04
Galatia plus FBA	70.45	233.45	3.33E-04
Galatia plus PFA	65.35	180.25	2.89E-04

From Figure 6.2 it is clear that the additives are inhibiting the devolatilization steps under these conditions. The FBA sample increased the activation energy of devolatilisation of Galatia. These higher Ea values also resulted in slower reaction rate constants than that of the coal alone- these results are consistent with the peak temperatures observed, Table 6.2.

Overall, the addition of ash appeared either to decrease or to at least have no noticeable effect on the reactivity of all three coals, perhaps with the exception of FBA for La Loma, and possibly PFA for the Galatia coal.

6.3.1 HHR volatile yields

It is well known that under conditions of HHR and high temperature the volatile yields increase due to the rapid cracking of the coal matrix which releases volatiles before they re-polymerise to form char (Kambara et al., 1994). It was of interest to compare the results in this work to previous data, to see if similar trends were followed. The four coals, when plotted against data collated by King fall along the trend line, y 1.5x as shown in Fig. 6.3 (King, 2016).

The low reactivity Ffos-y-fran sits to the left on the graph. The three bituminous coals all sit close together between 50 and 60% total high temperature volatile yields (daf). Thus, the coals are behaving as would be expected under these conditions. The biomass data point is close to the y=x (dotted) line. In the presence of the additives the high heating rate volatile yields generally increase relative to the proximate volatile yield, although many of the data points are still within the scatter of data from previous work. The results for olive cake showed that the addition of the coal PFA results in an increase in high temperature volatile yield, while proximate volatile yield is virtually unchanged. Ffos-y-fran data indicates that, when the additives are present, the high temperature volatile yield is increased significantly compared to the change in proximate volatile content. This shows that (i) the lower volatile coals are affected more by the additives than the more reactive coals (ii) the additives are more effective at

enhancing volatile yield at high temperatures and heating rates than they are under conditions of proximate analysis.

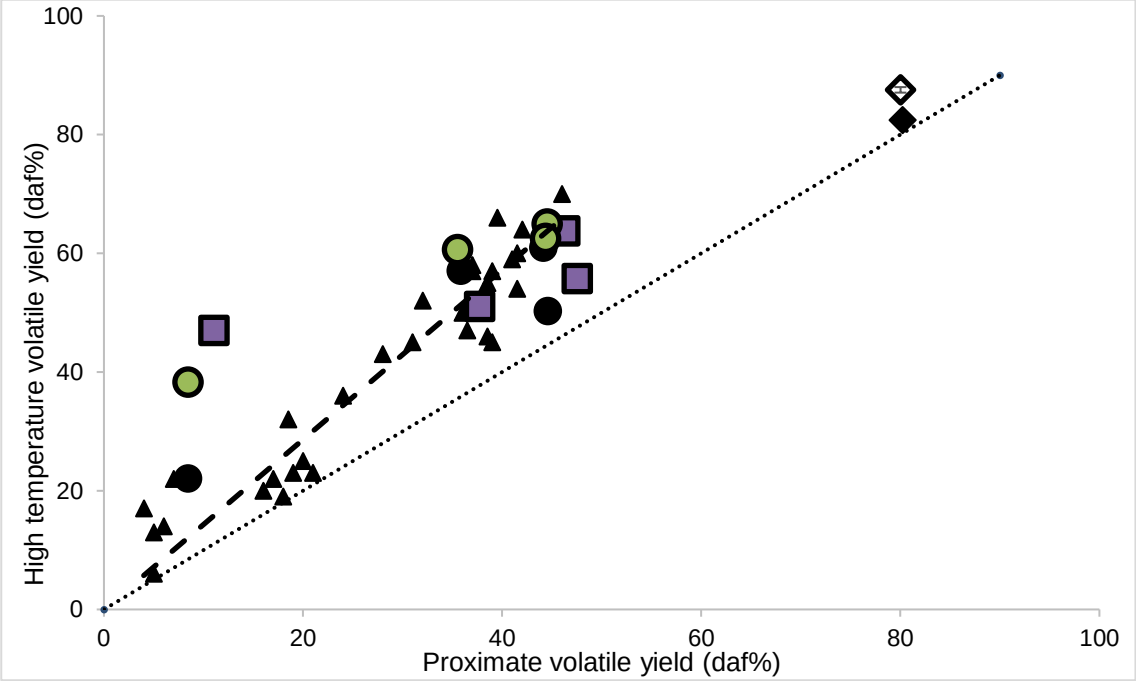

Figure 6.3 Comparison of high temperature volatile yield and proximate volatile content DT1. Symbols: ● Coals, ● Coals+PFA, ■ Coals+FBA, ♦ olive cake, ◇ olive cake plus coal PFA. ▲ Data from King, with dashes line. (King, 2016). The dotted line is the 1:1 reference line.

Chars from DTF1 were collected and analysed for proximate and ultimate analysis. The burnout (%) is calculated using the ash tracer method, which assumes no loss of metals and ash species through devolatilisation, as given in Equation. 6.1 (Steer, 2015).

$$Burnout\ (\%)\ =\ (A_1 - A_0)10^4\ /A_1\ (100 -\ A_0) \qquad \text{Eq 6.1}$$

Where:

A_0 is the ash content of the coal (%)

A_1 is the ash content of the char (%)

The carbon conversion for the fuels during devolatilisation in 1–2% O_2 at 1373 K is given in Figure 6.4.

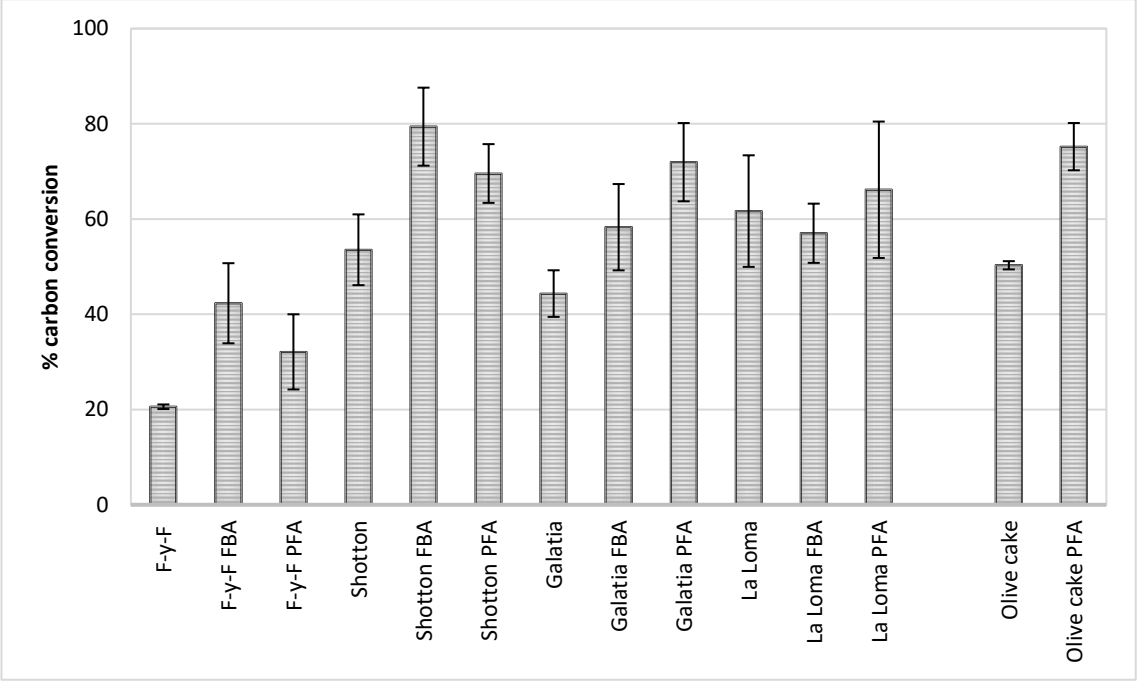

Figure 6.4. Carbon conversion of the fuels and fuels with additives during devolatilisation at 1373 K in DTF1.

The level of conversion ranged from ~20% for Ffos-y-fran to 62% for La Loma. A very interesting effect is observed in the presence of both of the additives, where there is a very large increase in carbon conversion- with the exception of La Loma. For example, conversion reaches to over 80% for Shotton when co-fed with FBA, and over 70% for Galatia when co-fed with PFA. A similar trend is observed for all coals, and for the olive cake when co-fed with coal PFA, Figure 6.5.

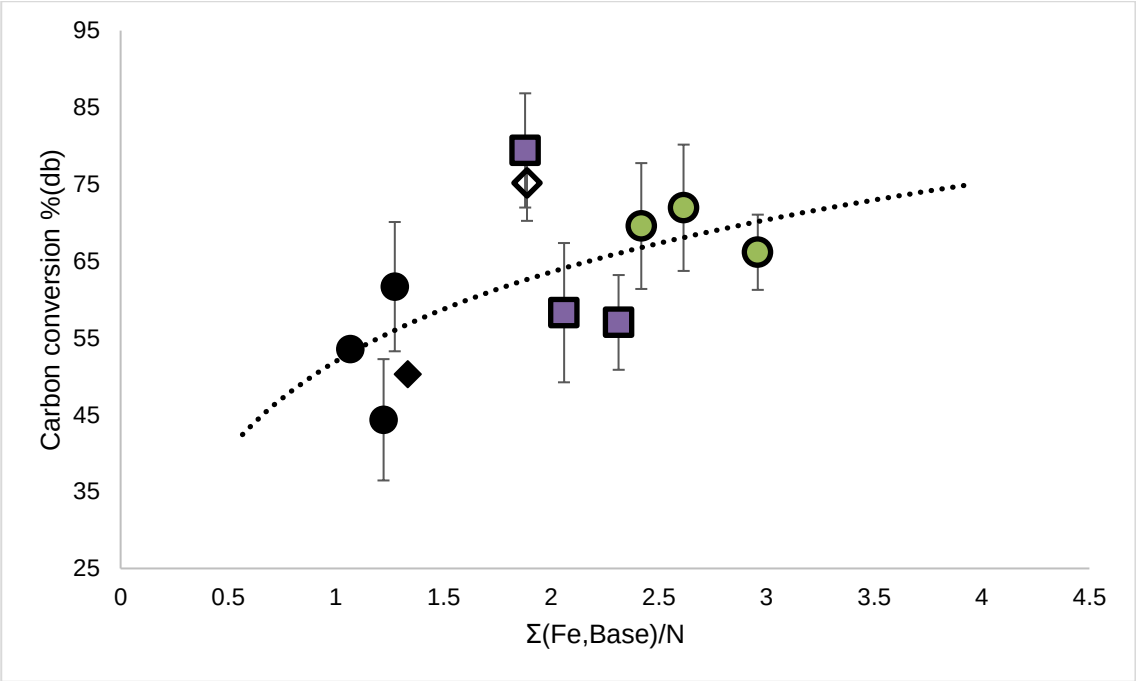

Figure 6.5 Carbon conversion (DTF) as a function of mass ratio of alkali and alkaline earth metals to N-content of the feed, Σ(basic components in the feed)/N. Symbols: ● Coals, ● Coals+PFA, ■ Coals+FBA, ♦ olive cake, ◇ olive cake plus coal PFA.

6.3.2 HHR volatile-N release (TGA)

Figure 6.6 shows the results of HHR volatile nitrogen release from TGA (ballistic heating), compared to total volatiles (daf) measured by the proximate method.

The coals under test were plotted against the trend line for previous published data from heated wire-mesh reactor experiments which have higher heating rates, and shorter residence time compared to the TGA (Gibbins, 1995). Results from the current work for N-partitioning from pure coals and biomass fall along the 1:1 relationship, with HHR volatile nitrogen release in the range 8–45% for the coals and 85 % for the olive cake. Thus for the most part volatile nitrogen release follow total volatiles, and there is a concentration of nitrogen in the char for the low volatile content coal. This is why there is a well-known relationship between NOx and FR (Mitchell, 1998).

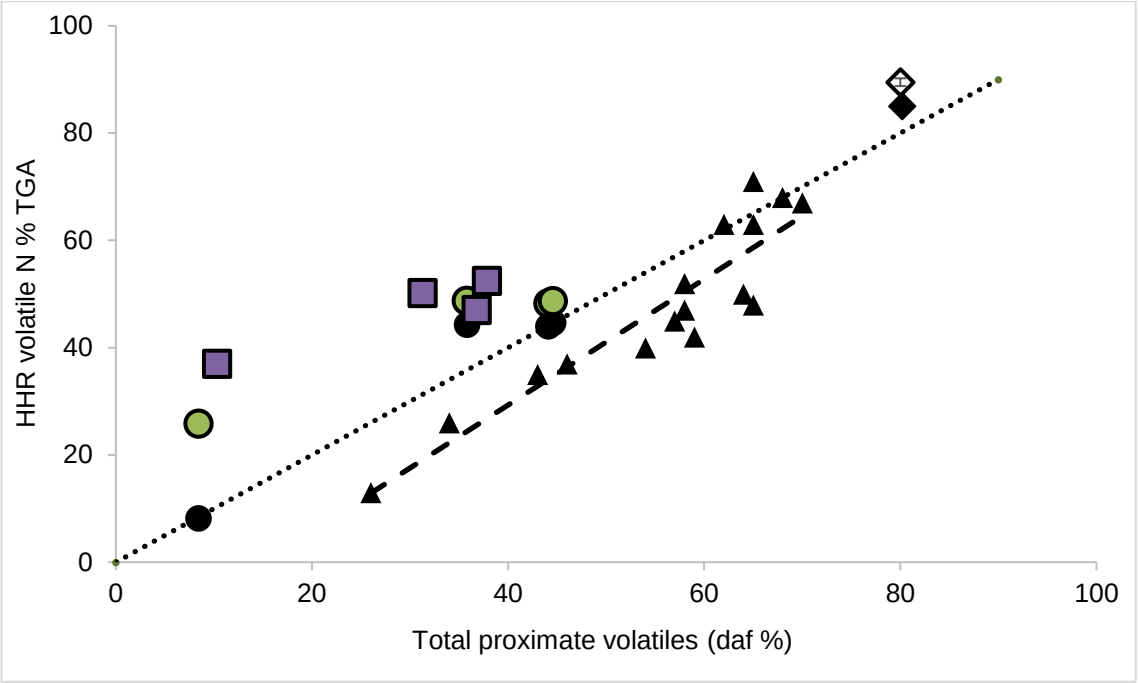

Figure 6.6. Synergy of HHR (TGA) volatile N compared to total volatile matter contents. Dotted line is a 1:1 relationship. Symbols: ● Coals, ● Coals+PFA, ■ Coals+FBA, ♦ olive cake, ◇ olive cake + coal PFA. and ▲Previous data from (Gibbins, 1995) (trend line for the latter given by the dashed line).

When the additives were mixed with the coals (and olive cake) there was a very significant change in the nitrogen released during devolatilisation. The addition of FBA or PFA both resulted in an increase in the fraction of N in the volatiles; in some cases this more than doubled compared to volatile-N from the pure fuels. The increases in HHR volatile-N release across all of the fuels indicates that catalysis is taking place with the additives. Within the TGA, the fuels and additives are held in close physical proximity and the additives clearly influence the decomposition of the coal matrix. Furthermore, as seen in previous studies (Ohtsuka, 1997; Tsubouchi and Ohtsuka, 2008) it is possible that as the coal matrix decomposes and the volatiles are released from the fuels, they interact with the surface area of the additives, which can provide reaction zones for enhanced reduction of NO to N_2. These reaction zones could be from reactive elements within the additives. For example, (Ohtsuka, 1997; Tsubouchi and Ohtsuka, 2008) showed coals with iron on the surface could instigate a reduction of NO to N_2 from char. In the case of the additives studied here, there are high levels of

Fe_2O_3, K_2O, CaO, MgO and Na_2O, and elevated levels of potentially reactive carbon in the ash additives, Section 5.3.

6.3.3 HHR volatile-N release (DTF1)

It was observed in the previous section that both additives can catalyse the release of nitrogen into the volatile phase when the fuels are reacting rapidly in a bed and the additives and fuels are in close proximity. Of interest to this work, is whether the same influence is observed when the fuel and additive particles are entrained in the DTF. Nitrogen partitioning was calculated from the char yields and N-contents of fuels and chars.

Figure 6.7 shows the distribution of nitrogen between volatile and char phases. The coals without additives all retained high levels of nitrogen in the chars ranging from 44 to 78% (i.e. 22–56% released into the volatiles). This is different to the results of Figure 6.6 which showed that at the heating rates attained in the ballistic TGA, although it is still enhanced, there is less Fuel-N released into the volatiles.

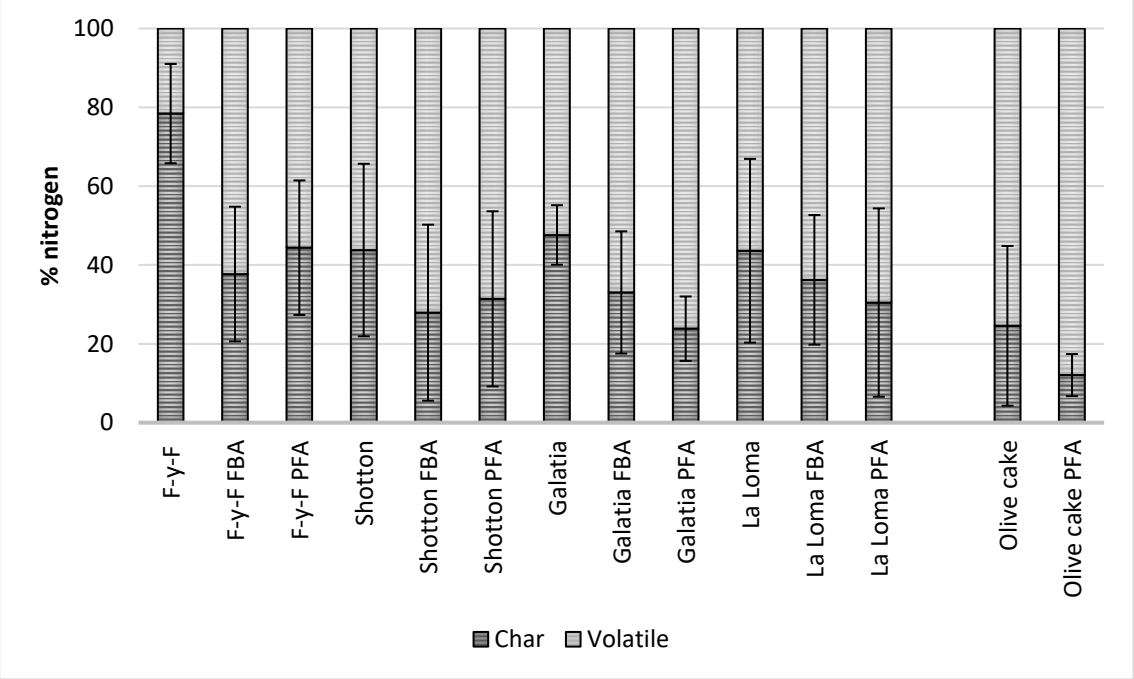

Figure. 6.7 Nitrogen partitioning of the fuels and fuels with additives during devolatilisation in DTF1. Dark grey=char-N %, Light grey=volatile-N %.

When additives were co-fed into DTF1 there was a change in the distribution of the nitrogen. The addition of the PFA resulted in a decrease of the nitrogen retained in the chars during devolatilisation across all four coals. The lower volatile coal (Ffos-y-fran) in particular showed a marked reduction in the char N with both additives. The FBA addition also resulted in a higher volatile-N yield. Thus, both additives showed reductions in the nitrogen retained in the char for all of the coals. A similar, although smaller trend was observed for the olive cake: The N retained in the char fell from 25% to 12% with the addition of coal PFA, as shown in Figure 6.7. The reason for the trends seen in Figure 6.5 might be explained by the extent of conversion in the DTF.

Literature suggests that carbon conversion (i.e. both devolatilisation and char oxidation) can be used as an indicator for nitrogen release, and there is a known correlation between carbon conversion and nitrogen devolatilisation in coals, as reviewed in (Mitchell, 1998). Consensus of the relationship differs dependent of coal type and heating regime. Jones et al. reported that nitrogen devolatilisation was slightly lower than carbon conversion, in a DTF at 1400°C. (Jones, 1994). Woitowicz et al. (Woitowicz et al., 1995) suggested nitrogen devolatilisation and carbon conversion was dependent on temperature profiles.

Figure 6.8 shows the relationship between nitrogen partitioning and carbon conversion. Included in Figure 6.8 is the trend line based on previous data presented in Kambara et al. (Kambara et al., 1994). The four coals all fall along the plotted trend line (and within the scatter of data in (Kambara et al., 1994)) which is very close to the monotonic relationship given by the dotted line in Figure 6.8.

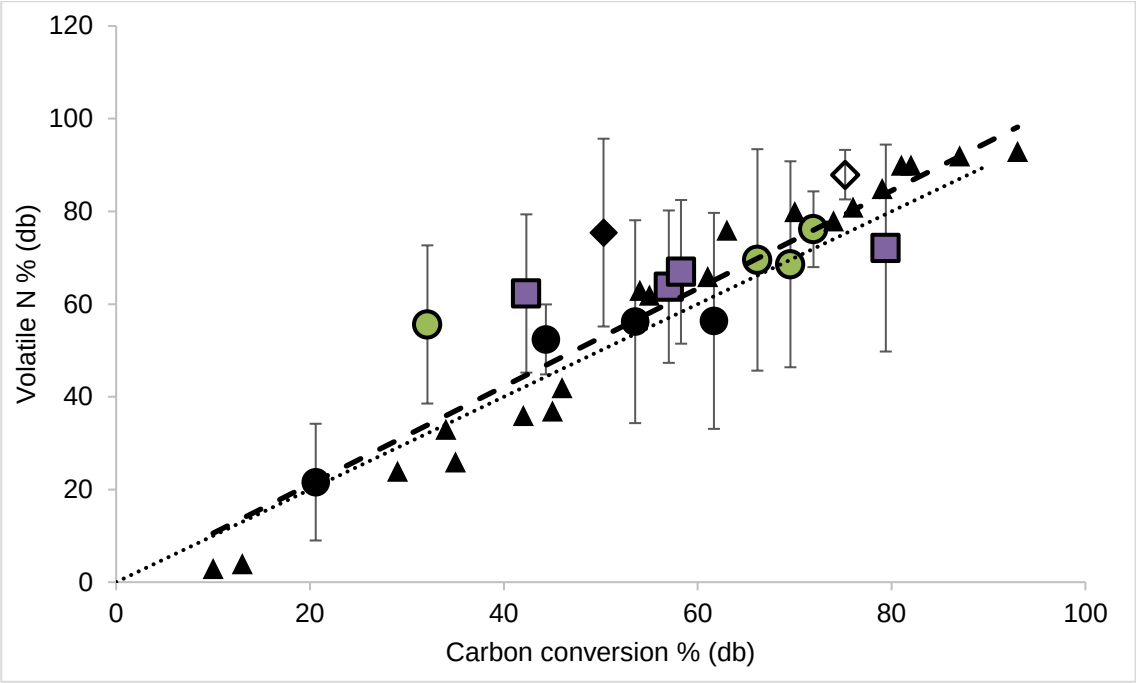

Figure 6.8 Volatile N as a function of carbon conversion during devolatilisation at 1373 K in DTF1. Previous published data (+) from (Kambara et al., 1994) is represented by the dashed trend line. The dotted line represents a monotonic relationship between volatile-N and carbon conversion. Symbols: ● Coals, ● Coals+PFA, ■ Coals+FBA, ♦ olive cake, ◇ olive cake plus coal PFA.

When the coals are co-fed with PFA there is an increase in both the volatile N release and the carbon conversion. The general trend is for the carbon conversion and the volatile nitrogen release from the coals to move to the right on the graph but still follow the trend line. This would indicate the coals are behaving as higher volatile coals in the presence of the additive. Figure 6.9 shows the change in volatile N release for the coals and coals blended with additives. There is an apparent natural log relationship in the increase in volatile N release when comparing the bituminous coals to the coals with additives.

This is an important finding, coal combustion in full-scale plant, equipped with low-NOx burners, show a general relationship of decreasing NOx with increasing volatile matter content (Mitchell, 1998). For Ffos-y-fran with additives there was enhanced volatile-N release compared to the carbon conversion, and these data points are therefore above the trend line (and above the scatter in the data given in (Kambara et al., 1994)).

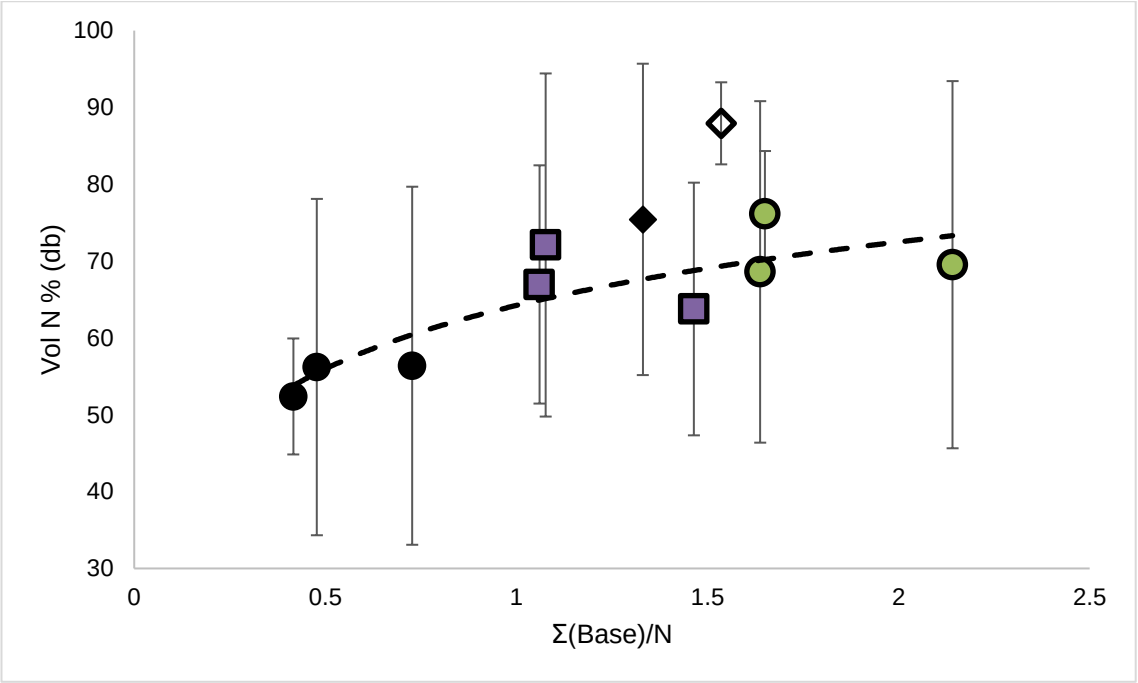

Figure 6.9 Volatile N release (DTF1) as a function of mass ratio of alkali and alkaline earth metals to N-content of the feed, Σ(basic components and iron in the feed)/N. Symbols: ● Coals, ● Coals+PFA, ■ Coals+FBA, ♦ olive cake, ◇ olive cake plus coal PFA.

The olive cake data also shows a greater volatile N release compared to the carbon conversion, and the addition of the coal PFA to the fuels increases both the carbon conversion and the volatile N release. The result draws the biomass data closer to the trend line. Across all of the fuels, and fuels with additives the general trend of volatile-N following carbon conversion is maintained. Higher values are achieved with the additives, indicating catalysis is taking place during devolatilisation. Since there is 1–2% O_2 in DTF1 it is possible that the rate of char oxidation is also being increased in the presence of the additives.

Nevertheless, various researchers have demonstrated that reactive elements within biomass (and coal) can participate in reactions which can result in a decrease in NOx emissions (Daood et al., 2014; Chen and Gathitu, 2011; Daood et al., 2017; Illan-Gomez et al., 1995a; Illan-Gomez et al., 1995b; Illán-Gómez et al., 1998; Karlström et al., 2017; Lissianski et al., 2001; Su et al., 2010) One mechanism by which this can occur is via catalysis of the fuel-N release (i.e. enhanced fuel-N release) in early stages

of combustion. During pulverised fuel coal combustion, low-NOx burners promote the release of fuel-N in low oxygen environments which enhances the formation of N_2 over NOx. Results from both TGA (ballistic heating) and DTF1 show that the additives enhance the conversion of the fuel (and concomitant release of N), which is clearly a desirable attribute to help lower NOx emissions. It is interesting that enhanced volatile (and volatile-N) release happens under both fixed-bed and entrained flow conditions, where in the latter case, there may not be close contact between the reacting fuel and the additive. Daood et al also saw a decrease in NOx through fly ash addition to the coal feed for a staged, 100 kW_{th} down-fired combustion test facility (Daood et al., 2013; Daood et al., 2017). In this case, the catalytic effect was attributed to fly ash entering the coal matrix during decomposition reactions and also interacting with volatiles as they are released. In this case, iron components within the fly ash were highlighted as potential catalytic sites, because Fe/char (Zhu, 1997) and iron additives are known catalysts for NOx reduction (Daood et al., 2014; Jones JM., 1999). Similarly biomass fly ash has been shown to be effective at reducing NO at temperatures of 300–600°C (Chen and Gathitu, 2011). Such a mechanism could partly explain the results seen here, although the O_2 concentration in DTF1 is low, and NO-carbon or NO-ash reactions are expected to be of much lesser importance because the NO concentration will be low. If the solid additive is able to interact with the coal matrix, then the alkali and alkaline earth metals may also interact with the devolatilisation step (Liu, 2007; Liu, 2019). Nanoparticles of CaO and MgO are known to form during coal (and biomass) combustion (Silva and da Boit, 2011) and it is feasible that these ultra-fine particles become embedded in the forming char particle and react. Alternatively, the alkali metal salts, and fine particles of alkaline earth metal salts may enter the vapour phase and influence gas phase reactions. Hernandez and Kilpinen (Hernandez, 2005) showed a reduction of NOx during biomass staged and non-staged combustion through the effects of K and Na. Figure 6.9 demonstrates a clear effect of the alkali and alkaline earth components within the feed on the partitioning of nitrogen into the volatiles. Yao and Che observed a mechanism whereby a combination of Ca and Mg promoted the

formation of NO_X. Conversely, Fe, K and Na realised a suppression of the formation of NO_X during coal combustion. (Yao and Che, 2007). The onset of NO_X formation was at different temperatures for the different coal types under test with additives.

6.4 Further investigation of N partitioning

A third method of N partitioning was investigated. The method involved using small sample quantities, approx. 2-2.5 mg of sample subjected to high temperatures in a furnace (the Low-N analyser described in Chapter 4.7). The results were in the form of NO released during devolatilisation and char combustion, observed as two separate peaks. The methods of preparing the sample, and the procedures followed are in Chapter 4.7. The results show a similar trend to those from the ballistic TGA and DTF1, where the volatile N for all the coals were similar values to the HHR volatile values. When the coals were blended with the additives, there was a significant increase in the volatile N release for all coals and with either additive. There was a difference in the data comparing the FBA and PFA additives however, Figure 6.10. The FBA appeared to yield a greater percentage of volatile N than the PFA across all of the coals under test, despite the FBA having a lower percentage of alkali and alkaline elements.

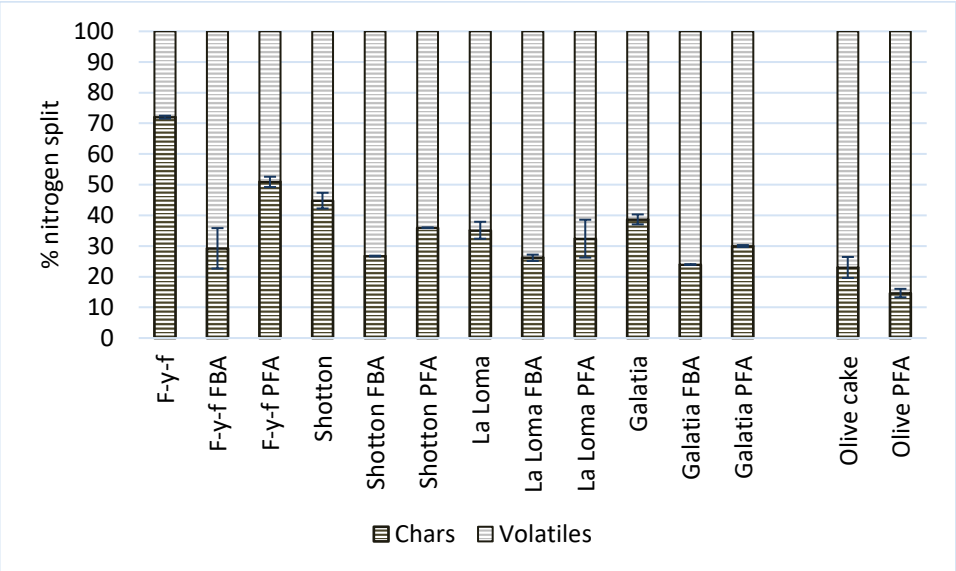

Figure 6.10 N partitioning from the Low N analysis. Light grey is volatile N, dark grey is the char N

Figure 6.11 attempts to separate the impact of the different additives of the N partitioning. A natural log relationship is again shown for the coals and additives; however, this has been separated out for the two different additives. Whilst the data from the Low N analysis has some similarities to the other HHR analyses, there are some differences in the process. The temperature is maintained at 1050°C throughout the procedure. The devolatilisation gas is argon, and the combustion gas is O_2, therefore complete combustion is carried out on the samples, with only ash as the remnant.

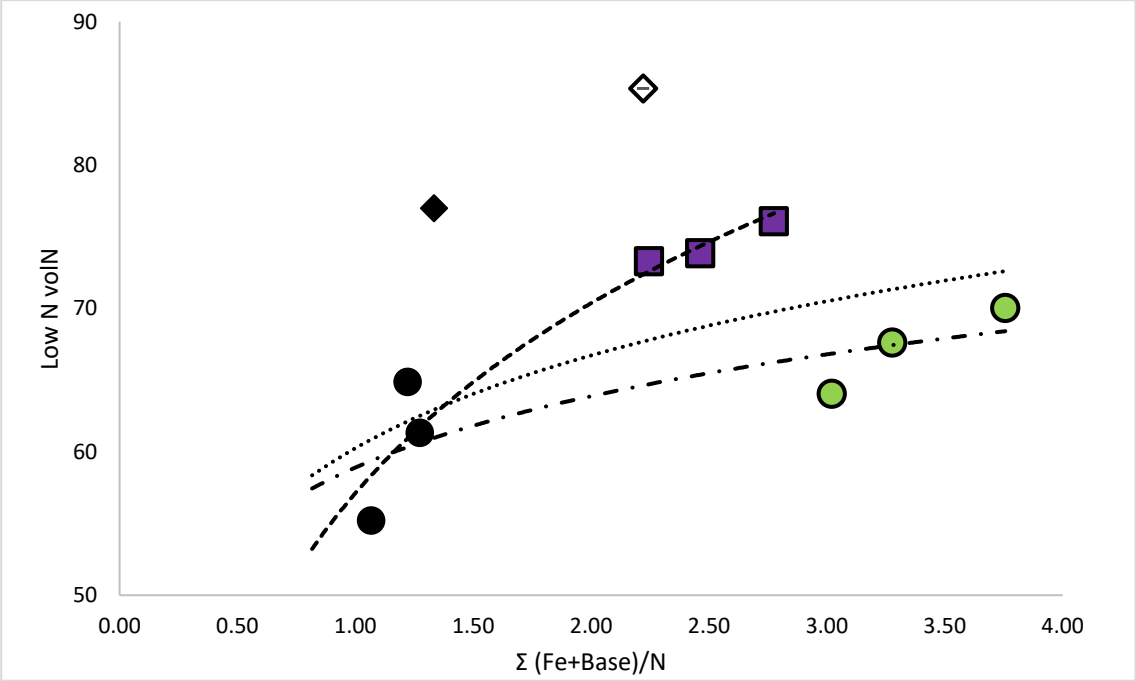

Figure 6.11 Volatile N release Low N analyser, as a function of mass ratio of alkali and alkaline earth metals to N-content of the feed, Σ(basic components in the feed)/N. Symbols: ● Coals, ● Coals+PFA, ■ Coals+FBA, ♦ olive cake, ◇ olive cake.

Appendix 1 shows the profiles for all of the coals with and without additives. Integration of the curves was carried out to establish the division of volatile N and char N. The Low N analysis takes the data direct from the analyser, whilst the data from the TGA and DTF1 is calculated by difference. The chars produced are then analysed using the Flash Element Analyser. The difference in the fuel N and char N are used to calculate the volatile N release. In the case of the Low N analyser, the ash tracer method highlighted in Equation 6.1 was not required for the N partitioning. In the case of the Low N analyser, the ash tracer method relies on the complete ash content remaining,

which may contain carbon content left if complete combustion does not occur. The FBA contains higher levels of carbon in the additive, which may account for the apparent higher volatile N release. The ash tracer method makes assumptions that some of the ash is lost, however exact values of the losses are not known. Further to this, the ash tracer method and N partitioning calculations carry an inherent large standard deviation error through the propagation of error in the equations.

6.5 Chapter summary

Through this chapter, devolatilisation of the coals with and without additives was studied using two main methodologies, LHR and HHR devolatilization were analysed using a TGA, and in the latter case, also using a DTF. The TGA, LHR analysis of the devolatilisation process revealed there were some changes to the OD, PT and ED for all of the coals when blended with the additives. However, generally and inhibiting effects of the additives was apparent at LHR's. The devolatilization kinetics were derived from the coals (and coals + additives) and these parameters are utilised later in the model development (Chapter 8.2.6).

Using HHR techniques, the total volatile and volatile N releases were investigated. There was a marked increase in the HHR volatile release compared to the proximate volatile release for the coals without additives. When the coals were blended with the additives, a further increase in the HHR volatiles was observed. To compliment this the same was observed for volatile N release. Under HHR conditions, volatile N release increased compared to proximate volatile N release. When the coals were blended with either of the additives, an enhanced volatile N release was observed. Catalysis appears to be taking place, liberating volatiles (including fuel N) more readily with the addition of the FBA and PFA to the coals.

Carbon burnout is also enhanced when the coals are blended with either of the additives under HHR conditions found in both the ballistic TGA and DTF analysis. The

known relationship between carbon burnout and volatile N release is still maintained, with both increases showing parity.

Chapter 7 Char characterisation and combustion

7.1 Introduction

This chapter focusses on the chars, their characteristics and the emissions of N-species during char combustion. The results are presented from elemental and proximate analysis, SEM images from the chars produced in DTF1, NO emissions from DTF2, char nitrogen split from an STA-MS and N functional groups taken from XPS analysis.

During combustion of a coal, several distinct phases develop: devolatilisation, gas phase, tar production and char formation. This chapter analyses the char combustion rates produced in DTF1. During devolatilisation in the drop tube, much of the gases are given off during devolatilisation and through the processes used in the DTF's, gases and tars diffuse rapidly from the forming chars. The nitrogen within the coal is also partitioned between the volatiles and the chars. The nitrogen partitioning can be affected by the elemental composition of the coal and the additives present during combustion. The nitrogen in the coal is in the form of functional groups, which can change during combustion through destruction and reforming of chemical bonds. The influence of alkali and alkaline metals may elicit changes in the partitioning of nitrogen through catalysis. Within coals the principle N-groups are pyrrole, pyridine, pyridinic and quaternary.

7.2 Elemental and proximate analysis

Elemental and proximate analysis of the coal chars and the ash additives were carried out using the procedures in Chapter 4. Of particular note is the nitrogen percentage values. These are reduced compared to the coal nitrogen values shown in Chapter 5. Some of the carbon, nitrogen, hydrogen, sulphur and oxygen was lost during devolatilisation. From the proximate analysis there was a significant reduction in the

volatile and moisture contents. Table 7.1 shows the percentage details from the elemental and proximate analysis.

Table 7.1 Elemental and proximate analysis of the coal chars % db

Char db	Ffos-y-fan	Shotton	La Loma	Galatia	FBA	PFA
Carbon	82.07	86.50	68.90	75.00	39.48	4.50
Hydrogen	1.07	0.03	0.80	1.00	1.99	0.07
Nitrogen	0.92	1.53	1.20	1.50	0.12	0.03
Sulphur	0.63	0.23	0.50	0.90	0.00	0.10
Oxygen	9.86	1.50	7.30	6.20	0.44	7.62
Volatiles	0.00	0.00	0.00	0.00	25.74	2.88
Fixed carbon	94.55	87.99	78.70	84.60	16.29	9.44
Ash	5.45	12.01	21.30	15.40	57.97	87.68
Moisture	0.00	0.00	0.00	0.00	2.40	0.40
HHV[a]	28.10	28.99	23.26	28.49	15.94	0.24

Note: a=HHV-Milne for the coals and DuLong for the ashes

7.3 SEM

DTF1 was used to prepare chars for further analysis to establish if there were changes to the morphology and chemical structures of the coal chars through blending with the additives.

7.3.1 Char morphology

The morphology of chars was originally proposed by Bailey et al, where chars were subjected to pyrolysis at 1500°C sectioned, polished and SEM analysis carried out (Bailey et al, 1990). The samples were initially divided into 11 main categories, eight of which are shown in Figure 7.1 and characterised by physical and optical properties of the chars. The characterisation then divided the chars further by particle shape, vesicle volume, shape and orientation, wall thickness and anisotropy. The initial work focussed on seven Australian coals, four used in power production and a further 3 that could be used for electricity generation.

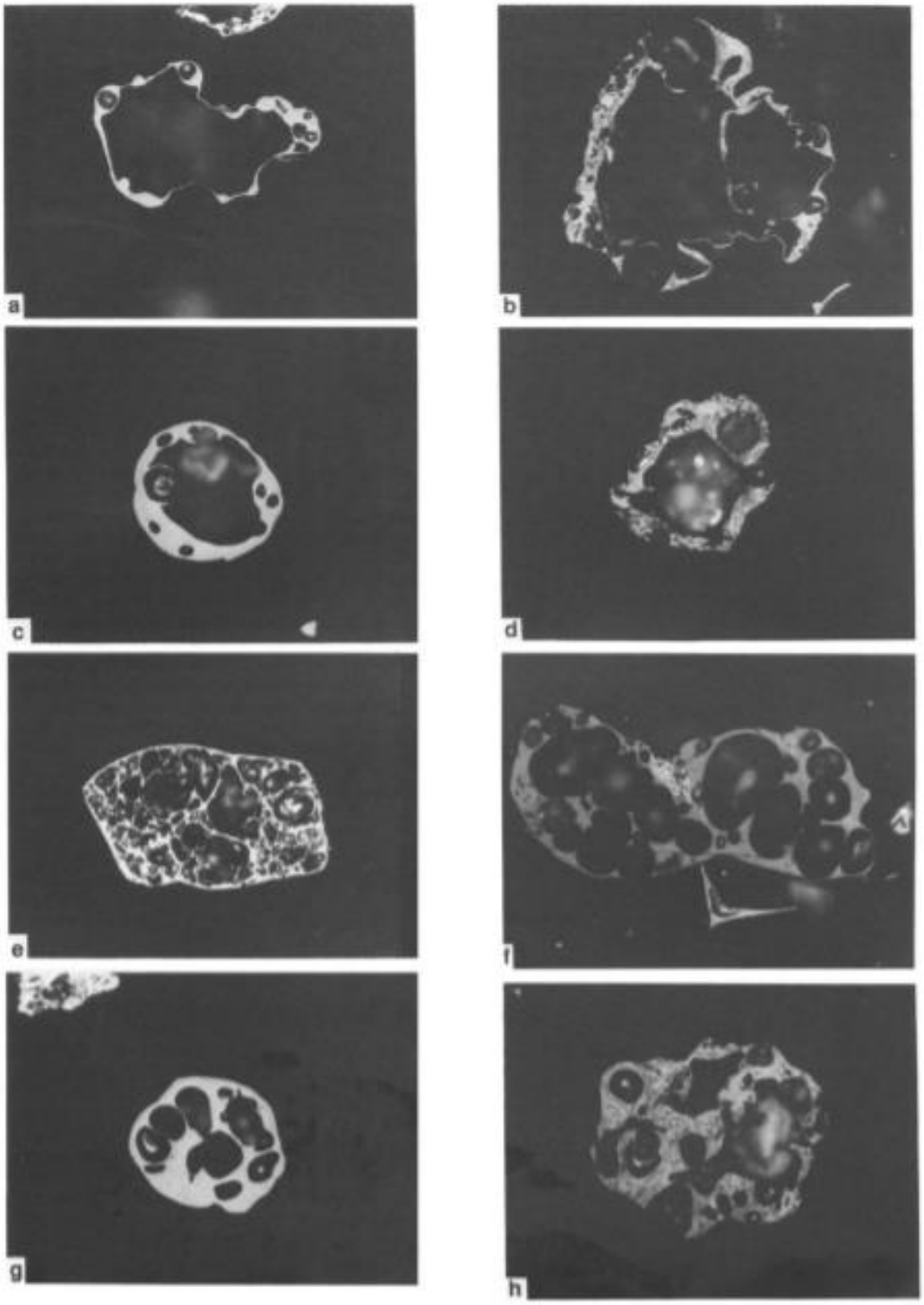

Figure 7.1 Eight char morphology categories as depicted by Bailey et al. a. isotenuisphere, b, anisotenuisphere; c. isocrassisphere, d. anisocrassisphere; e. isotenuinet f. anisotenuinet g. isomesosphere h. anisomesosphere (Bailey et al, 1990).

Further work by Lester et al, extended the work to establish potential leading particulars of the chars to define the morphology further (Lester et al, 2010). The categorisation used an unfused category system, and then sub-divided this with

porosity and wall thickness, Figure 7.2. Similar to Bailey, Lester produced the chars, took a slice of the char, polished the section then used SEM for characterisation. Figure 7.3 shows some of the salient categories from the Lester study (Bailey et al, 1990, Lester et al, 2010).

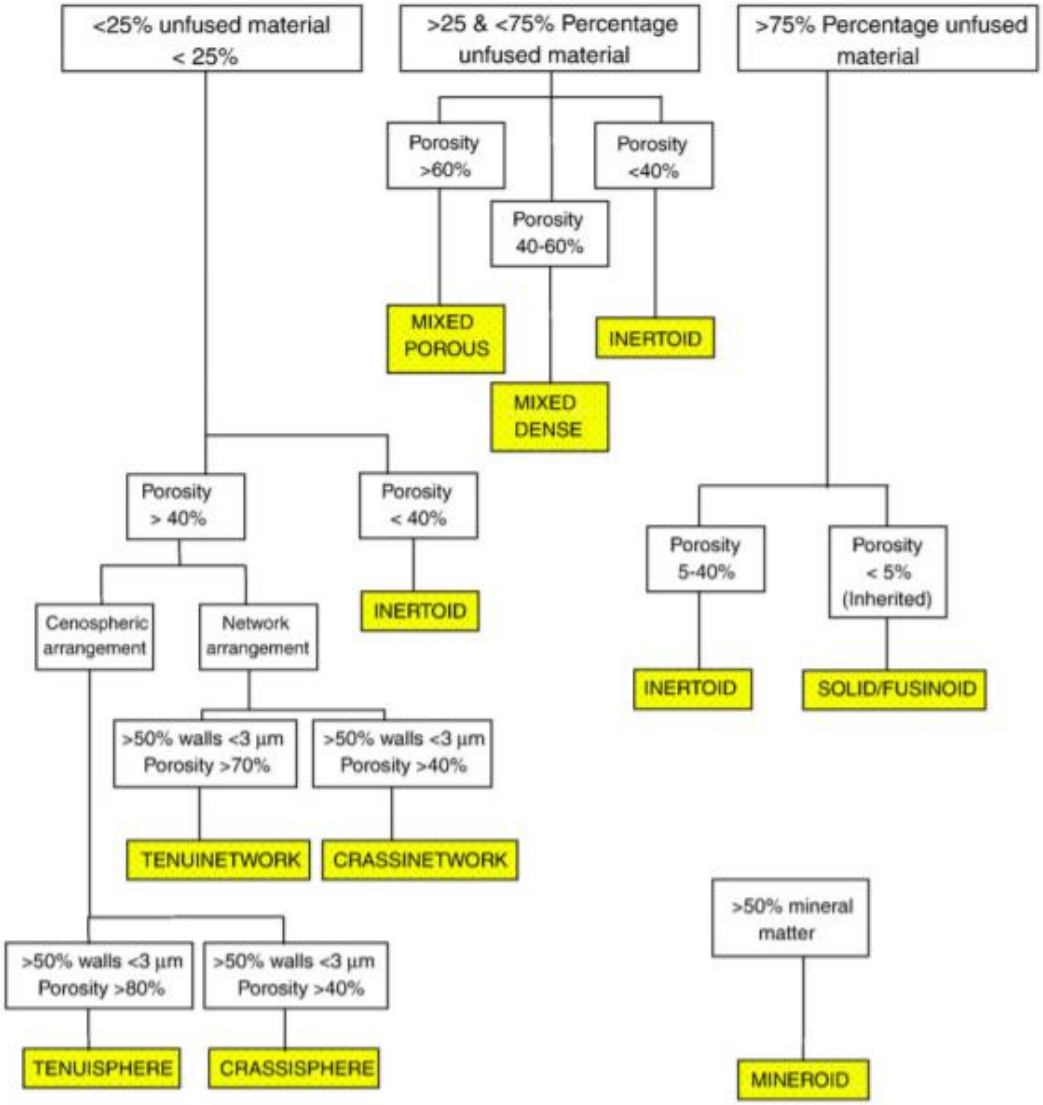

Figure 7.2 Logical tree for classification of chars (Lester et al, 2010)

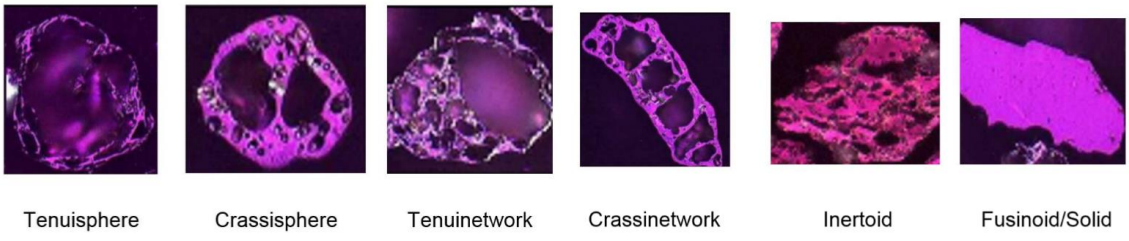

Figure 7.3 Images of the main classifications of chars (Lester et al, 2010)

7.3.2 Coal chars

From the chars produced in DTF1, samples of the coal chars and the coals blended with the ash additives chars were processed in a Zeiss SEM, in accordance with the procedures shown in Chapter 4.9. The char images in this chapter can be compared to the coal SEM images in Chapter 5.3. Study of the chars can give a good indication to the burnout of a coal and a potential area for improving complete combustion (Bailey et al., 1990). From Figures 7.4 a-d, all four of the coals have behaved differently during devolatilisation.

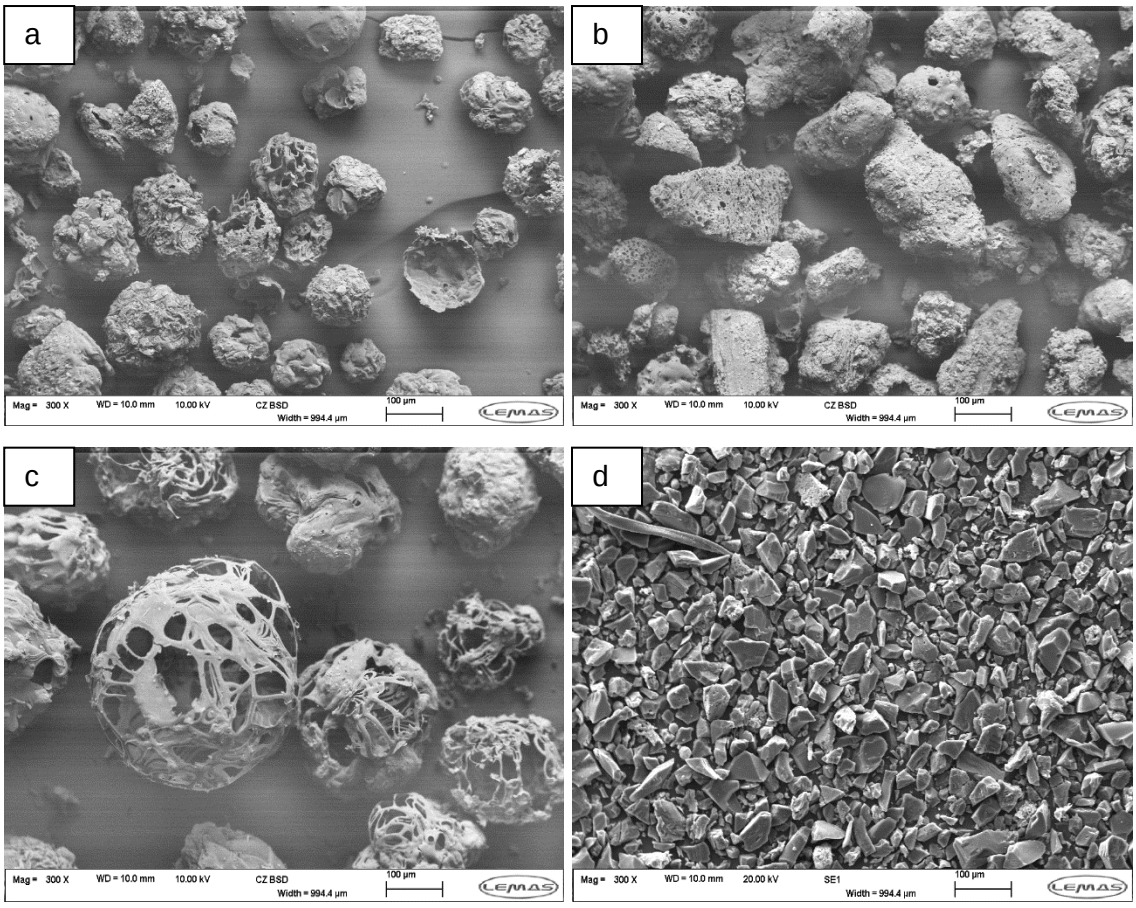

Figure 7.4 Coal chars after devolatilisation in DTF1 at 1100°C in an N_2 atmosphere. a=Shotton, b=La Loma, c=Galatia, d=Ffos-y-fran

The three bituminous coals have shown some changes in morphology, with swelling of many of the particles to greater than 100 µm for all three of the bituminous coals. Shotton and Galatia have shown large amounts of the surface area development as pore structure, where the volatiles have escaped from the malleable chars. The

predominant char structures are cenospheres (Bailey et al., 1990, Lester et al, 1995, Lester et al, 2010). Shotton char has none of the small particles remaining that were present in the coal SEM images, Figure 5.3. Shotton char does have some smaller fragments visible in Figure 7.4a. The smaller fragments shown are most likely from the destruction of the cenospheres from rapid volatile ejection.

La Loma has exhibited changes to the morphology, where the coal has become malleable and formed inertoids (Bailey et al., 1990, Lester et al 1995, Lester et al, 2010). There are some pore holes visible where the volatiles have escaped the structure during devolatilisation. The reformed surface of the chars on the La Loma are indicative of tars forming but not completely dissipating during pyrolysis.

The Ffos-y-fran has not shown any significant changes to the structure of the coal particles after passing through the DTF. The temperature and residence time in the DTF may not have been sufficient to show significant changes to the visible physical structure of the low reactivity coal. The high carbon content and low volatile content may be instrumental to the reduced morphology change.

7.3.3 Coal blended with ash additives chars (DTF1)

When the coals were blended with the PFA, there was no apparent change in morphology of the chars for Shotton, La Loma or for Ffos-y-fran. All three of the coals show the same visual characteristics as the chars without ash blends. Galatia has shown some changes to the physical structure and the pore density has an apparent increase. From the image in Figure 7.5 a-d, there has been some disintegration of the chars leading to a mix of cenospheres and fragments. The fragmentation is indicative of more explosive release of the volatile contents during devolatilisation of the Galatia coal char.

When the coals were blended with the FBA, the same type of results were observed, where there was an increase in fragmentation of the Galatia and some increase in pore

density in the Shotton. The Shotton also showed the reduction in smaller fragments of coal, possibly indicating complete combustion of smaller particles, (Note, the O_2 concentration in the DTF was ~1-2%, therefore some char conversion is expected when the reaction rate is fast enough). The La Loma showed the same characteristics as when blended with the PFA, where the surface appears to have become malleable under heat, but no significant increase in visible volatile release in the SEM images.

The Ffos-y-fran blended with FBA show little to no change in the morphology when compared to the char without additives.

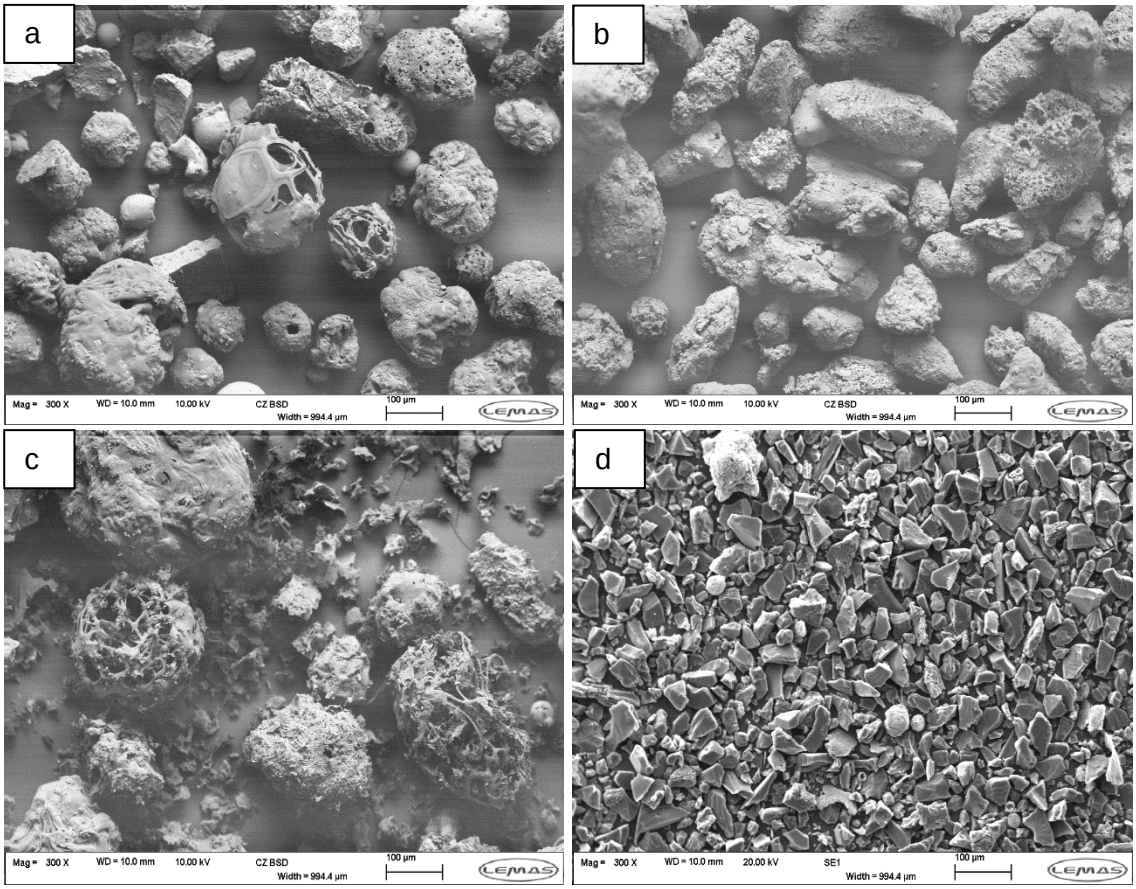

Figure 7.5 Coals chars blended with PFA from DTF1 at 1100°C in an N_2 atmosphere. a=Shotton plus PFA, b=La Loma plus PFA, c=Galatia plus PFA, d=Ffos-y-fran

7.4 Coal nitrogen functional groups (XPS)

Using chars from DTF1, XPS analysis was carried out to ascertain the N-functional groups on the coal chars with and without additives using the procedures in Chapter 4. The analysis was carried out for the chars with and without additives. The signal

detection was low and there was some spectra noise in the signals, therefore there is some uncertainty in minor peak detection.

7.4.1 Coal chars

For the coal chars without additives, all four chars now predominantly contain nitrogen in quaternary form, this is shown with peaks at ~401.4 eV and a second smaller peak at ~399.2 eV. Ffos-y-fran char also possibly shows some pyridinic N-6 at 398.7 eV. When this data is compared to the coals in Chapter 5.6, there is a significant change from pyrrole in the coals to quaternary nitrogen species in the chars. Figure 7.6 shows the functional groups from the coal chars. The percentage of nitrogen functional groups in each char are presented in Table 7.2.

Table 7.2 % functional groups within the coal chars

Chars	Functional group1	% in group 1	Functional Group 2	% in group 2
Shotton	Quaternary	64	Quaternary	36
La Loma	Quaternary	66	Quaternary	34
Galatia	Quaternary	66	Quaternary	34
Ffos-y-fran	Quaternary	77	Pyridinic	23

Under high heating rate conditions, nitrogen in pyridinic groups tend to be more stable than those in pyrrole or quaternary groups and pyridine is more prevalent in higher rank coals (Nelson, 1992b). The cracking of the N-5 rings releases H radicals from the heterocyclic rings. In the case of Ffos-y-fran, the H radicals can then attack the N-6 compounds, helping to liberate the nitrogen bound in the rings. (Deng et al., 2016) If the coals are behaving as higher volatile coals (when blended with either of the additives), then the resultant chars may be in the form of higher-grade coal chars. This may account for the increase in N-6 formations after devolatilisation. N-6, however is also known to form during lower intensity pyrolysis (Pels, 1995b; Pels, 1995a), see Figure 7.9, whilst quaternary is the main product of N functional groups during pyrolysis under more severe conditions.

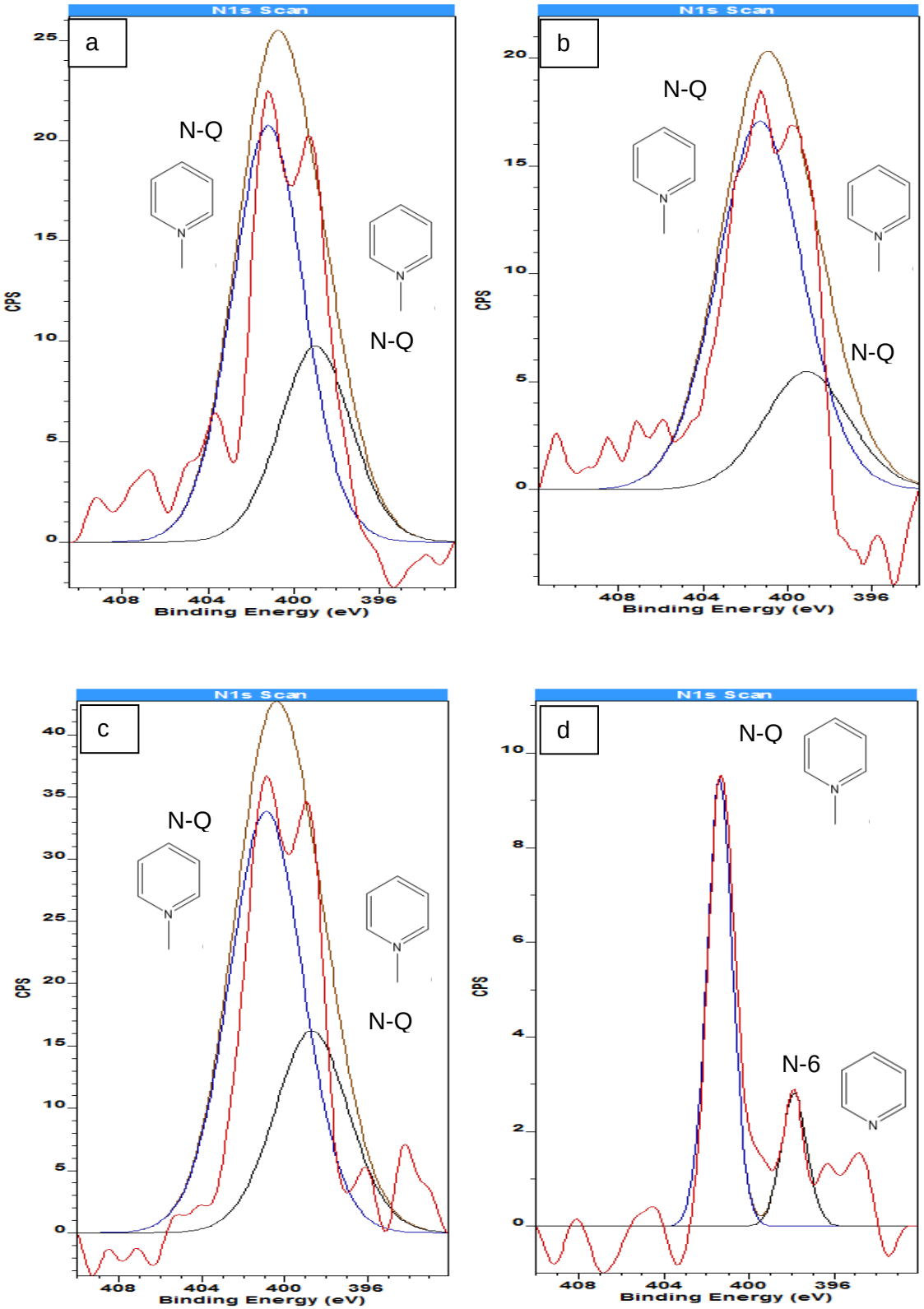

Figure 7.6 Bituminous coals N-Q, Ffos-y-fran N-Q and N-6 Pyridinic. —— 1st Functional group, —— 2nd Functional group —— raw data (smoothed)

When pyrrole degrades under heating conditions, HCN and propyne molecules tend to form in preference to NH_3. Liu et al (Liu, 2019) using a Density functional theory

suggested the addition of Na^+ and K^+ may actually inhibit the formation of HCN. When examining the meta position of H in the pyrrole functional group however, Na^+ and K^+ may act as catalysts for opening the pyrrole ring. The catalytic effect may spread as far as assisting in lowering the energy required for breaking the C-H bonds within the pyrrole cyclic rings. It is further postulated Na^+ and K^+ may play an important role in the thermal decomposition of nitrogen containing compounds such as indole and carbazole (Liu, 2019).

7.4.2 Chars blended with additives

When the chars were generated from the coals blended with the FBA, the functional groups in the chars have shown a change from the chars without additives, Figure 7.7. Table 7.3 shows the proportional amount of each of the functional groups in the chars blended with FBA.

Table 7.3 % functional groups within the coal chars plus FBA

Chars	Functional group1	% in group 1	Functional Group 2	% in group 2
Shotton	Quaternary	78	Nitroso	22
La Loma	Quaternary	67	Pyridinic	33
Galatia	Quaternary	74	Pyridinic	26
Ffos-y-fran	Quaternary	100	N/A	

From Figure 7.7, it can be seen the bituminous coal Shotton shows a single peak of quaternary nitrogen at ~401.4 eV. The Galatia and La Loma has still retained the second quaternary peak at 399.2 eV. Ffos-y-fran has retained the quaternary peak, however it has lost its N-6 peak. It is interesting to note that shotton shows a distinct peak for pyridinic nitroso, which is not present in the other chars.

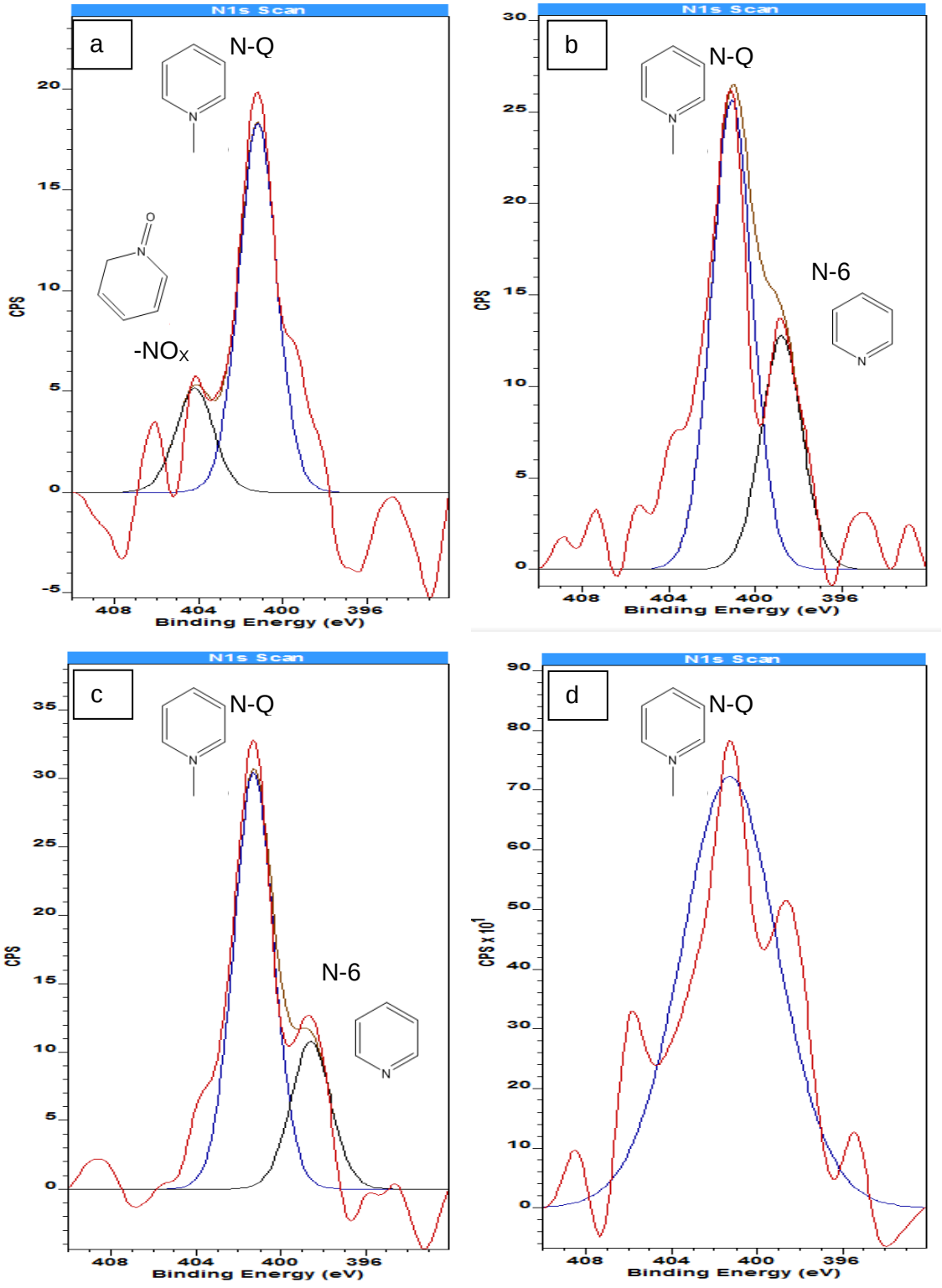

Figure 7.7 Functional groups for the chars with FBA —— 1st Functional group, —— 2nd Functional group —— raw data (smoothed)

Figure 7.8 shows the results of combustion of the chars blended with PFA. Table 7.4 contains the percentage of N 1s species within each blend.

Table 7.4 % functional groups within the coal chars plus PFA

Chars	Functional group1	% in group 1	Functional Group 2	% in group 2
Shotton	Quaternary	67	Pyridinic	33
La Loma	Quaternary	100	N/A	
Galatia	Quaternary	78	Pyridinic	22
Ffos-y-fran	Quaternary	100	N/A	

When the coal chars are blended with the PFA, a similar pattern is observed for all four coals compared to the coal chars with FBA, however the Galatia has now lost its secondary quaternary peak. La Loma has maintained the second N-Q peak. The Ffos-y-fran exhibits the same characteristics as the char with FBA, with the one quaternary peak at 401.4 eV. The results indicate that the coals have gone through a change in devolatilisation of the N functional groups when the coals are blended with the either additive and subjected to devolatilisation. As both additives increase the percentage of alkali and alkaline earth metals, there is an assumption when either additives is combined with a coal, the additives are presenting a catalyst to enhance reactions within the coals. The enhanced reactions are liberating the nitrogen during devolatilisation from the N-5 group. (Liu, 2019; Liu, 2007).

The bandwidth of the XPS spectra of Ffos-y-fran char with PFA is wide compared to those of the other chars with PFA. It could be argued that there is some N-6 within the profile at 398.7 eV, however there is no distinct peak at this value, therefore only N-Q is highlighted. As the severity of the thermal processing of a coal/char increases, so the conversion of pyrrolic N1s to pyridinic is likely to increase. Therefore, under severe pyrolysis, any nitrogen remaining in the chars is likely to be in the form of pyridine-N or graphene-N at 401.4 eV (Pels, 1995b), and bound in six ring heterocyclic membered rings, which are incorporated into carbon structures of graphene, Figure 7.6 (Pels, 1995a).

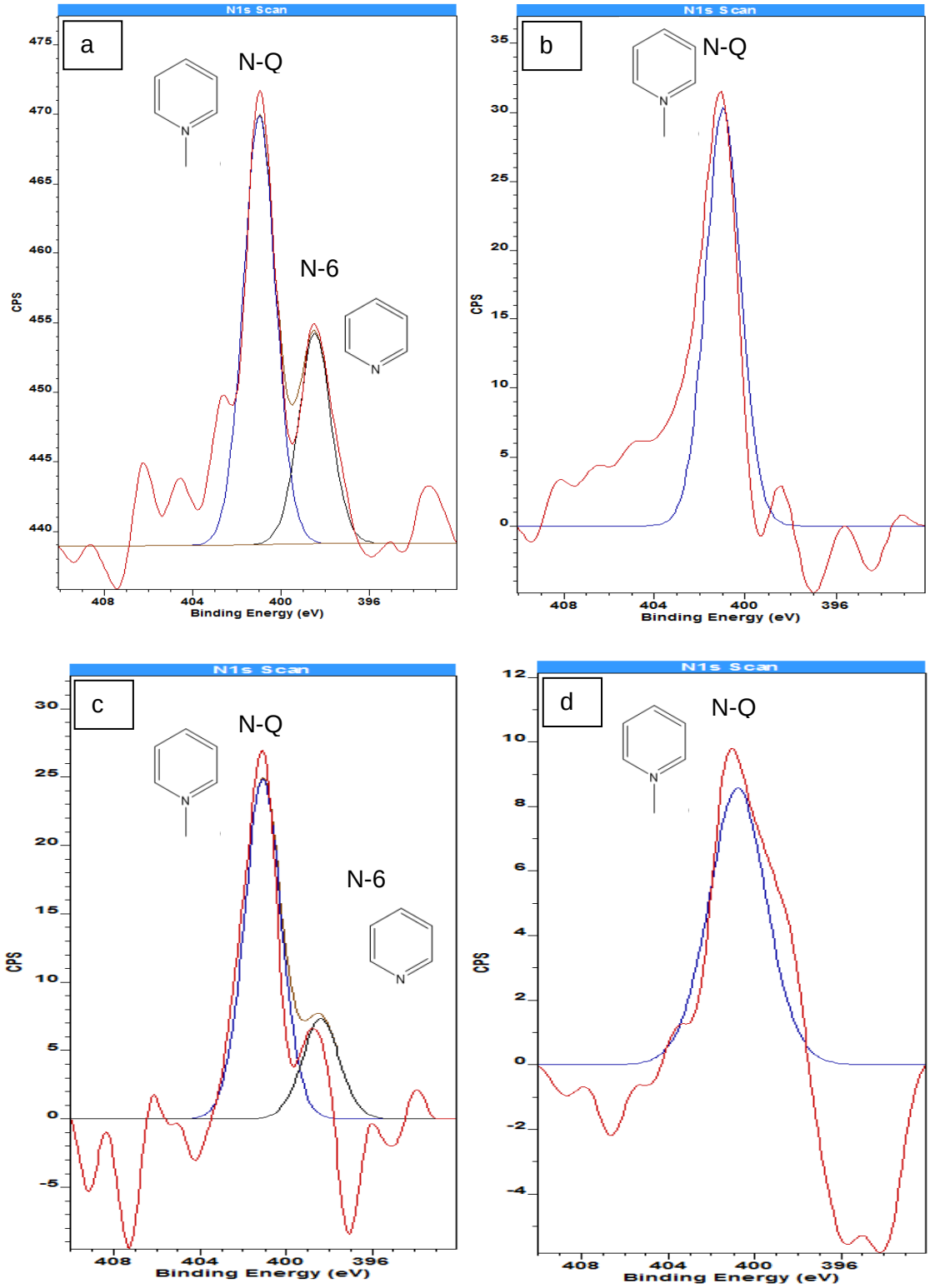

Figure 7.8 Functional groups for the chars with PFA —— 1st Functional group, —— 2nd functional group —— raw data (smoothed)

The coals chars without additives, showed only NQ groups. When the chars with FBA were analysed, there was some $-NO_X$ in the Galatia and N6 was present in Galatia and La Loma chars. The main nitrogen group was NQ. The N 1s functional groups from the

chars with PFA, showed the predominant groups to be NQ, with some N6 formations in the Shotton and Galatia. The evolution of the N 1s functional groups to NQ and N6 would indicate the addition of either FBA or PFA may be causing the chars to behave as they would under more severe pyrolysis as shown in Figure 7.9. The evolution of nitrogen functional groups may be intrinsically linked to the formation of nitrogen species C2N2, HCN and NO, see section 7.6

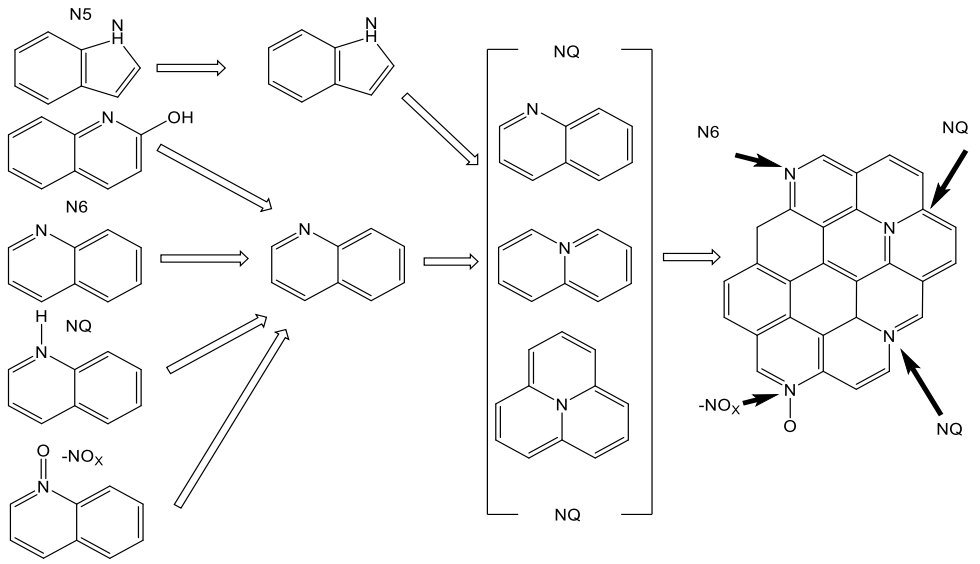

Figure 7.9 Evolution of coal functional groups as the severity of pyrolysis increases from left to right. Adapted from Pels (Pels, 1995a).

7.5 DTF2 (Gas analysis-NO)

From DTF2 (excess air) the emissions characteristics were taken for the three bituminous coals during combustion. Gas analysis was taken for each of the coals, with NO_X being the main area of interest. The NO_X was recorded as NO and NO_2 as per Chapter 4.4.3. Throughout this section, NO_2 was not detected in the gas analysers, therefore only NO is cited for NO_X. To establish the data in line with industrial standards EN 14792:2005 (E), they can be presented as NO_X ppm by volume or as NO_X mg/Nm. To calculate the NO_X emissions on an mg/Nm basis, the emissions data from the analysis equipment was converted from ppm (v/v) to mg/Nm using Equations, 7.1-7.6.

$$ppm\ (v/v)\ to\ mg\ m^{-3} = \frac{ppm \times molar\ wt}{Molar\ vol} \quad \text{Eq 7.1}$$

$$mg\ Nm^{-3}(stp) = mg\ m^{-3} \times Ft \times Fp \times Fo \times Fm \quad \text{Eq 7.2}$$

$$Fo = \frac{20.9 - O_2\ ref}{20.9 - O_2\ sample} \quad \text{Eq 7.3}$$

$$Fp = \frac{Pref}{Psample} \quad \text{Eq 7.4}$$

$$Ft = \frac{T\ sample}{Tref} \quad \text{Eq 7.5}$$

$$Fm = \frac{100}{100 - H_2O} \quad \text{Eq 7.6}$$

Where:

$Fo =$ oxygen correction, $Fp =$ pressure correction, $Ft =$ temperature correction, $Fm =$ moisture correction, $molar\ wt\ (NO) = 30.01$, $molar\ vol = Vm = \frac{RT}{P}$, $O_2\ ref = 6\%$

$Pref(STP) = 101.325kPa$, $Tref = 273.15K$

A simple conversion for ppm to Nm^3 for NO and for NO_2 can be used when operating at 273 K and 101.325 kPa by using the conversion factors shown in Equations 7.7 and 7.8:

$$1\ ppm\ (v/v)NO = 1.34\ mg\ Nm^{-3}\ NO \quad \text{Eq 7.7}$$

$$1\ ppm\ (v/v)NO_2 = 2.05\ mg\ Nm^{-3}\ NO_2 \quad \text{Eq 7.8}$$

Having established that the additives have a strong influence on devolatilisation, shown in Chapter 6 (in low O_2 environments), combustion in DTF2 was undertaken for the bituminous coals and coals plus additive blends. The combustion emissions from DTF2 were measured in an excess air environment for all of the bituminous coals and olive cake, and for each fuel blended with their respective additives.

The equivalence ratio was calculated using Equation 7.9.

$$\Phi = \frac{\frac{mfuel}{mair\ (sample)}}{\frac{mfuel}{mair\ (st)}}$$ Eq 7.9

Where:

$mfuel$ =mass of coal or biomass

$mair$ =mass of air

st =stoichiometric

Values for equivalence ratios, ϕ were in the range 0.4–0.6 for the coals (with and without additives), and 0.25–0.3 for the olive cake (with and without additive). NO_X measurement results are given in Figure 7.10a and 7.10b. At first inspection (Figure 7.10a), a correlation is possible between NO_X emissions and FR (R^2=0.9747), but work by Ren et al (Ren et al., 2017) demonstrated that there is a different correlation for biomass fuels compared to coal or torrefied biomass fuels. In fact, the NO_X emissions given in Figure 7.10a are in close agreement with these previous findings, and the curves from (Ren et al., 2017) are reported in Figure 7.10b for comparison. Ren et al. (Ren et al., 2017) also observed that a high-N biomass can yield higher NO_X than coal under the conditions in DTF2.

One would expect that in the DTF CH radicals from the volatiles would react with NO thereby producing the well-known correlation of decreasing NO_X with decreasing FR (Wendt, 1995). However, for high-N fuels, a high fraction of fuel-N enters the volatiles, and for biomass, the volatiles have high O species. Thus it is possible that for some biomass, NOx will be more dependent upon Fuel-N content. Of course, competition between NOx formation versus reduction routes is also profoundly influenced by excess air. For the fuel lean stoichiometry used here, one would expect increased NOx emissions, and thus it is less easy to observe the impact of the additives than it is in devolatilisation.

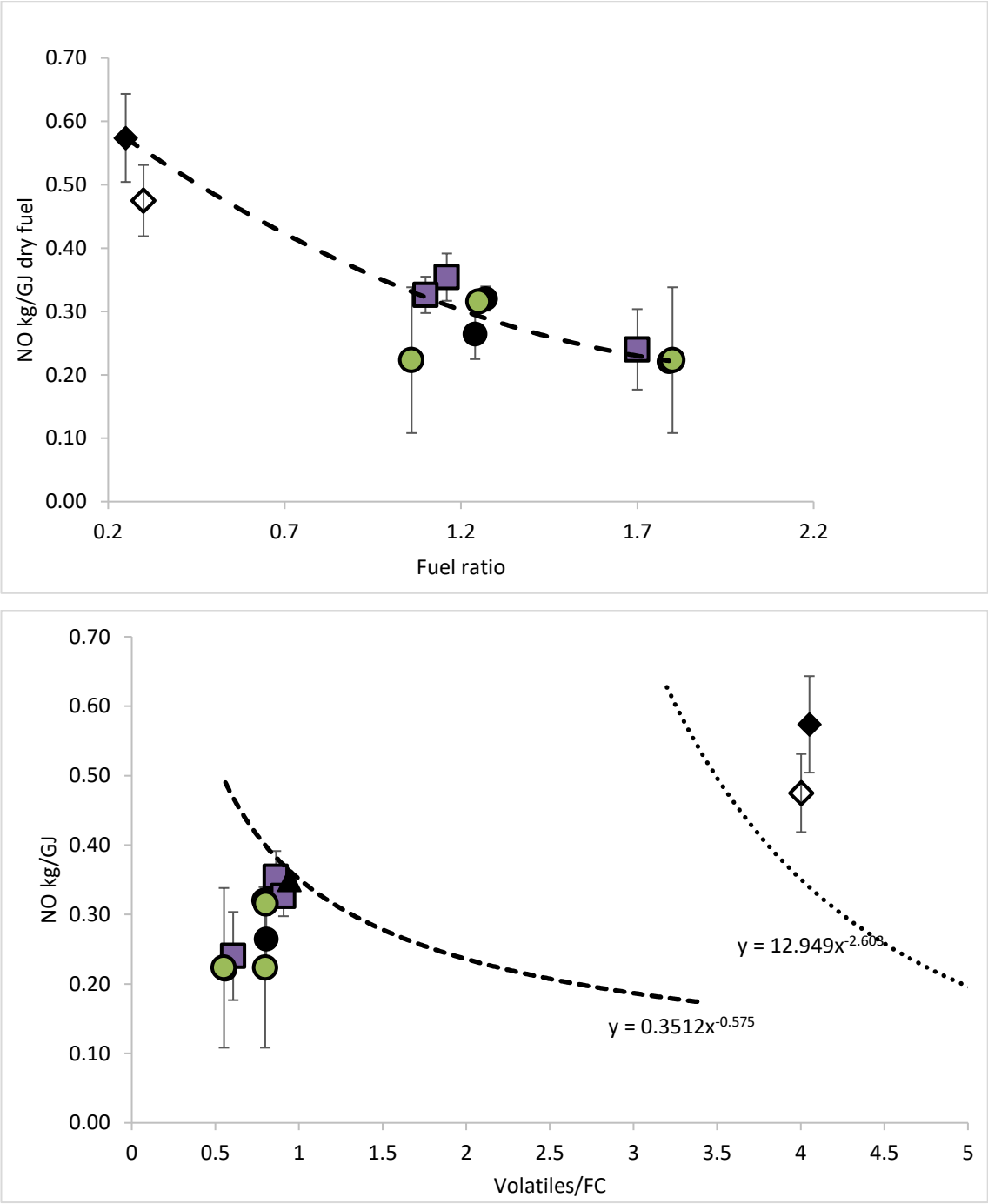

Figure 7.10 Fuel NOx emissions from combustion at 1373 K in DTF2 (kg GJ^{-1}) as a function of (a) fuel ratio (FC/VM), (b) VM/FC. Symbols: ● Coals, ● Coals+PFA, ■ Coals+FBA, ♦ Olive cake, ◇ olive cake+coal PFA, and ▲ coal studied in (Ren et al., 2017) with trend lines based on data in Ren et al (Ren et al., 2017) for coals/ torrefied fuels (dashed line) and biomass fuels (dotted line).

It should be noted that while the effects are not as large as seen in devolatilisation (DTF1) some effect of the additives was apparent: As the volatiles increased (FR decreased), so there was a greater reduction in NO emissions in the presence of additive, particularly when using the PFA additive. The olive cake, with the lowest fuel

ratio showed a reduction of emissions from 0.57 kg/GJ to 0.47 kg/GJ (±0.01 kg/GJ). Co-feeding PFA (coal or biomass derived) resulted in a reduction for NOx kg/GJ, across all of the fuels, coals and olive cake.

The PFA had higher values of alkali and alkaline earth metals compared to the FBA and the coals as shown in Table 5.2 and 5.3. Figure 7.11a and b explores the influence of alkali and alkaline earth metals on NOx emissions from the test in the un-staged DTF (in excess air).

The curves in Figure 7.11a are based on data for combustion of coals/torrefied biomass and raw biomass from (Ren et al., 2017). A trend of decreasing NOx with increasing reactive metal components is observed, which could point to a mechanism whereby fine nanoparticles of metal oxides embed into the fuel/char particles at reactive sites. Once in close contact with the fuel matrix they can influence the heterogeneous reaction chemistry and decrease NOx. The curves and data in both Figures 6.8 and 7.11a and 7.11b suggest that there is a limit to the effectiveness of this mechanism. Results for the raw fuels are in agreement with (Ren et al., 2017), and there are modest reduction in the NO emission (17% decrease in NO for the olive cake and 5% decrease in NO for the coals in the presence of PFA, which has the greatest amount of alkali and alkaline earth metals). This is demonstrated further in Figure 7.11b. However, the presence of excess air in DTF2 is influencing the efficacy of the gas-phase NOx reduction chemistry.

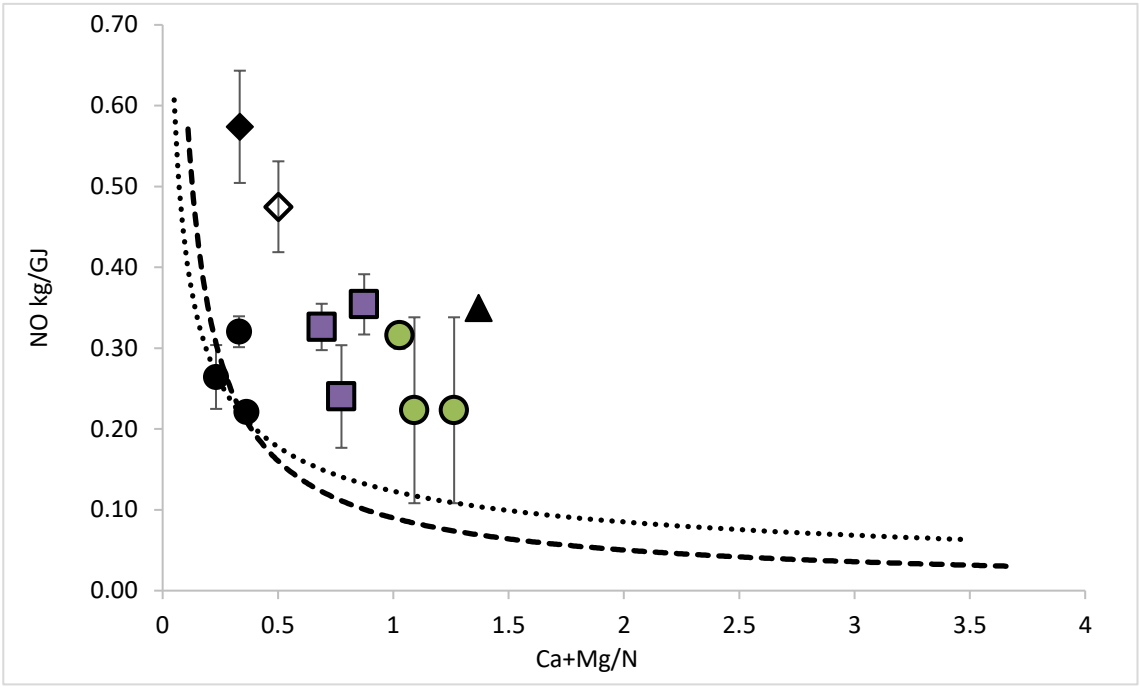

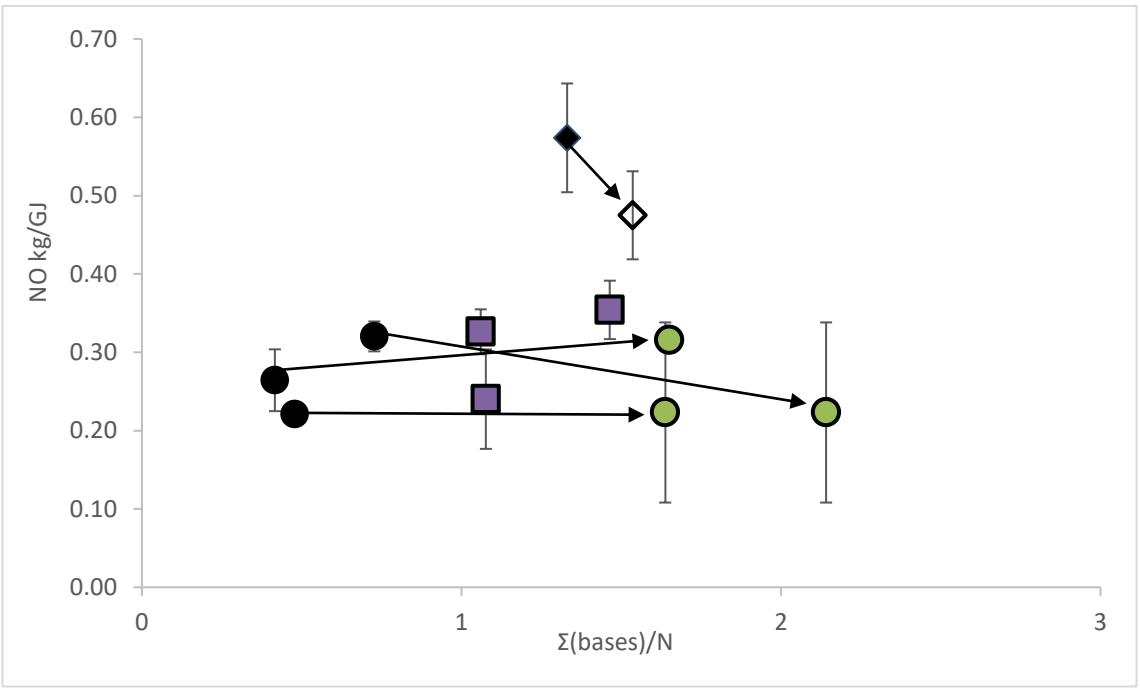

Figure 7.11. NO emissions from combustion at 1373 K in DTF2 with respect to mass ratios of potential reactive elements in the feed (normalised for nitrogen in the feed). (a) alkaline earth metals (dashed and dotted lines represent the relationship for coal/torrefied biomass, or biomass respectively from (Ren et al., 2017)) (b) alkali+alkaline earth metals. ● Coals, ● Coals+PFA, ■ Coals+FBA, ♦ Olive cake, ◇ olive cake+coal PFA. Arrows denote change in NO emissions for fuels with PFA.

If the additives were used in a staged combustion system, then the reduced oxygen in the near burner region, together with enhanced fuel-N release in the presence of

additives (as seen in DTF1 and ballistic TGA), should be conducive to NOx reduction, although the combustion would need optimising for each fuel-additive combination.

The modelling work in Chapter 8 has shown that calibration curves can be used to combine bituminous coals with additives (when the chemical analysis is known) to predict: both the N partitioning from a DTF and the NO_X emissions from a furnace.

7.6 Char nitrogen evolution profiles (STA-MS)

Using chars produced in DTF1, char combustion was carried out in the STA-MS, following the procedure in Chapter 4.12. Figures 7.12-7.15 shows the Gs evolution profiles for CO_2, C_2N_2, HCN and NO for the four chars with and without both additives.

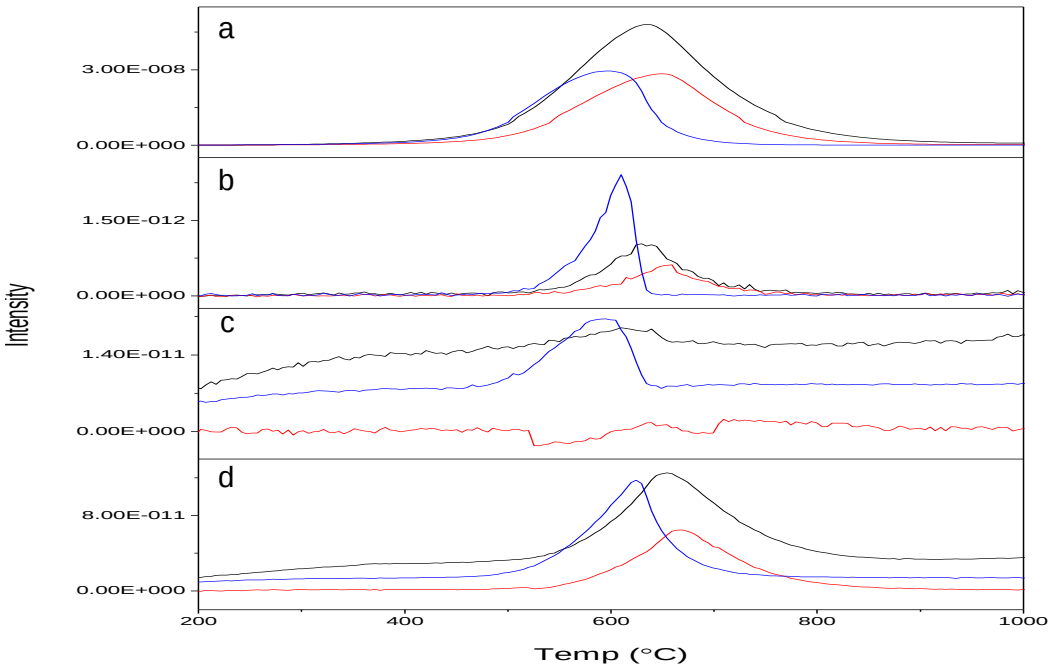

Figure 7.12 Ffos-y-fran char with and without additives emissions profiles for; a. CO_2, b. C_2N_2, c. HCN and d. NO. —— Chars —— chars plus FBA —— chars plus PFA

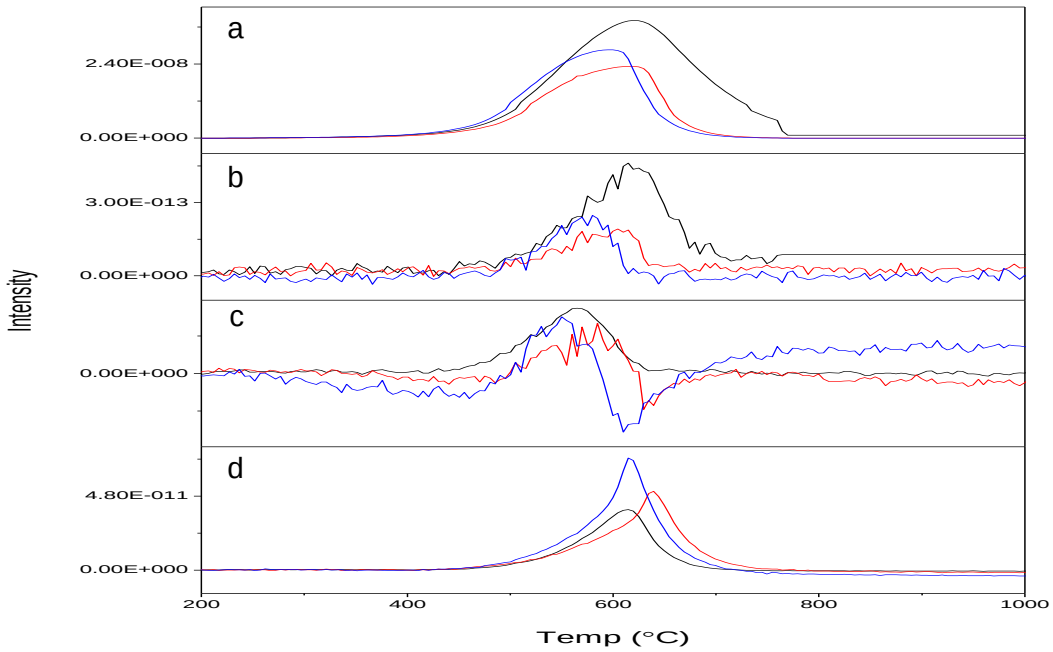

Figure 7.13 Shotton char with and without additives emissions profiles for; a. CO_2, b. C_2N_2, c. HCN and d. NO —— chars —— chars plus FBA —— chars plus PFA

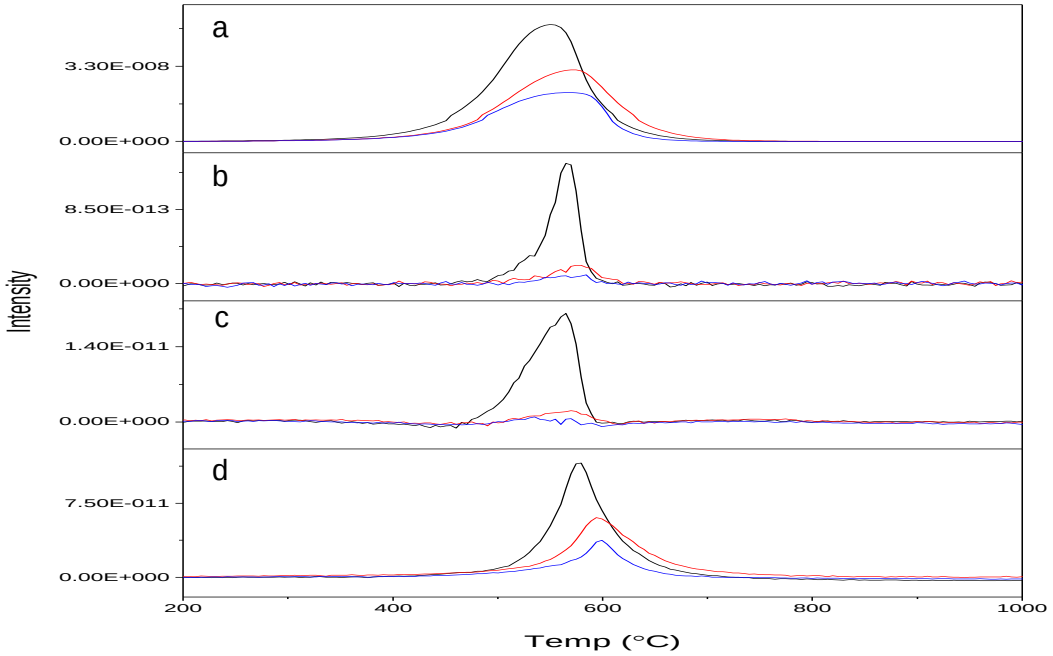

Figure 7.14 La Loma char with and without additives emissions profiles for; a. CO_2, b. C_2N_2, c. HCN and d. NO —— Chars —— chars plus FBA —— chars plus PFA

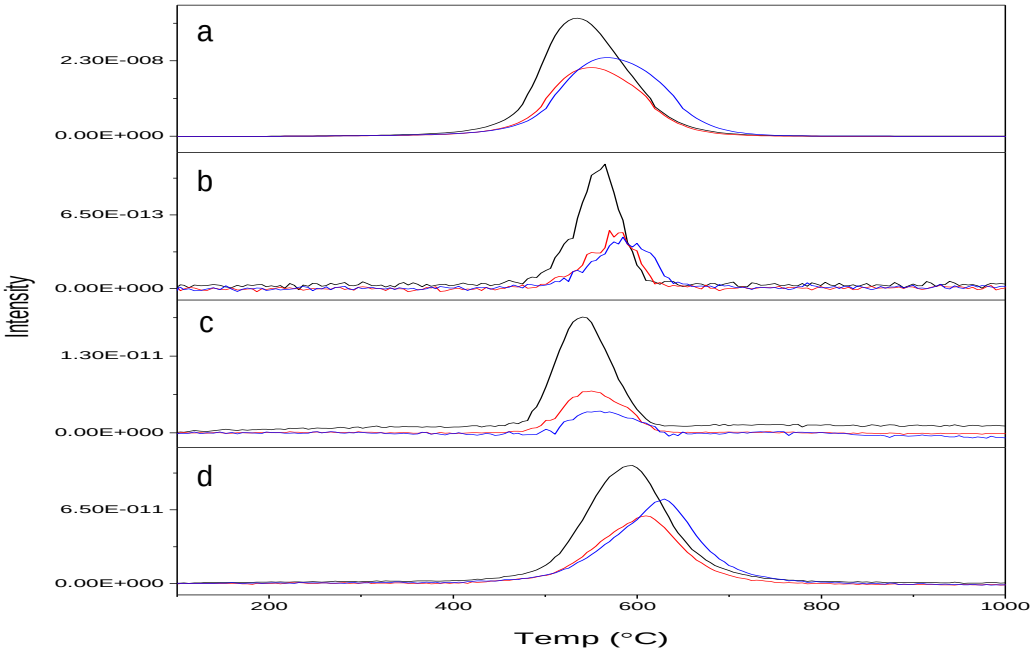

Figure 7.15 Galatia char with and without additives emissions profiles for; a. CO_2, b. C_2N_2, c. HCN and d. NO —— Chars —— chars plus FBA —— chars plus PFA

All three of these nitrogen compounds are important in the formation and potential control of NO_X in a furnace. The NO and the HCN has been discussed in Chapter 3 and in Equations 3.1-3.16. The C_2N_2 is an intermediate in the mechanism to form NO_X. (Setser, 1965). C_2N_2 can often be seen leading the formation of NCH and NO as shown in Figures 7.12 – 7.15, where all four of the coals show some C_2N_2 formation. Whilst this does lead the HCN and the NO, there is an overlap in the formation, indicating not all of the C_2N_2 goes on to form HCN or NO. Equations 7.13 to 7.15 shows one process for the formation of HCN and NO from the C_2N_2.

$$O + C_2N_2 \rightarrow NCO + CN \qquad \text{Eq 7.13}$$

$$O + NCO \rightarrow NO + CO \qquad \text{Eq 7.14}$$

$$O + C_2N_2 \rightarrow HCN + CO \qquad \text{Eq 7.15}$$

The Ffos-y-fran however, does shown a consistent increase in HCN up to ~600 °C, then maintained at this intensity level across the full range of the rest of the temperatures shown in Figure 7.12c, (this could be attributed to baseline drift), for the coal without additives whilst the C_2N_2, only starts to show formation at ~ 550°C. Ffos-y-

fran is the only coal under test to show this characteristic. As a char without additives, Ffos-y-fran is the only coal char to show pyridinic (N-6) formation, Figure 7.6. Work by Li and Tan indicated that when pyridine was present, in shock tube experimentation, more NH_3 and NH_3 as a precursor to NO, was formed in preference to HCN (Li and Tan, 2000). Axworthy et al showed, in a quartz reactor, pyrolysis of coals in a helium atmosphere yielded the following: pyrrole showed a 50% decomposition at 905°C, and pyridinic nitrogen increased from 40% at 960°C up to 100 % at 1100°C. However it was unclear if the HCN was from a primary or secondary reactions (Axworthy et al., 1978). Whilst these works were focussed on pyrolysis of coals rather than the chars, they may be indicative that pyridine forms more readily into NH_3 rather than HCN at lower temperatures. Both NH_3 and HCN are known precursors to NO_X formation, as shown in Chapter 3. At higher temperatures, the pyridine is more likely to convert to HCN. Within this work, the C_2N_2 appears to show a peak conversion temperature leading the peak formation temperature of HCN and consequently the NO, when the chars were blended with the additives Figure 7.12-7.15.

All of the chars formed without additives are predominantly composed of quaternary nitrogen species, Section 7.4.

When the chars were made from coals blended with the additives, the emissions characteristics changed for all four of the chars. The intensity of the peaks are an indication of the amount of the gases released. Across all of the bituminous coal chars, the intensity of the gases is significantly diminished for all gases with both additives. For the Ffos-y-fran chars with PFA, the C_2N_2 profiles shows an increase in intensity, indicating more C_2N_2 gas is released when blended with the PFA. Across all of the coal chars, when blended with the PFA, the gas peaks are all at lower temperatures than for the coal chars without additives. The move to lower temperatures is a good indication catalysis is taking place, particularly when the chars are formed with the PFA.

The data from the STA-MS was used for two separate calculations: nitrogen species evolution (NO/N, HCN/N, C_2N_2/N) and char reactivity, shown in Section 7.7. To

calculate the respective ratios of NO, and its precursors, HCN, C_2N_2 to fuel-N, Equations 7.10-7.12 were used, with the data from the Quadupole MS. The ratios were converted to percentages and presented in Table 7.5.

$$Char\frac{C_2N_2}{N} = \frac{C}{N} \times \frac{[C_2N_2]}{[CO+CO_2]} \quad \text{Eq 7.10}$$

$$Char\frac{NO}{N} = \frac{C}{N} \times \frac{[NO]}{[CO+CO_2]} \quad \text{Eq 7.11}$$

$$Char\frac{HCN}{N} = \frac{C}{N} \times \frac{[HCN]}{[CO+CO_2]} \quad \text{Eq 7.12}$$

From Table 7.5 the totals of the nitrogen evolution species are less than 100%. Due to the mass of N_2 being the same as CO, it is unable to be detected with the equipment, therefore we have to make the assumption that the remaining N species not shown in the table is in the form of N_2.

Table 7.5 Percentage nitrogen split for the chars and chars plus additives

Chars	NO/N	HCN/N	C_2N_2/N	Total %
Ffos-y-fran char	44.85	15.89	0.02	60.76
Ffos-y-fran plus FBA char	16.61	1.12	0.11	17.84
Ffos-y fran plus PFA char	6.26	2.53	0.32	9.11
Shotton char	16.78	1.39	0.05	18.22
Shotton plus FBA char	8.50	0.14	0.05	8.69
Shotton plus PFA char	8.03	0.68	0.03	8.74
La Loma char	8.40	1.13	0.05	9.58
La Loma plus FBA char	9.41	0.39	0.02	9.82
La Loma plus PFA char	5.59	0.14	0.01	5.74
Galatia char	16.40	2.50	0.10	19.00
Galatia plus FBA char	14.20	1.17	0.07	15.44
Galatia plus PFA char	13.26	0.41	0.05	13.72

Where the chars were blended with the additives, it can be seen in Table 7.5 that there is a reduction across all of the species, with the exception of La Loma plus FBA, where

an increase in NO/N is felt. The reduction seen in the total nitrogen species can be inferred to show there is an increase in N_2, showing catalysis from the additives.

7.7 Char reactivity

Char reactivity was calculated for all four of the chars with and without additives, and the results shown in Table 7.6. The bituminous chars without additives all show an increase in activation energy (Ea) compared to the respective coals. Ffos-y-fran char shows a slight decrease in Ea value compared to the coal. All of the bituminous coals show a reduction of Ea with the addition of either of the additives.

Table 7.6 Kinetic parameters of coal chars and coal chars/ash blends

Sample (Chars)	E_a (kJ/mol)	A (cm^3/s)	k_{773K}/s
Ffos-y-fran	163.49	5.74E+08	5.13E-03
Ffos-y-fran plus FBA	163.83	1.62E+08	1.38E-03
Ffos-y-fran plus PFA	193.63	6.46E+10	5.31E-03
Shotton	169.77	1.75E+09	5.90E-03
Shotton plus FBA	120.29	2.70E+05	1.55E-03
Shotton plus PFA	91.70	2.44E+03	2.01E-03
La Loma	100.3	5.05E+04	8.43E-03
La Loma plus FBA	75.52	2.50E+02	1.97E-03
La Loma plus PFA	69.66	5.39E+01	1.06E-03
Galatia	163.11	2.92E+08	2.77E-03
Galatia plus FBA	126.69	6.39E+05	1.76E-03
Galatia plus PFA	112.25	4.35E+04	1.13E-03

However the calculation of the rate constant at 773 K gives a means of comparing the reactivities of the coal chars. For all of the chars, produced from the coal-additive blends, there is a reduction in the reaction rates. The reduction in reaction rates is particularly pronounced for the blends with FBA. The addition of PFA to the coal chars also shows a reduction in the reaction rates for the Ffos-y-fran, Shotton and Galatia. This may be related to the extent of burnout and annealing that each of the chars have undergone in the DTF. It was seen in section 6.3 that the additives enhance the burn-out of the chars, such that each char-additive combination has undergone a different

extent of burn-out, as shown in Figure 6.5. In fact, there is a good correlation of k_{773} and % carbon conversion for Shotton, and Galatia, whilst La Loma (the highest volatile content coal/lowest carbon content) shows a modest increase as shown in Figure 7.16. As the k value decreases so carbon conversion increases as the char undergoes burn-out the remaining material becomes less and less reactive. (Hurt et al, 1998).

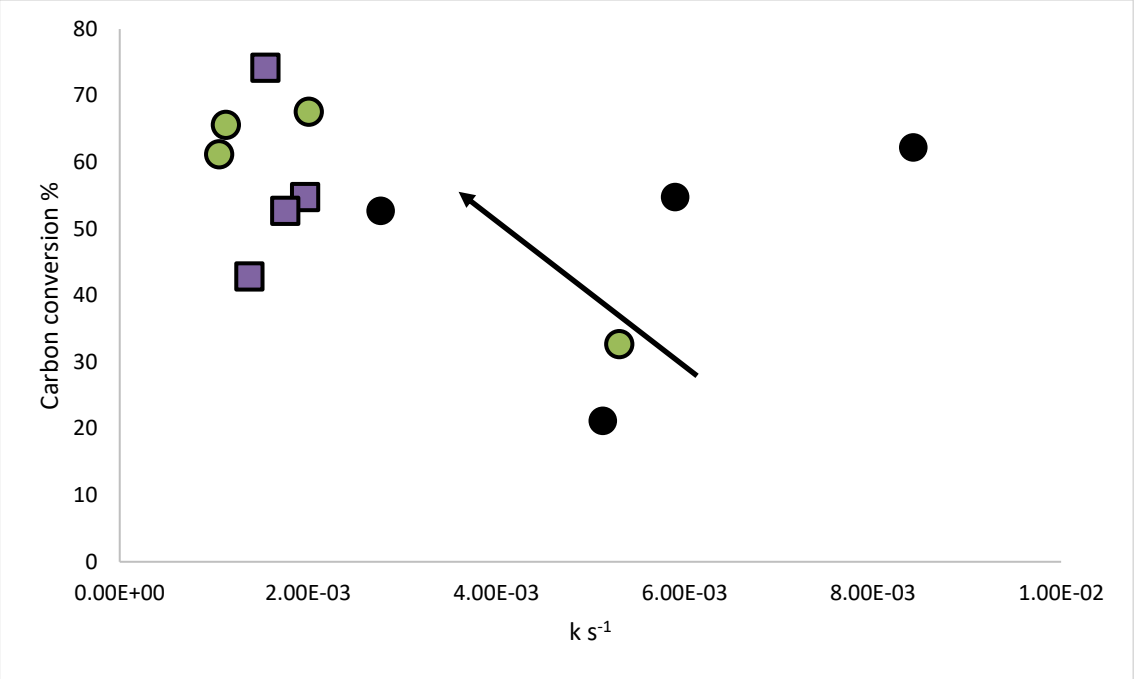

Figure 7.16 Carbon conversion as a function of k_{773}. The arrow indicates the trend of carbon conversion as k decreases. ● Coals, ● Coals+PFA, ■ Coals+FBA.

7.8 Chapter summary

Within this chapter, the chars produced from coal and coal with additive blends have been investigated for N-functionality, morphology, reactivity and char-N release during combustion. The bituminous coal chars have shown changes to their respective coals when subjected to HHR testing and analysis. The bituminous coal chars have shown changes in their morphology, through softening of the particles and the release of volatiles. The Shotton and Galatia chars display characteristics of rapid expansion and expulsion of volatiles, resulting in highly visible pore structures and comparatively thin char walls, cenospheres. La Loma showed swelling of the coal particles, however there were not the same density of visible pore structures of the other two bituminous coals

(Shotton and Galatia). La Loma has become malleable, but through the retention of some tars, the surfaces have remained mainly intact. The Ffos-y-fran has shown no apparent change to physical morphology compared to the bituminous coal.

When blended with the additives, there was some change to the physical structures of all three of the bituminous coals. The Shotton and the Galatia both show an increase in surface pore density. Galatia showed the greatest increase in pore density, indeed showing some increased explosive release of volatiles, resulting in fragmentation of the cenospheres. La Loma showed some increase in reactivity, whereby there are some clearly visible pores in the char surfaces.

The functional groups have shown a change in the chars compared to the coals, where the N-5 groups have been converted to N-Q. Shotton also showed some nitroso $N\text{-}O^-$ content. Ffos-y-fran showed a change to N-Q, however, there was also some signs of pyridinic nitrogen (N-6).

When blended with the additives, there was some noted changes to the functional groups within the chars. Galatia and La Loma maintained the N-Q as their principle functional group. Shotton showed a change by releasing the nitroso and developing an N-6 peak at 398.7 eV. Ffos-y-fran showed a single peak of N-Q, however this was of a wide bandwidth, and may incorporate some N-6 functionality. The development of N-Q from N-5 is a known process, under high heating rate pyrolysis conditions. (Pels, 1995a). N-Q is less stable than N-6, therefore if more extreme heat conditions were applied, then a decrease in N-Q and an increase in N-6 could be expected. This may be accelerated by the introduction of the PFA additive for coals.

NO emissions in an excess air combustion environment (DTF2) showed little change in the ppm values from the bituminous coals or chars when blended with the additives. Although a slight trend towards NO reduction was observed when compared to the Σ(Fe+ basics)/N in the blends. The work from DTF2 showed the known relationship between FR and NO emissions was maintained even when the coals and chars were blended with the additives.

Chars from DTF1 were used to study the char nitrogen species evolving during combustion. The fraction of char-N converted to C_2N_2, HCN and NO were decreased when the chars were blended with the FBA and PFA, implying enhanced conversion of char-N to N_2.

In the Shotton and Ffos-y-fran, the addition of the PFA to the chars tends to show the formation of the C_2N_2 leading the HCN and NO respectively. C_2N_2 is a potential precursor to the formation of NO during coal and char combustion. If the release of the precursors can be liberated at lower temperatures, then the resultant NO can be reduced in a Low-NO_X burner.

The higher volatile coal chars (Galatia and La Loma), show a tendency for the C_2N_2 to be released at the same temperature as the HCN and NO, however all three of the emissions were released at lower temperature with respect to the chars without additives for the two higher volatile coals. This indicates that the char combustion process is faster in the presence of additives.

The results from the STA-MS indicate a reduction in the amount of C_2N_2, HCN and NO from all four of the chars when blended with the additives, this indicates that there is enhanced conversion of char-N to N_2.

Chapter 8 Modelling

8.1 Introduction

In this chapter there is: a review of modelling relevant to the research, including the key components that have been utilised in the furnace model, a results section for the modelling carried out and a chapter summary for the model. Modelling is a key component to design of a furnace. The use of models can be applied to an engineering system to find a representation of expected, calculable and predictable results.

A problem facing operators of large-scale furnaces is the implementation of emissions regulations which have come in retrospect to the furnace build and for the design of future furnaces. The emissions directives (discussed in Chapters 2 and 3) in the future are expected to become more stringent, in particular for large furnaces operating with pulverised fuel combustion. With new furnaces expecting to have life expectancies of 40-60 years, controlling the emissions whilst maintaining efficiency, in the present and the future is one of the key requirements in combustion. If models can be utilised to predict the performance of a furnace and the emissions output, then alternate methods of operation of the furnace can be trialled to find emissions reduction strategies. Historically there have been several models developed to investigate combustion processes. Of importance within this work, are the Chemical Percolation and Devolatilisation (CPD) and Carbon Burnout Kinetics (CBK 8) models. These two model approaches have been integrated into a furnace slice model developed in (Waldron, 2005). For this work, the modelling is focussed on the devolatilisation and char combustion of bituminous and sub-bituminous coals during pulverised fuel combustion in the presence of additives. The outputs from the models are in the form of nitrogen partitioning from CPD and NO_X emissions from the slice model.

8.2.1 Devolatilisation and combustion modelling

Model development is essential to predict the thermo-chemical processes and emissions characteristics of a fuel. If model predictions can be carried out before any combustion takes place, the efficiency of the furnace can be optimised, a higher achievable energy per kg of fuel consumed can be realised and emissions characteristics can be calculated for known fuels. If a furnace operation is more efficient, the amount of waste, in both energy lost and non-combusted carbon in the ash can be reduced. Higher efficiency of combustion can also lead to less harmful pollutants being created in an emissions-controlled furnace.

There is often a compromise in a furnace between emissions characteristics of any fuel and the furnace operating conditions. The combustion profile within a furnace can change the distribution of fuel emissions given off from any fuel. A furnace operating at lower efficiencies, or the use of lower oxygen content, would favour CO over CO_2. A lower efficiency combustion process would seem undesirable. With respect to the reduction of NO_X, lower furnace temperatures are favourable to reduce thermal NO_X, but lower temperatures affect the extent of carbon burnout. To predict the emissions in particular for this research, NO_X, the use of a model can be instrumental in finding reduction strategies. (Mitchell, 1998; Popescu, 2010).

In this project the two biomass additives, FBA and PFA, are being used as catalysts to change fuel nitrogen partitioning. If the fuel nitrogen can be released during devolatilisation, then firing strategies can deliver optimum performance to reduce NO_X emissions at the stack.

Coal is a complex heterogeneous fuel. Owing to this, modelling the output from coal combustion, for both energy and emissions can be complicated. Coal combustion can be considered in three principle stages:

- Particle heat up, including moisture loss
- Devolatilisation

- Char burnout

These three processes do not happen in isolation or necessarily sequentially. Even in a well-mixed furnace, in the near burner flame, particles of coal can go through different gas environments, some containing relatively higher levels of oxygen. With the variation in oxygen content, there is an overlap between devolatilisation and char combustion. (Gurgel Veras et al., 1999). Depending upon the heating environment and burner conditions, all three can occur concurrently, although char combustion is inevitably the last to complete. Figure 8.1 shows a representation of the stages of combustion of a coal particle, and how the combustion process can be fed into a model.

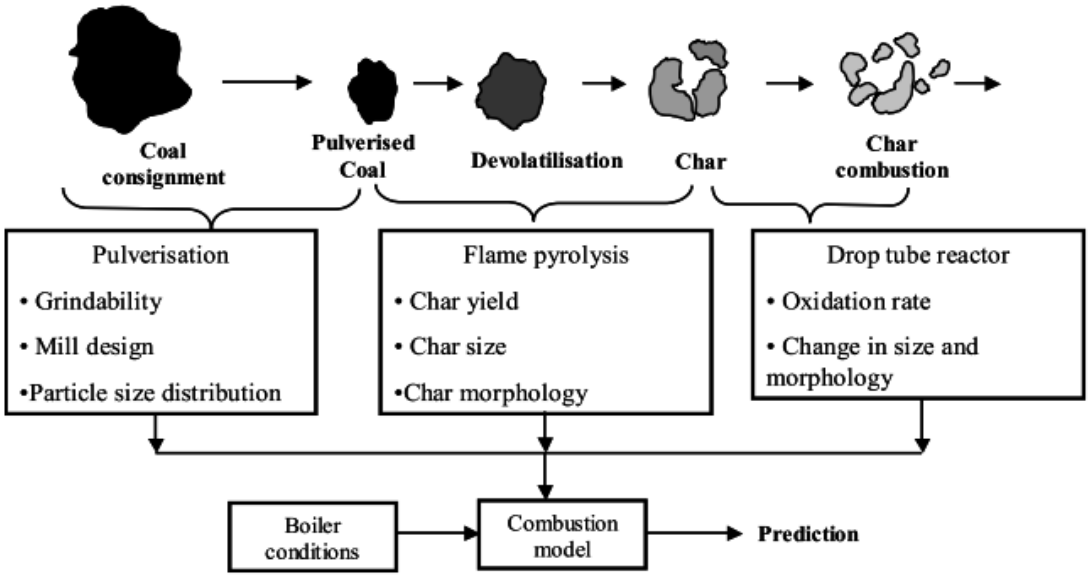

Figure 8.1 The process of coal combustion and the feeds into a model (Unsworth, 1991; Waldron, 2005)

There are two distinct phases for building a model for a furnace, from a solid fuel perspective. Devolatilisation/pyrolysis and char combustion. A number of mathematical models have been proposed and developed in the past. The models range from simple correlation models based on empirical data up to models that utilise information about the fundamental coal structure. There is a variety of sub-models that have been implemented to explain the combustion process.

Figure 8.2 highlights a breakdown for the modelling process, from four different approaches to devolatilisation, and two methods of char combustion modelling.

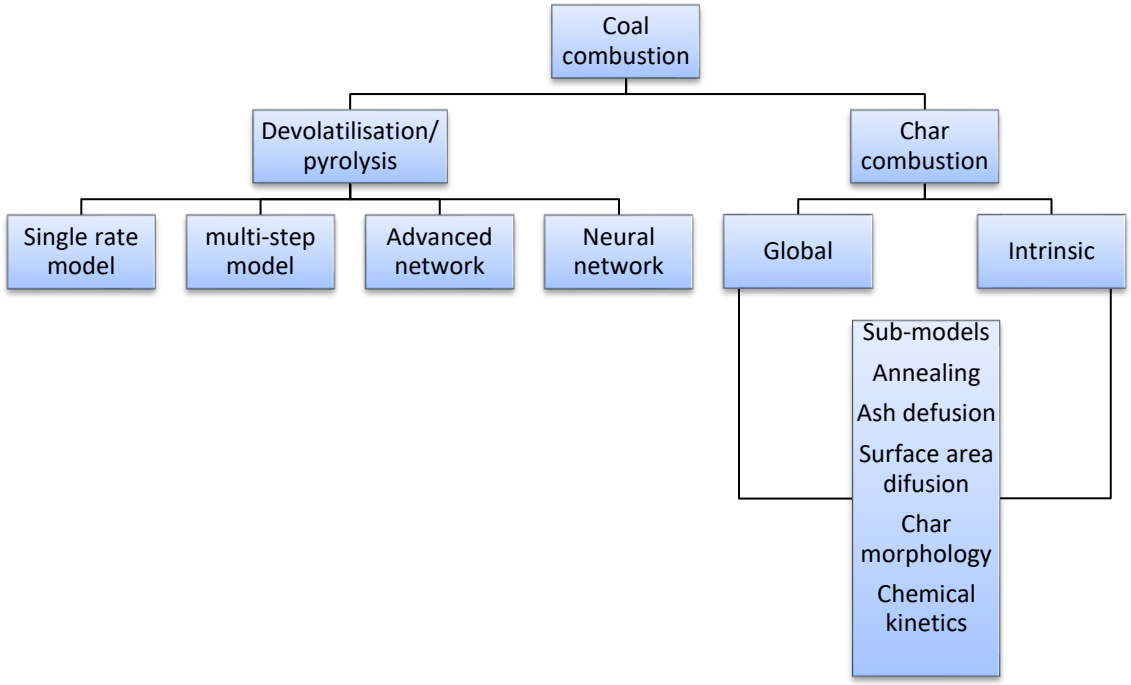

Figure 8.2 Model development for coal combustion, adapted from (Waldron, 2005)

Computational fluid dynamic (CFD) modelling can utilise sub-models to describe the combustion process, however these often require input from empirical data from experimental or laboratory work (Waldron, 2005).

For the development of NO_X from solid fuel combustion, the single rate and multi-step models are not sufficient, therefore the advanced models are required to accurately predict nitrogen devolatilisation within a furnace (Waldron, 2005; Williams, 1993).

8.2.2 Devolatilisation modelling

Whilst it is dependent on the coal type and heating regime, devolatilisation occurs between ~300-700°C. In bituminous coals the metaplasts and clusters remaining after devolatilisation become malleable at ~500°C, after this, at ~550°C they solidify again into chars. Above 700°C, the carbon matrix will break down and react at appreciable

rates, resulting in the gasification of the char and the development of CO/CO_2. (Fernando, 2014), see Section 8.3.2.

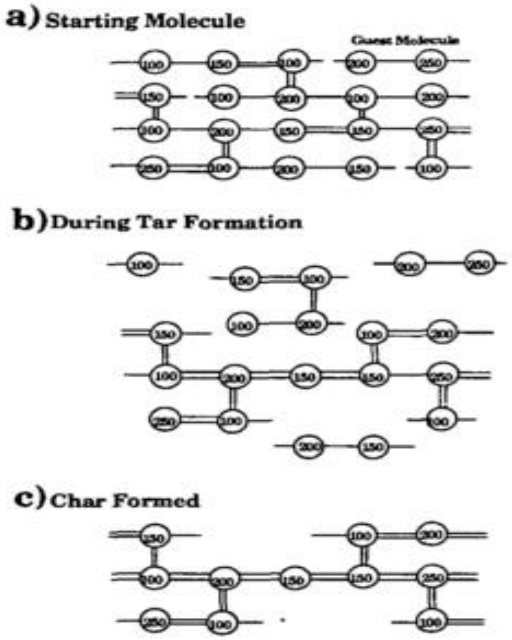

Figure 8.3 Representation of the dissociation of a coal molecule during devolatilisation. (Solomon et al., 1992)

The representation in Figure 8.3, is based on the Functional Group-Devolatilisation, Vaporising and Cross-linking (FG-DVC) model developed by Solomon and Serio, but the principle is relevant for devolatilisation and char formation across other combustion and devolatilisation models. (Solomon et al., 1992) From the starting molecule, light functional groups and aliphatic compounds break off as side chains and labile bridges break. The single lines represent easily broken bonds, whilst the double bonds require higher levels of energy to dissociate. Numbers represent the molecular weights of the aromatic structures (Solomon et al., 1992).

Devolatilisation is an important process for building a coal combustion model. Pyrolysis of a coal can release as much as 70% of the mass loss and 50% of the heating value. (Fernando, 2014; Kobayashi, 1977). During pyrolysis, the labile bridges and side chains are broken, leaving aromatic rings with masses much less than the original coal. The aromatic rings from the parent coal, form the tars and further cross-linking to form

chars. The fragments with low molecular weights will often form light gases, heavier gases and tars. Under continued heat, the tars subsequently break down into light and heavier gases. Fragments and gases with higher molecular weights and low vapour pressures, can reattach to the char lattice. (Fernando, 2014)

Much work has been carried out to establish the chemical composition and compounds within coal volatiles, however the structures and compounds are still not completely understood. Volatile matter, predicted within models is often therefore treated as an assumed representative structure, especially in computationally expensive modelling such as CFD. (Arenillas, 2001; Baum, 1971; Hashimoto, 2012).

The heating regime, heating rate and final temperature, are the most important factors in coal devolatilisation and thus essential in establishing a model for predicting coal combustion and burnout. Higher heating rates tend to release higher percentages of volatiles compared to proximate values. Kobayashi *et al*, showed the comparison between a lignite and a bituminous coal at the same final temperature, heating rate and residence time (Kobayashi, 1977). Both coals had very different chemical compositions but showed similar devolatilisation rates and total volatile release with short residence times of 10-200ms.

To establish a model, there are some key assumptions required about coal combustion.

- Different coal ranks and coal types devolatilise at different rates:
- Rates of devolatilisation of functional groups within coals are independent of the coal type
- The chemical composition of the tars is based on the composition of the virgin coal. (Hashimoto, 2012; Solomon, 1987; Solomon, 2007)

Devolatilisation is often modelled on the numerical devolatilisation model of Badzioch (Badzioch, 1970; Niksa, 1996a; Niksa, 1996b; Solomon, 1987; Solomon, 2007), where an apparent first order single rate Arrhenius equation is used to calculate the rate of

devolatilisation. The rate of devolatilisation is dependent on the amount of volatiles remaining in the fuels at any given time, as given in Equation 8.1.

$$\frac{\mathrm{dV}}{dt} = \mathrm{k}(\mathrm{V}^* - \mathrm{V}) \qquad \text{Eq 8.1}$$

where

$$k = k_0 exp^{\frac{-E}{RT}} \qquad \text{Eq 8.2}$$

V is the volatiles at time t, V* is the total volatiles. Whilst the first order approach may have its limitations, it is widely adopted and yields a good representation of devolatilisation from different coals. (Fletcher, 1998; Hashimoto, 2012; Solomon et al., 1992)

Further devolatilisation models have been developed using a two stage devolatilisation process, with two competing reaction rates, Figure 8.4. (Fletcher, 1998; Hashimoto, 2012; Kobayashi, 1977; Solomon et al., 1992; Baum, 1971).

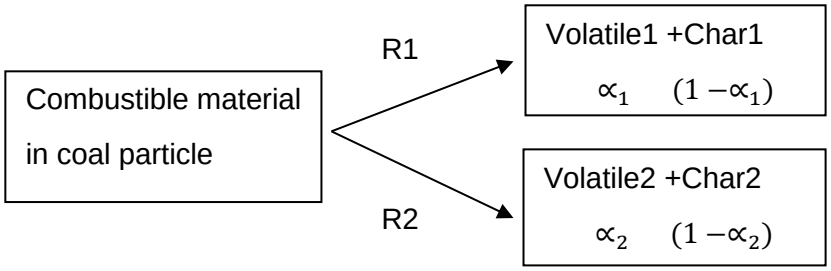

Figure 8.4 Two stage devolatilisation model (Baum, 1971)

$$R_1 = A_1 exp^{\frac{-E_1}{RT_p}} \qquad \text{Eq 8.3}$$

$$R_2 = A_2 exp^{\frac{-E_2}{RT_p}} \qquad \text{Eq 8.4}$$

Where A_1 and A_2 are the pre exponential rates and E_1 and E_2 are the activation energies for the two devolatilisation reactions, α_1 and α_2 are mass stoichiometric coefficients.

With the two reaction rates, volatile release and devolatilisation rates can be calculated dependent upon the heating rates. This approach can be extended to model multiple reactions. The drawback of this method is obtaining the six parameters required before running the simulations.

8.2.3 Network models for predicting coal devolatilisation

The three main models that have the facility to calculate the devolatilisation and account for nitrogen partitioning are:

FLASHCHAIN (Niksa and Kerstein, 1991)

Functional group – depolymerisation, vaporization and cross-linking-FG-DVC- (Solomon, 1987; Solomon et al., 1992).

Chemical percolation and devolatilisation-CPD. (Fletcher, 1998)

The network models for predicting the behaviour of coal devolatilisation, FLASHCHAIN, FG-DVC and CPD use the structural characteristics of the coals to calculate an approximation of their thermal decomposition. These models calculate the decomposition based upon some chemical composition assumptions. The three models adopt a different mathematical approach for the devolatilisation of the fuel. (Hurt, 1998; Solomon et al., 1990).

8.2.4 FLASHCHAIN

Within the FLASHCHAIN model, coal is considered to consist of a mix of chain fragments. The coal structure is further broken down into 4 key features:

- labile bridges
- char links
- aromatic clusters
- peripheral groups i.e. aliphatic chains.

The coals devolatilise into aromatics, hetero-aromatics and aliphatic compounds. The coals devolatilise through bridge scission, spontaneous condensation, bimolecular recombination and peripheral group elimination.(Niksa and Kerstein, 1991) All of the nitrogen within the coal is assumed to be contained inside the aromatic compounds.

8.2.5 FG-DVC

Devolatilisation of coal using FG-DVC predicts the volatiles, tars and individual gases, distribution of tar molecules and the fluidity of char (Bassilakis et al., 1993). It subjects the assumed macromolecular structure network to various reactions, combining crosslinking, labile bridge breaking, tar vaporisation and tar reformation, Figure 8.3 (Solomon, 1987). To determine coal devolatilisation kinetics and the composition of volatiles, thermogravimetric Fourier transform infrared (TG-FTIR) is employed.

The model is based on the following principles:

- Labile bridge breaking
- Gas evolution through crosslinking
- Tar transportation, breaking into lighter fragments and light gases
- Determination of molecular fragmentation
- Decomposition of the coals to produce tar and char
- Functional group decomposition to produce light gases

Under heat, the coals matrix decomposes into smaller mass fractions. The lightest fractions become volatile gases, some of the lighter fractions and the intermediary fractions evaporate or condense to form tars. The heaviest fragments form the metaplasts and chars, Figure 8.3. (Solomon, 1990)

8.2.6 CPD

Within the CPD model, coal is treated as a macromolecular network system with aromatic rings connected via labile bridges, side chains connecting aliphatic compounds to the aromatic compounds. The nitrogen and oxygen are considered to be contained within the aromatic rings. This is based on a Bethe lattice 2-dimensional structure. Figure 8.5.

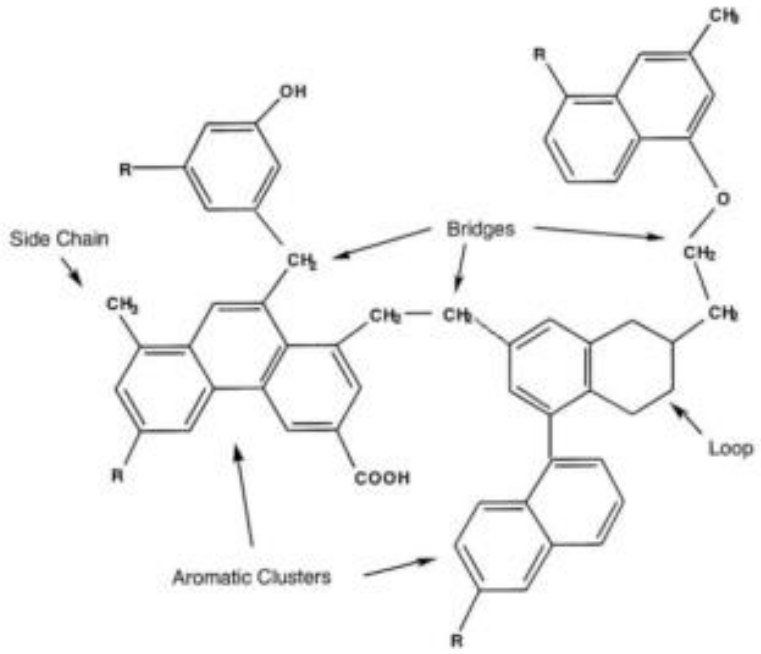

Figure 8.5 Representation of a coal structure, labile bridges and side chains shown Bethe lattice 2-dimensional structure (Fletcher et al., 1990)

Chemical structures are determined from 13C NMR analysis, which are considered to be coal dependent parameters. The kinetic rates of dissociation of the labile bridge and sidechains are taken as independent of the coal type. (Fletcher et al., 1990).

Percolation statistics are employed to calculate the tar precursor generation from the coal. Flash vaporisation is used to describe the cleavage of the labile bridges and side chains. Cross linking is used to account for the formation of chars and metaplasts. (Fletcher et al., 1990; Fletcher, 1998)

As the bridges and side chains disassociate, light gases and aromatics are released. As heating continues, heavier gases and tars are released from the lattice. The final structures left are the chars, metaplasts and mineral matter, which will form the ashes.

8.3.1 Model development

Figure 8.6 is a schematic representation of the combustion model proposed by Waldron, which incorporates several sub-models: volatile release model, gas combustion, soot model and a char model (Waldron, 2005).

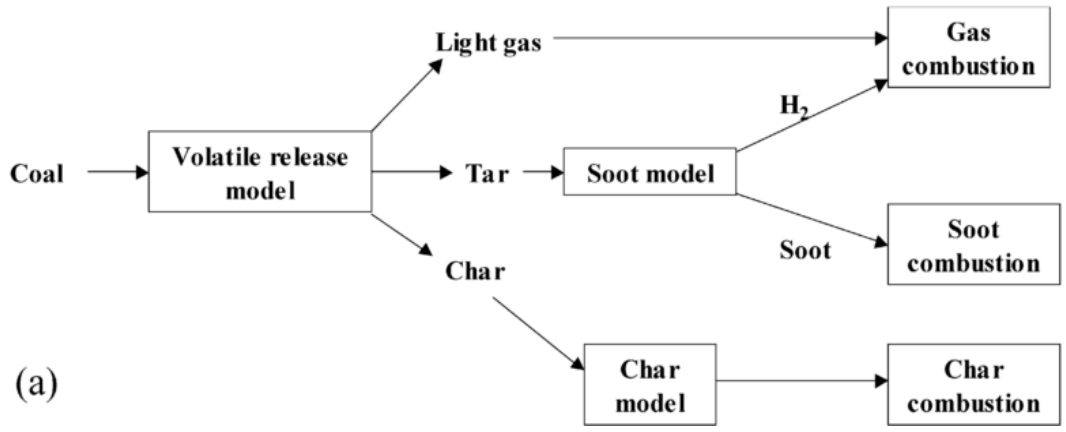

Figure 8.6 Schematic of the coal combustion model. (Waldron, 2005)

The volatile release model predicts the division of the coal into light gases, tars and char. The predictions from the three divisions are then applied to the sub-models. The volatile model can also be used to predict the high temperature volatile yield and the partitioning of volatile-N, tar-N and char-N. The soot model is used to predict the soot burnout, whilst the char model is used to predict the char burnout. A combustion model can be developed to predict emissions characteristics.

Devolatilisation within the DTF was modelled using default CPD values and validated using the default CPD values from Table 8.1 and Table 8.2, for the four reference coals. Figure 8.7 shows the relationship between composite rate of side chain breaking and char breaking, kδ/kc.

Table 8.1 Default values for HTVY calculations in the CPD module.

Item	Description	Value
1	Labile bridge dissociation pre exponential constant	2.602×10^{15} s^{-1}
2	Labile bridge dissociation activation energy constant	55400 cal/mol (232 kJ/mol)
3	Labile bridge dissociation constant	1800 cal/mol (7.54 kJ/mol)
4	Composite rate pre exponential constant (side chain breaking/char chain breaking kδ/kc)	0.9
5	Composite rate activation energy constant	0
6	Gas release frequency factor	3×10^{15} s^{-1}
7	Gas release activation energy	69 kcal/mol (289 kJ/mol)
8	St. Dev. for distributed Ea (gas release)	8100 cal/mol (33kJ/mol)
9	Cross linking pre exponential factor	3×10^{15}
10	Cross linking activation energy constant	65 kcal/mol (272 kJ/mol)

Note: Item 4 was optimised for use in the model when the coals were blended with the additives

Table 8.2 CPD default values for volatile N release from the coal matrix

Item	Description	Value
1	Pre-exponential factor fast light gas A_N	18.4 or 10 (note 1)
2	activation energy fast light gas E_N	6 kcal/mol (25kJ/mol)
3	initial fraction stable N, M_{cl}	0.03
4	High T slow N release pre-exponential factor	3.2×10^9
5	High T slow N release energy activation	90 kcal/mol (376 kJ/mol)

Note 1: Two default values have been proposed for Item 1, by Perry. (Perry, 1999) Perry was using a DTF operating at temperatures below 1000°C, where an A_N value of 18.4 was proposed. Thompson and Stainsbury were operating a DTF at temperatures of 1300°C. A better fit of A_N of 10 was found for the experimental work by (Thompson, 1993).

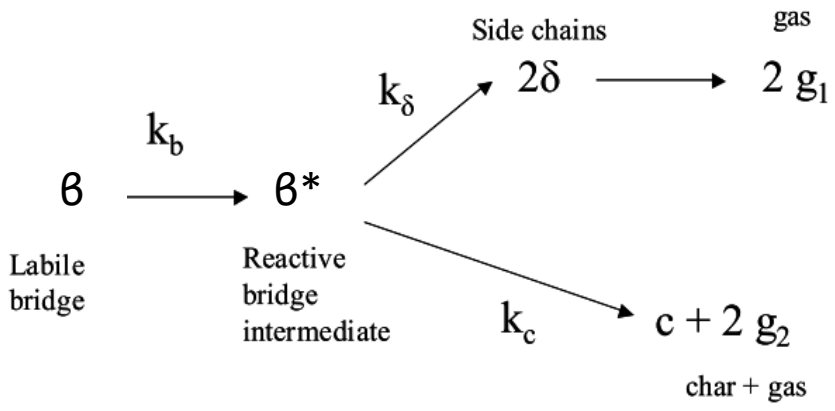

Figure 8.7 The connections between the aromatic cluster and side chains, and their respective cleavage constants (k). (Waldron, 2005)

The DTF model was used for the prediction of devolatilisation of coal. The validation was taken over two stages: HTVY and volatile-N release. Using the default CPD values in the model and with a temperature of 1100°C, heating rate 1 E05°C/s and residence time of 0.5s. The predictions from the model were in close agreement with the data from experimental work in the DTF, for both HTVY and for volatile-N release, Chapters 6 and 7, and shown later in this Chapter.

Within the CPD model, there is a library of coals, which forms the CPD database for the coals based on their molar ratios O:C and H:C. The atomic ratios of the library reference coals are shown in Figure 8.8. The coals are plotted on the modified Van Krevelen diagram and are joined to adjacent coals to form triangulation points. Coals under test can then be plotted on a template graph as shown in Figure 8.8.

The four reference coals were all plotted onto the modified Van Krevelen diagram, with predetermined CPD library coal data. See Section 8.5.2.

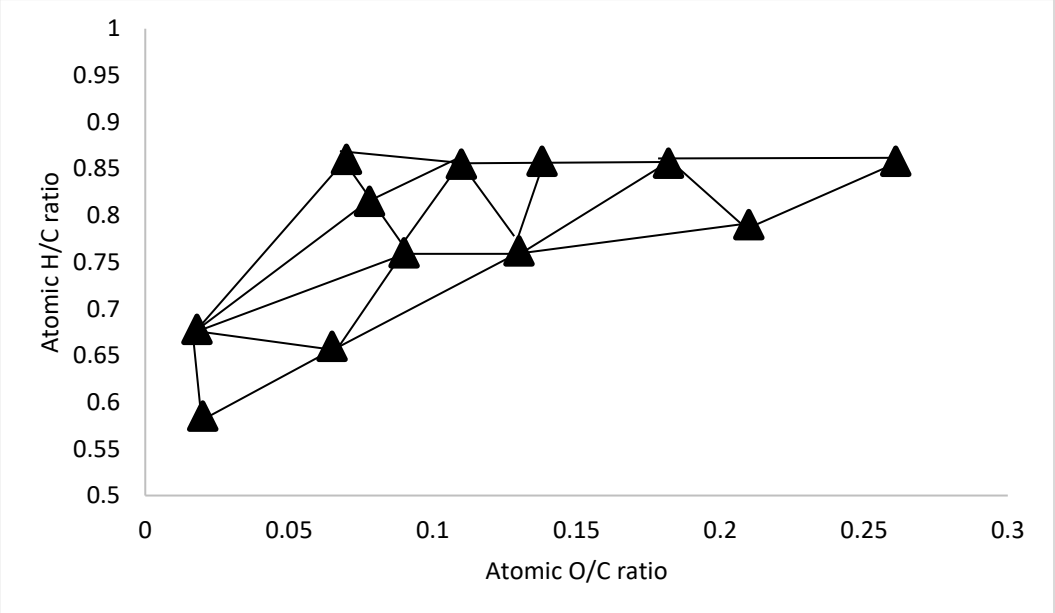

Figure 8.8 Matrix for CPD bituminious and sub-bituminious library coals on a Van Krevelen diagram (Waldron, 2005; Fletcher et al., 1990)

8.3.2 Char modelling

The process of char combustion is relatively well understood, (Waldron, 2005; Williams, 1993). For modelling of char combustion, two methods can be adopted, global and intrinsic. Both of these model approaches rely on sub-models to give accurate predictions.

Chars produced during coal combustion tend to be micro-porous solids, with pores in excess of 18 nm, refer to Chapters 6 and 7, for the transformation of coal to chars. Char particle surface areas for bituminous coals tend to be much higher than their respective coal. Heterogeneous gas-solid reaction zones occur on the surface of the chars in combination with the surrounding gases: O_2, H_2O, CO and CO_2 (Backreedy et al., 2005).

Dependant on temperature and stoichiometric ratios, there are two main products of char combustion, CO and CO_2. The fraction of carbon converted to CO_2 can be expressed in Equation 8.5.

$$C + \frac{1+\Psi}{2} O_2 \rightarrow (1-\Psi)CO + \Psi CO_2 \qquad \text{Eq 8.5}$$

Where Ψ=fraction of carbon converted to CO_2.

There is uncertainty in Equation 8.5 from the stoichiometric coefficient of oxygen when modelling char oxidation, therefore the CO_2 conversion is often considered as the simpler product ratio CO/CO_2. (Waldron, 2005).

The CO/CO_2 product ratio is critical to the prediction of the combustion temperature during the early and middle stages of carbon burnout. Figure 8.9 shows the idealised burning regimes of a porous char particle.

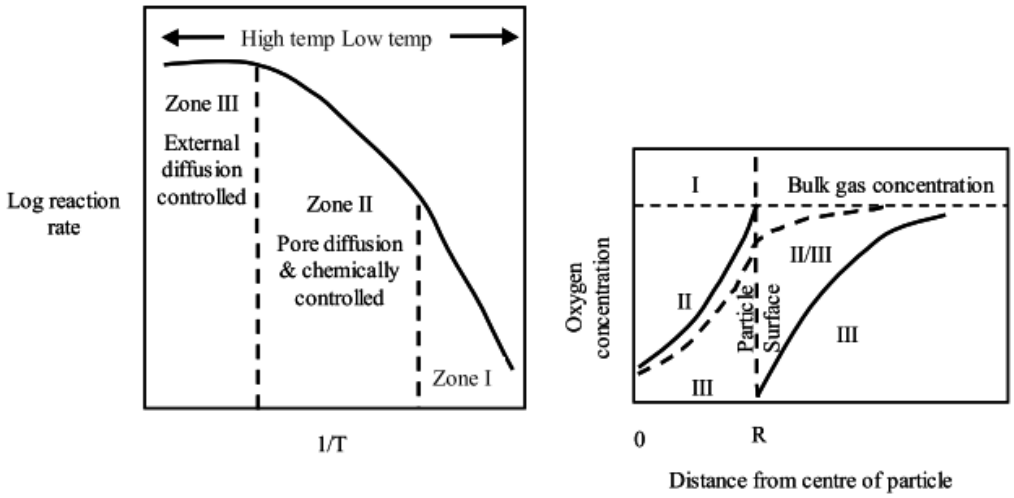

Figure 8.9 Idealised char burning regime (Waldron, 2005)

- Zone 1. The oxygen in the pores of the particle shows an even distribution throughout the particle and the boundary layer. The combustion process within zone 1 is chemically controlled.
- Zone 2. Through the increase in temperature, chemical reaction rate increase and oxygen penetrates less into the pores, with combustion taking place near the surface of the particle and in the pores. The reaction rates taking place in zone 2 are controlled by the diffusion rate of oxygen and by the chemical reactions. Oxygen penetration is determined by particle size. As combustion and burnout continue, particle sizes diminish and thus the oxygen penetration decreases.
- Zone 3. The higher temperatures in zone 3 result in a rapid reduction in surface area available for reaction. The increased chemical reaction rate, results in significant reduction in oxygen ingress into the pores, when O_2 ingress may equal 0. The combustion reactions now take place near the surface of the particle; thus the reaction rates are limited to the diffusion rates through the boundary layer.

Within this work there are two main model approaches for predicting the char combustion and the chemical reactivity on the surface of the char particles, Global and Intrinsic.

8.3.3 Global model char combustion

Global models, consider the reactions between the particles and gases to occur on the surface of the char. The limitation of this model approach is that it is considered the particles are impervious to pore diffusion, and so calculations are incorporated in chemical reaction constants. Figure 8.10 shows a representation of Global char particle combustion.

A boundary layer of stagnant gas is considered to surround the char particle during combustion, and the combustion occurs through bulk diffusion in the boundary layer between O_2 and the char surface. This method is limited in that it reveals no insight into the reaction mechanisms that take place on or in the char particle, and is therefore generally only used as an engineering tool (Nsakala, 1986).

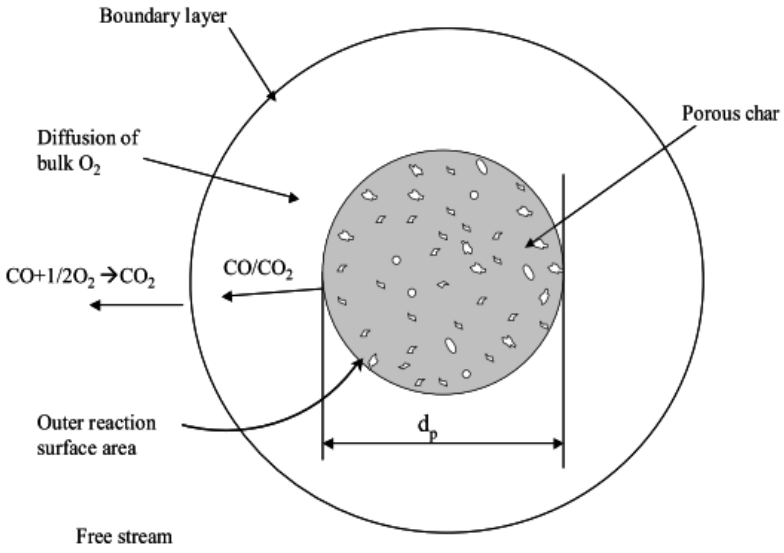

Figure 8.10 Representation of a char particle in the Global model (Waldron, 2005)

8.3.4 Intrinsic model char combustion

Intrinsic model, considers reactions to take place within the porous char surfaces. As shown in Figure 8.11, this method also relies on implementing sub-models for calculating oxidation on the porous surfaces and the diffusion of gases through the pore structures.

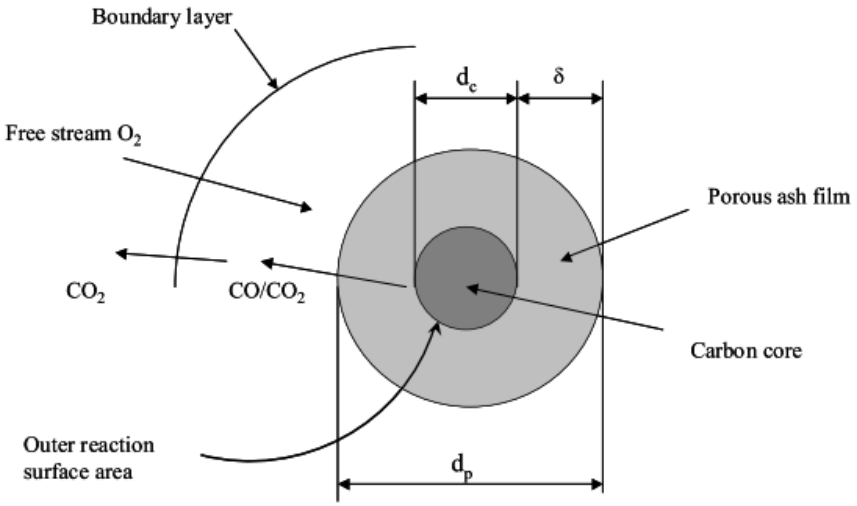

Figure 8.11 Representation of a char particle in the intrinsic model (Waldron, 2005)

Model developments by Backreedy 2004 and Hurt 1998, (Backreedy et al., 2005; Hurt, 1998) have incorporated the effects of ash inhibition, annealing and macerals for calculating their impacts on reaction rate. Intrinsic modelling techniques generally assume all reactiviy data is the same for all coals, i.e. there is an intrinsic reaction rate for the reaction of char (carbon) with oxygen, and the differences in observed reaction rates depends on other factors. These include: Measureable values of char structure, surface area, density, swelling factors and porosity are used to determine the frequency factors. The reaction rates and difussion of gases through the pores are essential for calculating the intrinsic reactivity for a given coal.

Within this work, a carbon burnout kinetic model (CBK 8) is used. CBK 8 uses an intrinsic modelling method, whilst the forerunner, CBK 7 adopted a global model approach. (Hurt, 1998).

8.3.5 Intrinsic reacivity

Intrinsic reactivity is an important factor in determining char burnout. Intrinsic reactivity is considered independent of coal rank and can be correlated using the Arrhenius form, Equation 8.5:

$$R_i = A_i e^{\frac{-E_i}{RTp}} \qquad \text{Eq 8.5}$$

Smith proposed model values of 179kJ/mols (42.8kcal/mol) and 305g cm^{-2}s for E_i and A_i respectively. (Smith, 1982). Backreedy has reported values of between 145-165 kJ/mol for E_i (Backreedy et al., 2005). Attempts to correlate data over a range of coals have been carried out, however these have only been completed on a limited catalogue of coals samples (Hampartsoumian, 1989; Sun, 2000). Whilst these predicted values can give an estimation of the potential values for intrinsic reactivity, measured values for individual coal chars will yield more precise values.

An approximation of intrinsic reactivity can be taken from historical data as shown in Figure 8.12 (Waldron, 2005). From the data in Figure 8.12, an approximation can be made using the correlation line, Equation 8.6. Figure 8.12 and Equation 8.5 show a correlation between the energy of reactivity and intrinsic reactivity.

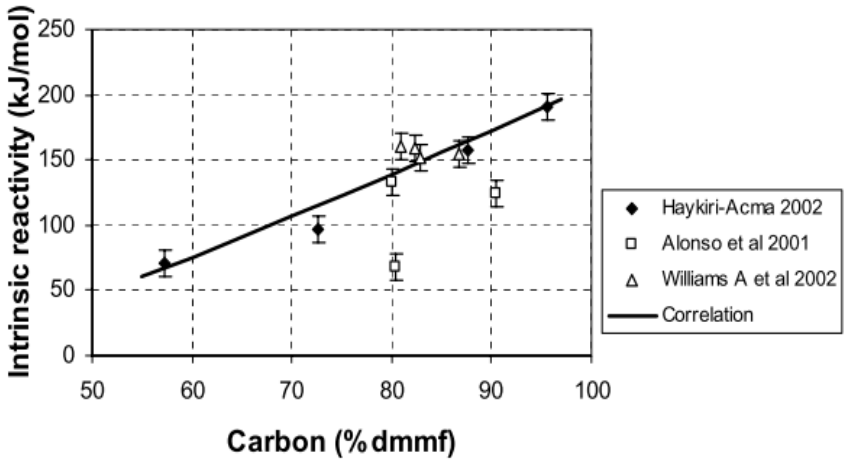

Figure 8.12 Relationship between intrinsic reactivity of coal chars and carbon content (Waldron, 2005)

$$R_i = 0.0074C^2 + 2.111C - 77.502 \quad \text{Eq 8.6}$$

It should be noted this approximation method is only valid for coal chars with carbon values in excess of 50% (dmmf).

8.3.6 CBK 8 model

CBK models are used to predict the burnout from coal char particles and can be applied to a wide range of particles size distributions. It should be noted, on their own they are not complete furnace models but can form part of a larger program to predict output data from a furnace through modelling. CBK models consider char combustion as an idealised mechanism, whereby the char particle is spherical, and the carbon rich core is surrounded by a layer of porous ash, Figure 8.11.

CBK 7 which used the global model gave reliable burning curves for previous DTF results up to ~70% conversion before the results started to deviate from experimental data (Hurt, 1998; Waldron, 2005). When the CBK 7 model was incorporated into CFD codes, excessive run times were experienced, indicating this approach was not suitable as a statistical method due to the time penalties. As with the global model, the particle is assumed to be surrounded by a stagnant gas layer that O_2 can pass through to react with the carbon core.

CBK 8, uses an intrinsic model approach and was developed to overcome the difficulties of CBK 7(Niksa, 1996b). CBK 8 was extended for applications to include pressures in excess of atmospheric (Niksa, 1996b). To obtain accurate data from the CBK 8 model, input data about the char morphology is generally required. Default values can be applied where specific data is not available however, this will lead to more generic output data.

8.4 Furnace model

In the simplest terms, a furnace is a water cooled combustion chamber, heat is transferred to the walls via thermal radiation (Goodridge, 1976), where heat is extracted by water, losses through leakage and from the exhaust gases. To model a furnace, simple mathematical, and more complex approaches are used.

- Empirical modelling
- A range of furnace modelling from complex mathematical model through to CFD modelling.

Within the more complex models, a range of engineering codes have been utilised to predict the radiative fluxes and gas temperatures in the furnace. (Bueters, 1974; Stephenson, 1994; Unsworth, 1991; Waldron, 1998). Most of these codes use a system of dividing the furnace into discrete sections. Figure 8.13 shows representations of four of these methods. The CFD models are generally the most complex of these with discrete segments of as much as $1x10^6$. Within this thesis the slice furnace model is applied, more details can be found in Section 8.5.8.

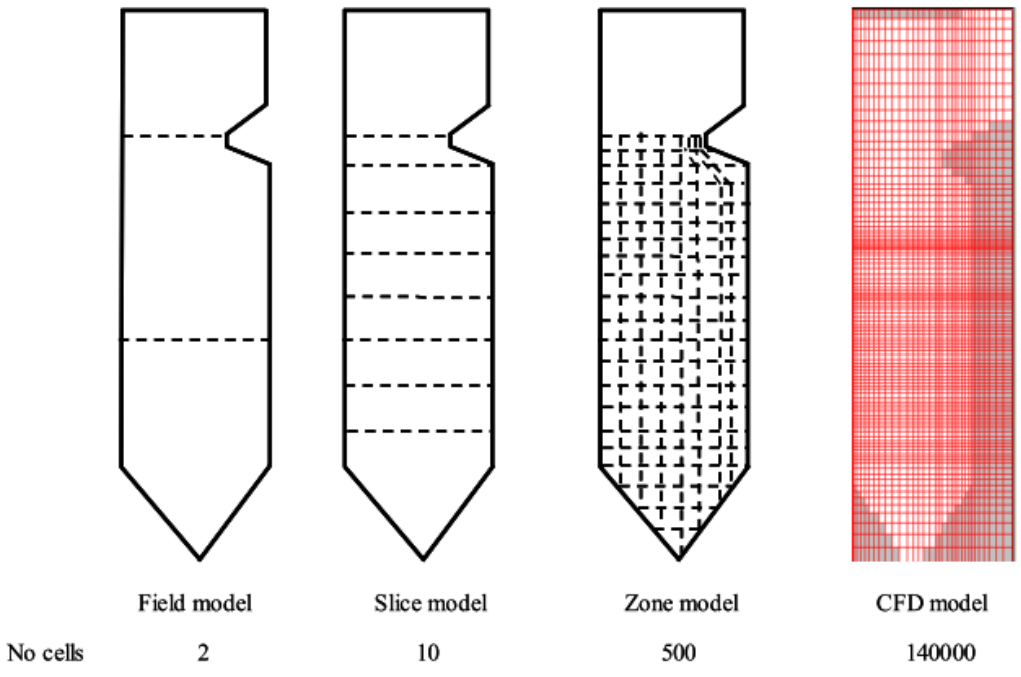

Figure 8.13 Variations of furnace model types (Waldron, 2005)

8.5.1 Results

The results are separated out into coal information and model development and results.

8.5.2 CPD model inputs

The atomic H/C and O/C ratios of the four reference coals were plotted on the modified Van Kevelen diagram. The CPD library is constructed on bituminous and sub-bituminous coals. The H/C ratios of steam coals are much lower than bituminous coals. Figure 8.14, shows the Van Krevelen diagram with the triangulation points and the four coals under test. From Figure 8.14 it can be seen the 3 bituminous coals all fall within the matrix of the library coals, whilst the Ffos-y-fran falls outside the matrix. The low reactivity coal (Ffos-y-fran) does not fit into the matrix. When coals fit within the CPD library matrix, then the input data can be interpolated from the matrix. For the Ffos-y-fran, the closest CPD library coal was selected as a representative value for Ffos-y-fran. This made the modelling of Ffos-y-fran unreliable.

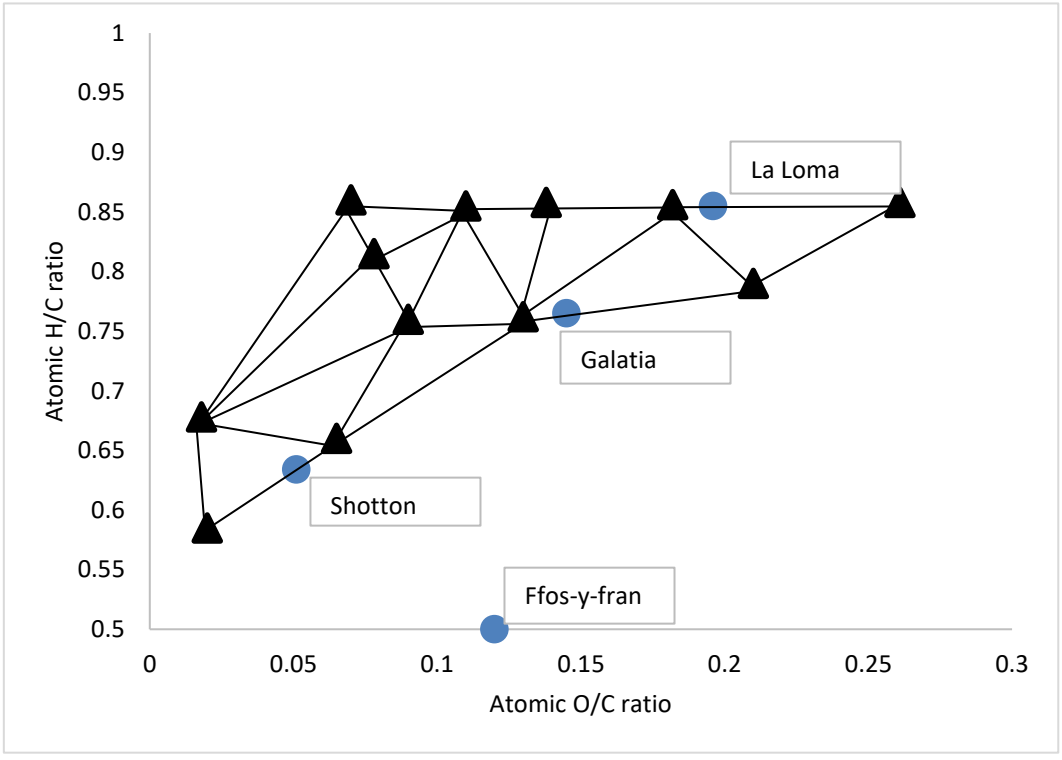

Figure 8.14 Library model from CPD with reference coals overlain. ▲CPD library coals, ● reference coals. Adapted from Waldron, (Waldron, 2005; Fletcher et al., 1990)

8.5.3 Prediction of high temperature volatile yield using CPD

The use of the composite rate, side chain breakage/ char chain breaking (kδ/kc) from Table 8.1, was selected based on the assumption all of the nitrogen is bound in the aromatic clusters, therefore increasing the breaking of the labile bridges will not yield the increases in volatile N found experimentally. The HTVY was particularly sensitive to changes in the composite rate. The breaking of the side chains only would also not yield increases in volatile N, however the ratio of side chain breaking compared to char dissociation can change the ratios if all of the nitrogen is in the aromatic clusters, as these form the chars and metaplasts.

To calibrate the model, coal data and experimental data on HTVY's and nitrogen partitioning from the DTF analysis was used, Chapter 6 and Birley et al 2018 (Birley, 2018). In addition, within the paper there is information with respect to the potential effects of the alkali and alkaline earth metals on the release on volatile-N from the fuels.

8.5.4 Modelling

The modelling results are separated into the three model sections, CPD-HTVY, nitrogen volatiles and the furnace model incorporating the CBK 8 code. Validation and calibration of the CPD model was carried out using experimental data from DTF1 (i.e. high temperature volatile yield and N-partitioning). Application of the calibrated CPD model and CBK 8 in a furnace slice model was then used to estimate NOx reduction from combustion of the coals in the presence of the additives.

8.5.5 Calibration of the CPD model for HTVYs of the coals and coals with additives

Using the default values from the CPD model, the four coals were tested for HTVY predictions compared to the experimental data given in Chapter 6.3.3 (DTF 1). With the CPD default values, the model produced data that was consistent with that of the experimental data for all four of the coals. Table 8.3 shows comparison between measured HTVY values and those predicted from the HTVY model at default values kδ/kc=0.9.

Table 8.3 HTVY, predicted values at kδ/kc=0.9, compared to experimentally measured values (%)

Coals	HTVY measured	HTVY predicted at kδ/kc=0.9
Ffos-y-fran	22.06	26.46
Shotton	57.03	47.49
Galatia	60.57	58.96
La Loma	50.22	62.18

Experimentally the additives produced enhanced levels of HTVY, increased carbon conversion and reduced levels of char, refer to Chapter 6.3.3, and this was not replicated in the model. Within the model for HTVY, there are several areas for potentially adjusting the volatile yields. As experimentally there was an increase in volatiles and a reduction in chars, the ratio between side chain breaking and char cracking kδ/kc was deemed the most viable factor for balancing the changes seen. Figure 8.15 highlights the changes in kδ/kc required for modelling both coals and coals with additives.

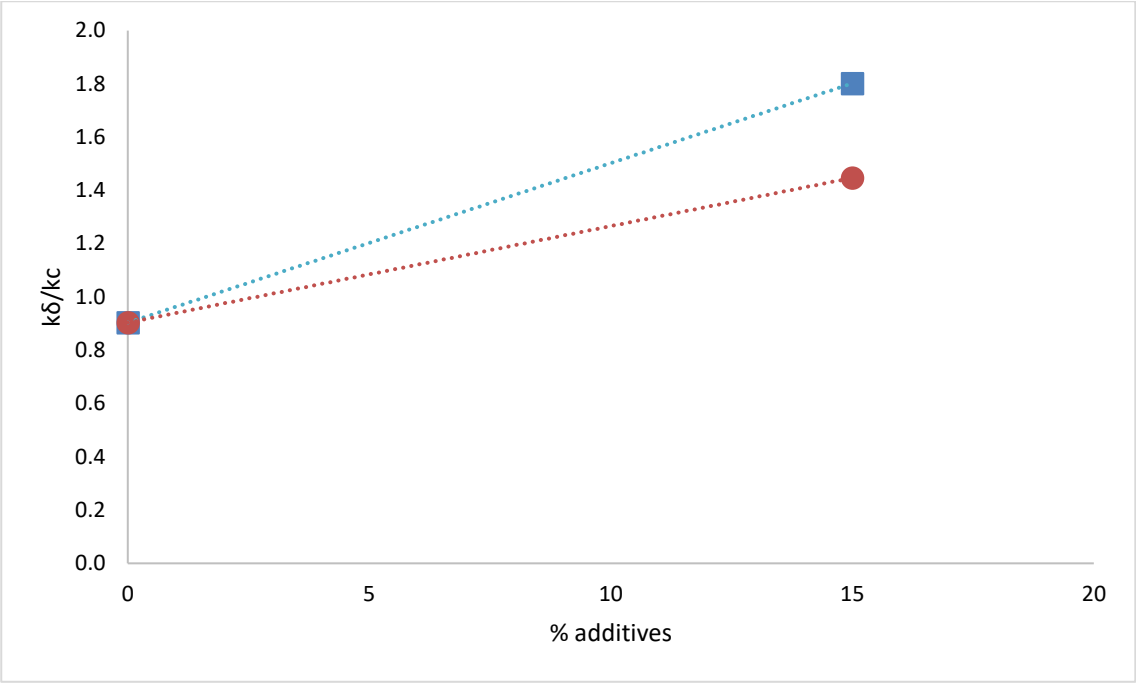

Figure 8.15 Optimisation of kδ/kc for the modelling of coal plus additives using CPD. kδ/kc values for the coals without additives as kδ/kc=0.9, and kδ/kc values for the coals with both FBA and PFA additives. kδ/kc=1.45 for coals blended with FBA, kδ/kc=1.8 for coals blended PFA. All values of kδ/kc are the same for all of the reference coals. ■ Coal plus PFA, $y = 0.06x + 0.9035$, ● Coal plus FBA, $y = 0.0362x + 0.9035$

Here kδ/kc for the coals only was 0.9 (default value), and this increased to 1.45 and 1.8 for all of the 4 coals with FBA and PFA respectively. These values gave HTVY results similar to the experimental data from DTF1, Chapter 6. The results from these changes are presented later.

The relationship in Figure 8.15 can be extended to yield values of kδ/kc for other weights % additives. Figure 8.16 shows the values of kδ/kc required to model the three bituminous coals, with varying mass values of the additives (FBA and PFA). With all of the values, a calibration with a straight line can be plotted.

Further to this, it can be postulated that for any coals within the range of bituminous coals, combined with additives containing Fe, Na, Ca, K and Mg, kδ/kc can be calculated using this method with default values of 0.9 for coals without additives, up to 1.45 for 15% FBA and 1.8 for 15% PFA. Whilst it could be proposed these equations continue as a straight

line past 15% additives, the values have not been validated. Values higher than 15% may not calibrate to the straight lines shown in Figure 8.16.

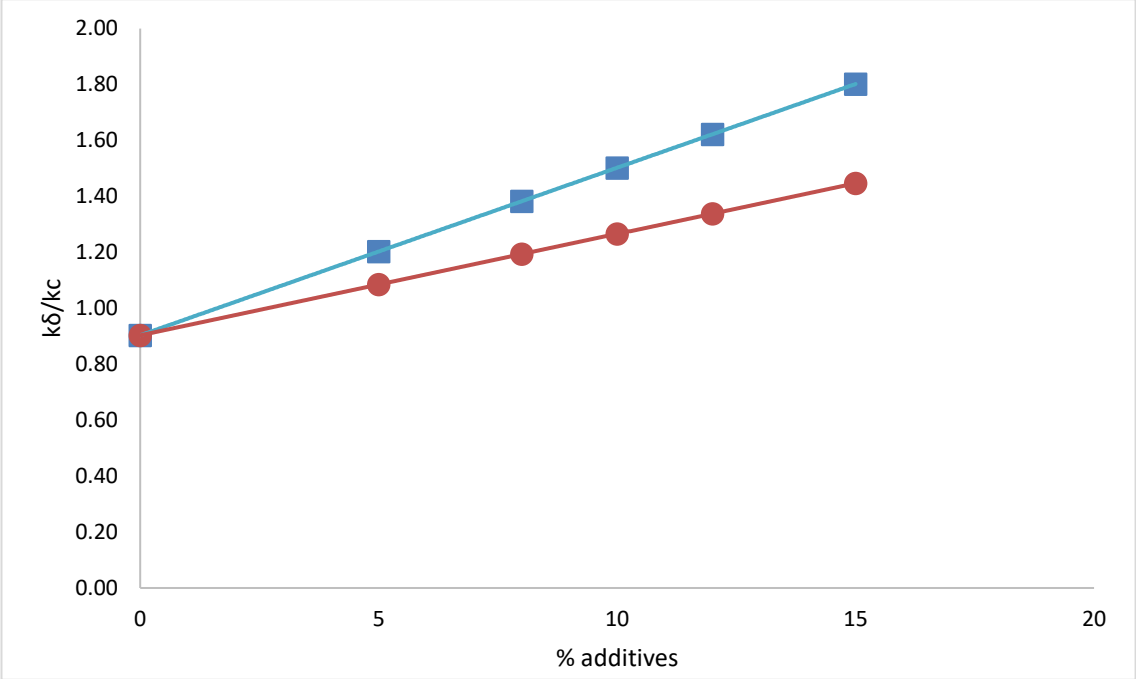

Figure 8.16 kδ/kc values plotted for percentage values of additives (0, 5, 8, 10, 12, 15)% for coals with FBA and PFA. ■ Coal plus PFA, ● Coal plus FBA

Figure 8.17 shows the three bituminous coals and coals with the additives, FBA and PFA, comparing the kδ/kc values against the Σ(Fe, Na, Mg, Ca, K)/ fuel-N. For each coal type there is a correlation between the kδ/kc values and the reactive components in each coal plus additive. The kδ/kc values can be directly related to the percentage of additives, thereby allowing a mechanism for predicting the HTVY for a given percentage of additives. The kδ/kc value taken from Figure 8.17 can be used in the CPD model to predict the HTVY for a given value of alkali and alkaline earth metal content in any coal and coal plus additive combinations, providing the coal properties sit within those of the CPD coal library. A straight line could be plotted through all of the data to produce a mean straight line of $y = 0.421x + 0.406$.

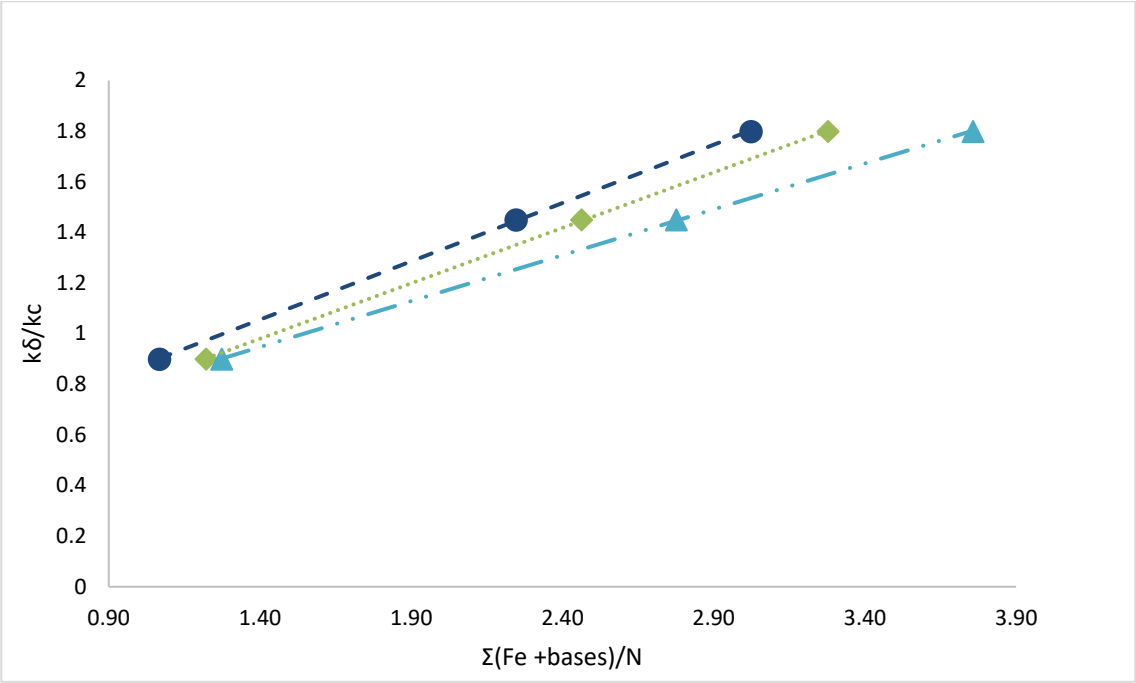

Figure 8.17 Values of kδ/kc as a function of the summation of alkali and alkaline earth Σ(Fe +alkalines)/N. ● Shotton, ♦ Galatia, ▲ La Loma

The values of kδ/kc can be taken from the straight-line plots in Figure 8.17, and these can then be used to calculate the percentage of HTVY from the model for any given percentage value of the reactive components up to 15%. When the HTVY prediction is plotted against the percentage additives for each fuel type, the HTVY shows a polynomial relationship. The relationship follows that seen experimentally, where the effects of increasing the reactive components reduces in effectiveness as higher percentage values of additive are used. From Figures 8.16 and 8.17, all three bituminous coals show the same trend, with both additives. The higher volatile coals (Galatia and La Loma) show a larger amount of HTVY. With both additives, there is an increase in HTVY release. Of the two additives, the FBA has a higher level of volatiles, so would be expected to have a higher HTVY compared to the PFA. Conversely, from Figure 8.18, it can be seen across all three bituminous coals, when blended with the PFA, a higher level of HTVY is achieved. There is a higher percentage of reactive compounds in the PFA.

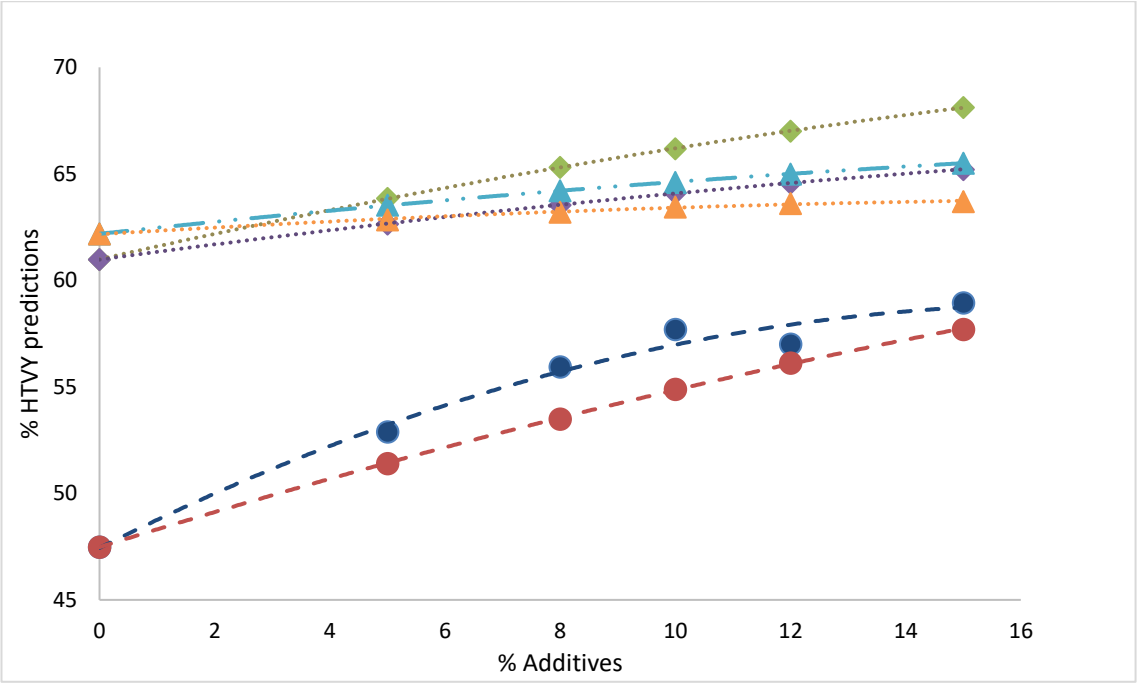

Figure 8.18 Model predictions of HTVY (%) for the three reference bituminous coals blended with 0, 5, 8, 10, 12 and 15% FBA and PFA additives. ● Shotton plus PFA, ● Shotton plus FBA, ♦ Galatia plus PFA, ♦ Galatia plus FBA, ▲ La Loma plus PFA, ▲ La Loma plus FBA.

Figure 8.19 shows the predicted and experimental data for HTVY. When the predicted values of HTVY from the model are compared to experimental data, it can be seen all four of the coals align close to the centre 1:1 line, Figure 8.19. When the HTVY correction for the additives is applied, the data points for the blends fall closer to the 1:1 line, most of the predicted data in within 10% of the parity line.

The coals blended with PFA shows the best correlation, with all of the data falling within the 10% margins. The correction values of kδ/kc=1.45 for the coals with FBA, and 1.8 for the coals with PFA, realise good correlation between model predictions and experimental data.

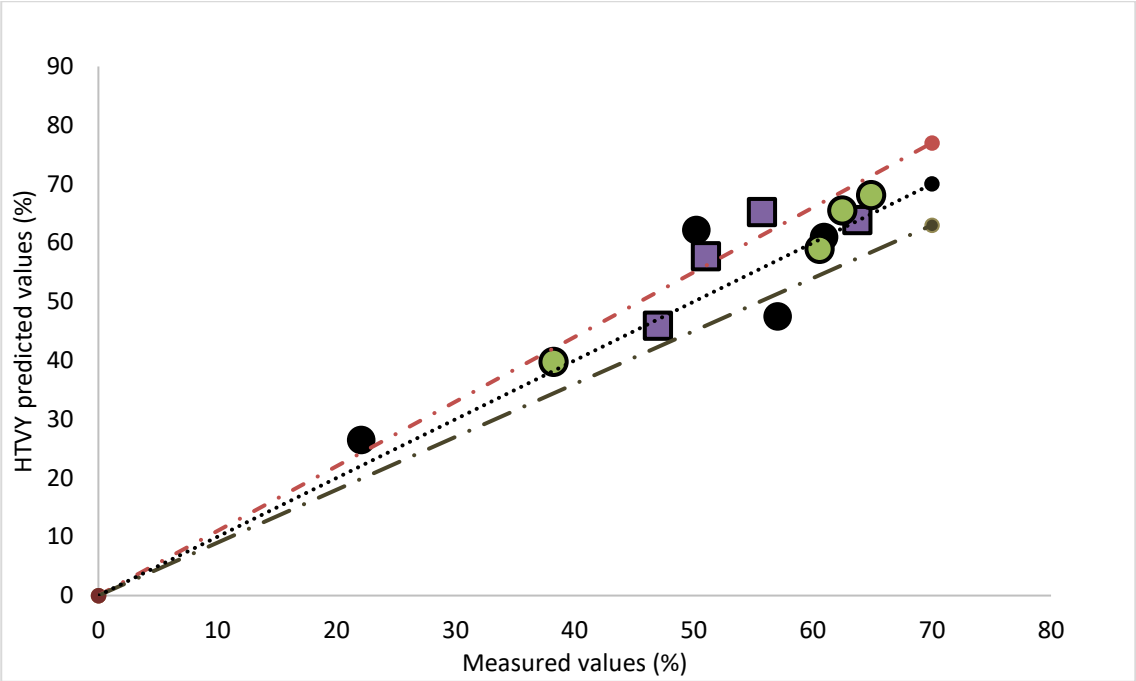

Figure 8.19 HTVY comparison of Experimental values and predicted values form CPD model with kδ/kc values adjusted for additives for 15% additives. ● Coals, ● Coals+PFA, ■ Coals+FBA, Central single dotted line 1:1, upper dashed and dotted line 1:1 plus 10%, lower dashed and dotted line 1:1 -10%.

8.5.6 Prediction of Volatile-N using the CPD model

For the volatile nitrogen release predictions from the CPD model, the values of volatile-N release at 0 and 15% additives were established from experimental data. Using the default values within the model and with pre-exponential value for nitrogen of A_N=10 (Item 1, Table 8.2) the model produced prediction results that agreed well with experimental data for the coals without additives. When these input values were used for the coals blended with both additives, the resultant data did not agree well with the results from DTF 1. The predictions from the model were significantly lower than experimental results. Thus the value of A_N required optimising for both additives to accommodate the increased volatile-N release observed in experimental work.

Through iteration, the values of A_N were adjusted for the blended fuels to the values of 12 for coal with FBA and 13.5 for coal with PFA for all three of the bituminous coals. Figure 8.20. These value of A_N gave good agreement with the experimental data, as shown in Section 8.5.7.

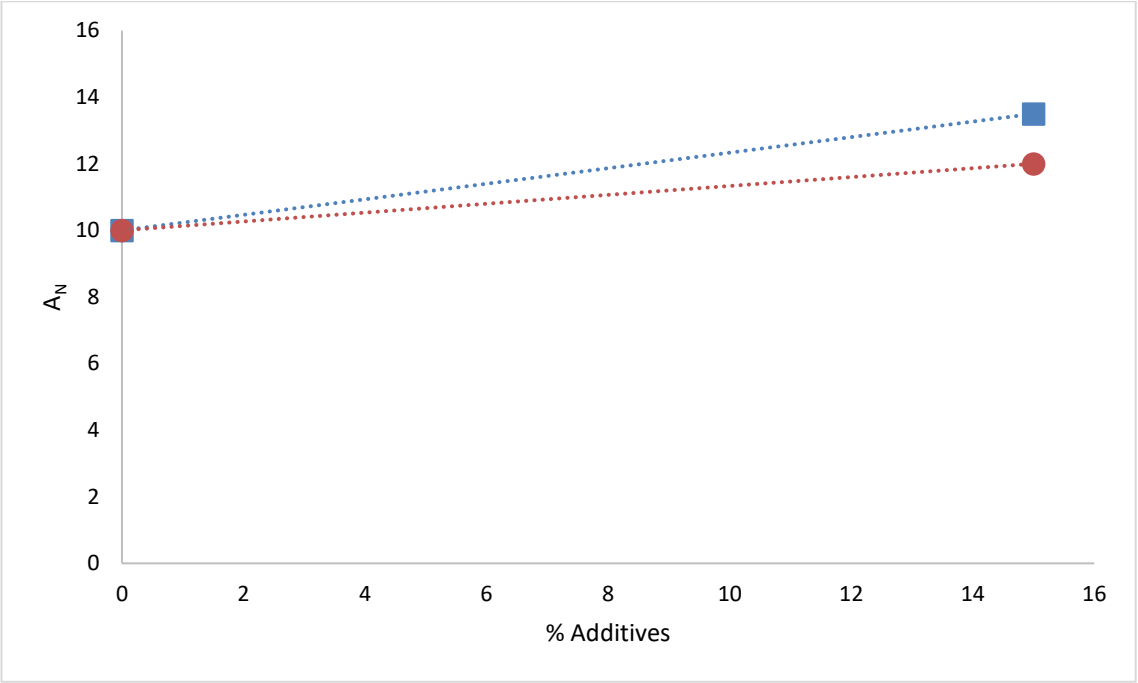

Figure 8.20 Measured A_N values for the coals at 0% and 15% additives for the three bituminous coal plus FBA and PFA, compared to experimental data for volatile nitrogen release. ■ Coal plus PFA, ● Coal plus FBA

Furthermore, the values of A_N can be interpolated for any percentage of additives between 0 and 15%. Values of 0,5,8,10,12, and 15%, as are shown in Figure 8.21.

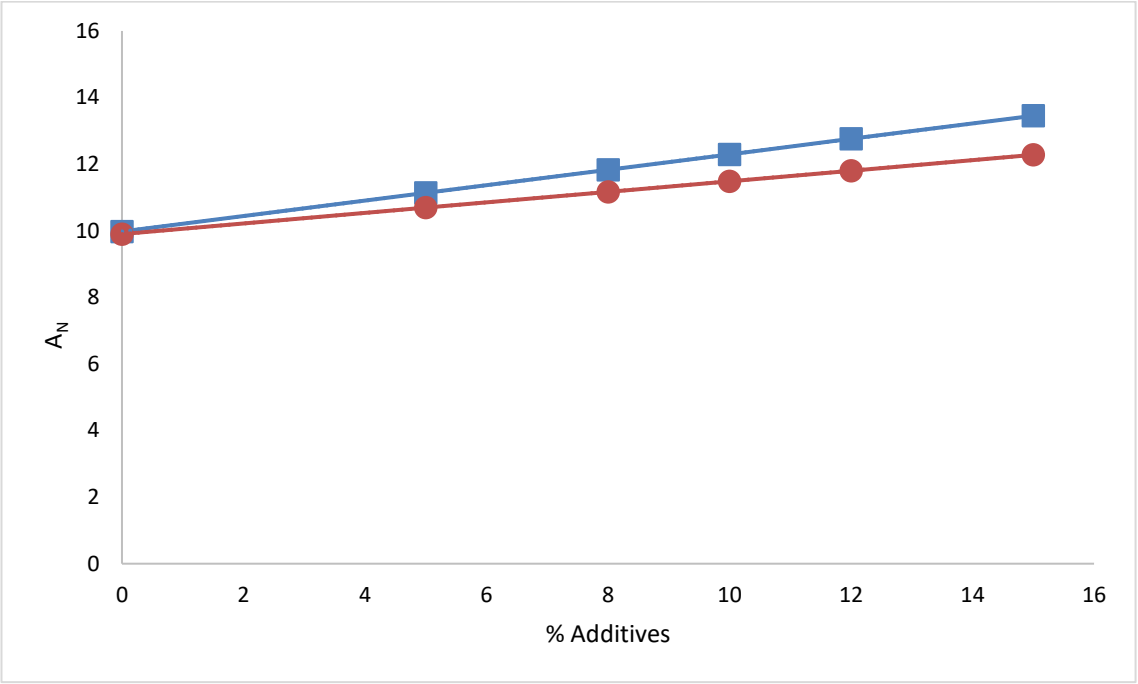

Figure 8.21 A_N values for the coals, coals with FBA and coals with PFA at 0% additives and 15%, an predicted A_N values at percentage additives of 5, 8, 10, and 12% ■ Coal plus PFA, ● Coal plus FBA

Figure 8.22 shows the calibration for A_N as a function of the ∑(Fe, Ca, Mg, K, Na)/N for the three bituminous coals (A_N values of 12 for FBA and 13.5 for PFA). The masses and percentage values of ∑(Fe, Ca, Mg, K, Na)/N are different for each coal type, and thus each has its own gradient line, even though the A_N values are the same for each coal.

. From the trend lines for each fuel type, Figure 8.22 can be used to estimate how the mass of reactive components relate to the A_N values. This allows for calculating the release of volatile N. Each of the bituminous coals shows a different amount of reactive components at any given value of A_N. However, when the volatile-N is predicted from the model, they show comparative results to experimental data, Figures 8.23 and 8.24.

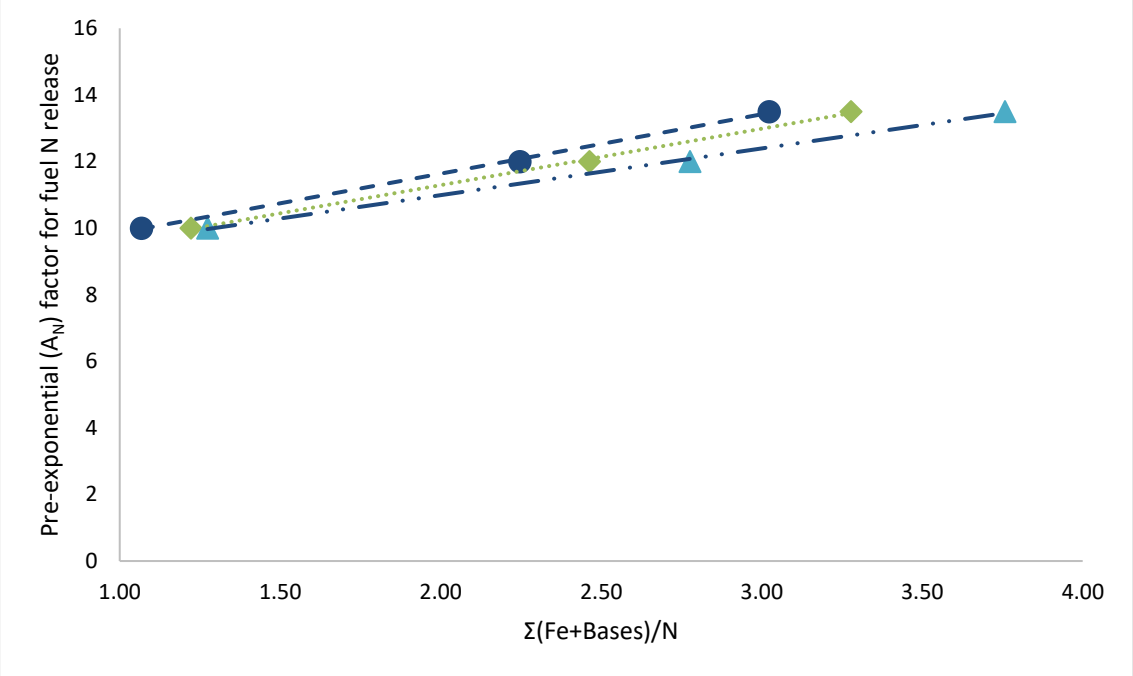

Figure 8.22 A_N for the three bituminous coals and coals blended with both additives. ● Shotton, ♦ Galatia, ▲ La Loma

There is a linear correlation for the coals, coals with FBA and coals with PFA. As greater w/w values of ∑(Fe, Ca, Mg, K, Na)/N are present in the fuels, so the value of A_N also shows an increase. A straight line can be plotted through all of the data for a mean value of $y = 1.626x + 8.052$.

8.5.7 Volatile-N release from coals blended FBA and PFA

The predictions of the percentage of volatile nitrogen for the bituminous coals and coals blended with additives are presented in Figure 8.23. With additives at 0, 5, 8, 10, 12 and 15%, the figure shows a polynomic relationship. As larger percentages of additives are added, the accumulative effect of the reactive compounds diminishes. This is the same result as seen experimentally, where proposed saturation of the catalyst by nano-particles is proposed as a mechanism for the reducing effect of catalysis. The modelling of nitrogen release thus shows result in good agreement with those from experimental data.

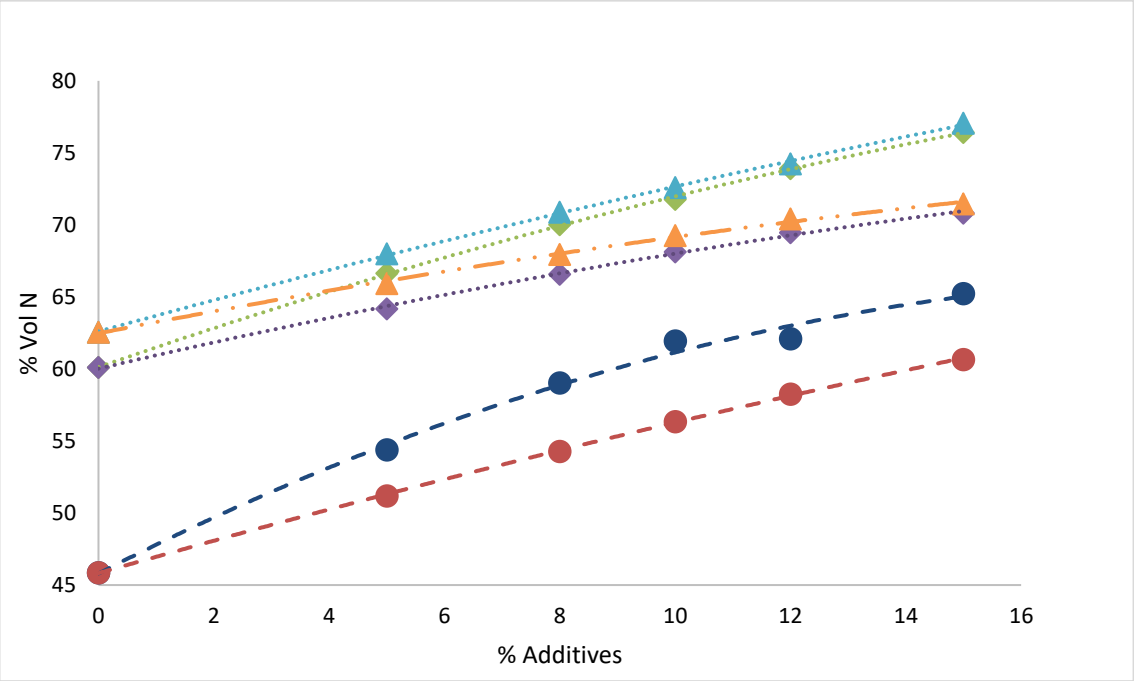

Figure 8.23 Prediction of volatile N with percentage of additives at 0, 5, 8, 10, 12 and 15%. . ● Shotton plus PFA, ● Shotton plus FBA, ♦ Galatia plus PFA, ♦ Galatia plus FBA, ▲ La Loma plus PFA, ▲ La Loma plus FBA.

In Figure 8.24, the volatile-N data is shown for the four coals and coals with both additives, using the calibrated A_N values in the model. For the bituminous coals, the model yields predictions close to the volatile N release observed during experimental work. The low reactivity coal shows good correlation between the CPD model and experimental work. However for this coal (Ffos-y-fran) when blended with the additives,

the same A_N values show large inaccuracies compared to experimental values. The lower reactivity coals showed the greatest increase in volatile-N release observed during experimental work. Therefore fuels with higher fuel ratio values, i.e. those that fall outside the range of rank in the CPD coal library, will require further validation and corrected values to A_N to achieve more accurate results.

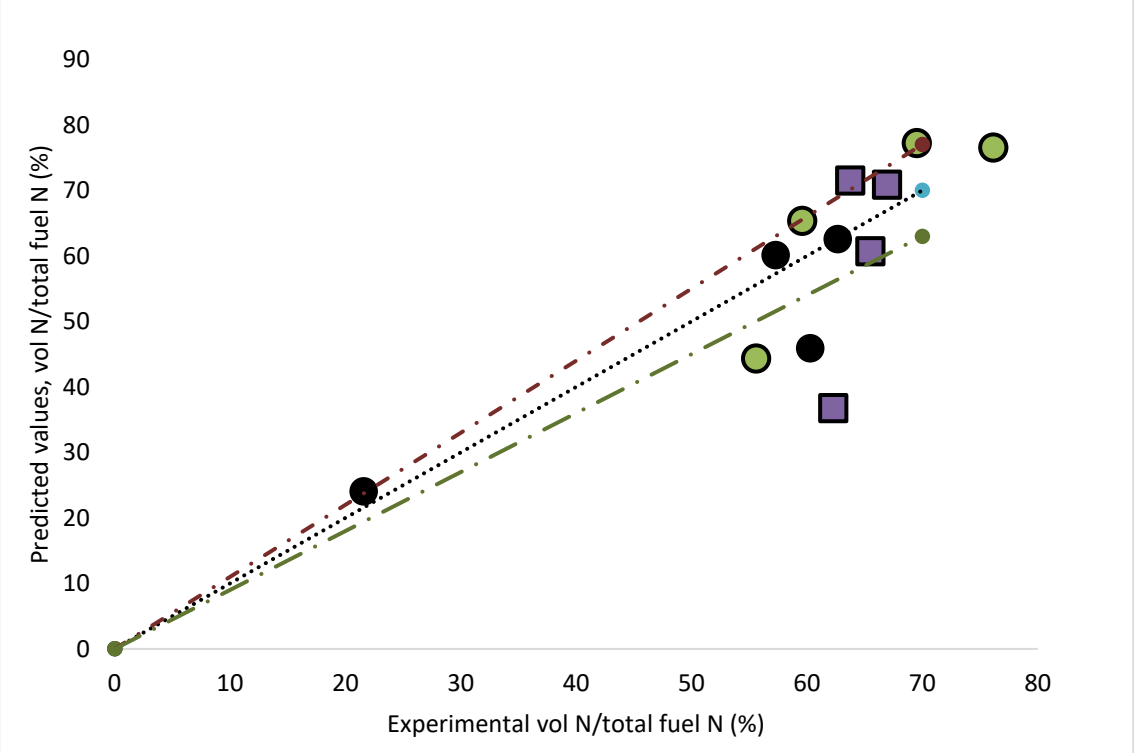

Figure 8.24 Model prediction of volatile-N release and experimental volatile-N release. Coal prediction values set at default CPD values. Coal blended with FBA, kδ/kc=1.45, A_N=12. Coals blended with PFA kδ/kc=1.8, A_N=13.5. ● Coals, ● Coals+PFA, ■ Coals+FBA, Central single dotted line 1:1, upper dashed and dotted line 1:1 plus 10%, lower dashed and dotted line 1:1 -10%.

The volatile-N release is closely related to the HTVY, i.e. when the HTVY increases, so the volatile N can be expected to increase proportionally. Two sets of calculations were therefore used to make the adjustments for the volatile-N conversion. From the HTVY calculations, the kδ/kc was selected based on the HTVY release and for the volatile-N calculation, adjustments to A_N. were applied.

8.5.8 Furnace model

The furnace model was a slice furnace model developed by Waldron (Waldron, 2005). A representation is shown in Figure 8.25. Using the model, a furnace is divided into cross-section areas. Each of the rows for fuel/air injectors occupies its own slice. The top of the furnace is considered to be the furnace outlet plane (FOP), which delineates the top of the last slice. The cross-sectional areas are used to calculate a 3-dimensional representation of the furnace.

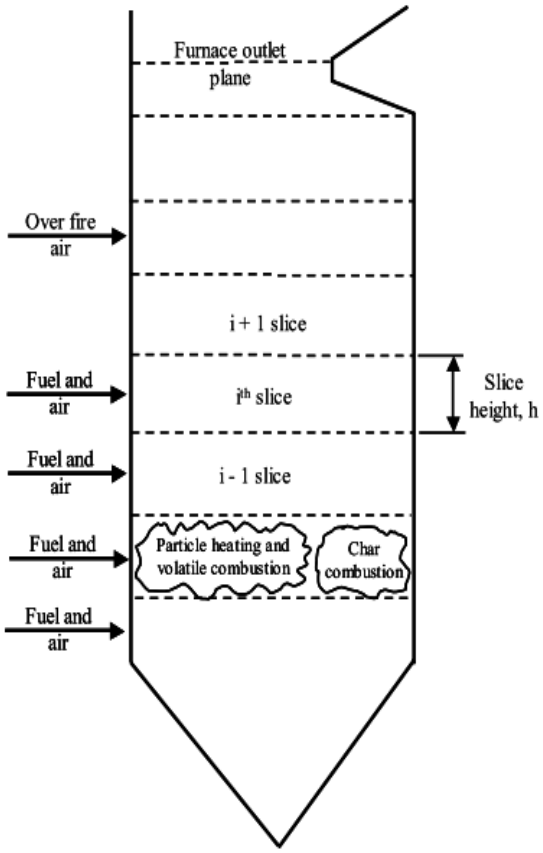

Figure 8.25 Representation of the furnace model showing the division of the slices

Each slice is calculated independently, and the output from a slice is used as an input to the slice above, the total output from the model at the FOP is the summation of all of the slices. The furnace model uses CPD, CBK 8 sub models to describe devolatilisation and char burn-out respectively, together with furnace geometry and furnace operating conditions.

8.6.1 Furnace geometry

The reference furnace data used for validation and examination of the three bituminous coals was from a large-scale furnace. Original data for a bituminous coal was provided for a coal with similar characteristics to the La Loma coals under test. Figure 8.26a shows the geometry data required for the furnace model. Figure 8.26b shows the fuel/air injectors and the slices for the industrial furnace. The injectors were arranged in five rows and six columns on both the front and rear of the furnace. The injectors were fed fuel from 8 mills. The furnace used for modelling was separated into eight segments. The first slice incorporating fuel/air injector 1, also included the hopper section. Slices 2-5 were of equal size, determined by the positions of the injectors. Slices 6-8 were separated as having the same height.

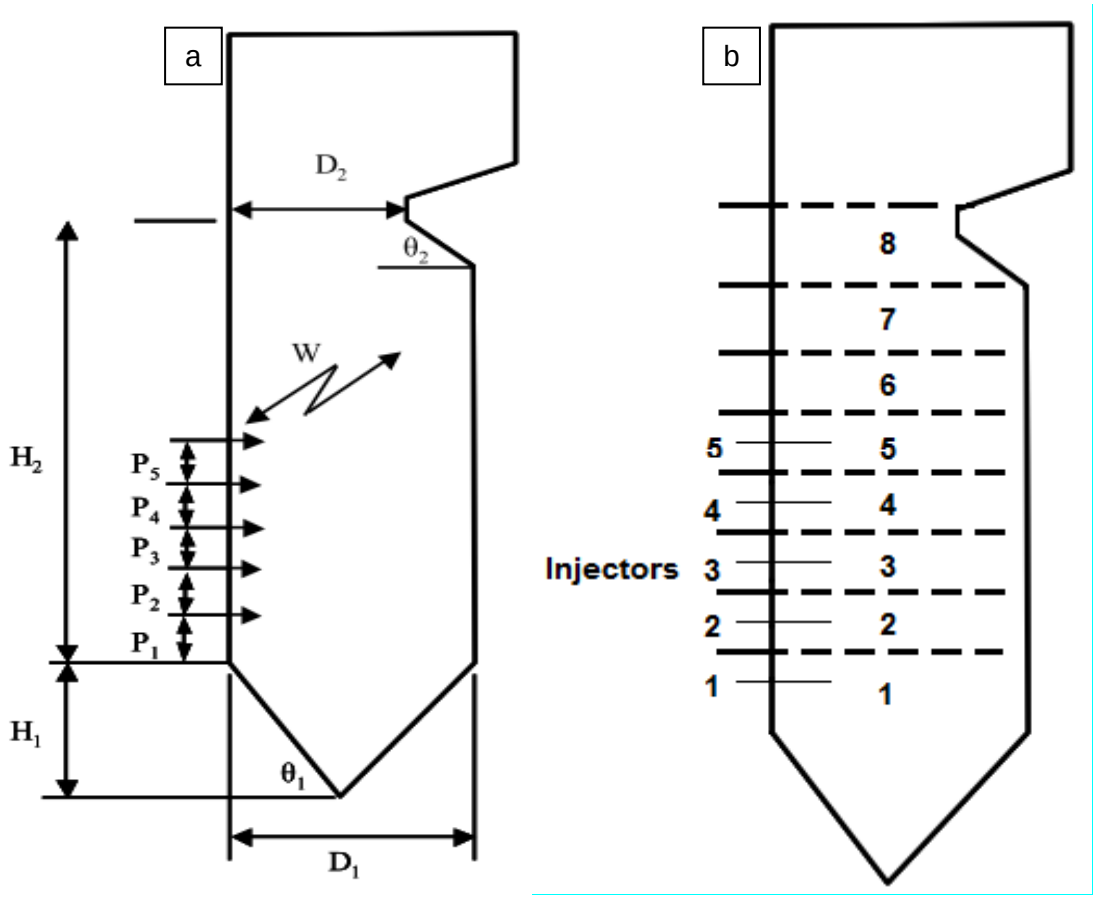

Figure 8.26 a. Representation of furnace used for model.(Waldron, 2005) b. Industrial furnace used for validation with fuel/air injectors and slices.

Table 8.4 shows the geometric data from an industrial furnace used as inputs to the furnace model.

Table 8.4 Furnace geometry

Geometry variable criteria	Furnace dimensions (m)
Hopper throat to H_1	7.5
Knuckle to nose H_2	22.5
Burner row P_1	2.25
Burner row P_2	2.25
Burner row P_3	2.25
Burner row P_4	2.25
Burner row P_4	2.25
Burner row P_5	2.25
Furnace depth D_1	25.5
Furnace depth D_2	15.0
Furnace width W	12
Hopper angle θ_1 (degree)	60
Arch angle θ_2 (degree)	30

8.6.2 Furnace operating data

To achieve an accurate output from the model, fuel and air data is required for the furnace. The fuel data for the injectors is shown in Tables 8.5 and 8.6. The fuel/air flow and particle size distribution from the industrial coal from the industrial furnace data was used for all of the bituminous coals with and without additives, as this was representative of the milling process for the furnace used for calibration.

Table 8.5 Fuel input data for furnace

	Fuel flow kg/s	Air flow kg/s
Injectors 1	8.8	101.2
2	9.1	102.4
3	7.7	93.8
4	9.1	102.3
5	8.7	99.9
Primary air tep °C	43	
Secondary air temp °C	350	

To produce NO_X emissions data from the furnace model, further information for the coals is required: HTVY, swelling factor, mass specific intrinsic reactivity, fuel density, activation energy, scale factor and surface area.

Table 8.6 Particle size distribution from the furnace mills

Particle size µm	37.5	112.5	225	300
% of each size	51.4	28.53	13.98	6.07

Default values can be selected for many of these values. For this work, the intrinsic reactivity was applied for each specific coal with and without additives based on the experimental work in Chapters 5 and 6.

Table 8.7 shows the R_i values used for the furnace model.

Table 8.7 R_i values used in the model for all coals plus additives

% Additives	Shotton	Galatia	La Loma
Coal only	169.19	161.59	137.78
Plus 5	153.38	151.23	122.13
8	143.89	145.01	112.74
10	137.57	140.87	106.49
12	131.24	136.73	100.23
15	121.75	130.51	90.84

8.6.3 Furnace model calibration

Initial work focussed on data for a coal from an industrial furnace. The calibration of the furnace model (using La Loma coal) was made against this data and is shown in Table 8.6. From the data in Table 8.8, it can be seen the model predicted the output from the furnace to within 7% for ppm and significantly less deviation on an mg/Nm basis.

Table 8.8 Data from furnace

	Data from a furnace	Slice model for coal used in furnace
Total NOx leaving furnace mg Nm^{-3}	1138	1164
Total NOx leaving furnace ppm	527	564

For the furnace model work, when the coal is blended with an ash additive, it is assumed to be fed into the furnace as a single fuel. It was found that the slice model needed calibrating in order to predict NOx for coal plus additive feeds. Since the additive changes the rate of char combustion The variable input data (intrinsic reactivity, R_i) for the bituminous coals with and without additives were validated. As with the HTVY and volatile N calibration, the output against percentage of additives was initially extrapolated. Figure 8.27 shows the values of R_i for the range of coals with additives from 0-15%. It can be seen the R_i values show a consistent decrease in values as the percentage of additive is increased.

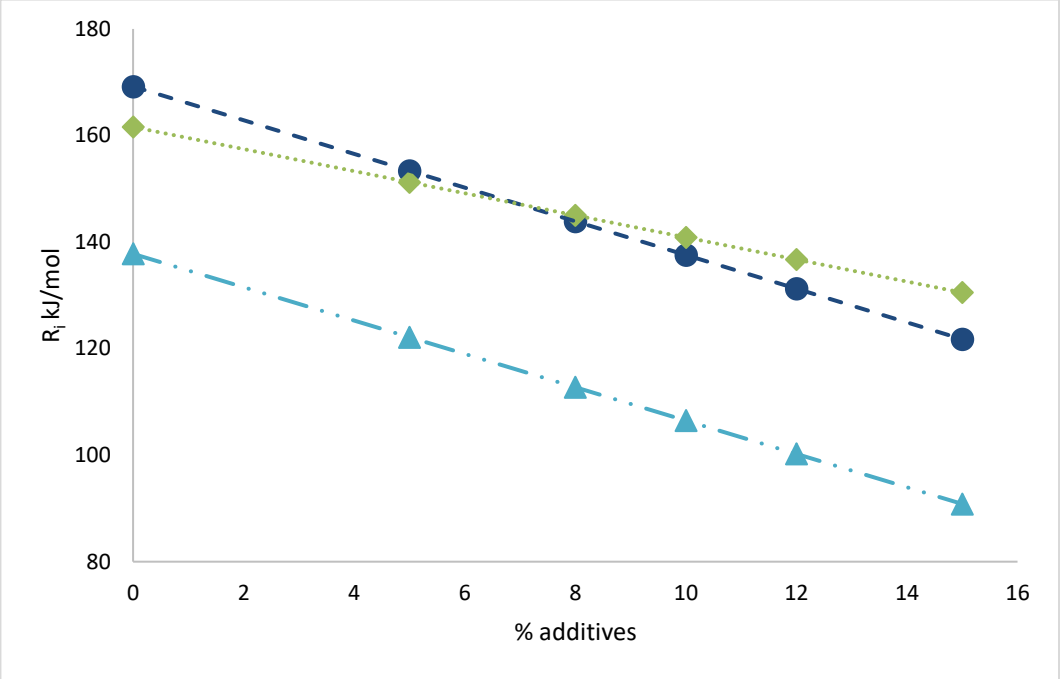

Figure 8.27 Char R_i as a function of % of additives. ● Shotton, ♦ Galatia, ▲ La Loma

Values are for measured activation energy. The equations were taken to plot the interpolated values for 8 and 12% additives, all other values were also calculated from the equations for use in the furnace model. For all of the bituminous coals with either additive, there is a general trend for a decrease in activation energy with increase in the percentage additives. As shown in Chapter 5, the increase in percentage of additives brings an increase in Σ(Fe+basics)/N.

The data from Figure 8.27 was then applied on a mass of reactive compounds in the additives. Figure 8.28 shows the relationship between R_i and the mass increase of Σ(Fe+Basic)/N.

The trend across all three of the bituminous coals is a straight-line relationship, where, as the mass of reactive compounds increases, so the intrinsic reactivity decreases. All of the bituminous coals show the same relationship.

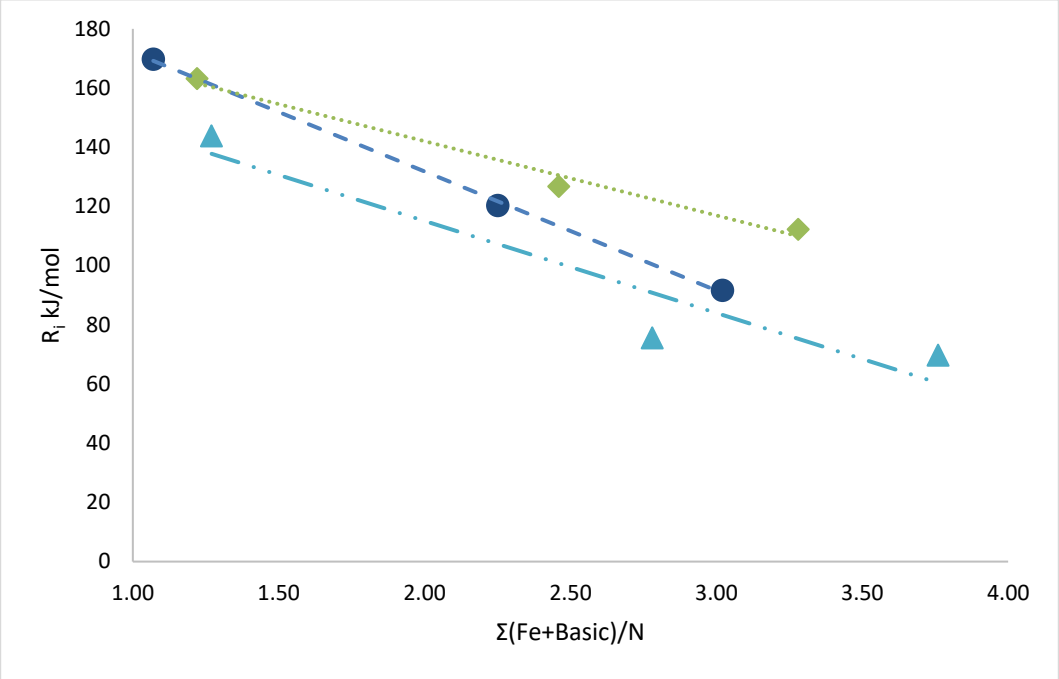

Figure 8.28 Char R_i as a function of Σ(Fe+Basic)/N. ● Shotton, ♦ Galatia, ▲ La Loma

8.6.4 Furnace model NO_X output

The data in Figure 8.29 shows there is a relationship between the Σ(Fe+Basic/N) and NO_X emissions reductions.

The data is shown for the coals, with both FBA and PFA at 15%. As the Σ(Fe+Basic/N) increases, the reduction in NO_X emissions increases. The relationship of volatile N release during pyrolysis (Chapter 6) can be linked to the reduction in NO_X. As nitrogen is released as volatiles in a reducing flame in a Low-NO_X furnace, it can form diatomic nitrogen, thus an effective reduction mechanism for NO_X can be realised. The data shown would indicate there is an effective upper and lower limit for NO_X reduction with

the inclusion of additives. For the Shotton, as the mass of reactive compounds increases, so the reduction appears to accelerate. Galatia tends to show a slowing up of effectiveness. Corrections for moisture and O_2 have not been applies at this stage.

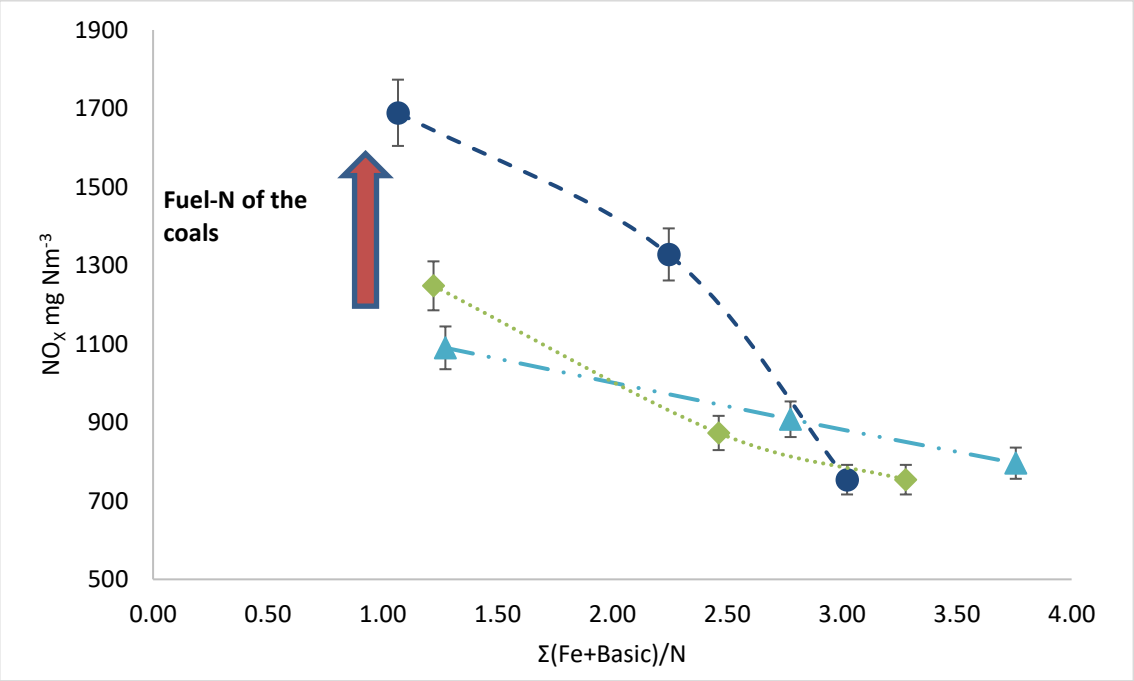

Figure 8.29 NO_X emissions from slice furnace model and the effects from Σ(Fe+Basic)/N, moisture and O_2 correction have not been applied to these values. ● Shotton, ♦ Galatia, ▲ La Loma

Note: Error bars set to ±5% uncertainty error of monitoring equipment in industrial data

8.6.5 Furnace model NO_X output (O_2 and moisture correction)

From Figures 8.30 a and b, it can be seen the model predicts a reduction for all of the coals with both additives. The least effective reduction seen is for the Shotton plus FBA. The Shotton without additives has NO_X values of 1638 mg/Nm^3. The addition of the FBA at 15%, reveals of reduction of NO_X from 1638 down to 1252 mg/Nm, Figure 8.30b. The values equates to a reduction of ~23%. The same percentage reduction (23%) is felt on the fuel ppm basis, Figure 8.30b. Galatia showed high levels of moisture and oxygen content, compared to the other reference coals, Chapter 5. To

normalise the predictions from the furnace model, moisture and oxygen correction was applied.

The greatest NO_X reduction is also felt across the Shotton blended with PFA. For the fuel NO_X, Figure 8.30a, the reduction is ~41%, whilst for the mg/Nm, the reduction is shown as much as 43% Figure 8.30b. The enhanced reduction may be accounted for as the high non-combustible ash content of the PFA, may be causing heat diffusion, and the reduced carbon content will have reduced the thermal properties of the fuel. The La Loma blended with the FBA realises the smallest NO_X reduction of 25%. The La Loma had the lowest percentage of nitrogen content of the coals under test. This is reflected in Figures 8.30, where La Loma has the lowest NO_X emissions of the three bituminous coals with and without additives.

When the fuel NO_X is viewed, the Galatia with FBA shows only a small reduction over the first 5% of additives. This reduced effect may be through the oxygen content of the fuel and additives, which can lead to oxygen and moisture in the exhaust. When the oxygen and moisture correction are applied, Chapter 7.5, the Galatia curves shows more consistency with the other coals plus additive curves. The greatest reduction is felt for all of the coals plus additives over the first 5-7% additives.

As the curves are polynomial, the optimum Σ(Fe+basics)/N for NO_X emissions reduction can be calculated from –b/2a. The curve fitting for La Loma plus PFA was utilised as this realises the lowest point for the y axis on the graphs, the equation for La Loma plus PFA is $y = 25.18x^2 - 259.51x + 1448.9$. For the Fuel NO_X, this equates to ~6.16 Σ(Fe+Basic)/N whilst for the mg/Nm^3, the value is decreased to 5.15 Σ(Fe+Basic)/N. The change in values is due to thermal NO_X and oxygen correction being taken into account.

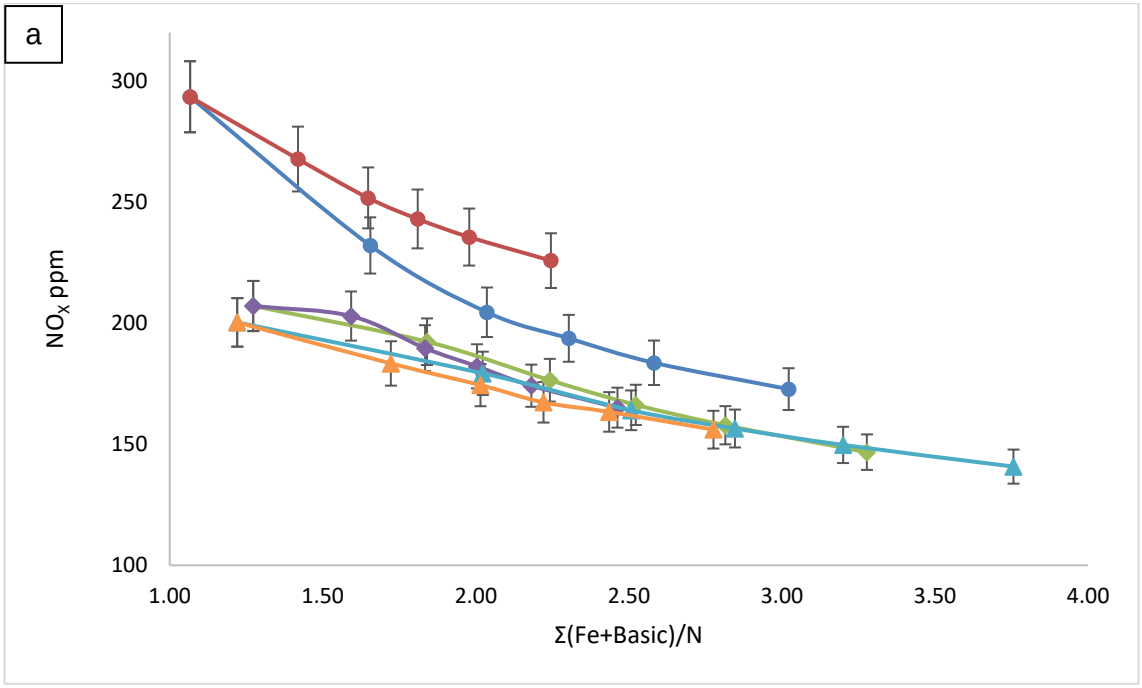

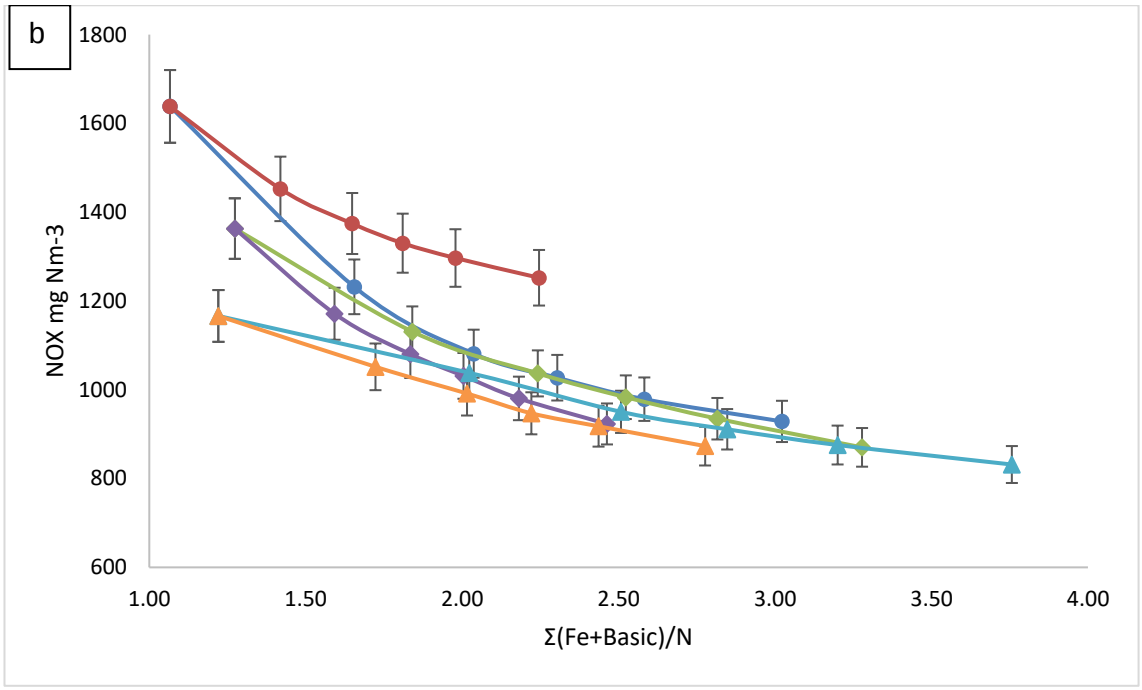

Figure 8.30 a and b. NO_X emissions predictions from the furnace model. a. NO_X emissions from the fuel, ppm. b. NO_X emissions from the furnace model including thermal NO_X and O_2 correction, mg/Nm^3. ● Shotton plus PFA, ● Shotton plus FBA, ♦ Galatia plus PFA, ♦ Galatia plus FBA, ▲ La Loma plus PFA, ▲ La Loma plus FBA.

Note: Error bars set to 5% uncertainty error of monitoring equipment in industrial data

It should be noted this might be the optimum value for NO_X reduction, however other factors such as furnace slagging and fouling and corrosion should be taken into account. Arvelakis and Frandsen noted the change in slagging, fouling and corrosion

during co-combustion of coal and biomass, attributed to the increase in alkali and alkaline metals (Arvelakis and Frandsen, 2010). Barisic, noted an improvement in the resistance of agglomeration when pulverised coal ash was used as an additive during biomass combustion in a $1MW_{th}$ circulated fluidised bed. It was also noted there were no adverse effects on fouling or corrosion, as some of the biomass alkalis were captured in the coal ash additives. (Barišić et al., 2013) Further considerations should be given to the effect on combustion characteristics if the additives are from biomass ashes, as the increased ash content of the additive may cause heat diffusion. Heat diffusion can change the combustion characteristics of a fuel. There will also be a reduction in combustible materials with higher ash contents, leading to lower heating values through a reduction of carbon content. In Chapter 6, it was noted however that with the percentage of biomass ash additives applied in this work, carbon conversion of the blended fuels showed an increase. (Birley, 2018). Priyanto noted in a furnace at 1300 °C, that blending low ash biomass with coal did not change the blended combustion ash properties. When coal was blended with higher ash biomasses >1% ash, there was a significant increase in high calcium mineral slagging in the blended combustion ash. (Priyanto et al., 2016).

From the model predictions, the NO_X emissions for bituminous coals with nitrogen contents and compositions similar to the coals under test can be assumed to fall within the boundaries shown in Figure 8.30a and b. Shotton with FBA forming the upper limit and La Loma with FBA demoting the lower limits of NO_X reductions. It can be seen there appears to be a limit to the Σ(Fe+basics)/N ratio, whereby above this value further additions would provide no further benefit as a NO_X reduction technique.

8.6.6 Generalisation of the model

From the data for the three bituminous coals with and without additives under examination, it is possible to postulate that the three variables kδ/kc, A_N and R_i can be standardized for any given Σ(Fe+basics) mean mass value. Using the data from the

bituminous coal without additives and coals with 15% FBA and PFA respectively, the equations in Table 8.9 were found.

Table 8.9 Standardised values for furnace

	Equation	R^2
kδ/kc	$0.3913 \times x + 0.4655$	0.9412
A_N	$1.5149 \times x + 8.2814$	0.9402
R_i	$-33.429 \times x + 197.61$	0.8223

Note: x = Σ(Fe+basics)/N based on wt% in the coal/additive blend

As the iron and basics act as the catalysts for the reduction of NO_X in this work, Table 8.7 shows the equations for each of the variables and the R^2 values for the masses of Σ(Fe+basics)/N. From the equations in Table 8.7, input data can be calculated for any values of Σ(Fe+basics)/N from 0-15% of the FBA or PFA, on a mass of reactive element basis.

8.7 Chapter Conclusion

Through this chapter, the data from DTF 1 for HTVY and nitrogen partitioning (from Chapters 5-7) has been used in a range of models culminating in the prediction of NO_X emissions from a furnace model.

8.7.1 CPD

To predict NO_X emissions from the furnace model, the CPD model can be used to predict the HTVY and volatile N release. To achieve accurate data from the CPD model across the three bituminous coals with and without additives, calculations for the input data was required.

8.7.2 HTVY

Using default values for CPD, accurate predictions for HTVY could be achieved using the default values in the model, when compared to experimental work for devolatilisation of the coals alone. When the default values were applied to the coals

blended with either FBA or PFA, the model predictions became less reliable. Using the experimental data for the bituminous coals with additives, the variable ratio kδ/kc was isolated as a method to calibrate the CPD model prediction of HTVY values with those from experimental work. Using kδ/kc ratio values of:

- 0.9-All three bituminous coals
- 1.45-Bituminous coals plus 15% FBA
- 1.8-Bituminous coals plus 15% PFA

The above data was used to formulate kδ/kc ratio values for Σ(Fe+basics)/N on a mass basis. Using the kδ/kc ratio values, accurate predictions for HTVY could be made across a range of additives based on the reactive elements.

The Ffos-y-fran was also tested on the CPD for HTVY with lower but with reasonable accuracy. This coal had properties that fall outside of the CPD coal library data.

8.7.3 Volatile N release

The CPD model was further developed to predict the volatile N release from the three bituminous coals with and without additives. Volatile N release is dependent on HTVY, therefore, the kδ/kc ratios were also used for volatile N release. Using the default values for the bituminous coals without additives, the CPD model accurately predicted the volatile N release compared to experimental data. When the default values were applied to the CPD model for the bituminous coals with either additive, the predicted results were less accurate. Using the activation energy values (Ea) for the coals and additive, and calibrating the pre-exponential value A_N, accurate volatile N predictions could be achieved.

Accurate predictions for the bituminous coals were achieved with A_N values of:

- A_N=10- Bituminous coals
- A_N=12- Coals plus FBA
- A_N=13.5- Coals plus PFA

The Ffos-y-fran results were less conclusive, with predicted results for volatile N release for the Ffos-y-fran with either additive far less accurate compared to experimental data. Low reactivity coals may not be able to be accurately predicted using CPD without significant adjustments for each individual coal.

8.7.4 Furnace model

The furnace model required data inputs from CPD (HTVY and volatile N), CBK 8, the furnace geometry and operating data and an environmental module. For calculating the NO_X emissions from the bituminous coals with and without additives, some assumptions were made based on the validation data supplied from the industrial furnace:

- Stoichiometric values fuel and air flow values
- Injector firing patterns
- Industrial milling fuel size distribution
- Furnace geometry

The furnace model was validated against a coal used in the furnace over a two hour period. Comparison was made to La Loma which had similar proximate and elemental analysis to the sample coal from the furnace. The predictions from the slice model predicted similar NO_X outcomes within 7% of the furnace NO_X data.

In order to expand the furnace model to the other coals studied here it was necessary to change the intrinsic reactivity activation energy for char oxidation in line with experimental findings. Using the calibrated data for CPD (HTVY and volatile N), input data from the char intrinsic reactivity activation energy was calculated from experimental data, for CBK 8. Using the input data, the furnace model predicted trends in NO_X emissions from the industrial furnace when using bituminous coals with and without additives. The furnace model showed that as the reactive elements increased in the coal with additive blends, so the NO_X emissions decreased. The model was able to predict the reduction in NO_X based on the catalysis from the Σ(Fe+basics)/N.

8.7.5 Generalised model

Using the variable input data for HTVY, volatile N and char intrinsic reactivity, standardised equations could be calculated. For any given value of Σ(Fe+basics)/N (within the range under examination) the values of kδ/kc, A_N and R_i can be used with bituminous coals to predict NO_X emissions from a furnace with known operating data.

Chapter 9 Feasibility study

9.1 Introduction

The main body of this research has been to investigate the viability of using biomass ash as an additive to reduce NO_X emissions from coal combustion. To compliment this work, a short feasibility study was carried out with a biomass (olive cake) and an additive coal PFA. Olive cake is a waste product from the olive oil industry. The olive cake is the remains of the flesh, skins and stones after pressing to release the oil. Biomass tends to be higher in volatile content, with reduced carbon and consequently heating value is also reduced. Biomass is used in co-combustion with coal as a method of reducing emissions. Co-combustion of coal and biomass can be an effective method of reducing CO_2, SO_X and NO_X in a fuel flexible furnace (Kruczek et al., 2006; Sahu et al., 2014; Wu et al., 2011). Biomass can have varied chemical compositions based on the growing environments, see Chapter 3.7.2 (Bogush et al., 2018; Gudka, 2015; Lanzerstorfer, 2015). Olive cake tends to have high nitrogen content, which can be counterproductive to reducing NO_X during combustion.

Coal PFA differs from the biomass ashes shown in Chapters 4-7. Coal ashes tend to have higher levels of potential catalysts in the nominal form of Fe_2O_3, and lower values for the alkali and alkaline earth metals. Coal PFA can also have relatively high levels of heavy metals, however these have not been included in this research.

The study presented in this chapter involved blending the olive cake with the coal PFA at the same ratios as in the coals with biomass ashes, i.e. the coal ash at 15% w/w. The research was to investigate if a NO_X reduction strategy can be achieved for biomass combustion using coal combustion by-products.

The chapter is a summary of the results from the olive cake with and without coal PFA. The chapter is broken into the fuel characteristics: particle size distribution, elemental and proximate analysis, ash analysis, mass loss and nitrogen functional group

analysis. Reference is made to Chapters 4-7 for some of the data: devolatilisation, volatile N release and NO emissions.

9.2 Experimental methodology

All of the experimental procedure are given in Chapter 4. Where possible, the same procedures as for the coals with and without additives were followed. Where procedures were different, these have been highlighted in Chapter 4.

9.3 Results

Results for the olive cake with and without additives are presented in Chapters 6 and 7 for devolatilisation and NO emissions. Where the data is not shown in previous chapters, it is presented in this chapter.

9.3.1 Proximate and elemental analysis

Proximate and elemental analysis was carried out as per Chapter 4.5. The results of the proximate and elemental analysis are presented in Table 9.1. The data is presented on a daf basis.

Table 9.1 Characteristics of the olive cake and coal PFA (%)

	Olive cake	Coal PFA
Carbon[a]	51.9±0.5	87.2±0.13
Hydrogen[a]	6.8±0.1	1.2±0.01
Nitrogen[a]	3.0±0.07	0.0±0
Sulphur[a]	0.4±0.02	0.0±0
Oxygen[ad]	37.9±0.7	11.6±0.14
Volatiles[b]	72.3±0.18	2.3±0.01
Fixed carbon[ab]	17.8±0.23	1.8±1.3
Ash[b]	9.9±0.5	95.9±1.21
LOI	-	2.8±0.2
Moisture[c]	13.4±0.1	0.5
Fuel ratio	0.25	0.8
HHV (MJ/kg db)[be]	18.90	-

a=daf, b=db, c=as received, d=by difference, e=Friedl

For the olive cake it can be seen there are high levels of volatiles. The HHV of 18.90 MJ/kg is significantly lower than those of the coals, however it is consistent with those of biomass. The olive cake ash content (9.9% db) is higher than many biomass ash contents. (Gudka, 2015). The value of 9.9% ash is comparable with the bituminous coals under examination. The fuel ratio of 0.25 is of interest compared to the coals which have fuel ratios in the range of 1.24-1.8. As shown in Chapter 7.5, FR may be instrumental in the analysis for NO_X reduction. The nitrogen content is of particular note at 3% (daf). The coal PFA is also presented on a daf basis. The ash content of the PFA is high at 95.9% on a db. The high ash content gives a misleading value for the carbon content, which is shown as ~87% daf, however this is only 3.6% on a db.

9.3.2 Metal analysis

The major metals analysis was carried out on the olive cake and the coal PFA and the results are shown in Table 9.2, assuming stable oxides.

Table 9.2 Oxide analysis of the ashes

Wt % db	Olive cake	Coal PFA
SiO_2	11.2	56.0
Al_2O_3	1.2	23.3
TiO_2	0.9	0.8
Fe_2O_3	0.1	9.4
CaO	10.3	3.8
MgO	3.0	2.2
Na_2O	0.6	2.8
K_2O	32.3	1.7
Mn_3O_4	0.1	0.0
P_2O_5	5.0	0.0
SO_3	2.4	0.0

As with the biomass ash additives, the CaO, MgO, Na_2O and K_2O are high values, with the K_2O of particular interest. Potassium is one of the main areas of research as a potential catalyst for the reduction of NO_X during combustion. The olive cake however shows very high levels of both K_2O and CaO when compared to all of the other fuels

and additives under investigation. Comparatively, the K_2O in the coal PFA is low, however the Fe_2O_3 values are high compared to the olive cake. It should be noted that these values based on percentage in the ash contents of the olive cake and the coal PFA. When the olive cake results are based on the ash contents of the olive cake, the true mass of the elements became clear. Whilst the K_2O is high in the olive cake, the K content of the olive cake ash was actually 2.65%, with the coal PFA being at 1.38%. The Ca also showed a significant increase when comparing the coal PFA with the olive cake, 2.63% and 0.73% respectively. Nether the less, anions and cations may be available to have a significant catalytic effect on the formation and reduction of NO from the olive cake.

Table 9.3 Elemental analysis of the ashes of the olive cake with and without additives (mg/kg)

	Olive cake	Coal PFA
Ca	0.73	2.63
Mg	0.18	1.29
K	2.65	1.38
Na	0.04	1.99
Fe	0.01	6.29

9.3.3 Ion mobility from the coal PFA

The cation mobility of the alkali and alkaline earth metals of the coal PFA was examined using the method in Chapter 4.10. When cations are released through washing, this can be indicative they can be released during combustion (Shannon and Fine, 1974, Yao et al., 2015). If the cations are released during combustion, then they are available to act as catalysts. Table 9.4 shows the mobility of the cations during washing.

The coal PFA showed a similar trend as the two biomass ashes, whereby the calcium exhibited the greatest mobility. The sodium and potassium ions also showed some

mobility, particularly during the first wash. For the K and Ca, this mobility is of importance as these are potential for the strongest catalytic effects on NO reduction.

Table 9.4 Coal PFA ion mobility as a % of ions in ash

	Wash 1	Wash 2	Wash 3	Wash 4	Total
Sodium	8.19	2.04	1.81	1.46	13.50
Calcium	27.73	6.72	2.22	0.00	36.67
Potassium	3.95	0.00	0.00	0.00	3.95
Magnesium	3.32	2.24	2.10	1.47	9.13

9.4 Particle size distribution

Particle size distribution for the olive cake and the coal PFA was carried out in the Malvern 2000E as per Chapter 4.3.6. The olive cake shows a large range of particle sizes ranging from 0.3 µm up to as much as 700 µm. The range of particle sizes are an indication of the difficulties in processing the biomass sample. It does however show a distinct peak at 40-50 µm, with a plateau at 5-15 µm. As with the coals, for further analysis of this data in the CPD and slice furnace models, the size distribution was divided into four percentage categories, 50 µm, 75 µm, 100 µm and 150 µm, Figure 9.1.

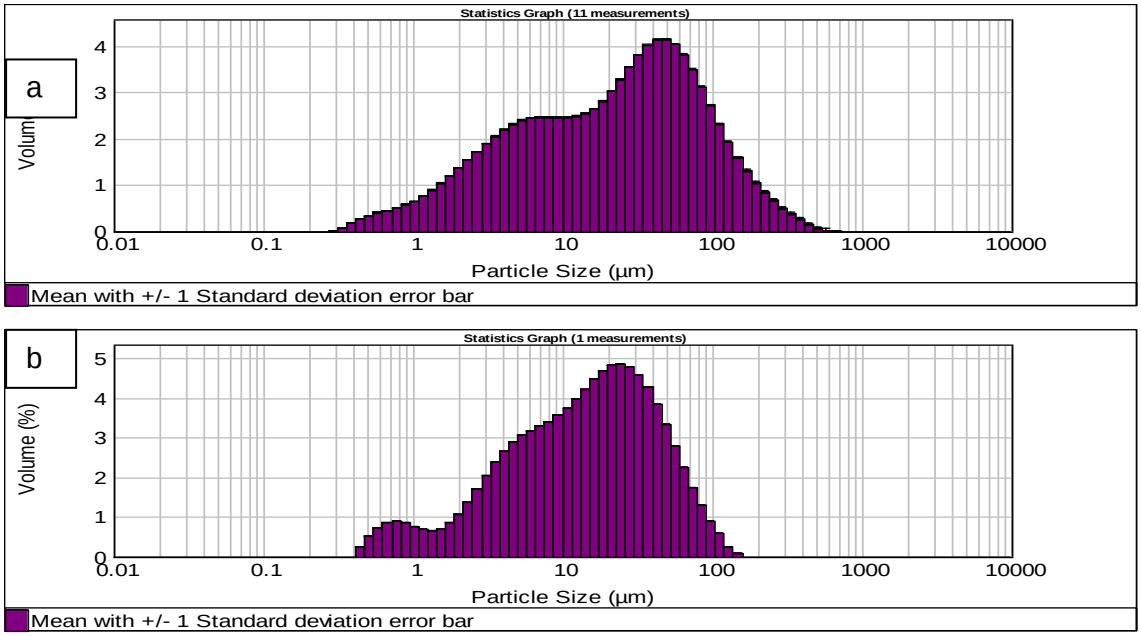

Figure 9.1 Particle size distribution of Coal PFA a. olive cake b. olive cake with coal PFA

The coal PFA showed a similar characteristic as the biomass PFA in Chapter 5.5.2. There is a main distribution peak at 20-30 µm, with a secondary peak at 0.7-0.8 µm.

9.5.1 Temperature programmed combustion (burning profiles)

Burning profiles were established using the methodology in Chapter 4.8. First derivative curves (dm/dt) were used to establish the reactivity of the olive cake with and without additives and mass loss through pyrolysis and char combustion. Figure 9.2 shows the DTG curves for both olive cake with and without additives. The profiles show a similar pattern, with the volatile content leading the char combustion as two distinct peaks. This is as anticipated for biomass pyrolysis and char combustion. The shape of the olive cake blended with coal PFA curve follows that of the olive cake without PFA. The mass loss of the blended fuel is reduced however compared to the unblended sample. The carbon content of the blended fuel is lower than that of the pure olive cake, therefore the mass loss curve is expected to be reduced.

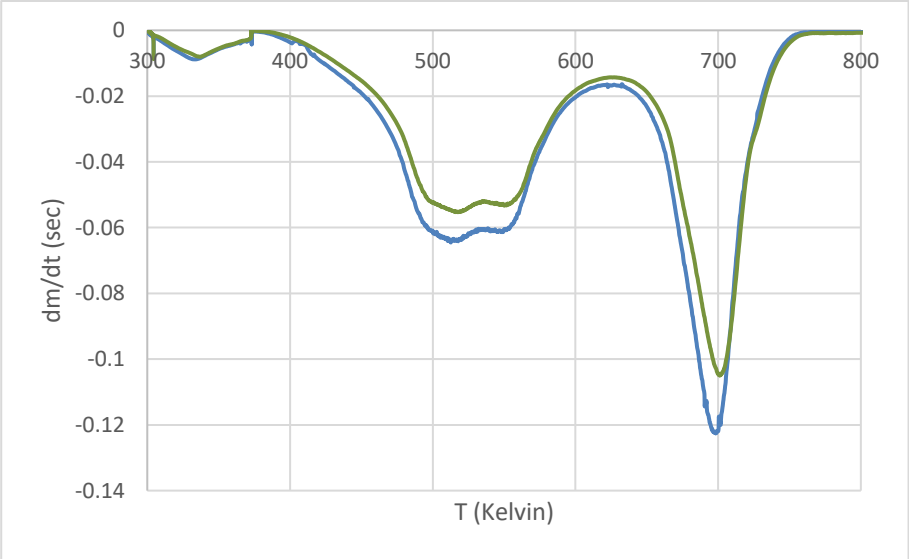

Figure 9.2 DTG curves during temperature programmed combustion, showing the influence of the coal PFA additive on olive cake. olive char olive char plus coal PFA

9.5.2 Olive cake reactivity

As for the coals and coal and ash blends, the onset of combustion (OC), PT and burnout temperature (BT) can be calculated from mass loss curves and the first derivative profiles. To calculate the reaction rates for a biomass, the first order reaction rate for volatile oxidation was used. From Figure 9.2, it can be seen there are two onset values, one for OC and the other for char combustion. Previous work has shown the use of the first order oxidation is the most consistent (Gil et al., 2010; Saddawi et al., 2009; Saeed et al., 2016; Darvell et al., 2012). The reaction rates were calculated over a 5 % range to prevent errors through heat diffusion. When blended, the onset of devolatilisation is retarded compared to the olive cake without additive, 432 K and 424 K respectively. The onset of char combustion is again delayed when the olive cake is blended with coal PFA, as shown in Figure 9.2. The peak and burnout temperatures are unaffected by the addition of coals PFA, Table 9.5. These results would suggest there is a change to the reactivity of the olive cake during devolatilisation, delaying the release of volatiles and slightly the onset of char combustion.

Table 9.5 Onset, peak and burnout temperatures for olive cake with and without additive in Kelvin

	OD	PT	ED	OC	PT	BT
Olive Cake only	424	517	622	648	702	737
Plus coal PFA	432	520	624	658	702	738

Figure 9.3 shows the Arrhenius plots for the olive cake with and without additive for volatile release. From the profile in Figure 9.3, it can be seen there is a small change in the reactivity from the olive cake with and without additives, where the activation energy has been slightly increased in the presence of the additive. Given the differences in physical and chemical composition, but under the same heating regime, a change in the reaction rates can be expected (Jones J.M, 2004).

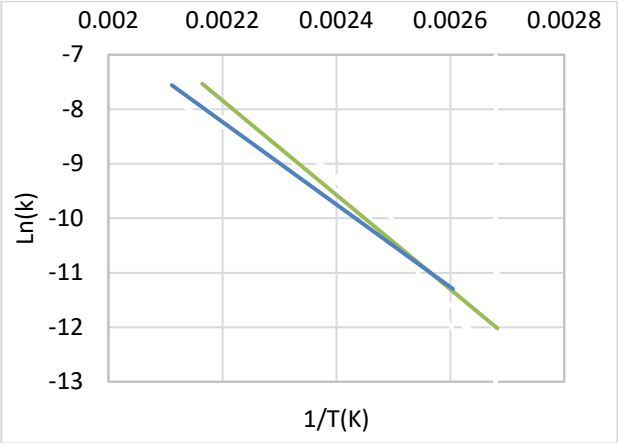

Figure 9.3 Arrhenius plots for volatile release for olive cake with and without coal PFA
olive cake, olive cake plus coal PFA

The data in Table 9.6 shows there is an increase in the activation energy (Ea) from 50.3 kJ/mol for olive cake to 63 kJ/mol for the olive cake with coal PFA and a significant increase in the pre-exponential factor A. The introduction of high percentage values of ash cause diffusion of heat delaying the onset of combustion. The increase in both of these values result in an increase of the constant k_{450K} from 1.77E 10^{-4} /s for olive cake and 2.25E 10^{-4} /s for the blended fuel. These indicate, when blended with the coal PFA, less energy is required for the onset of combustion.

Table 9.6 Kinetic evaluation of devolatilisation of olive cake with and without additive

	Ea (kJ/mol)	A (cm^3/s)	K_{450K}/s
Olive cake	50.3	122.17	1.77E-04
Olive plus Coal PFA	63.0	4651.76	2.25E-04

9.6 Devolatilisation under high heating rates

The process for devolatilisation analysis was the same as used for the coal with and without additives. To maintain context, some of the results are presented in Chapter 6, where this is the case the figures will be referred to.

9.6.1 HHR volatile yield

As shown in Chapter 6.3.2, the addition of reactive components show an increase of carbon conversion and volatile nitrogen for the coals. It is interesting to note any changes to total volatile content. Referring to Chapter 6.3.3 and Figure 6.9, the data for the olive cake with and without additives was plotted against data presented by King (King, 2016), high temperature volatile yields compared to proximate volatile yields. Whilst the coals followed a trend of y=1.5x, the olive cake was very close to the 1:1 line with proximate volatile content of 80% and high temperature volatiles of 82%. The olive cake/coal PFA blend was 80% and 87% respectively. It can be seen there is a significant increase in the total volatiles released when the reactive compounds were increased. It has been shown by Hernandez and Kilpinen that earth metal salts can enter the vapour phase and instigate reactions during the gas phase (Hernandez, 2005), resulting in a reduction of NO_X. Conversely, Yao and Che found a mechanism whereby Ca and Mg promoted NO_X formation, but Fe, Na and K delivered a reduction mechanism for NO_X reduction for coals at different temperatures (Yao and Che, 2007).

9.6.2 HHR nitrogen partitioning (TGA)

With reference to Chapter 6, Figure 6.3, the nitrogen release from the olive cake with and without additives are shown. The Figure focusses on the results of nitrogen release under HHR conditions in a ballistic TGA. The results plotted against work by Gibbins, however in the Gibbins work, the use of a single particle of coal and wire mesh was the main area for the results. (Gibbins, 1995). The results presented from this work are from a HHR in a TGA, see Chapter 4.8. The HHR volatile N release for the olive cake is close to the 1:1 line indicating the release of nitrogen is commensurate to proximate volatile release (85% for the HHR volatile N and 80 % for the proximate volatile N). As the olive cake matrix breaks down, the volatile N is released, under high heating conditions, more volatile N is released. When the olive cake blended with coal PFA is reviewed, the volatile N release under HHR conditions has increased to ~89.5

%. The increased Fe_2O_3 in the coal PFA may be providing increased reaction zones for the fuel matrix to degrade into a higher volatile content under high heat conditions. Alternatively, previous work has shown that Fe_2O_3, can act to reduce NO to diatomic nitrogen for coal chars. (Ohtsuka, 1997; Tsubouchi and Ohtsuka, 2008). The mechanism within the TGA is heterogeneous, as the solid particles of olive cake and coal PFA are in close proximity. As the fuel matrix degrades, some homogeneous reactions may take place.

9.6.3 HHR nitrogen partitioning (DTF 1)

The DTF procedure was the same as for the coals in Chapter 4.4. Chars were collected from DTF 1 for the olive cake with and without coal PFA. The nitrogen contents of the chars were measured and the calculation for nitrogen released was by difference. The ash tracer method was used as per Equation 6.1 (Steer, 2015) in order to estimate char yield and allow a N mass balance. Referring to Figure 6.4, it can be seen for the olive cake, the nitrogen partitioning shows nitrogen retained in the char at ~24.5%. For the blended sample, however the retention is reduced to ~12%. This indicates there is additional nitrogen release from the olive cake in the presence of coal PFA. For coal there is a known correlation between carbon conversion and nitrogen devolatilisation (Kambara et al., 1994). For coals, Jones et al (Jones, 1994) reported nitrogen devolatilisation was less than carbon conversion at 1400°C. It was also suggested by Woitowicz that carbon conversion and nitrogen devolatilisation were heating rate and temperature dependant (Woitowicz et al., 1995).

The carbon conversion for this experimental work in shown in Figure 6.5 and 6.6. In Figure 6.5 it can be seen the olive cake carbon conversion is at ~50%. When blended with the coal PFA, the carbon conversion increases to ~75 %. Within this work at 1373 K and 1-2% O_2, there is a direct relationship between carbon conversion and nitrogen release (Kambara et al., 1994). Within Figure 6.6, it can be seen, as the iron and basics increase, so the carbon conversion increases with a natural logarithmic

relationship. Figure 6.7 shows the data for the olive cake with and without additives compared to data from Kambara (Kambara et al., 1994). It can be seen (as with the coals) the parity between carbon conversion and volatile N release is maintained.

The volatile nitrogen was also examined against the Σ(Fe + bases)/N, Figure 6.8, where a natural logarithmic relationship was again found. Much research has been carried out to show the reactive compounds in coals and biomass can have a catalytic effect on the release of volatile nitrogen (Daood et al., 2014; Chen and Gathitu, 2011; Daood et al., 2017; Illan-Gomez et al., 1995a; Illan-Gomez et al., 1995b; Illán-Gómez et al., 1998; Karlström et al., 2017; Lissianski et al., 2001; Su et al., 2010). The release of nitrogen as volatile is desirable in a Low-NO_X furnace, where volatile N can be reduced to diatomic nitrogen.

9.6.4 Study of N-partitioning using the low-N analyser

Nitrogen partitioning was also studied by use of the low N analyser described in Chapter 4.7, the results were presented in Chapter 6.4 and Figures 6.10 and 6.11. The nitrogen release profiles are shown in Appendix 1. From Figure 6.10, (N split) it can be seen the data is similar to the figures in the volatile N release from the DTF, Figure 6.4. From the Low N analyser, the nitrogen split for the olive cake was 23% retained in the char. For the olive cake and coal PFA, the char-N fell to 14.5%. The trend is the same as for the DTF chars. There are some slight numerical differences, however, for the Low N analyser, the ash tracer method was not required, as there are no potential losses in the analyser. The addition of the increased reactive components, has again realised a reduction in the nitrogen retained in the char. By difference, the volatile N release has therefore increased.

Figure 6.11 shows the volatile N release as a function of Σ(Fe + bases)/N using the results from the Low N analyser. The volatile N increases from 77% to ~85.5% for the olive cake without and with coals PFA respectively. These results strengthen the

results shown in Chapter 6 and in Sections 9.6.1-9.6.2, where the addition of reactive compounds can have an effect of the volatile N release from olive cake.

9.7 Functional groups (XPS)

Analysis of the functional nitrogen groups N1s, in the olive cake, olive cake char with and without additives were carried out using the same procedure as described for the coals in Chapter 4.11.

The olive cake N-functionality was dominated by a peak at ~400 eV which could be assigned as pyrrole (N-5), or NH_2 type groups in amino acids. Plant based nitrogen can be in the form of NH_2 from chlorophyll, which has a signature at 400.4 eV (Darvell et al., 2012), however it is difficult to separate the two signatures out from the profiles presented in Figure 9.4. N5 is the same principle functional group that was in all four of the coals under test, Chapter 5. As with the coals, N-5 are thermally unstable forms of nitrogen, and the heterocyclic rings readily break under elevated heat conditions. The breaking of the rings releases H radicals which can form hydrogen cyanide. (Deng et al., 2016; Liu, 2019).

The olive cake char was analysed in the same way, and the functional group had evolved into quaternary (N-Q), this process is again the same as for most of the coals, where N-Q was the principle N1 s derivative in the chars. It could be assumed the same process is in place, whereby the pyrrole functional group undergoes heterocyclic ring scission and reforms as quaternary nitrogen see Figure 7.6. (Pels, 1995a).

When the olive cake is blended with the coal PFA and a char created, the functional group remaining is still N-Q. The addition of the coal PFA has no apparent effect on the functional group formation from the chars, where with or without additive, the resultant N 1s functional group is quaternary.

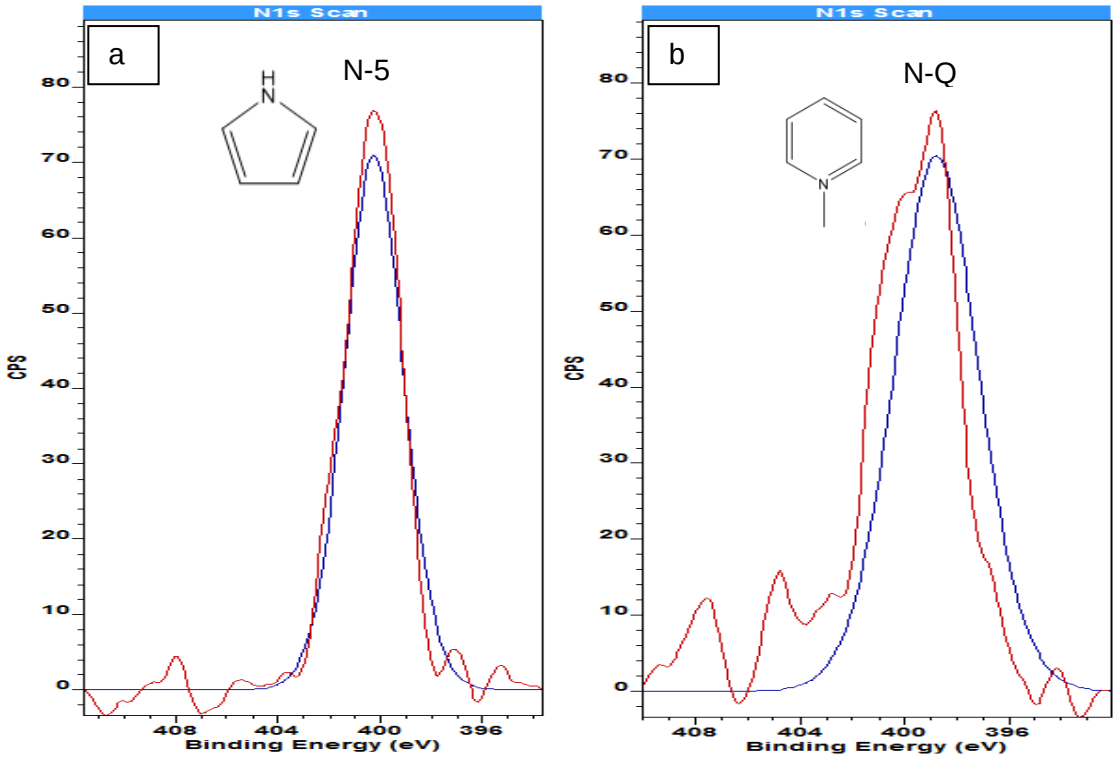

Figure 9.4 a. N 1s functional groups in olive cake. b. N 1s functional groups in olive cake char. —— 1st Functional group, —— raw data (smoothed)

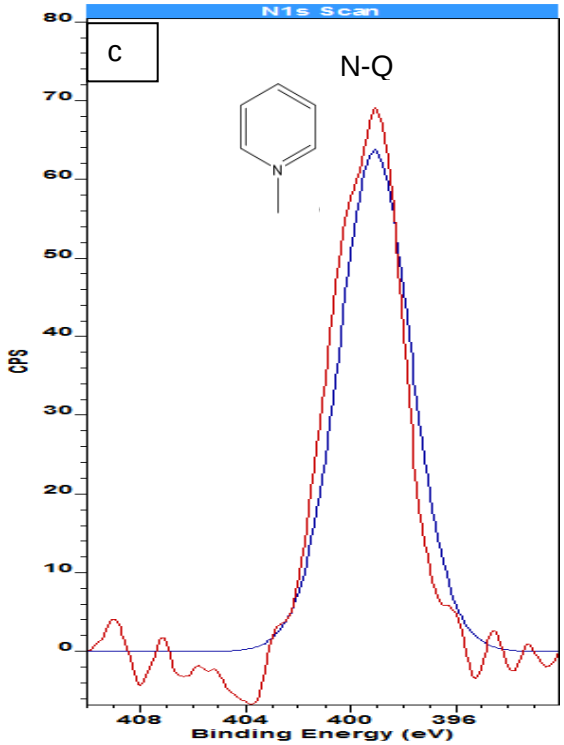

Figure 9.5 Olive cake plus PFA N 1s functional groups. —— 1st Functional group, —— raw data (smoothed)

9.8 Olive cake char combustion

A variety of methods for char combustion were carried out. Referring to Chapter 7, the NO from combustion was carried out using DTF 2 (Chapter 4.4.3). Nitrogen split was conducted using chars from DTF 1 Chapter 4.4.1 as described above. In addition, the chars were combusted using the STA-MS (Chapter 4.12) and the gas evolution profiles were detected and integrated to give the percent conversions of char-N to different N-species.

9.8.1 Fuel and fuel plus additive combustion in DTF 2

The data from DTF 2 and the effluent gas emissions equipment was recorded in ppmv, and converted to mg/Nm, using Equations 7.1-7.8. The equivalence ratio was calculated as for the coals using Equation 7.9. There is a known correlation between NO_X formation and FR. CH radicals form in the volatiles which can react with nitrogen species causing decreases in NO_X with reducing FR (Wendt, 1995). High volatile fuels tend to release more nitrogen as volatiles rather than retention as char-N. Biomass tends to be higher in oxygen than coals, which can react with nitrogen radical species and nitrogen species to form NO/NO_X. Work by Ren et al showed mineral matter can have an effect on the NO_X precursors HCN and NH_3 (Ren and Zhao, 2013). As the olive cake under examination is of a high N content, refer to Section 9.6.3 and 9.6.4, it is possible more nitrogen will be liberated during devolatilisation. The formation of NO_X is also dependant on available oxygen in excess air during combustion. The conditions for combustion in DTF 2 were fuel lean, therefore increases in NO_X were expected.

Figure 7.7a shows the NO kg/GJ as a function of FR. It can be clearly seen the olive cake with and without additives occupy the left most points with FR values of 0.25-0.3. The NO values of 0.57 kg/GJ for the olive cake and 0.47 kg/GJ for olive cake with coal PFA show an NO reduction far greater than simply the reduction of fuel bound nitrogen from the blend. The olive cake only forms part of the FR curve, whilst the olive cake

with coal PFA falls somewhat below the curve, indicating a greater reduction through the reactive compounds from the additive. Figure 7.7b has been used from Ren et al (Ren et al., 2017), where a correlation between NO kg/GJ to volatile/FC was shown in the trend-lines. The data from this work (using the same DTF and gas analysis equipment) showed some similarities in the data and correlation to the trends shown for the biomass trend line.

From Figure 7.8a, the NO kg/GJ is shown as a function of the Ca and Mg. Liu et al showed there is a connection between Ca and the initial breaking of pyrrole-N functional groups to form HCN (Liu, 2019). CaO and MgO have been shown to form nano-particles during combustion of coals and biomass, which can act as high surface zones for catalysis (Silva and da Boit, 2011). For the olive cake there is a significant reduction by 17% for the NO emissions when the coal PFA is added. The data from this research is in close comparison to that of Ren et al (Ren et al., 2017).

This work was taken a step further to make the comparison to Σ(Fe + bases)/N, in Figure 7.8b. As the same emissions data is presented, it is not possible from this data to establish which elements of compounds from the reactive components are principally responsible for the changes in NO emissions. It is certain that without the additives, the reduction does not occur. Using the chemical breakdown of the additives, it appears that the changes are brought about through catalysis with the reactive compounds. For the coal PFA, this is likely to be through the interaction of the Fe_2O_3. It has been shown through several researchers that reactive elements can have a reducing effect on NO_X emissions, particularly from biomass (Daood et al., 2014; Chen and Gathitu, 2011; Daood et al., 2017; Illan-Gomez et al., 1995a; Illan-Gomez et al., 1995b; Illán-Gómez et al., 1998; Karlström et al., 2017; Lissianski et al., 2001; Su et al., 2010).

9.8.2 Gas evolution profiles during char combustion

The chars of the olive cake and olive cake with coal PFA were analysed for temperature programmed combustion in the STA-MS as shown in Chapter 4.12, using the same process as for the coal chars.

During char formation the protein nitrogen is converted to pyrrolic and quaternary nitrogen. (Di Nola et al., 2010; Jones et al., 2012). The main primary products from the oxidation of the char containing these forms of nitrogen will be ammonia and HCN. Both hydrogen cyanide and ammonia are intermediary species for NO_X formation. Within this work NH_3 was not recorded, therefore the detected intermediary species were in the forms of cyano, C_2N_2 and HCN. The olive cake char showed distinct curves for all of the four gases, CO_2, C_2N_2, HCN and NO. The emissions of C_2N_2 leads the emissions of both HCN and NO. The onset of HCN is at a lower temperature than the NO. These results would indicate that in the olive cake char, the C_2N_2 and HCN are precursors to the formation of NO. Of note, there were two peaks for the HCN, and a ramp for the CO_2 leading up to the peak, which may be indicative of some volatile content still present in the chars.

The release of the gases from the chars occurs at higher temperatures than from the raw olive cake, Section 9.6.1. This is anticipated, as chars have lower reaction rates, through low volatile levels and cross linking of compounds forming stronger bonds. The stronger bonds require higher energy levels to break the bonds. The nitrogen species are released over the same range of temperatures as the CO_2 evolution from the chars. The NO peak aligns with the CO_2 emissions, which is commensurate with the carbon conversion and nitrogen partitioning shown in Chapter 6. Correction for $^{12}C^{18}O$ on the NO (m/z 30) signal were used in the calculations.

When the olive cake and coal PFA char blend was examined, the peaks for all of the gases have shown movement to the left compared to the olive char without additive. The lowering of the temperature at which the onset of gases was released and the lower temperature of the peak emissions suggests the addition of the coal PFA is

causing the peak of NO to be at lower temperatures, i.e. there is evidence of catalysis. This characteristic is desirable in a Low NO_X furnace, as Fuel N released earlier in the combustion in a fuel rich environment can be reduced to molecular nitrogen.

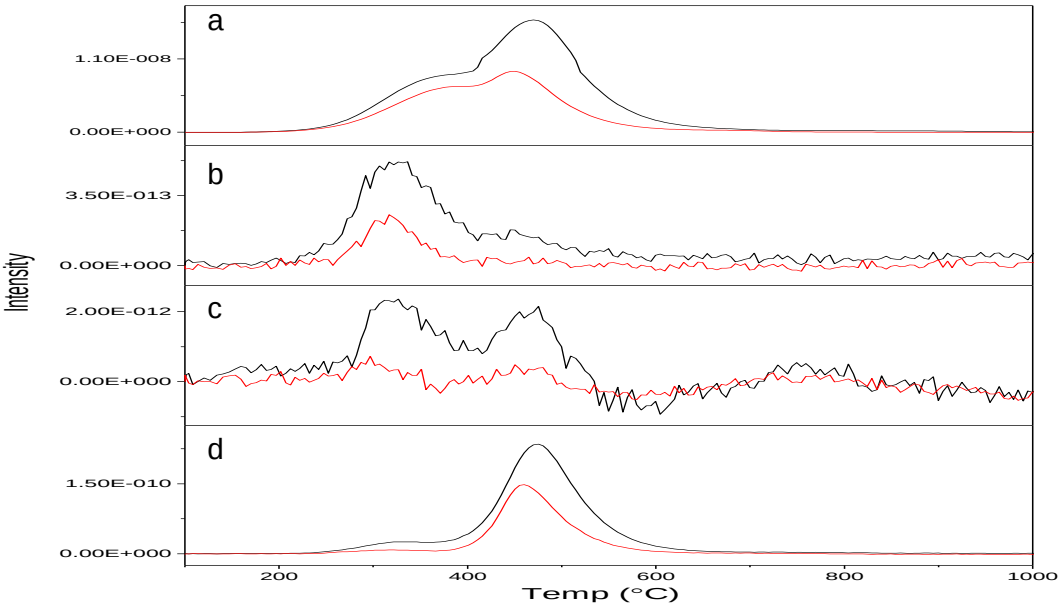

Figure 9.6 Emissions from olive cake char with and without coal PFA. —— Olive cake char —— olive cake char plus coal PFA a. CO_2, b. C_2N_2, c. HCN, d. NO

The percentage values of the nitrogen species released during the char combustion are shown in Table 9.7, all peak data was divided by the mg of sample. It can be seen the greatest proportion ~41% of the nitrogen species are in the form of NO, with less than 1% for each of the intermediary species (HCN and C_2N_2). Although the N_2 cannot be detected in the MS, as the m/z is the same as CO, as large quantities of CO are produced, it can be assumed all of the remaining nitrogen species are diatomic. As the percentage of N species/N decreases when the olive cake is blended with the additive, the percentage of diatomic N has increased.

Table 9.7 % values of Nitrogen species from the olive cake char with and without coal PFA

Chars	NO/N	HCN/N	C_2N_2/N	N species/N
Olive cake char	41.43	0.64	0.12	42.19
Olive cake plus coal PFA	38.01	0.05	0.05	38.11

9.8.3 Char reactivity

Using Arrhenius profiles as shown in Section 9.5.2, the reactivity of olive cake char with and without additive were calculated. The values are presented in Table 9.8.

Table 9.8 Kinetic parameters olive cake chars and chars/ash blends

Sample (Chars)	E_a (kJ/mol)	A (cm^3/s)	k_{630K}/s
Olive cake	69.76	13713.01	2.25E-02
Olive cake plus PFA	50.87	30.76	1.86E-03

When compared to the data in Table 9.6 (kinetic parameters for the olive cake and olive cake pus coal PFA), the olive cake has shown increase in the activation energy values from 50.87 kJ/mol for the olive cake to ~70 kJ/mol for the olive cake plus coal PFA char. The k value of 2.25E-02 for the olive char is a higher value than for the raw fuel at 1.77E-04. The olive cake blended with the coal PFA char, 1.86E-03 however, is an order higher than the olive cake char at 1.77E-04. From this value, it appears the coal PFA has increased the reactivity of the olive cake char. When the reactivity is compared to the emissions characteristics in Section 9.8.2, the onset of the emissions for the olive cake and coal PFA lags the olive cake char. The blended char gas evolution peaks for all of the gases (CO_2, C_2N_2, HCN, NO) in Figure 9.6 ahead of the gas peaks for olive cake without additive.

9.9 Chapter summary

The olive cake has a high volatile content, compared to the coals at, 72.3% (daf), however this is normal for a biomass, the nitrogen content is at 3% (daf). The high levels of volatile and nitrogen content resulted in high percentage levels of volatile nitrogen being released during pyrolysis. The addition of the coal PFA at 15% w/w, further enhanced devolatilisation, and increases in volatile nitrogen from 80% on a proximate basis, up to as high as 87% under HHR conditions in DTF 1. When the volatile N data was plotted against the iron and bases content, there was a correlation

showing a natural log relationship; as the Σ(Fe + bases)/N increased so the release of all volatiles (including volatile-N) increased.

The addition of the coal PFA to the olive cake yielded no apparent change to the functional groups formed. Olive cake appeared to contained pyrrole or NH_2 type groups, while the chars of olive cake and olive cake with coal PFA both showed only N-Q. It should be noted plant protein N 1s at 400.4 eV could be overlapping with the pyrrole signal 400.5 eV, from chlorophyll.

The reactivity of the olive cake increased when the coals PFA was added, with activation energies raising from 50 kJ/mol up to 63 kJ/mol. The $k_{(450)}$ constant also increased from 1.77E-04/s up to 2.25E-04/s.

An evaluation of the NO_X emissions in DTF 2 in an excess air environment, showed that there was no NO_2, therefore all NO_X readings were taken as NO. The NO data revealed the known connection between FR and NO_X emissions, whereby lower FR values tend towards higher NO_X values. The results when combined with the data from Chapter 7 for the coals suggests the FR, NO_X relationship is maintained across all of the fuels under test.

The evolution of nitrogen species during char combustion was assessed. For the olive cake, the release of CO_2 and NO were at the same temperatures, whilst C_2N_2 and HCN led the release of NO. When blended with the coal PFA, all of the peak temperatures for all four emissions gases (CO_2, C_2N_2, HCN and NO) were advanced, i.e. at lower temperatures. The blended fuel showed a reduction in the nitrogen species C_2N_2, HCN and NO, as a result it can be postulated the N_2 has increased. As C_2N_2, HCN pre precursors for NO, it can be assumed the increase in N_2 is at the expense of NO. The onset of emissions was similar to the unblended olive cake. Further to this, the C_2N_2 lead the HCN, indicating the C_2N_2 may be intermediary to HCN and NO formation.

The olive cake and coal PFA char showed a lowering of the activation energy from ~70 kJ/mol down to 51 kJ/mol, and $k_{(630)}$ was an order lower, at 1.86E-03.This result for the

char is the reversal of the reactivity changes for the raw biomass with and without additive.

This work has focussed on only one biomass, olive cake with a high nitrogen content. To consolidate this work, it requires extending out to a greater range of biomass materials to formulate a more comprehensive study.

Chapter 10 Discussion/ Conclusion

10.1 Discussion

The discussion is separated into two sections, the first reviews the results and the mechanism of catalysis, the second discussion explores the implications and potential outcomes for industry and future work.

10.1.1 Mechanism for impact of additive on N-partitioning

When the coals were blended with the ash additives, there was a change to the devolatilisation characteristics compared to the coals without additives. Across all of the coals there was an increase in LHR and HHR devolatilisation for all volatiles, and in particular the release of fuel bound nitrogen. Figure 10.1 highlights the reaction pathways for fuel nitrogen evolution and the effects of the ashes and the catalytic reaction pathways that appear to be taking place.

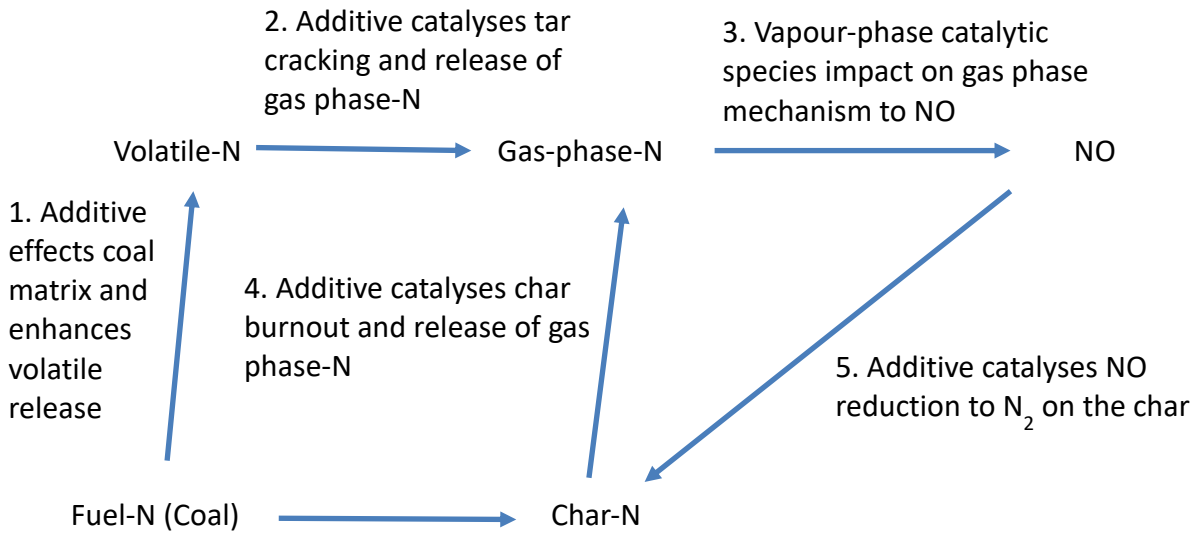

Figure 10.1 Reaction pathways for the evolution of nitrogen from the coal and the effects of the ash additives on the coal nitrogen evolution

The changes in the release of nitrogen from the coals through catalysis appears to be driven by a combination of the alkali and alkaline earth metals which are released

during both homogeneous and heterogeneous combustion. (Ohtsuka, 1997, Illan-Gomez, 1995a, Illan-Gomez, 1995b). The cations were shown to be released during washing, which is indicative that they are readily released during combustion. (Shannon and Fine, 1974). The additives showed a trend of reducing the temperature that the onset of devolatilisation started for all of the coals. From Figure 10.1 reaction pathway 1 shows the additives affect the coal matrix to increase the volatile N released during devolatilisation, resulting in a reduction of nitrogen retained in the char. (Hernandez and Kilpinen, 2005) Reaction pathway 2 shows an extra potential level of catalysis where the coal tars are cracked to increase the production of gas phase nitrogen. Pathway 3 highlights the impact of vapour phase catalysis and the impact on the mechanism for formation of NO versus reduction in N_2. Reaction pathway 4 shows the additives seem to catalyse the char nitrogen and enhances the gas phase nitrogen. Reaction pathway 5 shows an important mechanism, where the NO generated during combustion goes through reduction back to diatomic nitrogen. The reduction takes place through catalysis on the chars which have high surface areas and thus provide reaction zones for catalysis. (Lester et al, 199, Lissianski,, 2001) Under HHR conditions, volatiles are more readily released than during LHR. (King, 2006) The addition of the ashes enhanced the devolatilisation of the nitrogen under HHR condition. As the carbon content increased, so the effects appeared to be enhanced. The devolatilisation of the nitrogen appeared to be symbiotic with an enhanced carbon conversion across all of the coals, thus the increased release of nitrogen may be linked to carbon content. Illan-Gomez et al, 1993, Illan-Gomez et al, 1995a). Later work by Illan-Gomez, also showed a reduction of NO_X from potassium containing chars, however the results were in elevated O_2 conditions. (Illan-Gomez et al, 1998). The increased pore density of the chars and morphology changes of the chars may be instrumental to reaction pathway 4 (Figure 10.1), where the char-N conversion to gas phase N release appeared to increase through catalysis. Reaction pathway 5 may also have been enhanced through the increased surface areas created through the increased pore density, particularly on Shotton and Galatia chars. The presence of Fe

in the blended fuels, however, may also have had a catalysing effect on the NO emissions. (Daood et al, 2017) There was a change to NO_X intermediary species C_2N_2 and HCN, when the coals were blended with both additives. The reduction in NO and NO intermediary species indicate there was an increase in N_2. The results could not be verified as high levels of CO (which has the same molecular mass) mask the N_2 results. The PFA showed a marked increase in the release of C_2N_2 and HCN at earlier temperatures. There is indication the char combustion rate is also increased when the coals are blended with the additives. The functional groups seemed to show a change in their release when the coals were blended with the additives. When the PFA was added there was a reduction in the recorded N-Q. This may be indicative the quaternary nitrogen may release HCN at lower temperatures.

10.1.2 Practical considerations

According to the results obtained, the addition of biomass ash to coal was found to increase volatile release and thus volatile nitrogen fraction under both fixed-bed and entrained flow combustion conditions. This suggests that to see the beneficial effects of these additives, in practice the biomass ash would have to be introduced with the coal feed – whether co-milled with coal or injected closely together into the furnace. This would require optimisation of the combustion process, as mentioned in Chapter 6. In addition, fouling and slagging could be an issue with injecting biomass ash into the system. It is to be noted that the feed ratio has not been optimised in this work, and it is possible that a similar benefit could be seen on NOx with lower amounts of biomass ash. Nevertheless, volatile-K from the biomass ash would be of special concern, in particular for fouling (Plaza et al., 2009). In this regard, since this ash has already been through the boiler, it may have less mobile potassium than low temperature-ashed biomass ash (or a biomass fuel). Moreover, previous studies have shown that coal ash can react with volatile-K, so it is possible that coal ash could capture any remaining K as the coal burns (Clery et al., 2018). The cost trade-off between bringing NOx

emissions down and increasing of fouling and slagging propensity would have to be carefully assessed. There is potential that increasing the proportional levels of alkaline within the furnace may cause issues for accelerated corrosion within the furnace. Thus the use of biomass ash as an additive would require further study and optimisation, but it looks promising as a relatively cheap addition to NO_X reduction strategies in a power station that already has a flexible fuel inventory.

Further economic considerations would need to be evaluated. The FBA ash under test was high in carbon content, and therefore provided: a. a potential extra catalyst for reactions to take place. Activated carbon has high surface areas, and thus provide potential reaction sites for NO_X reduction b. the carbon content could be used as a secondary fuel within a furnace. The PFA however realised a better reduction strategy for NO_X. The addition of the PFA to coal may result in higher levels of more toxic ashes. These ashes would still require disposal and so would be subject to landfill taxation. With the increased carbon conversion resulting from the blend, there may be less total ash from the co-combustion system than if the two ashes were disposed of independently.

Biomass ashes have been shown to have some potential future uses, i.e. as a useful additive for the manufacture of concrete. There are some limitations for the use as a plasticizer for concrete, with a maximum addition of 20%. Additions above the value of 20% can lead to degradation of the structural integrity of the concrete. A further use for the PFA and FBA can be as an aggregate material for road building.

Further to the potential slagging and fouling issues within the furnace, there is an increased possibility of fouling or poisoning of SCR components. Due to the nature of the components in an SCR, the honeycomb structure have high surface areas. The fine particle nature of the ashes, and their nano-particle by-products may increase the risk of occupying the pores in the catalysts, reducing the effectiveness of the catalyst. K_2O, with particle sizes of <5 µm, is a known poison for SCR. (Baxter, 2005; Benson et al., 2005; Larsson et al., 2006). If the SCR catalyst effectiveness were to be reduced, the

reductions in NO_X from the furnace may be countermanded by the longer-term loss of effectiveness of the SCR. The cost for repair to a catalyst and the penalties for down time of a furnace may be counterproductive to the advantages gained from the ash.

To implement the ash into a furnace, there may be extra engineered parts required in the system. These may involve the inclusion of blending equipment prior to grinding to ensure correct percentage quantities were being added. The inclusion before grinding should ensure consistency of particle size entering the furnace.

A minor complication may be the storage of the ash prior to use. If the ashes were stored outside, this may affect the fuel quality of the ash. Storage outside may however result in leaching of the reactive components. The Ca and K have both shown to be susceptible to leaching in water. The loss of these elements may render the ash less effective as a NO_X reduction catalyst in the furnace.

Through the experimental work, the changes in nitrogen partitioning, showed a reduction with percentage of additive. As greater percentages of ash was used (reactive elements), the effectiveness on the nitrogen partitioning became reduced. The logarithmic nature of the curve indicated there is an optimum level of additives. Within a full-scale furnace, this restriction would be important for the effectiveness of the additives, however would be somewhat negated by the constant flow into the furnace of the fuel and additives. The constant supply of fresh material at the optimum level would ensure the reactivity of the ash would not diminish.

The experimental work also revealed an increase in carbon conversion. The increase in carbon conversion offers a potential for increased burnout of carbon within a furnace. The increased burnout would result in less ash from the coals. The fuel in the furnace would require extra consideration for stoichiometry. With the extra carbon burnout may come an increase in operational temperature. An increase in temperature may increase the risk of thermal NO_X. The ash does however offer some heat diffusion, which may counteract any increase in temperature from improved carbon conversion. The heat diffusion would help balance the NO_X emissions.

The addition of the coal PFA to the biomass also showed some positive effects on nitrogen partitioning and carbon conversion. Some of the potential problems associated with adding biomass ash to coal would also present potential issues for biomass combustion. The olive cake under test had high levels of K, Ca and Na, and to a lesser extent the Mg. The addition of a high Fe content ash however would offer a mechanism for creating an imbalance in the base/acid ratio. This would again offer a potential issue for slagging and fouling of a furnace. The increased iron can act to increase solidity of ash on a furnace wall, reducing the effectiveness of heat transfer.

A positive effect may be the proportional reduction of K_2O in the exhaust affecting the SCR.

10.2 Conclusion

Experimental studies were made of four coals and one biomass, in the absence and presence of power-station ash additives. During high heating rate devolatilisation, the coals retain 44–78% of their nitrogen in the char at 1373 K. In comparison, the olive cake loses 75% of its nitrogen under the same conditions. In the presence of the ash additives, a higher loss of Fuel-N is observed in the volatiles. This is most significant for high fuel ratio coal, Ffos-y-fran, where volatile-nitrogen increased from 22% to ~60% in the presence of the additives. This enhanced volatile-N release in the presence of the additives is related to the enhanced carbon conversion, and volatile-N correlates well with extent of conversion. Thus one role of the additives is to catalyse the devolatilisation (and char burning) stages. The additives all had elevated levels of the potentially catalytic species, CaO and K_2O, compared to the coal ashes. The effect of the additives for decreasing NO emissions was more modest in the studies under excess air. Nevertheless, the volatile fuel-N release shows a synergy with the base components (Ca, Mg, K, Na) in the feed (i.e. fuel or fuel + additive):

When the summation of base elements increase, so the volatile-N release increases, and NO decreases. A 17% reduction in NO for the biomass, and a 5% reduction in NO for the bituminous coals was achieved even under fuel lean conditions.

Results from experimental work were used for the validation of CPD and furnace modelling. Applicable to this work, CPD can be used to predict the HTVY and volatile N release from bituminous and sub-bituminous coals. To accurately predict the HTVY, the side chain/char chain cracking ratio was increased for the two additives, to allow for the increase in HTVY in experimental work. To achieve accurate model predictions for volatile N release for the coals when blended with either FBA or PFA, adjustments to the pre-exponential factor A_N were required. The values of the kδ/kc ratio and A_N values are dependent on the amount of reactive components (Ca .K, Mg, Na, Fe) and the percentage of additive applied. CPD gave accurate predictions for both HTVY and nitrogen partitioning release compared to experimental data.

The furnace model required three separate model input data ranges: CPD, CBK 8 and furnace data. CBK 8 required changes to the intrinsic reactivity for the bituminous coals under test. The furnace model was validated against an industrial furnace using data provided from industry. Using the three validation data sets for CPD, CBK 8 and the furnace, the furnace model was able to accurately predict NO_X emissions from an industrial furnace. With geometric and operating conditions for a furnace, standardised input data can be used to give a prediction of the emissions for bituminous coals with and without additives. The predictions are only extrapolated up to 15% additive.

Ffos-y-fran and olive cake were examined in the model, however the results were outside of the validation range.

The use of biomass ash, either FBA or PFA, could be used as a method for the reduction of NO_X emissions from a large-scale furnace operating with bituminous coals. This would operate as a primary reduction technique within a reducing atmosphere in a Low-NO_X burner. As part of an emissions reduction strategy, this could be used as a low-cost method of achieving emissions inside future regulatory standards. Further to

this, the use of a combined furnace slice model can be utilised to predict the emissions from a furnace operating with bituminous coals. Through this work, these would only be valid for additives up to 15% w/w with the current biomass ash additives. When converted to the reactive elements (Ca. K, Mg, Na, Fe) on a mass basis, different additives can be calculated within the ranges shown in this work.

As the ashes with lower calorific values than the coals under test were used, there is a slight reduction in potential heating value. The reduction in heating value could be of significance during power generation, as less heat would be available for transfer to the steam cycle, potentially reducing efficiency in a furnace. If less heat is available per kg of fuel, then more fuel would be required to achieve the same output. The additives however, improved the carbon conversion, which increases the burn out of the coal, thus more efficient use of coal and less unburnt carbon in the co-combustion ash. The increased efficiency of the carbon burnout compensates for the lower heating value of the blended fuels.

Consideration should be given to the potential negative impacts of fouling and slagging in a furnace and SCR poisoning although careful calculation of the base acid ratio should be used to mitigate these issues.

10.3 Future work

Within this work, the focus has been on the use of waste/ by-product of biomass combustion for catalysis during coal combustion as a method of primary NO_X reduction in a large-scale furnace. The main area of interest has been on bituminous coals currently used for power production. The theory was to explore if the reactive elements (Ca. K, Mg, Na, Fe) or their oxides, could act as method to increase nitrogen partitioning in favour of volatile N release compared to char N. The ash additives were applied at integrals up to 15%. Based on reactivity, 15% was used as the maximum, Chapter 4 and 5.

Within this work, the combined effects of these elements, led to increases in volatile N release and a decrease in char N, which is a positive effect for use in a Low NO_X furnace. It has not been established in this work if any single element, or which combination of elements actually resulted in the chemical change during combustion.

Secondary experimental work involved high and low reactivity fuels; olive cake (biomass with coal PFA additive) and Ffos-y-fran (coal with both of the biomass ash additives FBA and PFA).

Future work could be used to:

- Investigate the optimum ratio of the reactive elements for NO_X reduction from bituminous coals
- Isolate each reactive element and compound to explore the most effective reduction mechanism.
- Extend the work to lower than 15% percentage of biomass ash additives to investigate the extent of catalysis with both FBA and PFA on bituminous and sub-bituminous coal.
- Further work into the nitrogen evolution and the intermediate species could be explored to determine the exact route to NO_X from bituminous coals with additives.
- The low reactivity coal (Ffos-y-fran) had some positive results for HTVY and nitrogen partitioning. This work could be extended to explore if other low reactivity fuels showed similar effects.
- The high reactivity fuel (olive cake) and coal PFA, showed positive results in the release of HTVY and significant increases in volatile N release. Further biomass and high reactivity fuels should be investigated to ascertain if the addition of coals PFA could be used as a method of NO_X reduction for biomass fuels. This could potentially be extended to include coal FBA to explore the effects of carbon conversion and nitrogen partitioning.

Environmental consideration should be given to any final waste product produced during the co-combustion of fuels with additives.

- An investigation into the implications of the final ash on future uses i.e. cement enhancers, soil improvement etc should be investigated.
- Would the disposal of the ashes have further landfill implications, and would this be offset by the reduction in ashes direct from the furnace into landfill?

References

Adams, B.R. 2017. Mitigation of Airborne Pollutants in Coal Combustion: Use of Simulation. In: Meyers, R.A. ed. *Encyclopedia of Sustainability Science and Technology.* New York, NY: Springer New York, pp.1-36.

Arenillas, A., Rubiera, F., Arias, B., Pis, J.J., Faundez, J.M., Gordon, A.L., Garcia, X.A. 2004. A TG/DTA study on the effect of coal blending on ignition behaviour. *J. Therm. Anal. Calorim.* **76**, pp.603–614.

Arenillas, A., Rubiera, F., Pevida, C., Pis, J. J. 2001. A comparison of different methods for predicting coal devolatilisation kinetics. *Journal of Analytical and Applied Pyrolysis.* **58–59**, pp.685-701.

Arvelakis, S. and Frandsen, F.J. 2010. Rheology of fly ashes from coal and biomass co-combustion. *Fuel.* **89**(10), pp.3132-3140.

ASTM. 2012. 2012. *American Society for Testing and Materials, Standard Classification of Coals by Rank. 2012.*

ASTM. 2013. 2013. *ASTM D5865-13, Standard Test Method for Gross Calorific Value of Coal and Coke, ASTM International, 2013.*

Axworthy, A.E. et al. 1978. Reactions of fuel-nitrogen compounds under conditions of inert pyrolysis. *Fuel.* **57**(1), pp.29-35.

Backreedy, R.I. et al. 2005. Co-firing pulverised coal and biomass: a modeling approach. *Proceedings of the Combustion Institute.* **30**(2), pp.2955-2964.

Badzioch, S., Hawksley, Peter G. W. 1970. Kinetics of Thermal Decomposition of Pulverized Coal Particles. *Industrial & Engineering Chemistry Process Design and Development.* **9**(4), pp.521-530.

Bailey, J.G. et al. 1990. A char morphology system with applications to coal combustion. *Fuel.* **69**(2), pp.225-239.

Barišić, V. et al. 2013. Role of Pulverized Coal Ash against Agglomeration, Fouling, and Corrosion in Circulating Fluidized-Bed Boilers Firing Challenging Biomass. *Energy & Fuels.* **27**(10), pp.5706-5713.

Barranco, R. et al. 2006. The effects of pf grind quality on coal burnout in a 1 MW combustion test facility. *Fuel.* **85**(7–8), pp.1111-1116.

Bassilakis, R. et al. 1993. Sulfur and nitrogen evolution in the Argonne coals. Experiment and modeling. *Energy & Fuels.* **7**(6), pp.710-720.

Baum, M.M., Street, P. J. 1971. Predicting the Combustion Behaviour of Coal Particles. *Combustion Science and Technology.* **3**(5), pp.231-243.

Baxter, L. 2005. Biomass impact on SCR Catalyst performance .pdf. *IEA Bioenergy.* **32**.

Baxter, L.L. et al. 1996. Nitrogen Release during Coal Combustion. *Energy & Fuels.* **10**(1), pp.188-196.

Bell, R.D. and Buckingham, F.P. An overview of technologies for reduction of oxides of nitrogen from combustion furnaces.pdf.

Beltrán, M.G. et al. 2014. Mechanical and durability properties of concretes manufactured with biomass bottom ash and recycled coarse aggregates. *Construction and Building Materials.* **72**, pp.231-238.

Benson, S.A. et al. 2005. SCR catalyst performance in flue gases derived from subbituminous and lignite coals. *Fuel Processing Technology.* **86**(5), pp.577-613.

Berra, M. et al. 2015. Reuse of woody biomass fly ash in cement-based materials. *Construction and Building Materials.* **76**, pp.286-296.

BHEL. 2016. *New Environmental Norms on NOx for thermal power generation.* [Online]. [Accessed 27 January 2020].

Bilbao, R., Alzueta, M.U, Millers, A. 1995. Influence of stoichiometric ratio in the reburning zone on the concentration of different species. In: *Proceedings,2nd international conference on combustion technologies for a clean environment,* Lisbon, Portugal, 3-6 Jul 1995. *Lisbon, Portugal, Institute of Combustion: Portugese Section, vol II, Paper 27.1.* **II**, p8.

Bilger, R.W., Beck, R.E. 1975. 15th Symp. (Int'll) on Combustion, page 541. The Combustion Institute.
Birley, R., Jones, JM, Darvell, LI, Williams, A, Waldron DJ, Levendis YA, Rokni, E, Panahi, A. 2018. Fuel flexible power stations: Utilisation of ash co-products as additives for NOx emissions control. *Fuel.* **251**, p8.
Bogush, A.A. et al. 2018. Element speciation in UK biomass power plant residues based on composition, mineralogy, microstructure and leaching. *Fuel.* **211**, pp.712-725.
Bose, A.C., Dannecker, K.M., Wendt, J.O.L. 1988. Coal composition effects on mechanisms governing the destruction of NO and other nitrogeneous species during fuel rich combustion. *Energy and Fuels.* **2**(3), p457.
Boström, D.S., N.; Grimm, A.; Boman, C.; Öhman, M.; Broström, M.; Backman, R. 2012. Ash Transformation Chemistry during Combustion of Biomass. *: Energy Fuels* **26**(1), pp.85–93.
Bozkaya, U., Turney, J.M. Yamaguchi, Y., Schaefer III, H.F. 2010. *J. Chem. Phys.* **132**.
Bozzelli, J.W. and Dean, A.M. 1995. O + NNH: A possible new route for NO_X formation in flames. *International Journal of Chemical Kinetics.* **27**(11), pp.1097-1109.
Bozzuto, C.R. 1992. NO_X formation basics. Firth annual NO_X control conference. Long Beach, CA, USA, 10-11 Feb 1992. Burke, VA, USA, Council of Industrial Boiler Owners, pp1-17 (1992).
Bueters, K.A.C., J.G., Habelt, W.W. 1974. Performance predictions of tangentially fired utilily furnaces by computer model. *15th International symposium on combustion in Tokyo, Japan.*
Cahill, P., Smith M and Vallender SJ. 1991. Characterisation of British coals for low NOx combustion. Proceedings of the International Conference on Coal Science. *Proceedings of the International Conference on Coal Science, University of Newcastle-Upon-Tyne, United Kingdom.* pp.319-322.
Cai, H.Y., Guell, J., Chatzakis, N., Lim, J. Y., Dugwell, D.R., Kandiyoti, R. (1996). 1996. Combustion reactivity and morphology change in coal chars: effects of pyrolysis temperature, heating rate and pressure. *Fuel.* **75**(1), pp.15-24.
Chen, W.-Y. and Gathitu, B.B. 2011. Kinetics of post-combustion nitric oxide reduction by waste biomass fly ash. *Fuel Processing Technology.* **92**(9), pp.1701-1710.
Clery, D.S. et al. 2018. The effects of an additive on the release of potassium in biomass combustion. *Fuel.* **214**, pp.647-655.
Courtemanche, B. and Levendis, Y.A. 1998. A laboratory study on the NO, NO_2, SO_2, CO and CO_2 emissions from the combustion of pulverized coal, municipal waste plastics and tires. *Fuel.* **77**(3), pp.183-196.
Cumming, J.W., McLaughlin, J. 1982. Thermochimica Acta. **57**(253).
Dai, J. et al. 2008. Overview and some issues related to co-firing biomass and coal. *The Canadian Journal of Chemical Engineering.* **86**(3), pp.367-386.
Daood, S.S. et al. 2013. NOx control in coal combustion by combining biomass co-firing, oxygen enrichment and SNCR. *Fuel.* **105**, pp.283-292.
Daood, S.S. et al. 2014. Fuel additive technology – NOx reduction, combustion efficiency and fly ash improvement for coal fired power stations. *Fuel.* **134**, pp.293-306.
Daood, S.S. et al. 2017. Selective non-catalytic reduction – Fe-based additive hybrid technology. *Fuel.* **208**, pp.353-362.
Darvell, L.I. et al. 2012. Nitrogen in Biomass Char and Its Fate during Combustion: A Model Compound Approach. *Energy & Fuels.* p120216151727004.
Darvell LI, J.J., Ma L, Pourkashanian M and Williams A. 2010. Modelling NOx Formation in Pulverised Coal and Biomass Co-fired Boiler Units. *Proceedings of the Bioten Conference on Biomass Bioenergy and Biofuels.* pp.854-858.
Davidson, R.M. 1994. *Nitrogen in coal.* [Online].
Dayton, D.C.M., T. A. 1996. Laboratory measurements of alkali metal containing vapours released during biomass combustion:Laboratory measurements of

alkali metal containing vapours released during biomass combustion. *New York: Plenum Press.* pp.161-179.
Defra. 2019. *Defra National Statistics Release: Emissions of air pollutants in the UK, 1970 to 2017.*
Deng, J.J., & Li, H. L. 2008. Research progress of chemically inborn form and hot migration regularities for nitrogen element in coal. *Journal of Thermal Power Generation.* **37**, pp.12–17.
Deng, L. et al. 2016. Release of nitrogen oxides during combustion of model coals. *Fuel.* **175**, pp.217-224.
Di Nola, G. et al. 2010. TG-FTIR characterization of coal and biomass single fuels and blends under slow heating rate conditions: Partitioning of the fuel-bound nitrogen. *Fuel Processing Technology.* **91**(1), pp.103-115.
Doig, A., Morrison,G. . 1997. The use of natural gas in coal-fired boilers. IEAPER/35 London, UK, IEA Coal reseach. *IEAPER.* **35**.
Duan, L.L., D.; Chen, X.; Zhao, C. 2012. Fly ash recirculation by bottom feeding on a circulating fluidized bed boiler co-burning coal sludge and coal. *Appl. Energy* **2012**, pp.295–299.
EEA. 2010. *Nitrogen oxides (NOx) emissions.*
eia. 2018. *Oregan state profile and energy estimates.* [Online]. [Accessed 12 Nov 2019]. Available from: https://www.eia.gov/state/analysis.php?sid=OR.
eia. 2019. *Annual Energy Outlook 2019 with projections to 2050.*
Enerdata. 2019. *Global Energy Statistical Yearbook 2019.* [Online]. [Accessed July].
EPA, U. 2018. *www.epa.gov/climatechange/ghgemissions/gwps.html.* [Online].
EU. 2001. *Directive 2001/80/EC of the European Parliament and of the Council of 23 October 2001 on the limitation of emissions of certain pollutants into the air from large combustion plants*
EU. 2010. *Directive 2010/75/EU of the European Parliament and of the Council of 24 November 2010 on industrial emissions (integrated pollution prevention and control).*
EU. 2016. *Directive (EU) 2016/2284 of the European Parliament and of the Council of 14 December 2016 on the reduction of national emissions of certain atmospheric pollutants, amending Directive 2003/35/EC and repealing Directive 2001/81/EC.*
EU. 2017. *Commission Implementing Decision (EU) 2017/1442 of 31 July 2017 establishing best available techniques (BAT) conclusions, under Directive 2010/75/EU of the European Parliament and of the Council, for large combustion plants.*
Eurostat. 2018. *Air pollution statistics - emission inventories.* [Online]. [Accessed 26 July].
Evans, S., Pearce, R. 2019. *Mapped: The world's coal power plants.* [Online]. [Accessed 11 Nov]. Available from: https://www.carbonbrief.org/mapped-worlds-coal-power-plants.
Fenimore, C.P. 1970. Formation of Nitric Oxide in Premixed Hydrocarbon Flames. *Thirteenth Symposium (International) on Combustion, Combustion Institute, Pittsburgh, PA.* pp.373-380.
Fernando, R. 2014. *Developments in modelling and simulation of coal gasification.*
Finlayson-Pitts, B.J., Pitts, J.N., Jr. 2015. Final UK greenhouse gas emissions national statistics 1990-2013 Atmospheric Chemistry of Tropospheric Ozone Formation: Scientific and Regulatory Implications. *AIR & WASTE.* **43**, p1091.
Fletcher, T.H. et al. 1990. Chemical percolation model for devolatilization. 2. Temperature and heating rate effects on product yields. *Energy & Fuels.* **4**(1), pp.54-60.
Fletcher, T.H.K., Alan R. Pugmire Ronald J. Solum Mark, Grant David M. 1998. A chemical percolation model for devolatilization: Summary.
Francis, W. 1954. *Coal. Its foramtion and composition.* Edward Arnold Ltd.
Friedl, A. et al. 2005. Prediction of heating values of biomass fuel from elemental composition. *Analytica Chimica Acta.* **544**(1-2), pp.191-198.

Garba, M.U. 2012. Prediction of Ash Deposition for Biomass Combustion and Coal/Biomass Co-combustion.pdf.
Garcia, P., Espinal, J.F., Salinas, C. Martinez de Lecea, Mardragon. 1995. *Carbon.* **33**, pp.1641-1653.
Garner, L. 1997. Experience with low NOx burners. IEACR/99. London, UK. *IEA Coal Research.* p68.
Gibbins, J.R., Lockwood,F.C, Man,C.K, Williamson J. 1995. Implications of nitrogen release from coals at elevated room temperatures for NOx formation during pf combustion. In: *Coal science, proceedings of the 8th intermational confernece on coal science, Oviedo, Sp10-15 Sept 1995. Amsterdam, Netherlands, Elsevier Science BV. Coal science and technology.* Elsevier, pp.755-758.
Gil, M.V. et al. 2010. Thermal behaviour and kinetics of coal/biomass blends during co-combustion. *Bioresour Technol.* **101**(14), pp.5601-8.
Glarborg, P. 2003. Fuel nitrogen conversion in solid fuel fired systems. *Progress in Energy and Combustion Science.* **29**(2), pp.89-113.
Glarborg, P. et al. 2018. Modeling nitrogen chemistry in combustion. *Progress in Energy and Combustion Science.* **67**, pp.31-68.
Gomez-Barea, A.V., L.; Campoy, M.; Fernandez-Pereira, C. 2009. Plant optimization and ash recycling in fluidised waste gasification. *Chem. Eng. J. 2009.* **146**, pp.227–236.
Gong, B., Buckley, A. N., & Lamb, R. N. 1999. XPS determination of the forms of nitrogen in coal pyrolysis chars. . *Surface and Interface Analysis.* **28**, pp.126–130.
Goodridge, A.M.R., A.W. 1976. combustion & heat transfer in large boiler furnaces. *Prog energy combustion sci.* **2**, pp.83-95.
Greul, U., Rudiger, H. Spielthoff, H., Hein, K.R.G. 1996. NOx controlled combustion in a bench scale test facility. In: *Preceedings, 21st international technical conference on coal utilisation and fuel systems, CLearwater, FL, USA. 18-21 Mar 1996*. *Washington DC, USA coals and slurry technology association.* pp.711-722.
GRI2. 1996. GRI 2, Gas Research Institute
Gudka, B., Jones, Jenny M., Lea-Langton, Amanda R., Williams, Alan, Saddawi, Abby. 2015. A review of the mitigation of deposition and emission problems during biomass combustion through washing pre-treatment. *Journal of the Energy Institute.* **89**(2), pp.159-171.
Gurgel Veras, C.A. et al. 1999. Overlapping of the devolatilization and char combustion stages in the burning of coal particles. *Combustion and Flame.* **116**(4), pp.567-579.
Hampartsoumian, E.P., M. Williams, A. 1989. Combustionrates of chars and carbonaceous reisdues. *Journal Inst Energy.* **62**, pp.48-56.
Hashimoto, N., Kurose, R., Hwang, S., Tsuji, H., Shirai, H. 2012. A numerical simulation of pulverized coal combustion employing a tabulated-devolatilization-process model (TDP model). *Combustion and Flame.* **159**(1), pp.353-366.
Hayhurst, A.N. and Vince, I.M. 1980. Nitric oxide formation from N_2 in flames: The importance of “prompt” NO. *Progress in Energy and Combustion Science.* **6**(1), pp.35-51.
Hernandez, J.R., and Kilpinen, P. 2005. Homogeneous oxidation of volatile nitrogen (NH3, HCN) to nitrogen oxides: a modelling study of the effects of alkali vapors. *Turkish J. Eng. Env. Sci.* **30**, pp.163-174.
Hesselmann, G.J. 1997. Optimisation of combustion by fuel testing in NOx reduction facility. *Fuel.* **76**(13), pp.1269-1275.
Hurt, R., Sun, Jian-Kuan, Lunden, Melissa. 1998. A Kinetic Model of Carbon Burnout in Pulverized Coal Combustion. *Combustion and Flame.* **113**(1), pp.181-197.
IEA. 2018. *Pulverised coal combustion.* [Online]. [Accessed July 2019]. Available from: https://www.iea-coal.org/pulverised-coal-combustion-pcc/.
IEA. 2019. *Global Energy & CO2 Status Report.*

Illan-Gomez, M.J. et al. 1995a. NO Reduction by Activated Carbons. 2. Catalytic Effect of Potassium. *Energy & Fuels.* **9**(1), pp.97-103.
Illan-Gomez, M.J. et al. 1995b. NO reduction by activated carbons. 3. Influence of catalyst loading on the catalytic effect of potassium. *Energy & Fuels.* **9**(1), pp.104-111.
Illan-Gomez, M.J. et al. 1993. Nitrogen oxide (NO) reduction by activated carbons. 1. The role of carbon porosity and surface area. *Energy & Fuels.* **7**(1), pp.146-154.
Illán-Gómez, M.J. et al. 1998. Potassium-Containing Coal Chars as Catalysts for NOx Reduction in the Presence of Oxygen. *Energy & Fuels.* **12**(6), pp.1256-1264.
Oregon becomes the first US state to vote to go coal free. 2016. [Online database].
James, A. et al. 2012. Ash Management Review—Applications of Biomass Bottom Ash. *Energies.* **5**(12), pp.3856-3873.
Jayanti, S., Maheswaran, K., Saravanan, V. 2007. Assessment of the effect of high ash content in pulverized coal combustion. *Applied Mathematical Modelling.* **31**(5), pp.934-953.
Ji, Y., Tian,Y. P.,& Xu, D. L. 2009. Comments on NOx emission abatement in cement industry. *Journal of Xi'an University of Architecture & Technology.* **41**, pp.397–398.
Johnsson, J.E. 1994. Formation and reduction of nitrogen oxide in fluidized bed coal combustion. *Fuel.* **73**, pp.1399–1415.
Jones, A.R., Gibb, W.H, Irons, R.M.A. 1994. The effect of coal quality on the production of NOx and unburnt carbon levels. In: Proceesings, 1994 EPRI Workshop in NOx controls for utility boilers, Tuscon, AZ, USA, 11-13 May 1994, EPRI TR-104284, Palo Alto, CA, USA, Electric Power Research Institute, 13 pp(1994). p13.
Jones J.M, P.M., Williams A., Rowlands L., Zho Q. and Thomas K.M. 2004. Conversion of char nitrogen to NO during combustion.pdf. *Journal of Energy Institute.* **77**, pp.82-89.
Jones J.M., T.K.M. 1995. Carbon-13 materials as models for NOx and N_2O release during coal char combustion. *Carbon.* **33**.
Jones, J.M. et al. 2012. Combustion properties of torrefied willow compared with bituminous coals. *Fuel Processing Technology.* **101**, pp.1-9.
Jones JM., Z.Q., Thomas KM. 1999. Metalloporphyrin-derived carbons: models for investigating NOx release from coal char combustion. *Carbon.* **37**, pp.1123–1131.
Kambara, S. et al. 1994. Relation between functional forms of coal nitrogen and NOx emissions from pulverised coal combustion.pdf. *Fuel.* **74**(9), pp.1247-1253.
Karlström, O. et al. 2017. Role of ash on the NO formation during char oxidation of biomass. *Fuel.* **190**, pp.274-280.
Kazanc, F. et al. 2011. Emissions of NOx and SO_2 from Coals of Various Ranks, Bagasse, and Coal-Bagasse Blends Burning in $O_2/N_2$and O_2/CO_2 Environments. *Energy & Fuels.* **25**(7), pp.2850-2861.
Kelemen S. R., G.M.L., and Kwiatek P. J. 1994. Quantification of Nitrogen Forms in Argonne Premium Coal.pdf. *Energy & Fuels.* **8**, pp.896-906.
Kendall, R., Brown T., and Hetherington, L. 2010. Commodity profiles,. *British Geological Survey 2010.*
King, L. 2016. Doosan Babcock How UK thermal power plant cleaned up their act.....for what future? 65th Energy Science Lecture, University House, University of Leeds.
Kleinhans, U.W., Christoph, Frandsen, Flemming J. Spliethoff, Hartmut. 2018. Ash formation and deposition in coal and biomass fired combustion systems: Progress and challenges in the field of ash particle sticking and rebound behavior. *Progress in Energy and Combustion Science.* **68**, pp.65-168.
Klippenstein, S.J. et al. 2011. The role of NNH in NO formation and control. *Combustion and Flame.* **158**(4), pp.774-789.
Kobayashi, H., Howard, J. B., Sarofim, A. F. 1977. Coal devolatilization at high temperatures. *Symposium (International) on Combustion.* **16**(1), pp.411-425.

Kruczek, H. et al. 2006. The Effect of Biomass on Pollutant Emission and Burnout in Co-Combustion with Coal. *Combustion Science and Technology.* **178**(8), pp.1511-1539.
Landes, D.S., 1969. The Unbound Prometheus. Press Syndicate of the University of Cambridge
Lanigan, E.P., Golland, E.S., Rhine, J.M.,. 1994. The demonstration of gas reburninig at Longannet: Leading the world in low NOx technology. In *Proceedings, 60th Autumn meeting and gas 94 exhibition, London, United Kingdom, 22-23 Nov 1994. London, United Kingdom. Institute of gas engineering.* p30.
Lanzerstorfer, C. 2015. Chemical composition and physical properties of filter fly ashes from eight grate-fired biomass combustion plants. *J Environ Sci (China).* **30**, pp.191-7.
Larsson, A.-C. et al. 2006. Targeting by Comparison with Laboratory Experiments the SCR Catalyst Deactivation Process by Potassium and Zinc Salts in a Large-Scale Biomass Combustion Boiler. *Energy & Fuels.* **20**(4), pp.1398-1405.
Lester, E., Cloke,M. and Allen, M. 1995. Char Characterization Using Image Analysis Techniques.pdf. *Energy & Fuels.* **10**, pp.693-703.
Lester, E., Alvarez, D, Borrego, A.G., Valentim, B., Flores, D., Clift, D.A., Rosenberg, P., Kwiecinska, B., Barranco, R., Petersen, H.I., Mastalerz, M., Milenkova, K.S., Panaltescu, C., Marques, M.M., Thompson, A., Watts, D., Hanson. S., Predeanu, G., Misz, M., Wu, T. 2010. The procedure used to develop a coal char classification—Commission III Combustion Working Group of the International Committee for Coal and Organic Petrology. International Journal of Coal Geology 81 (2010) pp. 333–342
Li, C.-Z. and Tan, L.L. 2000. Formation of NOx and SOx precursors during the pyrolysis of coal and biomass. Part III. Further discussion on the formation of HCN and NH_3 during pyrolysis. *Fuel.* **79**(15), pp.1899-1906.
Lissianski, V.V. et al. 2001. Effect of metal-containing additives on nox reduction in combustion and reburning. *Combustion and Flame.* **125**(3), pp.1118-1127.
Liu, J., Zhang, X., Qinag, L., Shaw, A., Hu, B., Jiang, X. 2019. Mechanism study on the effect of alkali metal ions on the formation of HCN as NO_X precursor during coal pyrolysis. *Journal of Energy Institute.* **92**(3), pp.604-612.
Liu, Y., Che, D., Xu, T. 2007. Effects of Minerals on the Release of Nitrogen Species from Anthracite AU - Liu, Y. *Energy Sources, Part A: Recovery, Utilization, and Environmental Effects.* **29**(4), pp.313-327.
Liu, Y. et al. 2017. Experimental study on adsorption of potassium vapor in flue gas by coal ash. *Powder Technology.* **318**, pp.170-176.
Liu, Y.H., Che, D. F., & Li, Y. T. 2001. X-ray photoelectron spectroscopy determination of the forms of nitrogen in Tongchuan coal and its chars. *Journal of Xi'an Jiao Tong University.* **35**, pp.661–665.
Lovecz. 2006. *Effects of acid rain, woods, Jizera Mountains, Czech Republic.* [Online]. [Accessed 15 July].
MacPhail, J.M., Rhine, J.M, . 1997. The demonstration of gas reburning technology on a 600MWe boiler an Longannet, Scotland. In: *Combustion and emissions control III, Instutute of Energy, London, UK. Pergamon, Oxford, UK*. pp.340-350.
Malte, P.C. and Pratt, D.T. 1975. Measurement of atomic oxygen and nitrogen oxides in jet-stirred combustion. *Symposium (International) on Combustion.* **15**(1), pp.1061-1070.
Malvern. 2010. *Mie theory The first 100 years.* [Leaflet].
Maschio S., T.G., Piani L., Furlani E. 2011. Fly and bottom ashes from biomass combustion as cement replacing components in mortars production: rheological behavior of the pastes and materials compression strength Chemosphere. *85 (2011), .* pp.666–671
Matsuda, H., Minamizono,T., Kimoto, M., Makino, H. 1994. N_2O formation in pulverised coal combustion-the effects of combustion conditions. *In: Proceedings 6th International workshop on nitrous oxide emissions, Turku, Finland, 7-9 Jun*

1994, AAA-ILTF/FKF-94/10, Turku, Finland, Abo Akademi, Combustion Chemistry Research Group. pp.593-599
Mertens, J.D. et al. 1991. A shock tube study of the reactions of NH with NO, O_2, and O. *International Journal of Chemical Kinetics.* **23**(2), pp.173-196.
Miller, J.A. and Bowman, C.T. 1989. Mechanism and modeling of nitrogen chemistry in combustion. *Progress in Energy and Combustion Science.* **15**(4), pp.287-338.
Mitchell, S. 1998. NOx in pulverised coal combustion. *IEA Coal Research Report CCC/05.*
Molina, A. et al. 2009. Pathways for conversion of char nitrogen to nitric oxide during pulverized coal combustion. *Combustion and Flame.* **156**(3), pp.574-587.
Munir, S., Daood, S.S., Nimmo, W., Cunliffe, A.M., Gibbs, B.M. 2009. Thermal analysis and devolatilization kinetics of cotton stalk, sugar cane bagasse and shea meal under nitrogen and air atmospheres. *Bioresour. Technol.* **100**, pp.1413–1418.
Myhre, G., D. Shindell, F.-M. Bréon, W. Collins, J. Fuglestvedt, J. Huang, D. Koch, J.-F. Lamarque, D. Lee, B. Mendoza, T. Nakajima, A. Robock, G. Stephens, T. Takemura and H. Zhang,. 2013. *Anthropogenic and natural radiative forcing. In: Climate change 2013. : The Physical Science Basis. Contribution of Working Group I to the Fifth Assessment Report of the intergovernmental Panel on Climate Change [Stocker, T.F., D. Qin, G.-K. Plattner, M. Tignor, S.K. Allen, J. Boschung, A. Nauels, Y. Xia, V. Bex and P.M. Midgley (eds.)]. Cambridge University Press, Cambridge, United Kingdom and New York, NY, USA.* IPCC.
Nelson, P.F., Buckley A.N. and M.D. Kelly. 1992a. Functional forms of nitrogen in coals and the release of coal nitrogen as NOx precursors (HCN and NH_3).pdf. *Twenty-Fourth Symposium (International) on Combustion/The Combustion Institute.* pp.1259-1267.
Nelson, P.F. et al. 1990. Conversion of fuel nitrogen in coal volatiles to NOx precusors under rapid heating conditions.pdf. *Fuel.* **70**(March).
Niksa, S. 1996a. Coal Combustion Modelling. IEAPER/31, London, UK. *IEA Coal Research Report CCC/05.* p58.
Niksa, S., Cho, S. . 1996b. Conversion of fuel nitrogen in the primary zones of pulverised coal flames. *Energy and Fuels.* **10**(2), pp.463-473.
Niksa, S. and Kerstein, A.R. 1991. FLASHCHAIN theory for rapid coal devolatilization kinetics. 1. Formulation. *Energy & Fuels.* **5**(5), pp.647-665.
Nimmo, W. 2016. Energy Technology & Innovation Initiative Faculty of Engineering Pilot Scale Facility, PACT, Sheffield
Nizhou, J.F., Hamidou, S., Bouda, M., Koulidiati, J., Segda, B.G. 2014. Using Dulong and Vandralek Formulas to estimate the calorific heating value of a household waste model. *International Journal of Scientific & Engineering Research.* **5**(1), p6.
Nsakala, y., N., Patel, R.L., Borio, R.W. 1986. *Ce report TIS-8211, Presented at the 1986 ASME/IEEE Joint power generation conference, Portland, Oregan, October 19-23. An advanced methodology for prediction of carbon loss in commercial pulverised coal fired boilers.*
NSCEP. 1997. *Nitrogen Oxides: Impacts on Public Health and the Environment, EPA 452/R-97-002, National Service Center for Environmental Publications*
Nunes, L.J.R. et al. 2016. Biomass combustion systems: A review on the physical and chemical properties of the ashes. *Renewable and Sustainable Energy Reviews.* **53**, pp.235-242.
Ohtsuka Y, Z.W., Furimsky E. 1997. Effect of alkali and alkaline earth metals on nitrogen release during temperature programmed pyrolysis of coal. *Fuel.* **76**, pp.1361–1367.
Olanders, B. and Steenari, B.-M. 1995. Characterization of ashes from wood and straw. *Biomass and Bioenergy.* **8**(2), pp.105-115.
Pels, J.R. 1995a. *Nitrous Oxide in Coal Combustion.*
Pels, J.R., Kapteijn, F. Moulijn, J.A., Zhu, Q. Thomas, K.M. 1995b. Evolution of nitrogen functionalities in carbonaceous materials during pyrolysis. *Carbon.* **33**(11), pp.1641-1653.

Perry, S.T. 1999. *A global free-radical mechanism for nitrogen release during coal devolatilization based on chemical structure*. Doctor of Philosophy thesis, Brigham University.
Pevsner, N., Richmond, I., (2002). *Northumberland.* The Buildings Of England. New Haven, US and London: Yale University Press.
Plaza, P. et al. 2009. Use of a Predictive Model for the Impact of Cofiring Coal/Biomass Blends on Slagging and Fouling Propensity. *Energy & Fuels.* **23**(7), pp.3437-3445.
Anthropogenic air pollution sources.pdf 2010.
PowerstationsUK. 2019. *Power stations of the UK.* [Online]. [Accessed 29 July 2019]. Available from: http://www.powerstations.uk/coal-countdown/.
Priyanto, D.E. et al. 2016. Ash transformation by co-firing of coal with high ratios of woody biomass and effect on slagging propensity. *Fuel.* **174**, pp.172-179.
Rajamma, R. et al. 2009. Characterisation and use of biomass fly ash in cement-based materials. *J Hazard Mater.* **172**(2-3), pp.1049-60.
Ren, Q. and Zhao, C. 2013. NOx and N_2O precursors (NH_3 and HCN) from biomass pyrolysis: interaction between amino acid and mineral matter. *Applied Energy.* **112**, pp.170-174.
Ren, X. et al. 2017. Carbon, sulfur and nitrogen oxide emissions from combustion of pulverized raw and torrefied biomass. *Fuel.* **188**, pp.310-323.
Reynolds, O. 1901. Papers on mechanical and physicla subjects 2. (1881-1901). An experimental investigation of the circumferance which determines whever the motion of water shall be direct or sinuos and the law of resistance in parallel channels. 535. On the dynamic theory of incompressible viscous fluids and the determination of criteria.
Rokni, E. et al. 2018. Emissions of SO_2, NOx, CO_2, and HCl from Co-firing of coals with raw and torrefied biomass fuels. *Fuel.* **211**, pp.363-374.
Rosendaal, C.M., van Vliet H.N. 1996. Operational experience with low NOx pulverised coal fired boiler firing imported coals at Maasvalakte Poer Plant. *Paper presented at the Indonesian-Netherlands Seminar on Clean Coal Technology*.
Rolt, L.T.C and Allen, J.S. 1997. *The Steam Engine of Thomas Newcomen* (Landmark Publishing, Ashbourne 1997).
Rubiera, F., Arenillas, A., Arias, B., Pis, J.J. 2002. Modification of combustion behaviour and NO emissions by coal blending. *Fuel Process. Technol.* **77-78**, pp.111–117.
Saddawi, A. et al. 2009. Kinetics of the thermal decomposition of biomass. *Energy & Fuels.* **24**(2), pp.1274-1282.
Saeed, M.A. et al. 2016. Global kinetics of the rate of volatile release from biomasses in comparison to coal. *Fuel.* **181**, pp.347-357.
Sahu, S.G. et al. 2014. Coal–biomass co-combustion: An overview. *Renewable and Sustainable Energy Reviews.* **39**, pp.575-586.
Sami, M. et al. 2000. Co-firing of coal and biomass fuel blends 1-s2.0-S0360128500000204-main.pdf. *Progress in Energy and Combustion Science.* **27**, pp.171-214.
Sandbag, A.E.a. 2018. *The European Power Sector in 2017. State of Affairs and Review of Current Developments.*
Sarofim, A.F., Kandas, A.W., Goel, S. 1995. Char nitrogen: effects of coal type pore structure on NO/N2O evolution. *In: Procedings:12th Annual International Pittsburgh Coal Conference, Pittsburgh, PA, USA, Pittsburgh Coal Conference, University of Pittsburgh.* pp.1125-1130
Schumann, U.a.H., H. 2007. The global lightning-induced nitrogen oxides source. *Atmos. Chem. Phys.* **7**, pp.3923-3907.
Selgren, S.F., McLoughlin, P.W., Gellene G.I. 1989. *J. Chem. Phys.* **90**, pp.1624-1629.
Sen, S. 2010. An Overview of Clean Coal Technologies I: Pre-combustion and Post-combustion Emission Control. *Energy Sources, Part B: Economics, Planning, and Policy.* **5**(3), pp.261-271.

Setser, D.W., Thrush, B.A. 1965. Kinetics of reactions involving CN emission II. The reaction between oxygen atoms and cyanogen. *Royal Society.* **288**(A), pp.275-291.
Silva, F.C.C., Nuno C. Tarelho, Luís A. C. Rodrigues, Sónia M. 2019. Use of biomass ash-based materials as soil fertilisers: Critical review of the existing regulatory framework. *Journal of Cleaner Production.* **214**, pp.112-124.
Silva, L.F. and da Boit, K.M. 2011. Nanominerals and nanoparticles in feed coal and bottom ash: implications for human health effects. *Environ Monit Assess.* **174**(1-4), pp.187-97.
Skiba, U., Ball, B. 2006. The effect of soil texture and soil drainage on emissions of nitric oxide and nitrous oxide. *Soil use and management.* **18**(1), pp.56-60.
Skinner, B.J. 1976. Earth Resources, Figure 13, Prentice-Hall, Inc, Englewood Cliffs, NJ.
Smart, J.P., Weber, R. 1989. Reduction of NOx and optimisation of burnout with an aerodynamically air-staged burner and air-staged precombustor burner. *Journal of the Institute of Energy.* **62**(453), pp.237-245.
X-ray Photoelectron Spectroscopy. 2016. [Database]. City University of Hong Kong, UWO.
Smith, I.W. 1982. The combustion rates of coal chars: A review. *19th Symposium (International) on combustion.*, pp.1045-1055.
Solomon, P.R., Hamblen D.G, Carangelo R.M, Serio M.A. and Deshpande G.V. 1987. A General Model of Coal Devolatilization. In: *ACS Division of Fuel ChemistryAt: New Orleans, LA*, *August 1987*.
Solomon, P.R. et al. 1990. Network models of coal thermal decomposition. *Fuel.* **69**(6), pp.754-763.
Solomon, P.R. et al. 1992. Coal pyrolysis: Experiments, kinetic rates and mechanisms. *Progress in Energy and Combustion Science.* **18**(2), pp.133-220.
Solomon, P.R., Serio, M.A., Hamblen, D.G., Yu, Z.Z., and Charpenay, S. 1990. Advanced in the FG-DVC model of coal devolatilization. *United States: N. p.*
Solomon, S., D. Qin, M. Manning, Z. Chen, M. Marquis, K.B. Averyt, M.Tignor and H.L. Miller (eds.). 2007. Global climate projections. *Cambridge University Press, Cambridge, United Kingdom and New York, NY, USA.*
Steer, J., Marsh, R.,Morgan, D., Greenslade, M. 2015. The effects of particle grinding on the burnout and surface chemistry of coals in a drop tube furnace. *Fuel.* **160**, pp.413-423.
Stephenson, P.L. 1994. The mathematical modelling of utility flames. *BFRC flame days, Univeristy of Leeds.*
Su, S. et al. 2001. Techniques to determine ignition, flame stability and burnout of blended coals in p.f. power station boilers. *Progress in Energy and Combustion Science.* **27**(1), pp.75-98.
Su, Y. et al. 2010. Efficient and cost effective reburning using common wastes as fuel and additives. *Fuel.* **89**(9), pp.2569-2582.
Sun, J.-K., Hurt, R. 2000. Mechanism of extinction and near extinction if pulverised solid fuel combustion. *28th Symposium of combustion.* p2205.
Taniguchi, M., Kamikawa, Y., & Okazaki, T. 2010. A role of hydrocarbon reaction for NOx formation and reduction in fuel-rich pulverized coal combustion. *Combustion and Flame.* **157**, pp.1456–1466.
Thomas, L. 2002. Coal Geology. *John Wiley and Sons Ltd.*
Thompson, A.W., Stainsby, R.E. 1993. Nitrogen release and devolatilisation from power station from power station coals by drop tube furnace. Conference on NOx , basic mechanism of formation and destruction and their application to emissions control technologies. London , UK. 20-22 Apr 1993, Stoke Orchard, UK, Coal Research Establishment, Coal Reseach Forum. 5 pp (1993).
Tillman, D. et al. 2010. Coal Characteristics and Biomass Cofiring inPulverised coal boilers.pdf.

Tomeczek, J. and Gradon, B. 1997. The Role of Nitrous Oxide in the Mechanism of Thermal Nitric Oxide Formation within Flame Temperature Range. *Combustion Science and Technology.* **125**(1-6), pp.159-180.
Tsubouchi, N. and Ohtsuka, Y. 2008. Nitrogen chemistry in coal pyrolysis: Catalytic roles of metal cations in secondary reactions of volatile nitrogen and char nitrogen. *Fuel Processing Technology.* **89**(4), pp.379-390.
Tumuluru, J.S.S., S.; Wright, C. T.; Boradman, R. D.; Yancey, N. A. 2011. A Review on Biomass Classification and Composition, Co-firing Issues and Pretreatment Methods. *ASABE Annual International Meeting, INL/CON-11-22458, Paper no. 1110458, Idaho National Laboratory.*
Turns, S.R. 2012. An introduction to Combustion, Concepts and Applications. *Macraw Hill*
Tylecote, R. F. (1992). *A History of Metallurgy, Second Edition*. London: Maney Publishing, for the Institute of Materials. ISBN 978-0-901462-88-6
Unsworth, J.F. 1991. *Coal quality and combustion performance. Coals science and technology.*
Van der Kooj, J., Zellinger, G., Eeckhoundt, J., Postgaard, H., Bauer, E., Fuchs, P., Lawlor, G., Sala, M., Tosi, A., Pelet, C., O'Connor, M. 1997. The effects of coal quality on NOx emissions. Ref 02003Ren9769, Paris, France, UNIPEDE Thermal generation study committee group of Experts; Chemistry of Power Stations. p42.
Van Loo, S.a.J.k.e. 2008. The Handbook of Biomass Combustion & Co-firing. *Earthscan, London.* p236.
Vassilev, S.V. et al. 2013. An overview of the composition and application of biomass ash. Part 1. Phase–mineral and chemical composition and classification. *Fuel.* **105**, pp.40-76.
Veriskovsky, I. 1956. *Earth in upheaval.* Pocket Books.
Waldron, D.J. 2005. *The application of advanced coal combustion models to the prediction of furnace performance*. PhD thesis, University of Leeds.
Waldron, D.W. 1998. A semi-empirical approach to predicting carbon in ash from pulverised fuel fired boilers. *International flame research foudation, ToTeM12.*
Wang, C., Wang, F., Yang, Q., Liang, R. 2009. Thermogravimetric studies of the behaviour of wheat straw with added coal during combustion. *Biomass Bioenergy.* **33**, pp.50–56.
Watanabe, H., Yamamoto, J. I., & Okazaki, K. 2011. NOx formation and reduction mechanisms in staged O2/CO2 combustion. *. Combustion and Flame.* **158**, pp.1255–1263.
Wendt, J.O.L. 1995. Mechanisms Governing the Formation and Destruction of NO x and Other Nitrogenous Species in Low NOx Coal Combustion Systems. *Combustion Science and Technology.* **108**(4-6), pp.323-344.
WHO. 2006. <WHO_SDE_PHE_OEH_06.02_eng.pdf>.
Williams, A., Pourkashanian M., Bysh P. and Norman J. . 1993. Modelling of coal combustion in low-NO, p.f. flames.pdf. *Fuel.* **73**(7).
Wiser, W.H. 1975. Am. Chem. Soc. Div. Fuel Chem. Prepr. . **20**(122).
Woitowicz, M.A. et al. 1995. The fate of nitrogen functionalities in coal during pyrolysis and combustion.pdf. *Fuel.* **74**(4), pp.507-516.
WOU. 2006. *https://www.wou.edu/las/physci/GS361/Fossil%20fuels/.* [Online]. [Accessed 3 March 2019].
Wu, H. et al. 2011. Appendix A - Solid fuel interactions in co-combustion - a literature survey.pdf.
www.cmu.edu. 2019. www.cmu.edu/maty/materials/Nanostructured-materials/carbon-nanostructures.html.
www.ecn.nl/phyllis2. 2016.
Wynn, G., Coghe, P. 2017. *Europe's Coal-Fired Power Plants: Rough Times Ahead Analysis of the Impact of a New Round of Pollution Controls.*

Yao, M.Y. and Che, D.F. 2007. Catalytic Effects of Minerals on NOx Emission from Coal Combustion. *Energy Sources, Part A: Recovery, Utilization, and Environmental Effects.* **29**(11), pp.1005-1016.
Yao, Z.T. et al. 2015. A comprehensive review on the applications of coal fly ash. *Earth-Science Reviews.* **141**, pp.105-121.
Yokoyama, K. et al. 1991. Formations of OH(X2II, A2Σ+) in the Reaction of NH(3Σ−) with NO in Incident Shock Waves. *Bulletin of the Chemical Society of Japan.* **64**(6), pp.1738-1742.
Zeldovich, J. 1946. The oxidation of nitrogen in combustion and explosions *European Physical Journal A. Hadrons and Nuclei.* **21**, pp.577-628.
Zhang, L. et al. 2015. The effect of functional forms of nitrogen on fuel-NOx emissions. *Environ Monit Assess.* **187**(1), p4195.
Zhao, K. 2004. Empirical research of transformation of nitrogen in coal by means of model compounds. Xi'an:Xi'an Jiao tong University.
Zhong, B.J. et al. 2001. Effect of Catalysts on the NO Reduction During the Returning with Coal Chars as the Fuel. *Combustion Science and Technology.* **164**(1), pp.239-251.
Zhu, Q., Jones, JM; Thomas, KM. 1997. The influence of Fe catalysts on the release of nitrogen oxides during the gasification of nitrogen doped carbon-13 material. *CARBON.* **35**, pp.855-858.
Zou, C.W., L; Zhao, J; Shi, R. 2016. Effects of Calcium Peroxide on Desulfurization and Combustion Efficiency during Coal Combustion. *J. Energy Eng.* **143**(2).

Page intentionally blank

Study of N-partitioning using the low-N analyser

An alternate method of nitrogen evolution explored was the use of a Low N analyser, as shown in Chapters 6.4 and 9.6.4. The results were shown in Chapter 6.4. Presented below are the results profiles from the analysis.

Coals without additives

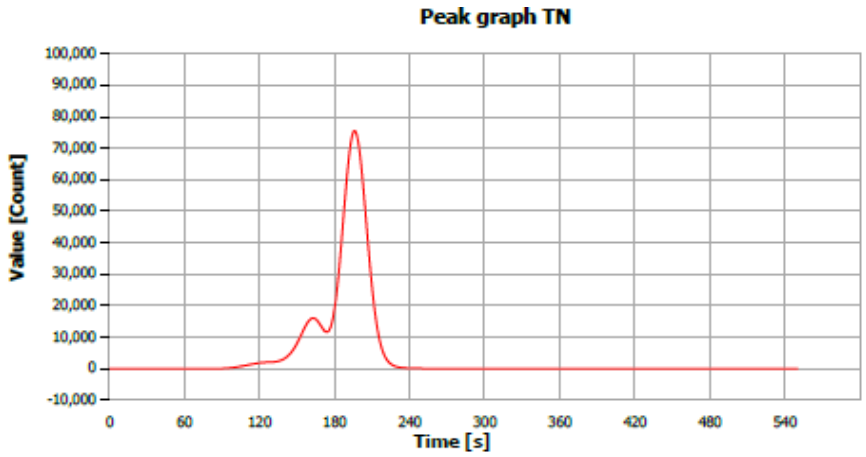

Ffos-y-fran coal

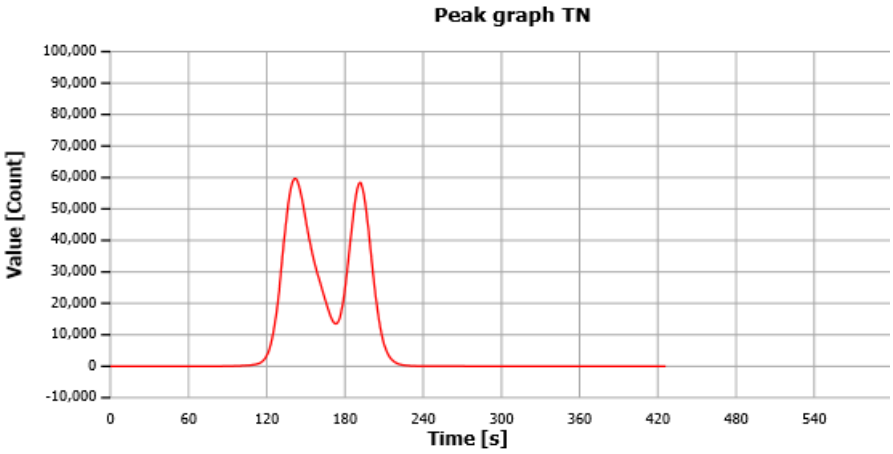

Shotton coal

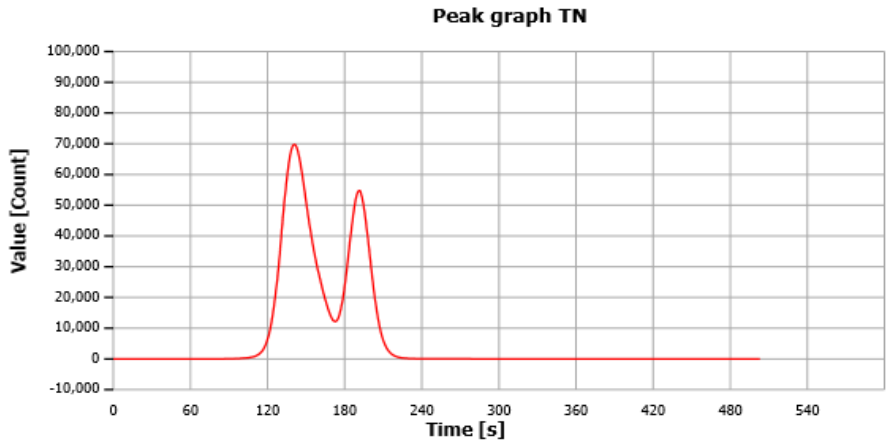

Galatia coal

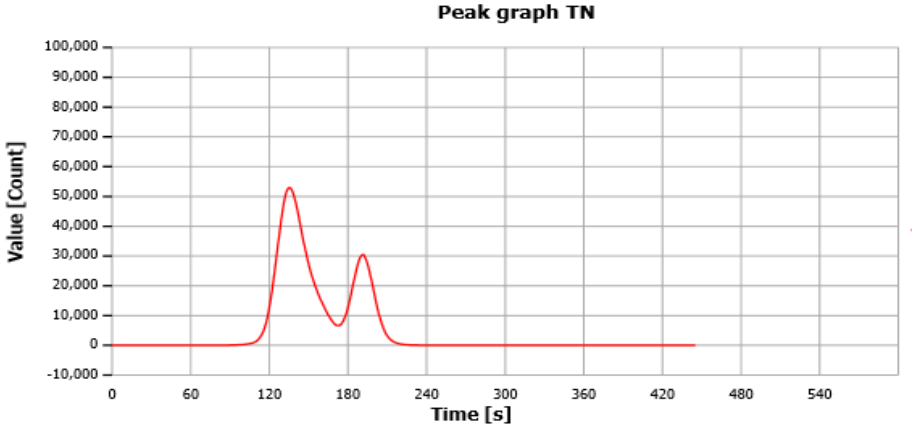

La Loma coal

Coals with additives

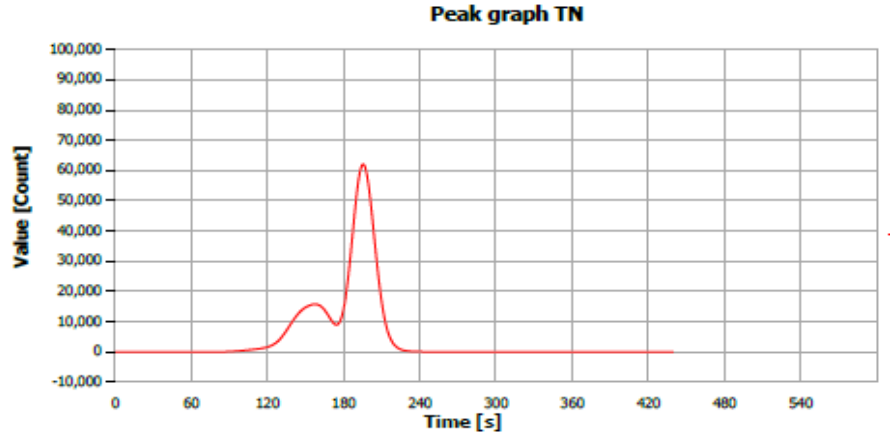

Ffos-y-fran FBA

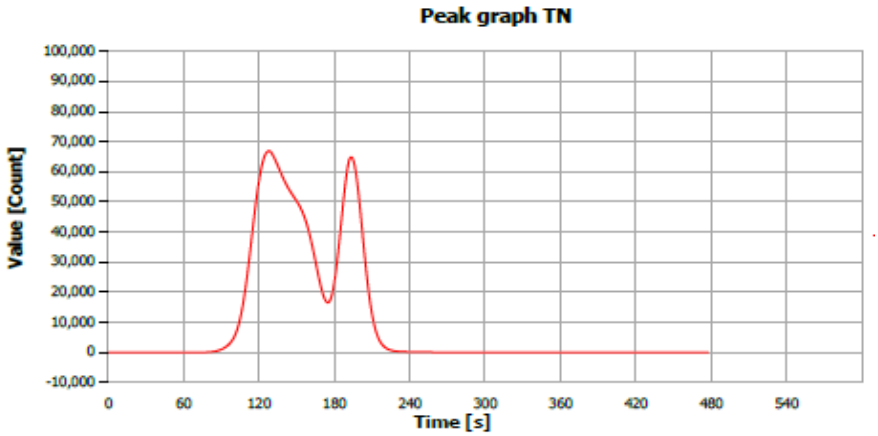

Ffos-y-fran PFA

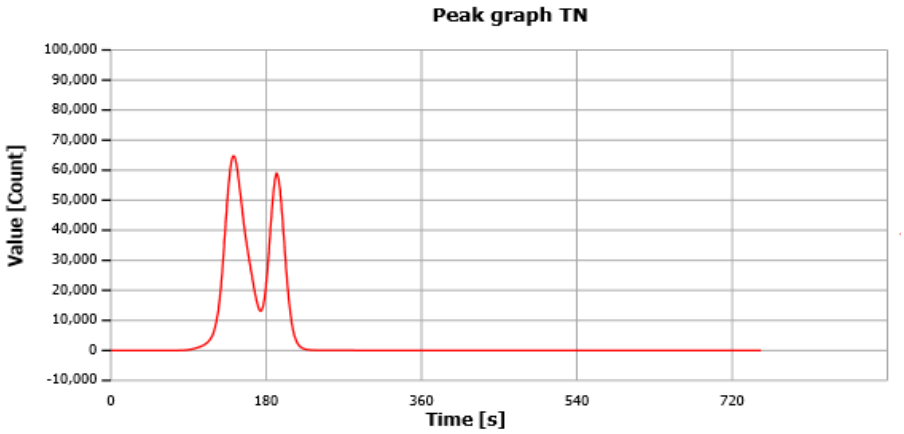

Shotton plus FBA

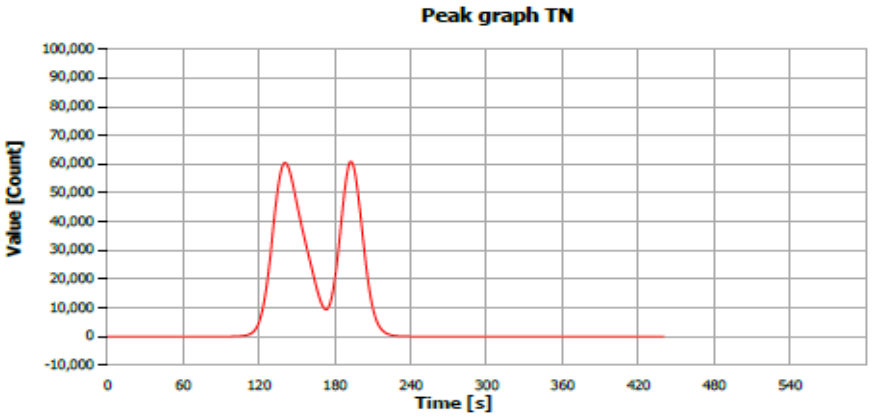

Shotton plus PFA

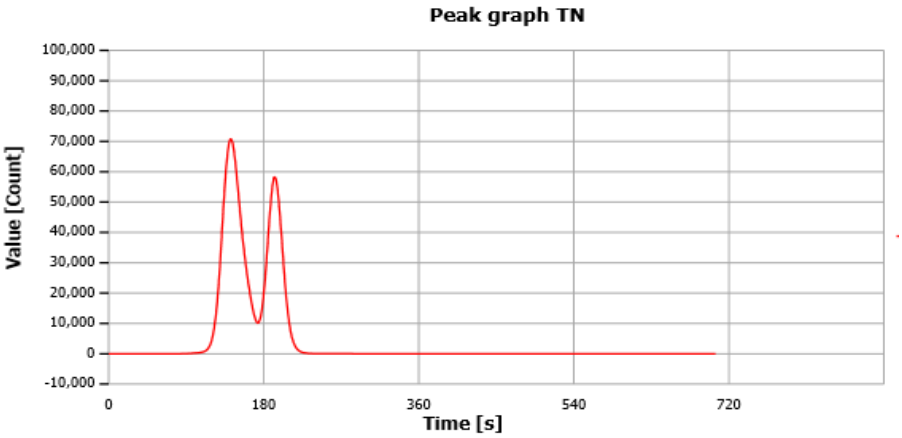

Galatia plus FBA

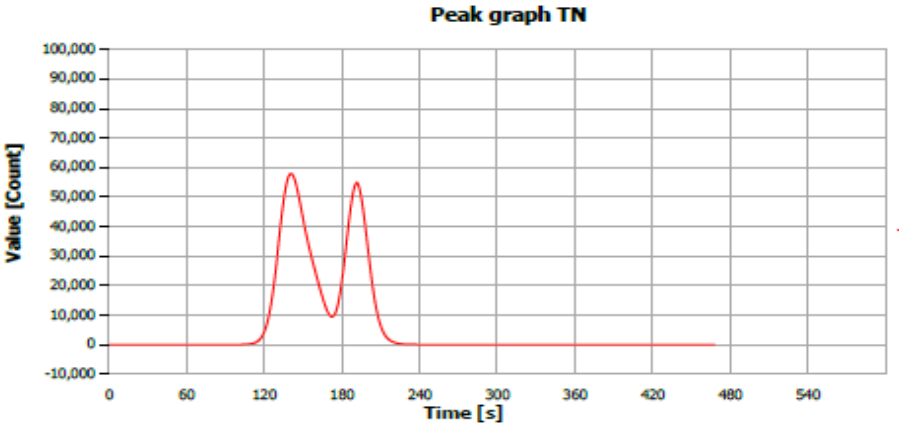

Galatia plus PFA

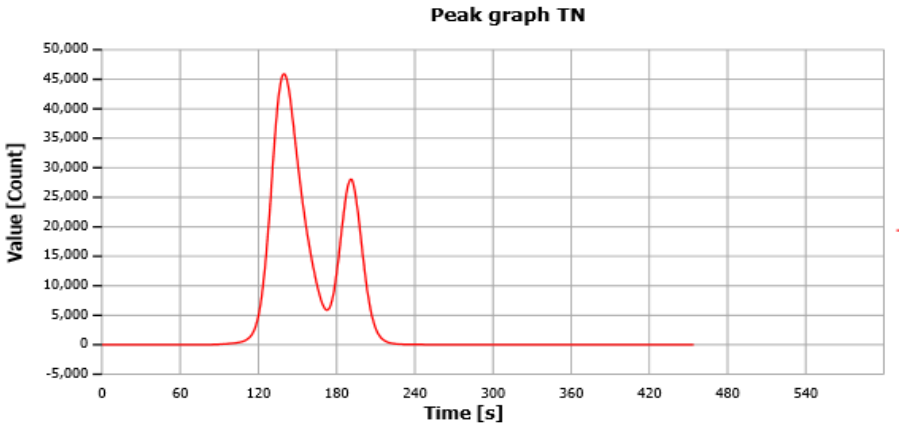

La Loma plus FBA

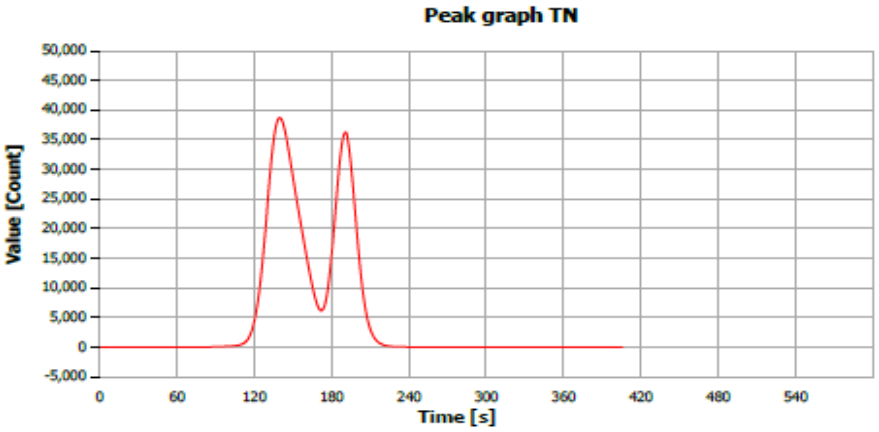

La Loma plus PFA

Coal chars

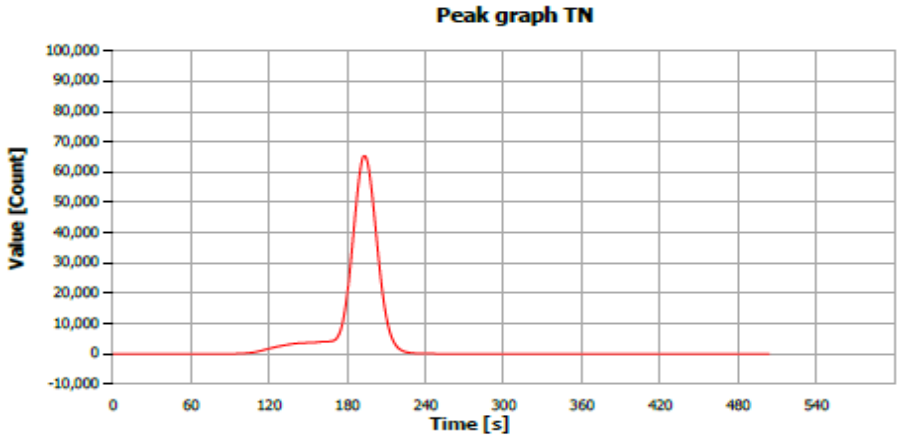

Ffos-y-fran char

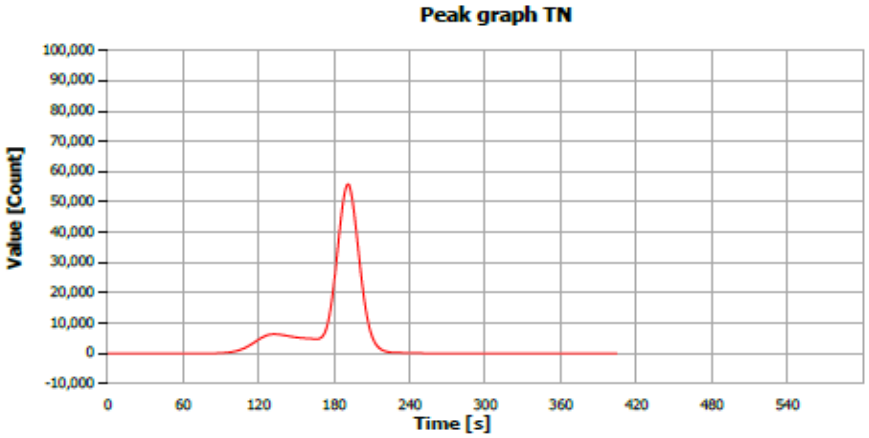

Shotton char

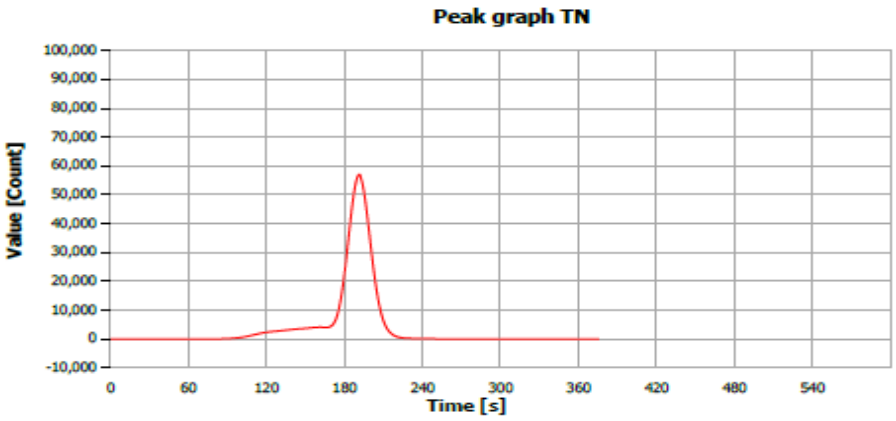

Galatia char

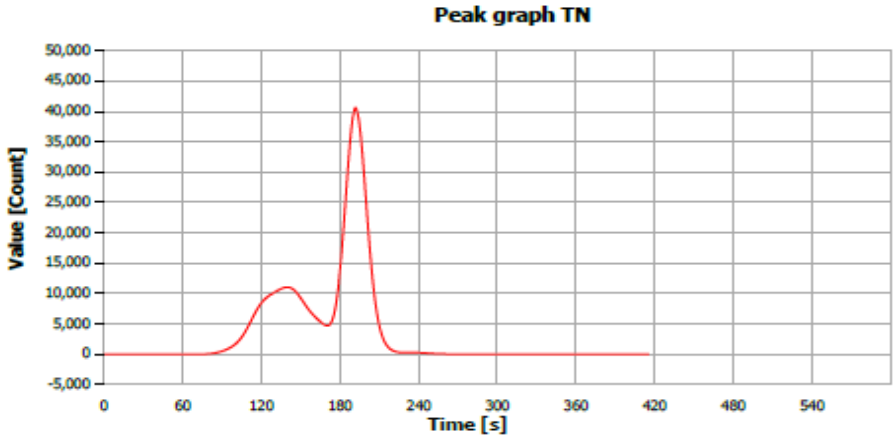

La Loma char

Coal Chars with additives

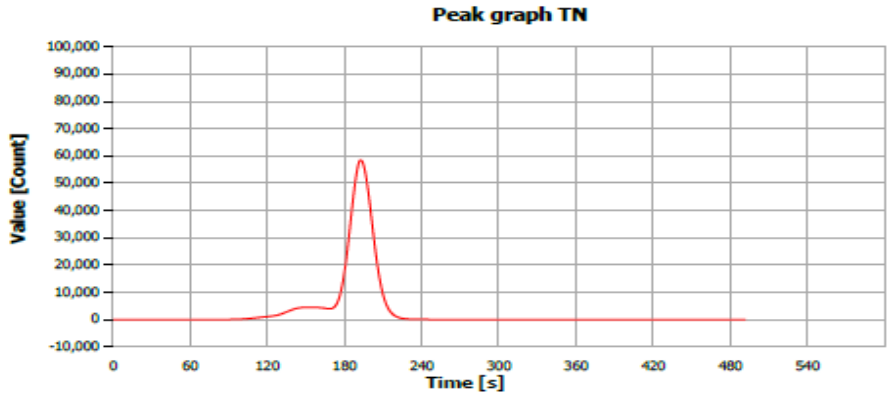

Ffos-y-fran FBA char

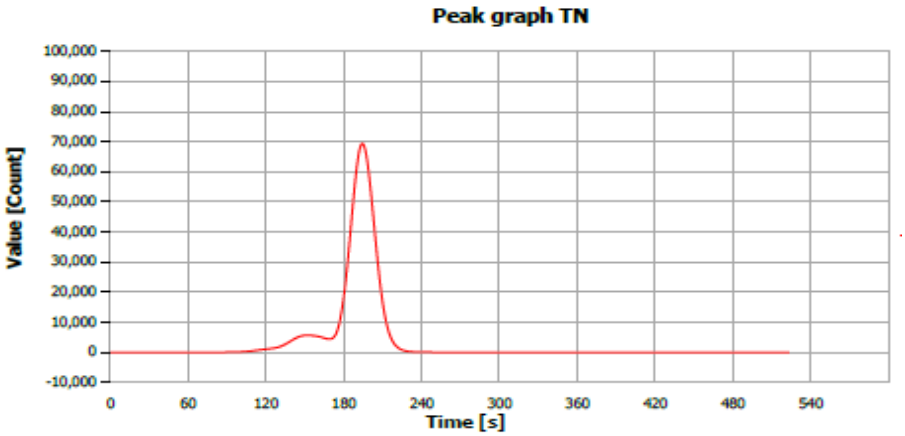

Ffos-y-fran PFA char

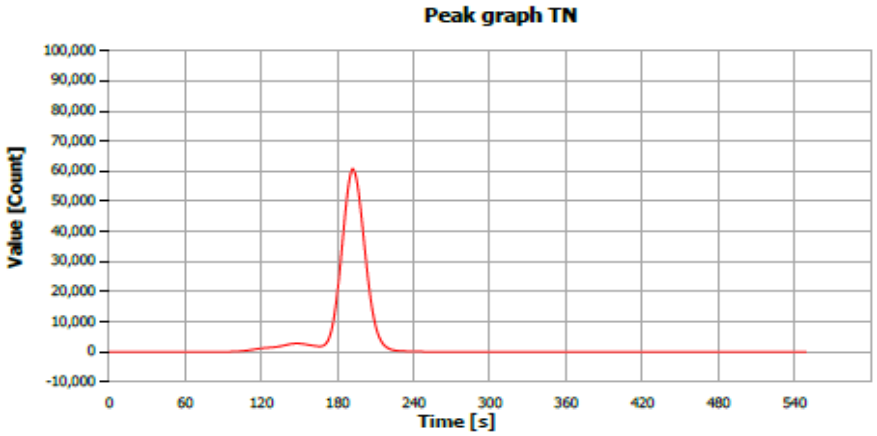

Shotton FBA char

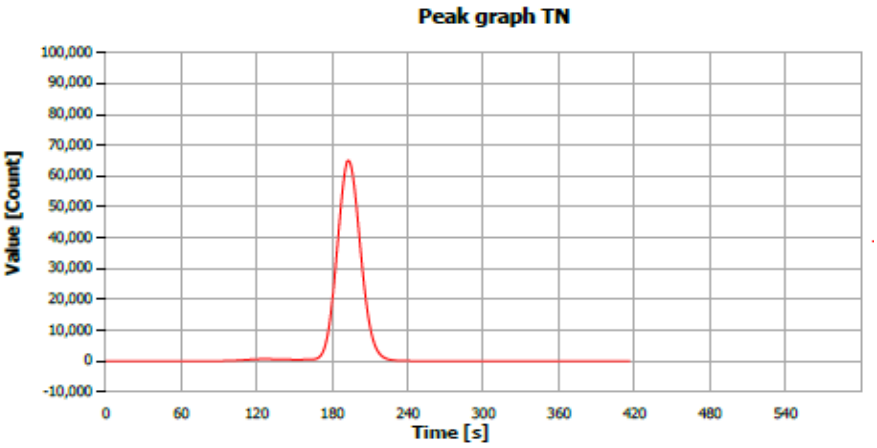

Shotton PFA char

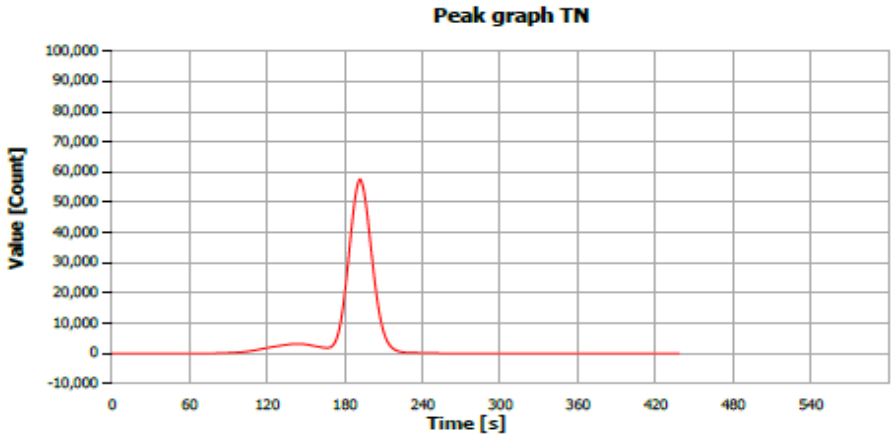

Galatia char FBA

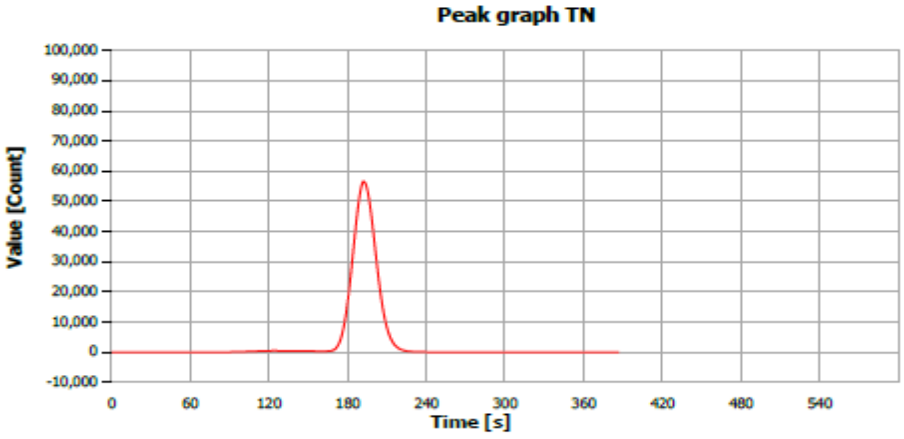

Galatia PFA char

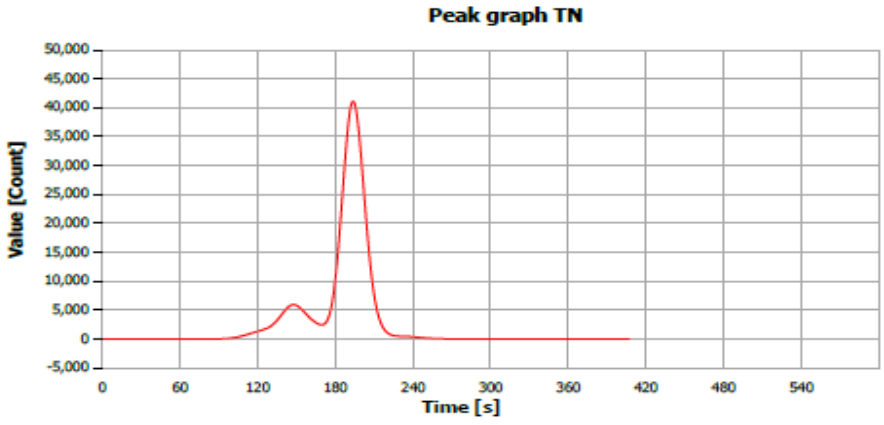

La Loma FBA char

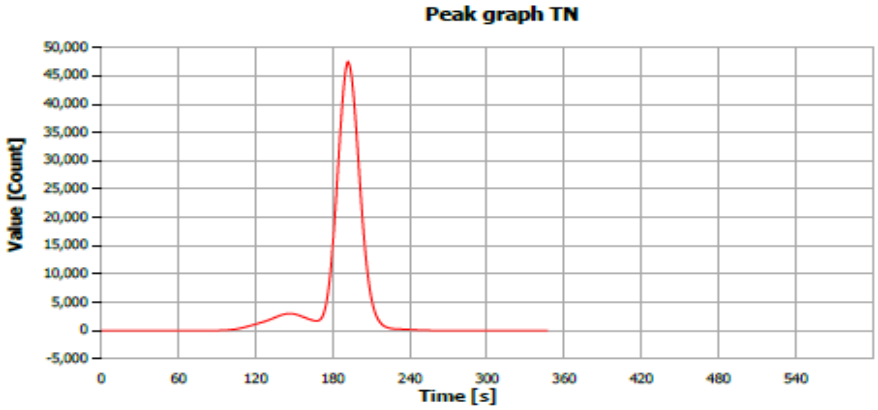

La Loma PFA char

Olive cake with and without additives

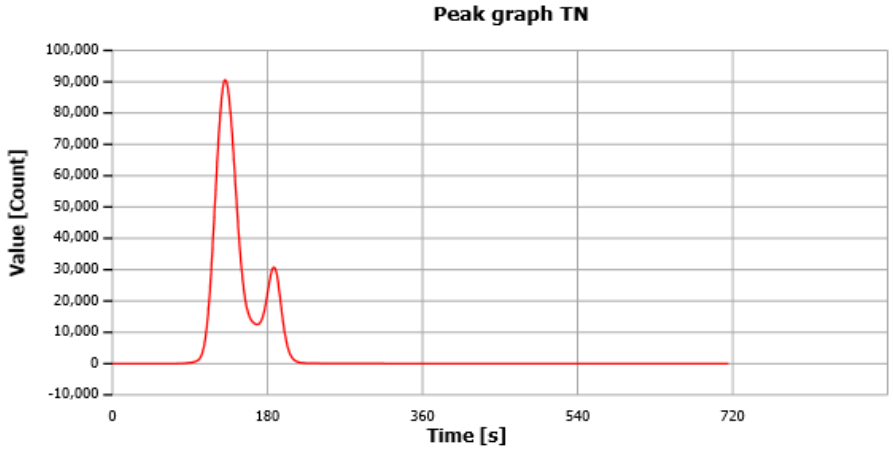

Olive cake

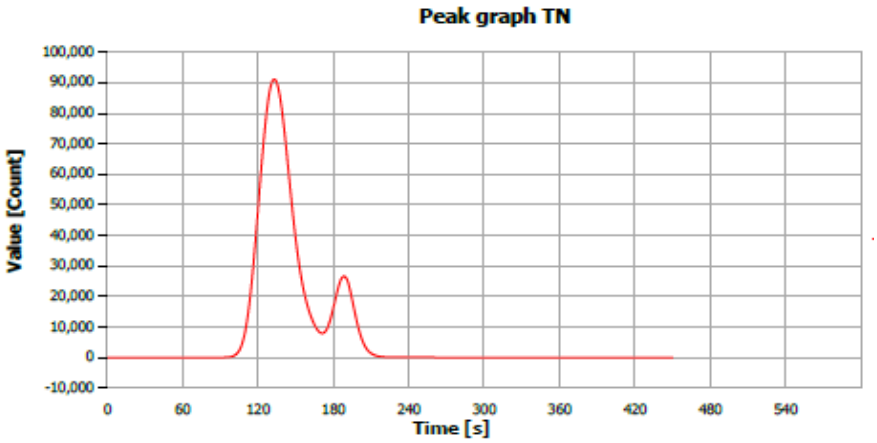

Olive cake plus coal PFA

Olive cake char with and without additives

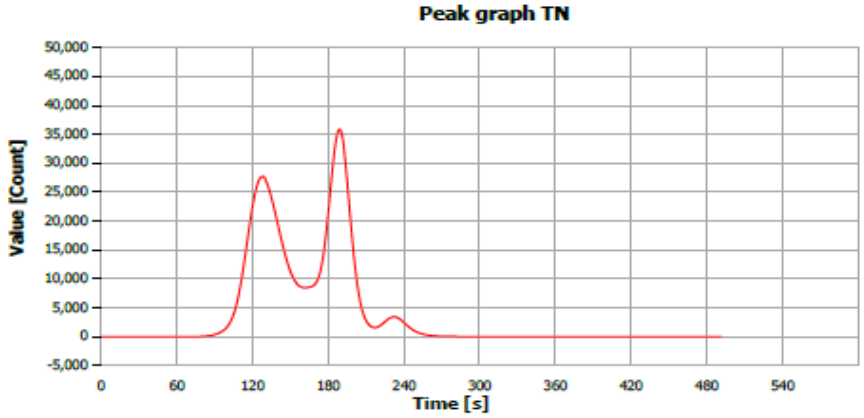

Olive cake char

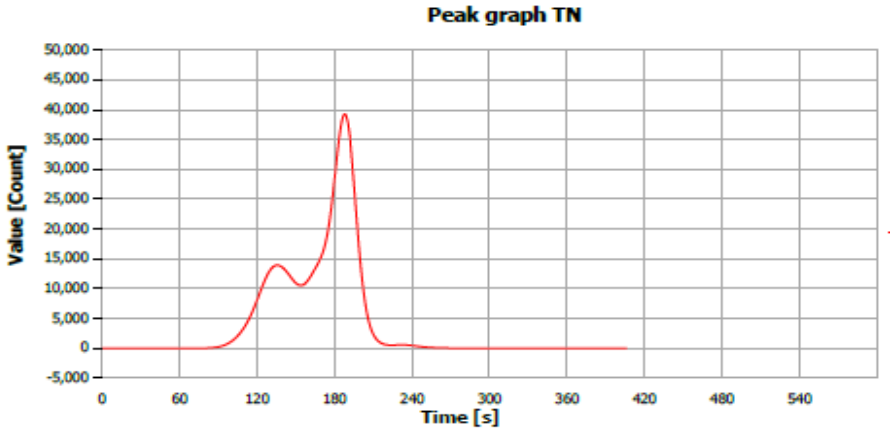

Olive cake plus coal PFA char

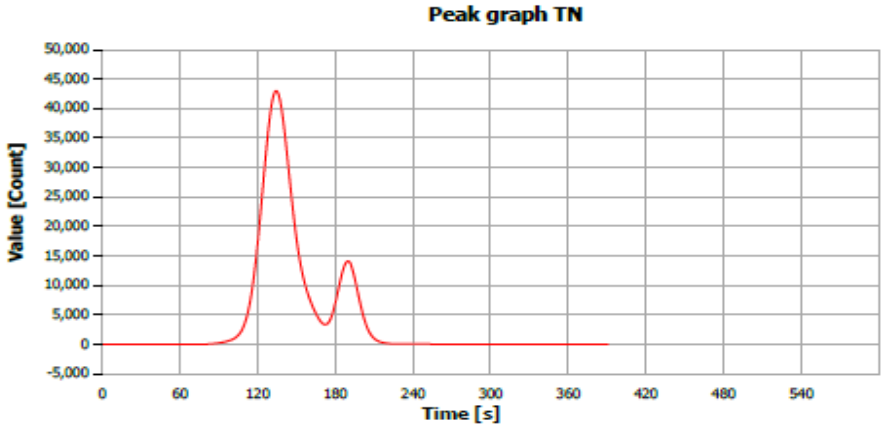

Olive stone standard